Development of macro/nanocellular foams in polymer nanocomposites

By

Subhendu Bhattacharya
B.Tech

A thesis submitted
for the fulfilment of the
requirements for the Degree of

Doctor of Philosophy (PhD)

Melbourne

August 2009

School of Civil, Chemical and Environmental Engineering
RMIT University
Melbourne, Australia

Acknowledgements

I would like to express my deepest gratitude to my Supervisors, Prof. Sati N Bhattacharya and Assoc. Prof Margaret Jollands. Apart from being encouraging and supportive of my ideas throughout my research degree candidature, they have immensely supported me in all my initiatives specially to convert research ideas to reality. Special thanks to Dr.Sumanta Raha for introducing me to the critical concepts in polymer rheology. I would also like to thank Mr. Phil Francis from the Department of physics (microscopic imaging) for his support in learning the various imaging techniques. I am also indebted to Dr. Rahul Gupta, Mr. Mike Allan, Dr Andrew Chryss and Dr. Ivan Ivanov who have helped me to get started with my research, by providing invaluable training in various experimental techniques. I also thank all my colleagues specially my close friends (Dr. Murali Reddy, Tim Harris, Swaroop Majumder, Hari Singh Parmar and Naishad Dave) who have always shared fun times with me. There support has helped me to keep my spirits high under trying circumstances. Most importantly I would like to thank my parents, for being assertive with all my endeavours. Their unconditional love, immense faith in my abilities, and unwavering support has provided me with the enthusiasm to keep going. Also last but not the least I would like to thank Steve Vai (Best rock guitarist) , John McLaughlin , Miles Davis and all other musicians who have through their music always provided me with a lot of energy and positive attitude to focus on my research objectives especially during times when I felt lonely.

Declaration

The work reported in this thesis, unless otherwise stated, is that of the candidate alone and has not been submitted previously, in whole or part, in respect to any other academic award. This research work has been carried out since the official date of commencement of the programme

Subhendu Bhattacharya

School of Civil, Chemical and Environmental Engineering

RMIT University

Melbourne, Australia

Publications arising from this work

1. **"Modelling of Gas solubility in HMS-PP/clay nanocomposites " CHEMECA (paper-073) Melbourne ,2006**

2. **"Foaming Behaviour of HMS-PP/clay nanocomposites",Polymer Processing society conference , Salerno , Italy (PPS)-24 , 2007**

3. **"Foam injection moulding of HMS-PP/clay nanocomposites", Polymer Processing Society conference (PPS)-25 , 2008**

4. **"Effect of polymer nanocomposite rheology on foam cell structure", Polymer Processing society conference Goa , India , (P-TSI-OP7),(PPS)-25 , 2008**

5. **Foaming behaviour of HMS-PP/clay nanocomposites, Polymer engineering and Science (accepted) ,(published online DOI 10.1002/pen-21343 ,2009)**

6. **"Clay compatibilization of immiscible PP/EVA blends , Polymer engineering and Science (accepted)**

Summary

Polymer foams have found use in a variety of industries due to their beneficial properties like high strength to weight ratio, improved insulating abilities and improved energy absorption capacity. Based on cell sizes, polymer foams can be classified as macrocellular (more than 100μm), microcellular (1-100μm), ultra microcellular (1 – 0.1μm) and nanocellular foams (less than100nm).The generation of nanocellular polymer foams would lead to further improvement in these properties along with additional improvements in tensile strength.

This thesis focuses on the generation of fine cell polymer foams using a heterogeneous nucleating agent (nanoclay), appropriate polymer blending strategies and accurate control of foam processing parameters. Foaming behaviour of High melt strength polypropylene (HMS-PP) /clay nanocomposites and HMS-PP/EVA/clay nanocomposite blends was studied using a batch and a continuous foam injection moulding system. Supercritical CO_2 as well as N_2 were used as the blowing agent. Polymer clay nanocomposites were processed in the Brabender twin screw extrusion system. PP-g-MA (12 wt %) (polypropylene grafted with maleic anhydride) with graft efficiency of 1% was used as a compatibilizer in both the blends. 12% PP-g-MA was used in both the nanocomposites. Since Ethyl vinyl acetate (EVA) was polar due to the presence of vinyl acetate, it intercalates clay galleries without the need of any compatibilizer. These nanocomposites were subsequently characterized and their thermal, mechanical and rheological properties were studied. Morphological studies using TEM and SEM led to a few interesting deductions. It was very difficult to attain complete exfoliation in case of HMS-PP/clay nanocomposites even at low clay loadings due to a non polar nature and low graft efficiencies of HMS-PP matrix. The addition of clay to an immiscible blend of HMS-PP/EVA results in compatibilization between the dispersed and the continuous phase. This compatibilization was due to improved adhesion between the blend components at the interphase. Subsequently foaming studies on the above mentioned nanocomposites was conducted in a batch and a continuous foam injection moulding system. A Box Benkhen experimental design approach was used to study the effect of foam processing parameters

(foaming time, foaming temperature, saturation pressure, and saturation temperature). Optimization studies revealed that the foam cell structure was highly sensitive to the foaming time and foaming temperature and the processing window for generation of fine cell foams was small (1 -2 degrees). Nanocellular foams (290 nm) were subsequently generated in the batch process at a foaming temperature of 147^{o}C and 25 seconds foaming time. Normally a low saturation temperature (near to the critical point of CO_2) and a high saturation pressure leads to increased supersaturation and hence reduced foam cell sizes but as such foam cell sizes are not very sensitive to these two parameters. It was observed that the addition of nanoclay, even in small proportions, leads to a reduction in foam cell size and in this case the smallest foam cell size was attained with 4 wt percent clay loading. Interestingly, the rate of cell coalescence increases with increase in clay loading and at very high clay loading the cells are completely ruptured and open cells foams are formed. Also, it was observed that the foam cell size reduction by addition of clay only happens till the rheologically determined percolation threshold was reached. After the percolation threshold, the foam cell sizes increase. It could also be said that foam cell sizes are reduced only when an exfoliated morphology, in case of polymer nanocomposites was attained.

The addition of immiscible EVA-28 to the HMS-PP matrix in presence of clay particles further results in reduction of foam cell sizes to 100 nm. The CO_2 attracting nature of the finely dispersed EVA -28 domains results in localization of the blowing agent within the dispersed phase and hence further reduction in foam cell sizes. The addition of clay particles also increases the melt viscosity and results in an extended strain hardening behaviour of the polymer matrix, limiting foam growth and hence cell sizes.

The effect of gas concentration, foaming temperature, injection pressure, and foaming time on foam cell size was studied. It was found that the foam cell size was highly sensitive to the injection pressure at the mould gate (hence pressure drop rate) and foaming temperature. The cell size linearly decreased with increase in gas concentration and foaming time. The sensitivity of foam cell sizes to changes in processing parameters decreases with increase in clay concentration.

The addition of clay particles to the polymer matrix results in a reduction of gas solubility within the polymer matrix. The presence of clay particles results in non random mixing within the polymer matrix and hence causes a change in the configurational entropy of the polymer matrix, which further results in a change in the overall thermodynamic properties of the polymer nanocomposites. This effect was simulated using statitistical thermodynamic tools to understand the molecular level impact of the addition of clay particles on gas solubility within the polymer. The level of supersaturation affects the foam cell structure. Hence to model the gas solubility and supersaturation in presence of clay particles Guggenheims quasichemical approximation was used. The partition function theory for a lattice combined with Guggenheim's approximation. A new contact fraction based equation for mixing within the polymer matrix was developed. Subsequently a new equation for Helmholtz free energy function was derived, which can be used to study other thermodynamic properties. Additionally rheological modelling studies are also performed to understand the role of dynamic and extensional rheological properties of polymer nanocomposites in controlling foam cell sizes. The simulation studies reveal that the dynamic viscosity was the controlling parameter for restricting foam cell sizes. The extensional viscosity increases rapidly during the first few seconds of foam growth and then becomes constant whereas the overall stress difference acting across the foam cells decays sluggishly and hence controls the foam cell sizes

TABLE OF CONTENTS

List of figures

List of Tables

Chapter 1: Background

1.1 Introduction

Polymer foams have been generally used in consumer products like cushions, packaging, insulations, and absorbents. It has also been used in high technology applications as scaffolds for tissue engineering applications or as a base material for production of bullet proof jackets and as smart materials (auxetic foams). Also interestingly the foamed products have better biodegradability characteristics as compared to pure polymer products and hence are more environmentally friendly (1). Because of multitude of applications the research in polymer foams is drawing increased attention. Polymer foaming is an interdisciplinary research area requiring a knowledge base from several different fields like polymer science, rheology, thermodynamics, mass & heat transfer, and process equipment design. Due to a broad range of skill requirement research in this area has been mostly experimental in nature. Hence understanding the theoretical principles which govern the polymer foam morphology becomes very important specifically in case of production of fine cell foams.

Traditionally microcellular foams are classified by cell sizes in the range of 1-10 μm and cell numbers higher than 10^9 cells/cm^3 (2). The characterization of foams based on cell sizes is debatable since it is difficult to relate the properties of polymer foams to cell sizes and density directly. Interestingly it has been found that generally microcellular foams have better impact strength as compared to macrocellular foams and also microcellular foams are rigid in nature as compared to macrocellular foams which are soft by nature (3). The generation of foam cell sizes below 1 micron would result in ultra fine or nanocellular foams. The generation of nanocellular foams is a relatively new area of research. Much of the research in this area has been directed in

the production of nanocellular foam cell structure in a batch process. It has been found that nanocellular foam cell sizes would result in additional advantages over microcellular foams (3). Specifically the tensile properties and insulation properties would be significantly improved. Also it would be more advantageous to use nanocellular foams in thin walled products like bottles, pipes, thin films, and sheets. The cell structure and cell density itself may have unique applications in areas like capsulation, filtration, insulation and absorption. Nanocellular foams may also have other multitude of applications which can only be realized once the production of such cellular materials becomes viable.

This thesis focuses on the physical foaming process using a physical blowing agent like supercritical CO_2 and nitrogen using either a batch or a continuous foam injection moulding system. The foaming process can be divided in to four basic steps (4) :

1) Mixing of the blowing agent or gas into the polymer matrix to form a homogenous polymer/gas composite. 2) Cell nucleation which is basically the process of phase separation caused by thermodynamic instability by either using a temperature superheat or a pressure decrease.

3) Foam cell growth or expansion of the critical nuclei to the desired size. This process is controlled by a host of factors like mass and heat transfer, morphology and thermal properties of the polymer and the rheological characteristics.

4) Foam cell stabilization which is a process to limit foam cell sizes by reduction of temperature of the matrix. The tendency of the foam cells to coalesce, collapse and distort during the quenching process makes it important.

The selection of physical blowing agent for generation of fine cell foams is of prime importance considering the potential effects on the environment and the effectiveness

of the blowing agent in terms of solubility and foam cell nucleation. The traditionally used blowing agents (chlorofluorocarbons) have been found to affect the ozone layer adversely and hence are not the recommendable option as blowing agents. Under such circumstances the choice is to use inert gases like CO_2, N_2, Argon or water. Out of all the mentioned inert gases CO_2 has some unique properties, which make it a suitable option. CO_2 is environmentally benign, non combustible, chemically inert and stable and is cheap as well. Also CO_2 has been found to have the highest amount of solubility in polymers as compared to other gases mentioned (5). Improved solubility of blowing agent provides better super saturation and hence also propels the rate of foam cell nucleation (6).

The critical point for CO_2 is 31^0C, and 7.4MPa, which is relatively low. Above this temperature and pressure, CO_2 is in the supercritical state. CO_2 in supercritical state has a liquid like density and gas like viscosity and diffusivity. Both of these aspects are supportive to the generation of fine cell foams. Also supercritical CO_2 has been found beneficial in other polymer processing applications, like extraction, dispersion of fillers in filled polymer systems, surface modification, and blending (5). The only drawback of using CO_2 as a blowing agent is the high pressure operation required and the fast gas escape during the foaming process. These drawbacks are not very significant as compared to the benefits of using CO_2 as a blowing agent.

1.2 Scope and objective of this research

In this study the production of foams using a batch and continuous foaming system is explored using supercritical CO_2 as the blowing agent. Polymer nanocomposites containing clay are used as the base polymer for foaming to produce foams with improved cell structure and properties. Experiments are carried out to study the effect

of five key processing parameters namely CO_2 content, foaming time, foaming temperature, pressure drop rate and clay content. Gas solubility studies using CO_2 is performed in a batch setup and the effect of CO_2 absorbing groups on equilibrium solubility is experimentally determined. Subsequently the change in gas solubility in presence of filler is modelled using statistical thermodynamic tools. Further rheological, thermal and morphological characterization studies are conducted on the polymer nanocomposites to understand the effect of clay particle dispersion and nanocomposites rheology on foam cell structure. Finally rheological modelling is performed to study the role of shear and extensional rheology on foam cell structure.

1.3 Polymer/clay nanocomposite foams

Homogenous nucleation and heterogeneous nucleation are the two different nucleation mechanisms that coexist in the polymer foaming process in the presence of fillers. The addition of filler to the polymer matrix greatly improves the nucleation rate by reducing the free energy requirement for foam cell nucleation (7). The foam cell morphology is affected by the shape, size, distribution and surface treatment of the filler material used (8, 9). As compared to conventional fillers the addition of a small amount of clay results in much finer cell sizes and higher foam cell densities (10). Nanometre sized clay particles as compared to conventional fillers have extremely fine dimensions and hence provide a much larger surface area for foam cell nucleation, In addition the functionalization of the filler results in intimate contact with the polymer matrix, and both these aspects affect the foam cell nucleation and growth mechanism. Open and closed cell morphology can be generated by controlling the dispersion state of the clay particles in the polymer matrix. The addition of nanoclay also improves the barrier properties, diffusion coefficient,

mechanical strength and heat resistance thus improving the range of applications of polymer foams generated by the addition of nanoclay to the polymer matrix.

1.4 Characterization of polymer/clay nanocomposites

The change in properties of the polymer matrix on addition of nanoclay affects the final foam cell morphology. Also the dispersion state of nanoclay particles affects the foam cell nucleation and growth mechanism. The rheological, thermal, and mechanical properties of the polymer are also affected on addition of clay particles and these properties also affect the foam cell structure. The improvement in melt strength characterized by the zero shear viscosity on addition of nanoclay helps in controlling foam cell sizes by improving the resistance to foam cell growth. The extensional viscosity of the polymer matrix on addition of clay particles also needs to be measured, since the polymer matrix in-between two growing bubbles experiences a bi axial stretching force which causes strain hardening of the polymer matrix (11). This behaviour in turn helps in restricting foam cell sizes (12). The change in crystallization temperature and crystallinity on addition of clay particles would also affect foam cell morphology by affecting parameters like gas solubility, cell nucleation and cell growth rate. The dispersion state of clay in the polymer matrix also affects foam cell morphology. It has been reported that exfoliated nanocomposites result in better foam cell densities and small foam cell sizes as compared to intercalated nanocomposites (10). Hence use of TEM and XRD becomes essential. Thus to better understand the role of clay in controlling foam cell sizes the characterization studies of polymer/clay nanocomposites become necessary.

1.5 Measurement of CO_2 solubility and modelling of gas solubility in polymer nanocomposites

The equilibrium solubility of the blowing agent within the polymer matrix influences the final foam cell morphology. The solubility of the agent dictates the level of super-saturation and the initial foam cell nucleation rate. Also the measurement of CO_2 solubility helps in calculating the foam expansion ratio and the degree of compatibility between the polymers and CO_2. A volumetric method using the batch setup has been designed to measure the solubility (13). The Sanchez Lacombe equation of state has been used to represent the phase equilibrium relationship (14).

The Sanchez Lacombe equation of state used to predict solubility of CO_2 in polymers is based on the lattice fluid theory, where a random mixing state between the polymer and the holes within the lattice is assumed. In case of polymer/clay nanocomposites, the presence of stationery interacting filler in the lattice results in non-random mixing of polymer and holes. The non randomized mixing state affects the configurational entropy of the polymer chains within the lattice (15). Also the presence of interacting filler also changes the internal energy of the polymer-clay-hole composite system. Hence the free energy of the entire system as compared to the case of randomized mixing state with only polymer and holes in the lattice is also affected (16). The change in free energy of the lattice would affect the gas solubility.

1.6 Thesis outline

This thesis includes six chapters starting with Background (chapter 1), followed by Literature review (chapter 2). The literature review provides a detailed insight into current research trends in generation of fine cell foams. Chapter 3 (Materials and

Measurement techniques) focuses on the experimental techniques used and the materials selected to generate and characterize polymer nanocomposite foams.

Chapter 4 (Results and discussions: Characterization studies) discusses the various experimental results obtained and compares them to current trends. Chapter 5 (Results and Discussions: Modelling and simulation) focuses on the modelling and simulation techniques used to verify experimental results. The conclusion from the research work is summarized in chapter 6. Recommendations for future work are also provided in this chapter. Finally some experimental data and programming codes are provided in appendices.

Chapter 2: LITERATURE REVIEW

2.1 Polymeric foams

Polymeric foams are defined as materials with gaseous voids of various shapes and sizes surrounded by a polymer matrix (17-20). The reduction in raw material requirement, the associated cost savings and a host of applications have resulted in an increasing interest in the area of polymeric foams in both academia and the industry. Foaming technology is an interdisciplinary area requiring a knowledge base from the areas of polymer science and engineering, thermodynamics, rheology, fluid dynamics, mass and heat transfer and process equipment design. Though research into foaming over the years has resulted in useful information about parameters affecting foam cell morphologies, the design of a foaming process is still experimental in nature. The probable reason is the necessity to scale up research results before designing a viable foam process for commercial applications.

Recent importance to environmental issues has resulted in several challenges to the foam processing industry. The foam process industry today is challenged by environmental issues like waste disposal, foam product life cycle, recyclability and use of environmentally friendly blowing agents and generation of microcellular/nanocellular foams due to there increasing demand and additional benefits (20-22). Considering the above aspects, current research into polymer foaming is concentrated to the use of environmentally friendly blowing agent substitutes and polymers. Also the generation of fine cell foams requires a better understanding of exact parameters governing foam processing and hence research into foam nucleation, thermodynamics and foam growth becomes crucial.

The demand for foamed plastic has been buoyant since the advent of microcellular foaming technology (22). The polymer foam market is expected to witness steady growth in the coming decade. The global polymeric foams market is projected to reach 20.5 million metric tons by 2010, at an average annual growth rate of more than 3.5% during 2000-2010. Asia-Pacific, the largest and the fastest growing foam market is projected to cross 6.5 million tons by 2010, at a CAGR (compounded annual growth rate) of more than 4% over the 2000-2010 periods (23). It is projected that the major demand for polymer foam products will be from the insulation and the packaging foam industry (23).

Polymer foams are classified as rigid and flexible foams. The classification is dependent on foam density, material consumption, foam cell morphology and physical and thermal properties of the foamed products. Rigid foams are used in applications like building and construction, appliance, ranks/pipes, transportation, packaging, furniture, flotation, mouldings, and food and drink containers. Flexible foams are used in applications like bedding and mattresses, textiles, toys, gaskets, automotive sealings, sport application, sound attenuation and shock absorption. Thus the major applications of polymer foams are in packaging, construction, insulation and as consumer products.

Polymer foams can also be classified on the basis of foam cell structure as open cell foams and closed cell foams. Closed cell foams are characterized by the presence of complete cell wall around each foam cells ,whereas open cell foams are devoid of cell walls and are left with only ribs and struts (18). The structure of the foam cells also influences the properties of polymer foams. Open cell foams generally have poor insulation properties for both heat and electricity; have higher permeation rates for gases, better sound absorption and insulation characteristics as compared to closed

cell foams. Also closed cell foams are normally rigid and open cell foams are flexible in nature. The generation of open cell foams or closed cell foams depends on the polymer material used and control of foam processing parameters. A typical foaming formulation consists of the polymer, foaming agent, nucleating agents, stabilizers and other additives. The final foam morphology and properties vary as per the combination of the formulation adopted. The selection of the base polymer for foaming is based on its properties like melt strength, crystallinity and degree of branching (23, 18, 24, 25). The selection of a blowing agent is based on the type of processing technique used for generation of polymer foams. There are two types of blowing agents that can be used to produce the gas phase in a foamed material: chemical blowing agent and physical blowing agent. A chemical blowing agent is premixed with the foam formulation. This blowing agent later on decomposes during processing and liberates water vapour, CO_2 or N_2. A physical blowing agents needs to be separately injected into the foam mixture using a high pressure injection device. The normally used physical foaming agents are chlorofluorocarbons (freons), volatile hydrocarbons/alcohols, and inert gases (CO_2, N, argon, or water).

The traditionally used foaming agents (freons) are environmentally hazardous, since they are responsible for the depletion of the ozone layer. Among the other three alternatives mentioned which are environmentally friendly in terms of depletion of ozone layer, CO_2 seems to be the best option due to its unique properties. As compared to freons, an equivalent amount of CO_2 can be dissolved in the polymer matrix under the supercritical state (elevated pressure). The diffusivity of CO_2 in the polymer melt under the supercritical state is large ensuring more efficient and quicker mixing (26). Also supercritical CO_2 is found to improve the dispersion of nucleating

agents in the polymer matrix (21, 26). The only challenges associated with use of super critical CO_2 are the high pressure operation and fast gas escape.

Homogenous nucleation and heterogeneous nucleation are the two nucleation mechanisms that coexist in a typical foaming process. The use of organic, inorganic, metal powders and other particles as nucleating agents results in heterogeneous nucleation. The addition of a finely dispersed particle to the polymer matrix results in the reduction of the free energy required for foam cell nucleation (27). This results in improved nucleation rate, uniform cells, and better control on foam cell sizes. Inorganic nucleating agents like talc, $CaCO_3$, titanium dioxide, diatomaceous earth, kaolin and clay are more commonly used (27). The nucleation efficiency of the nucleating agent is affected by the dispersion, shape, size and surface treatment of the nucleating agent. The nonuniform dispersion of a non – functionalized agent results in aggregation of nucleation agents at higher loadings. This behaviour results in increased foam cell coalescence, nonuniform cell size distribution and increased foam cell sizes. Recent studies on addition of functionalized nucleating agents like (clay, CNT, nanoparticles) have revealed that only a small amount of nucleation agent is required to obtain equivalent or higher nucleation efficiency as compared to the untreated nucleating agents. The reason is that a functionalized nucleating agent disperses uniformly throughout the polymer matrix (28). When the dispersion of the nucleating agent is at the nanometre level then the nucleation efficiency is the highest. Also, additional benefits like significant improvement in polymer/filler composite properties have also been reported. These polymer /filler composites are called as polymer nanocomposites (20).

The focus of this work is to generate fine cell foams using polymer/clay nanocomposites in a batch and an injection foam moulding system. The effect of

addition of clay particles on foam cell morphology will be studied. Additionally the use of another technique like (use of CO_2 philic groups) in presence of clay particles will also be explored.

2.1.1 Polymer Nanocomposites

Polymer nanocomposites are formed by the addition of functionalized fillers to the polymer matrix dispersed at the nanometre level. The nanocomposites can be formed using different types of functionalized fillers categorized on the basis of the shape, and functionality of the filler used. Our interest in this work is mainly the nanocomposites formed using layered silicates (clay) though other nanoparticles have also been found to be equally effective in terms of property enhancement.

The addition of pristine layered silicate (PLS) (clay) to the polymer matrix has resulted in remarkable improvement in multitude of properties (29-31). These improvements include enhancement in melt elasticity, increased tensile strength, improved thermal resistance, decreased gas permeability and flammability and improved biodegradability. The degree of enhancement of polymer properties is a function of the level of interaction between the polymer and the clay particles (32-34). The commonly used layered silicates belong to the family of phylosilicates. These particles physically are like a conglomeration of thin rectangular plates (layers) separated by exchangeable cations in between the layers. The layer thickness is around 1nm and the lateral dimension of these layers varies from 30 nm to several microns. The interlayer distance is produced thermodynamically by the Vander Wall forces generated due to the presence of exchangeable cations like $Na^{+,}$ K^{+}, Mg^{2+}, $Fe^{2+,}$ Al^{3+} etc. The net charge on the surface of these particles due to the presence of cations is expressed in terms of Cation Exchange Capacity (CEC) (35) denoted in mequiv/100gm. The CEC value is an average over all layers since the net charge

varies from layer to layer. Pristine layered silicates are hydrophilic in nature and can only intercalate with hydrophilic polymers like PEO and PVA. All other polymers can intercalate layered silicates only when they are modified with organic compounds making them organophilic. In absence of an organic modifiers layered silicates form an immiscible phase separated structure with most of the engineering polymers resulting in poor mechanical and thermal properties; hence organic modification becomes essential. Layered silicates are normally modified with primary, secondary, tertiary and quaternary alkyl ammonium or alkyl phosponium ions. Based on the surface charge density, chain length and reactivity of the modifier three different types of morphologies are established on addition of organo modified layered silicates to polymers, which are unmixed, intercalated and exfoliated (32). The unmixed polymer composite are formed when the polymer chains do not interact with the clay particles. This is a phase separated system of polymer and large layered silicate aggregates. The intercalated morphology is established when the polymer chain intercalates clay galleries. Intercalated polymer nanocomposites have an ordered and uniform distribution of clay particles throughout the polymer matrix. The exfoliated morphology is observed when there is a completely random distribution of clay particles within the polymer matrix. Also complete layer by layer separation is attained in case of exfoliated nanocomposites (36). Figure 2.1 shows the morphology of the three different types of nanocomposites discussed above.

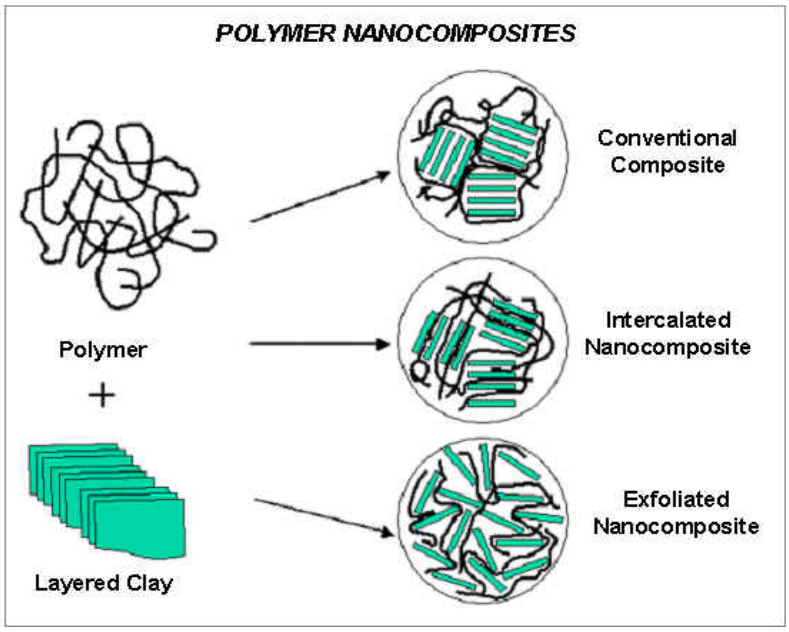

Figure 2.1: The three different morphologies that is observed in polymer nanocomposites (35)

Since the morphology of the polymer nanocomposites influences their properties, nanocomposite characterization studies become essential to analyze the effect of clay particles on polymer properties.

2.2 Morphological characterization of Polymer nanocomposites

The structural characterization of polymer nanocomposites generally has been performed using WAXD (Wide angle X-ray scattering) and TEM (Transmission electron microscopy). WAXD additionally can also be used to probe the kinetics of polymer melt intercalation into clay galleries (37). The nanocomposite structure (intercalated or exfoliated) is identified by analyzing the position, shape and intensity of the basal reflections originating from the silicate layers (35). In case of exfoliated nanocomposites the extensive delamination of the silicate layers results in complete absence of any coherent X-ray diffraction pattern (38). Alternatively in case of intercalated nanocomposites the layer expansion caused by the polymer chains results in appearance of a new basal reflection corresponding to the new gallery height.

Although WAXD patterns are easy to generate, they do not provide conclusive evidence about the structure of nanocomposites. The reason being that the experimentally generated WAXD patterns are normally averaged over the entire sample volume. As a result no conclusions can be drawn about spatial distribution of the silicate layers or the presence of any structural non-homogeneities. Hence TEM images become essential (39). TEM provides a direct visualization of the spatial distribution of clay particles and the structure of nanocomposites. However special care must be exercised to ensure that the sample analyzed truly represents the actual. Thus TEM in conjunction with WAXD provides conclusive evidence on the morphology of polymer nanocomposites. Figure 2.2 : TEM and WAXD patterns for different types of polymer nanocomposites (35) shows the possible WAXD and TEM patterns established for different polymer nanocomposite morphologies.

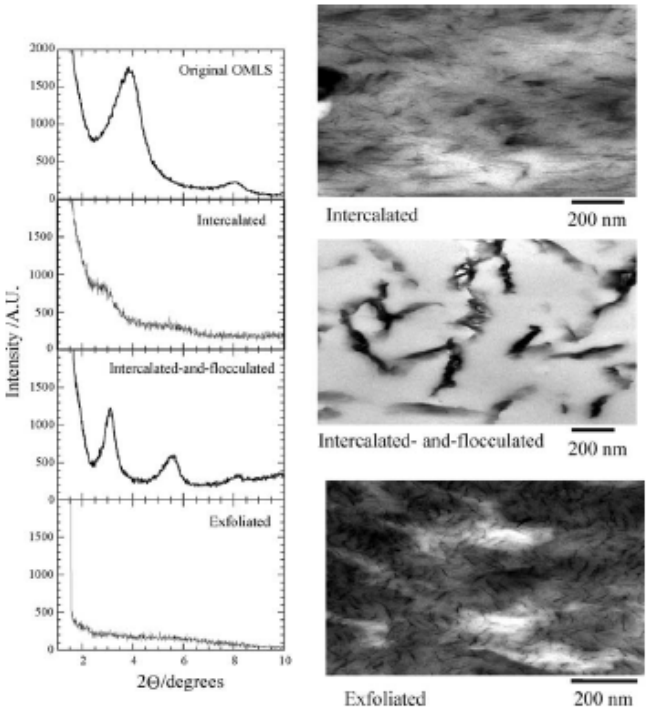

Figure 2.2 : TEM and WAXD patterns for different types of polymer nanocomposites (35)

2.3 Production of polymer nanocomposites

The preparation of polymer/clay nanocomposites can be carried out by three basic mechanisms. 1) Intercalation of polymer or pre polymer from solution 2) In situ intercalative polymerization and 3) Melt intercalation.

In the first case of interaction of polymer from a solution a common solvent in which the polymer is soluble and the clay particles is swellable is chosen (20 35). The commonly used solvents are water, chloroform and toluene depending on the type of polymer or pre polymer used. The clay is then first swollen in the solvent and then the polymer or pre polymer is added to the solution. Once this is done the polymer intercalates the clay galleries and displaces the solvent. Once the solvent is removed the intercalated structure remains. In case of in situ intercalative polymerization the clay particles are swollen in a solution of the monomer and subsequently polymerization is carried out within the interlayer to form the nanocomposites. The polymerization is initiated by heat, catalyst or organic initiator. The process of melt intercalation is a mechanical technique to produce polymer nanocomposites (40, 41). This process is the most commonly used commercial technique for the production of polymer nanocomposites. In this process, a well mixed mixture of polymer and the clay particles is annealed either statically or by using shear at a temperature above the softening point of the polymer. This process has a lot of advantages compared to the techniques mentioned previously. Firstly this process is environmentally friendly since it doesnot involve the use of organic or any kind of solvents. Secondly it is compatible with the industrial process of extrusion and injection moulding.

2.4 Foaming production techniques

2.4.1 Batch foaming

In a batch foaming process polymer samples are placed in a pressurized vessel and saturated with a blowing agent (CO_2 , N_2 , etc) at the desired pressure and temperature (42). The saturation time depends on the diffusivity of the gas or blowing agent into the sample. The saturation time can vary from few hours to several days in some cases. Once the sample has been saturated then there are two possible techniques for the production of foams. In case the saturation temperature and pressure is sufficiently high (above the glass transition temperature and nearby to the melting temperature) the saturation temperature can be treated as the foaming temperature. Subsequently foam cell nucleation can be achieved by a rapid release of pressure (43, 44).The rate of nucleation in this case is a function of the pressure drop and the pressure drop rate (45). In case the saturation temperature of the sample is very low (well below Tg or sufficiently below Tm); the nucleation of foam cells can be achieved by raising the temperature using an oil/water bath. In this case the rate of nucleation is dependent on the net temperature increase and the rate of temperature increase (46). The benefit of using the second technique is that gas solubility is higher at lower saturation temperature, hence increased solubility and possibly better foam cell structure could be attained. The other possible option is to use a combination of the two methods. Once nucleation is achieved the cell growth is controlled by the growth time and the cell growth temperature (47). After selection of suitable parameters for cell growth the next step is to quench the foamed samples below Tg or possibly below a temperature where the cell walls would be strong enough to sustain further foam cell growth. In commercial cases the quench temperature is normally the room temperature. Figure 2.3 below shows the schematic diagram of a batch process

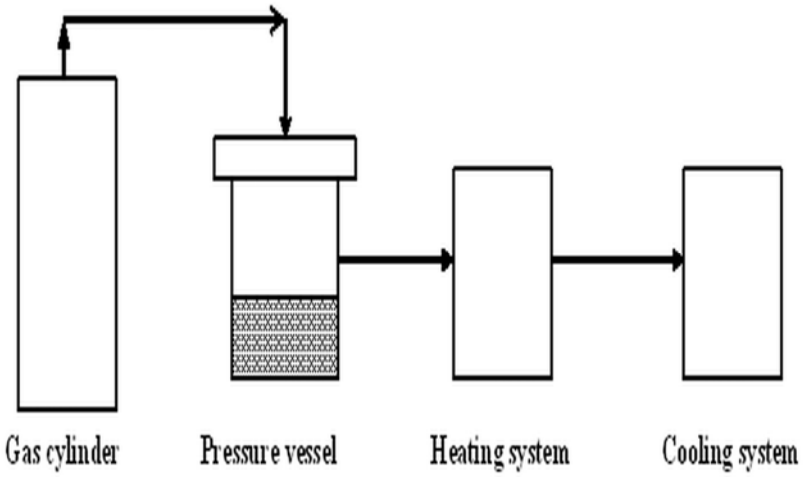

Figure 2.3 : A schematic representation of the Batch process for foaming

2.4.2 Semi continuous foaming

This process is very similar to batch foaming process and is used for the production of polymer sheets. In this process a roll of solid polymer sheet is formed with a gas permeable material inserted in between the polymer layers (23, 48, 49). This roll is then saturated with the blowing agent at high pressure and room temperature for sufficient time to attain the desired gas concentration. Finally the pressure is released and the material is unwound, separated from the gas permeable material and then subsequently drawn through a heating station maintained at the desired foaming temperature. This process is normally used for production of polymer foam sheets

2.4.3 Continuous foam extrusion

Figure 2.4 shows the typical processing steps involved in a continuous foam extrusion system. A continuous foam extrusion system is like a normal polymer extrusion system with a few modifications. The foam extrusion system has a port for injection

of the gas inside the system, a special mixing device to ensure the formation of a homogenous gas/polymer mixture and a specific foaming die (50, 51).

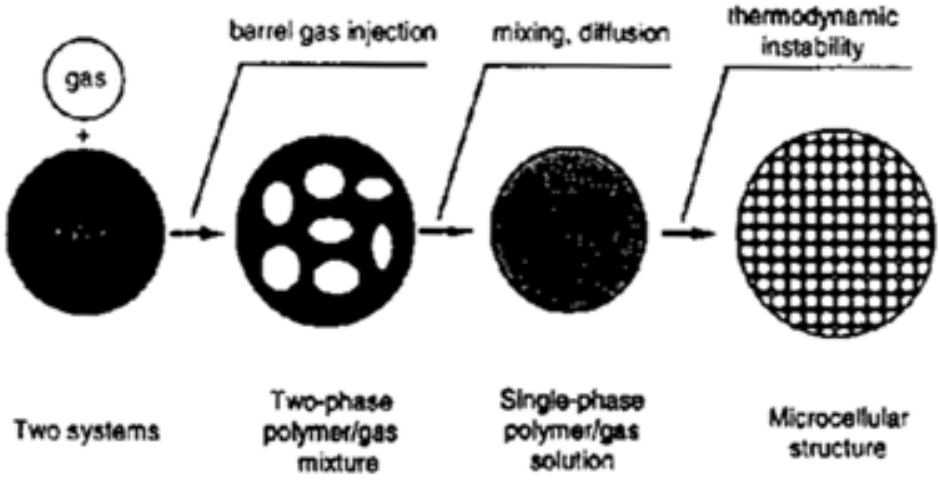

Figure 2.4 : The process steps involved in a typical foam extrusion process (41)

A typical foam extrusion system begins with a plasticization zone for melting of polymer resin before the injection of CO_2 at the injection port. A high temperature is maintained between the hopper and the injection port to ensure complete melting of the polymer resin. Then the blowing agent is injected. Once the gas is injected low barrel temperature can be applied due to viscosity reduction. The gas/polymer system then passes through a mixing zone. If required, an additional static mixer can be attached to the extrusion line. The mixing zone ensures that a homogenous dispersion of the gas is attained within the polymer melt (19, 52). The single phase mixture now enters the foaming section. The foaming die is preferably maintained at a lower temperature since better foam cell size control is attained at lower temperatures (53-55). The sudden rapid pressure drop through the die induces cell nucleation. After the nucleation die, a shaping die is required to control the foam expansion (growth) and foam structure. Once the temperature of the extrudate goes below Tg or room

temperature the foam samples can be collected for use. The difference between a continuous foam extrusion and a batch foaming process is that in case of a continuous foaming process a metered amount of gas is injected into the polymer matrix instead of saturating the polymer sample. Also in a continuous foaming system, the pressure drop gradient is dependent on flow rather than the saturation pressure and finally in a continuous foaming system the foaming die temperature is the foaming temperature. Also the additional mixing devices in case of a continuous foam extrusion system are needed since the polymer samples are not saturated with the gas (56, 57).

2.5 Foam injection moulding system

The foam injection moulding system consists of a foam extrusion line and an injection moulding unit for shaping of the foam extrudate into desired products. Compared to foam extrusion, foam injection moulding can be used to produce foamed parts with complex geometries. Generally, foaming injection moulding achieves increased melt flowability, lower injection pressures, faster cycle times, and greater dimensional stability and weight savings in moulded parts (58).The reduction in injection pressure can be associated to the possible pressure drop that can be attained at the mould gate(43). Also additionally, the reduced viscosity on injection of CO_2 results in further reduction of injection pressure. It also causes reduction in cycle time , injection speed and clamp tonnage (60, 61). Microcellular foams have been successfully generated using the foam injection moulding system (62-64, 44, 65). Modifications like improved screw design to ensure better mixing and a sealed barrel with gas injectors (66) have also helped in the generation of microcellular foams in injection moulding systems. Recently the foam injection moulding system has been used with filled polymers specifically with fibre reinforced polymers. It has been found that the melt

fracture of reinforcing fibres is avoided in the mould due to reduction in viscosity caused by the foaming agent (67-70).

2.6 Over view of foaming of polymer nanocomposites

The twin benefits of enhancement in polymer properties and improvement in rate of foam cell nucleation have led to intense research in the area of foaming of polymer nanocomposites recently. The foaming of polymer nanocomposites is relatively a new area and much of the research in this area has been experimental in nature and hence has been conducted in a batch scale setup. The foaming of polymer nanocomposites using continuous and semicontinuous foam setup is still relatively new.

2.6.1 Foaming of polymer nanocomposites in a batch setup

Foaming studies on amorphous as well as crystalline polymers have been conducted in a batch process. PS (Polystyrene) and HIPS (High impact polystyrene) are the most commonly used foams today. Since the first foams using HIPS was produced in 1982 (71), a lot of work has been done on the foaming of PS (72-73). Hence it was obvious to explore the foaming behaviour of PS/clay nanocomposites to begin with.

Han et al (73) studied the foaming behaviour of PS/clay nanocomposites. Two different PS/clay nanocomposites were prepared using commercially available cloisite 20A and using MMT (montmorillonite) modified with MHAB (2 – methacryloyloxyethylhexadecyldimetyl ammonium). The idea was to study the effect of clay particle dispersion and polymer –clay surface – CO_2 interaction on foam cell morphology. PS with 5 % cloisite 20A and 20 wt % MHABS was used for foaming. Interestingly it was found that an exfoliated morphology can be established with PS-MHABS system even at very high loadings. The average cell sizes in case of a 5 % cloisite 20A was around 15 micron. In case of exfoliated cloisite 20A nanocomposites

the average cell sizes was 10 micron. The cell sizes were comparatively smaller in case of 20 % MHABS. The reason is higher concentration of MHABS coupled with better dispersion results in decreased cell sizes. The average cell size range was in between 10 to 5 microns in case of MHABS.

PMMA like polystyrene was foamed with two different types of clay particles (80). The aim was to determine the effect of CO_2 interaction with the host polymer. The presence of carbonyl group (CO_2 attracting) in PMMA results in improved solubility of CO_2 in the polymer matrix which in turn improves nucleation efficiency. Hence it was found that under the same processing conditions and clay loading the foam cell sizes were significantly reduced with PMMA. To better understand the effect of CO_2 interaction on the clay polymer interface (PS-MHABS)-PMMA and (PMMA-MHABS)-PS were foamed. An exfoliated morphology was established in the former case where as an intercalated morphology was formed in the latter case. Interestingly in the former case PMMA domains were completely dispersed in the host polymer matrix whereas in the latter case the PMMA was attached to the clay surface. Hence in spite of having lesser nucleation sites (due to absence of an exfoliated morphology) smaller cell sizes were attained in the latter case. The presence of PMMA attached with the clay surface in the latter case resulted in the attraction of CO_2 to the clay surface improving the rate of nucleation and hence reducing the foam cell sizes. Thus it can be concluded that attainment of exfoliation is not the only technique to attain reduced cell sizes. The interaction of the polymer and clay particles with the nucleating agent is equally important.

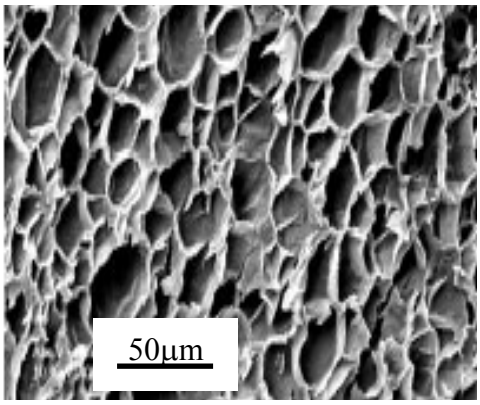

Figure 2.5: SEM PS with 5% Cloisite 20A (80)

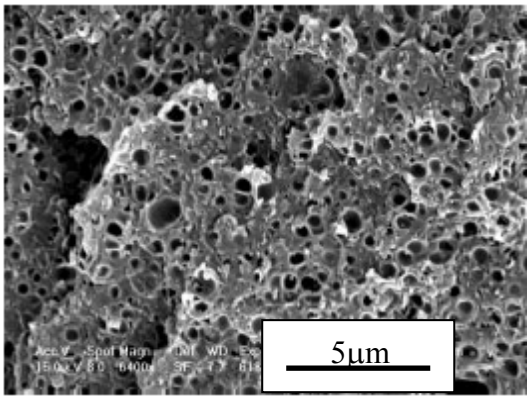

Figure 2.6: SEM PS with 5% MHABS (80)

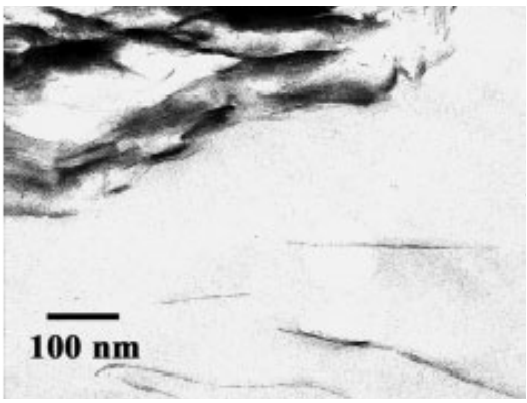

Figure 2.7: TEM of PS with 5% C20 (80)

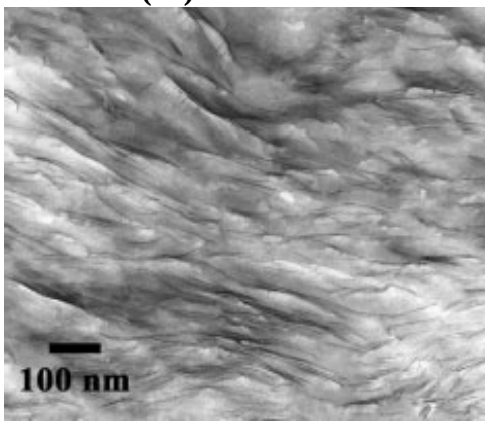

Figure 2.8 : TEM of PS with 5% MHABS (80)

Strauss et al (81) also foamed PS /clay nanocomposites with a view to study the effect of addition of a filler and foam processing parameters on foam cell morphology. PS/montmorillonite (MMT) nanocomposites were polymerized in situ using 0, 1 and 3 wt percent MMT. The samples were then subsequently foamed using the batch setup with CO_2 as the blowing agent. DSC studies conducted on the foamed samples revealed that the glassy region within the polymer nanocomposites increased after the addition of clay; the possible reason being the shear induced orientation of clay layers which improves the rate of crystal nucleation (82, 83). The foam cell sizes were reduced with the addition of clay and increased slightly as the clay concentration increased. Moreover the processing temperature and the pressure quench rate were the

factors that were found to critically influence foam cell morphology. The foam cell size increased with increase in foaming temperature. The increased gas diffusivity reduced matrix viscosity and increased chain mobility contribute to increase in foam cell sizes. Interestingly the overall pressure did not have much of an effect on foam cell size. The pressure becomes important only at very high values since then it actually improves the rate of homogenous nucleation. In the operating regimes used in this experiment (operating temperatures (60 – 85 ^{o}C) and operating pressures (6.5 - 10 MPa)) the applied pressure doesnot have a significant effect on foam cell diameters.

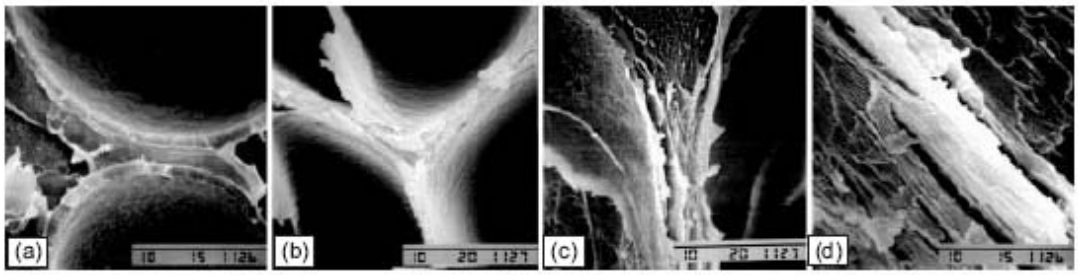

Figure 2.9: The alignment of clay platelets around foam cell walls (83)

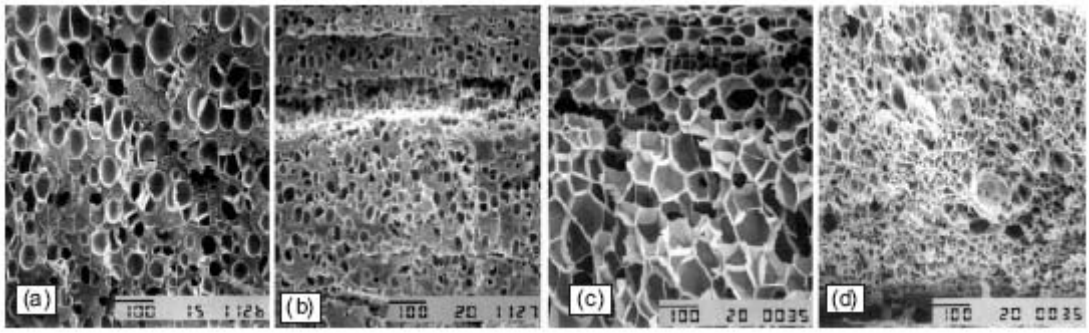

Figure 2.10: Reduction in foam cell sizes with increase in clay concentration (83)

The foaming behaviour of PU/clay (MMT) nanocomposites was studied by Cao et al (84). The effect of using different surface modifiers on foam cell morphology was studied. It was found that the higher chain length of the organo modifier improved the clay particle dispersion and overall intercalation of polymer chains into clay galleries. Commercially available MMT and MMT modified with Tin to provide a catalytic

functionality was used to prepare nanocomposites. The benefit of using a catalytic functionality was to improve the rate of reaction of nanocomposite formation during in situ synthesis. It was found that a better dispersion of clay was attained in case of MMT –Tin. The foam cell sizes were significantly lower with PU/MMT nanocomposites as compared to pure PU foams. A general increase in compressive strength was observed with the nanocomposite foams. The structure of PU greatly influenced the effect of the addition of clay on foam properties. It was observed that the PU/nanocomposite foams with high cross linked structure and higher urethane content showed reduction in properties as compared to PU nanocomposite foams with lower degree of cross linking and lower urethane content.

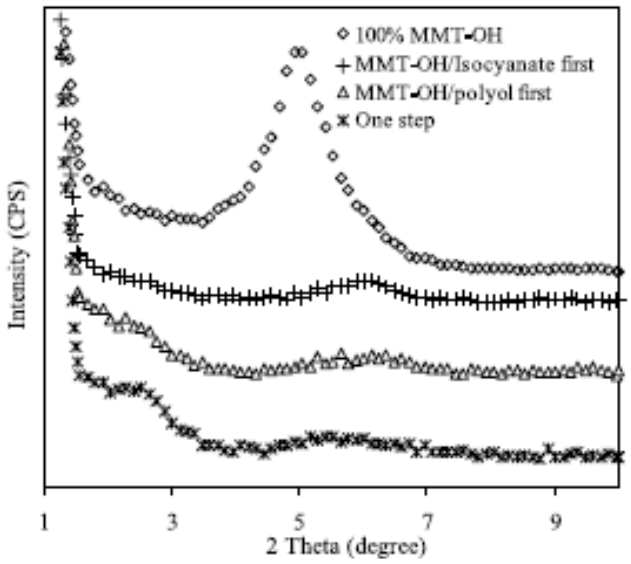

Figure 2.11: XRD plots of 5 % PU nano composite prepared by different mixing techniques (83)

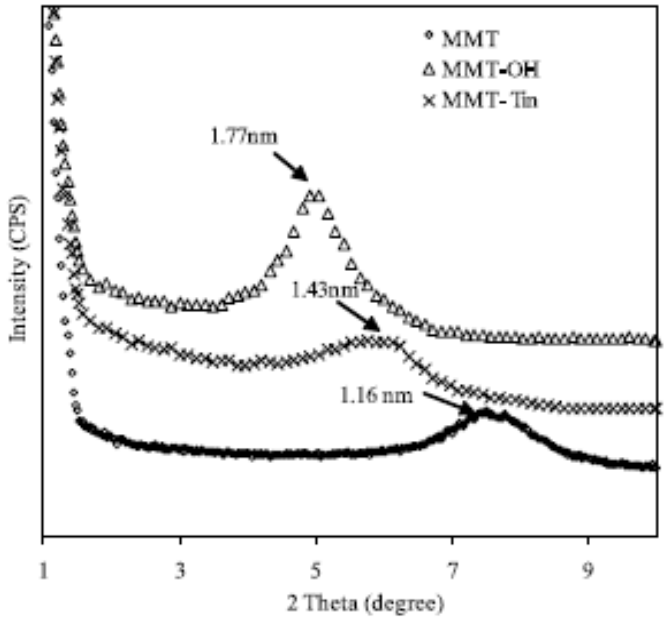

Figure 2.12: XRD plots of PU nanocomposites with different nanoparticles (83)

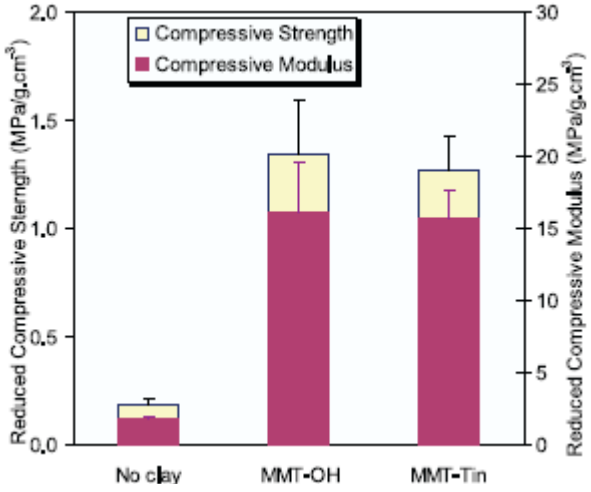

Figure 2.13: Compressive strength of PU Nanocomposites with 5% clay (83)

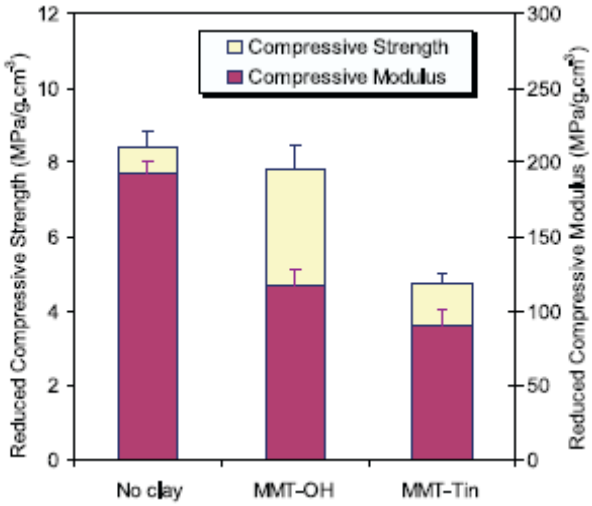

Figure 2.14: XRD plots of lower wt PU nanocomposite with 5% clay (83)

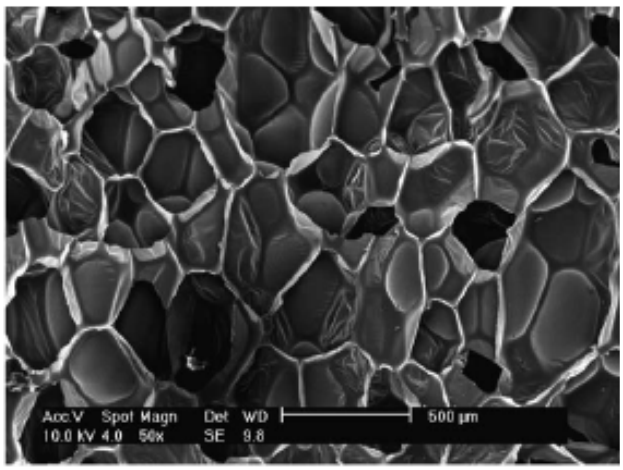

Figure 2.15: SEM of Pure PU foam (83)

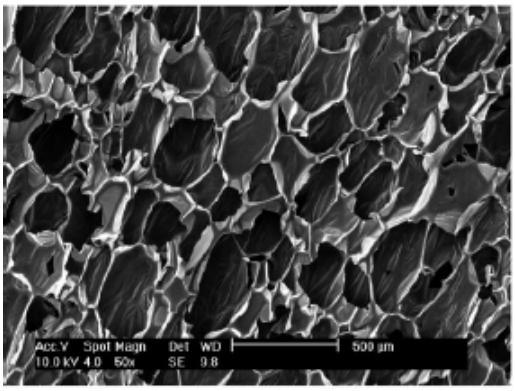

Figure 2.16 : SEM of PU foams with MM-OH (83)

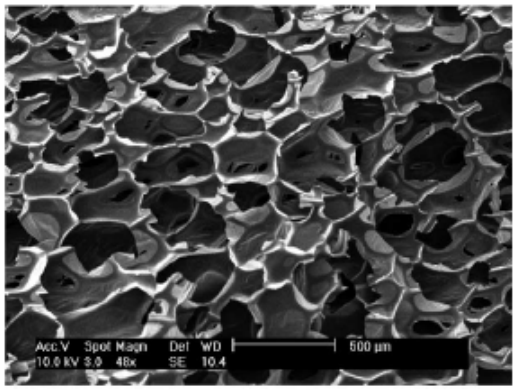

Figure 2.17 : SEM of PU foams with MMT -Tin (83)

PLA /clay nanocomposites have been one of the few polymer/clay systems which have resulted in the generation of nanocellular and ultra microcellular foams in a batch process.

Fujimoto et al (85) foamed PLA/clay nanocomposites with two different types of clay: one modified with octadecyl ammonium and another with octadecyltrimethyl ammonium. The dispersion state of clay particles was better in the latter case and nanocellular cell structure (360 nm) was attained. It was found that the dispersion state of clay particles influence cell sizes by affecting the rate of foam cell nucleation. Also the dispersion was better in the second case since the interaction potential between PLA and octadecyltrimethyl ammonium is higher as compared to the other

modifier used. The results also emphasized that the foam cell size is combinedly governed by the effective length of the particle, particle to particle distance and the melt elasticity respectively. Similar observations were made with other studies conducted on foaming of PLA/clay nanocomposites (86-90).

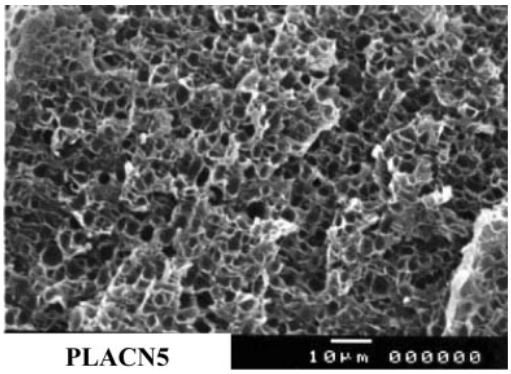

Figure 2.18: SEM of PLA/clay nanocomposite with 5 % clay (84)

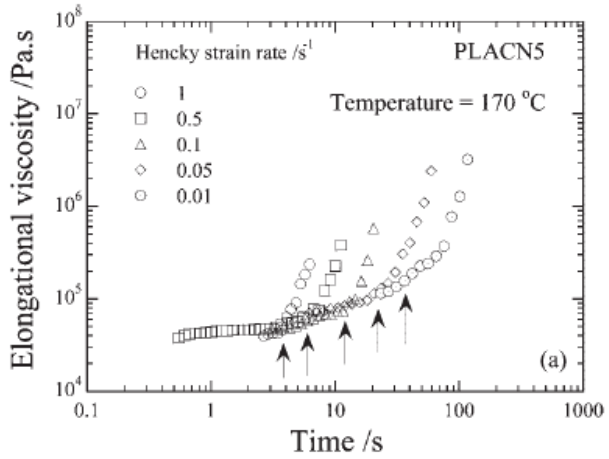

Figure 2.19: Strain hardening behaviour observed in PLA/clay (5%) nanocomposites (84).

Foaming behaviour of PC/clay nanocomposites was studied by Mitsunaga (91) , Fu et al (92). Foam cell sizes in the range of 10 -1 micron was attained in both cases. Exfoliated nanocomposites were found to show more uniform and smaller cell sizes as compared to intercalated nanocomposites. The cell coalescence was found to increase with increased particle clustering at higher clay loadings.

The foaming behaviour of HDPE/clay nanocomposites was investigated by Lee et al (93) in a batch process. Commercially available cloisite 20A was the clay used. The nanocomposites with 1 and 3 wt percent clay were subjected to foaming and compared to that of pure sample. It was found that the cell sizes and cell coalescence decreased with increased clay loadings. The increased rate of nucleation (heterogeneous nucleation) and improvement in melt viscosity resulted in smaller cell sizes and lesser degree of coalescence. Foam cell sizes in the range of 1 -0.3 micron was attained. It was found that crystallinity, rheology and the dispersion state of the clay particles critically influence cell sizes.

Nam et al (94) studied the foaming of PP/clay (montmorillonite) nanocomposites in a batch setup. PP/clay nanocomposites (PPNCs) were prepared in a twin screw extrusion process using 2, 4 and 7.5 wt percent clay. The samples were foamed at a constant saturation pressure of 10MPa and foaming temperature range of (130 – 146 ^{o}C) just below the melting point of the samples. Closed hexagonal and pentagonal cells were found to be formed at 2 wt percent clay loading. Spherical cells were generated with 4 and 7.5 wt percent clay loading. The effect of polymer nanocomposite rheology on foam cell structure was also investigated. TEM images revealed a biaxial flow induced alignment of the clay particles during foaming. This effect causes the polymer matrix to strain harden and provide more strength to the cell walls which in turn counteracts very high degree of cell growth. Cell sizes in the range of 30 -120 micron and cell wall thickness in the range of 5 – 15 micron were attained. Extensional viscosity studies on the nanocomposites revealed that all the nanocomposites exhibited strain hardening behaviour at stretch rates experienced during real time foaming.

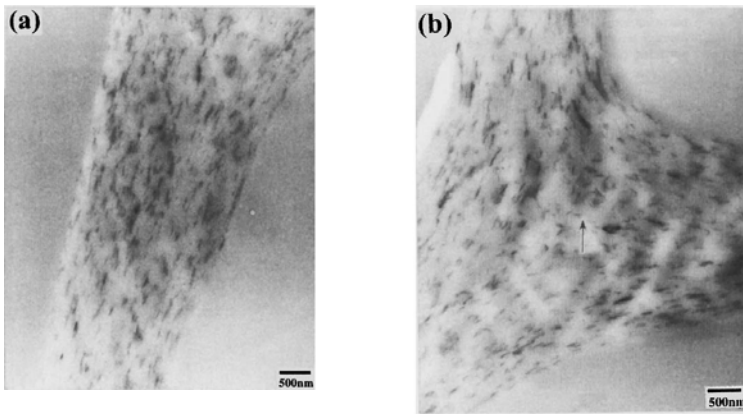

Figure 2.20: Biaxial flow induced alignment of clay particles in PP/clay nanocomposites (93)

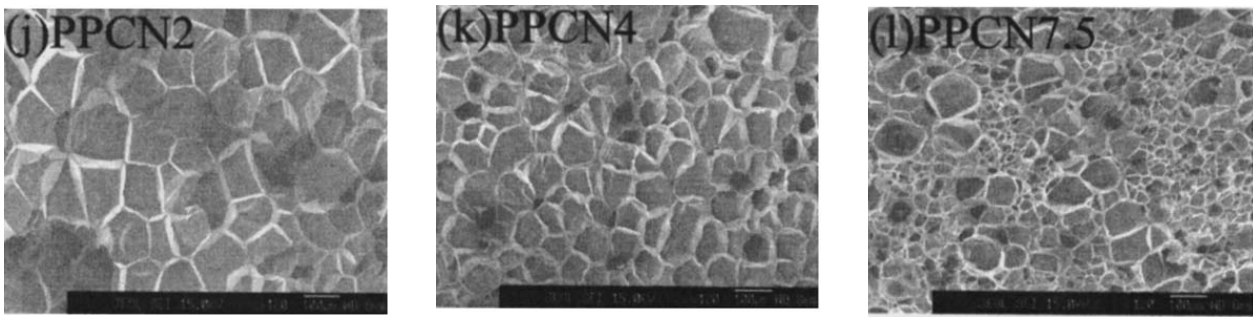

Figure 2.21 : Reduction in foam cell sizes with increase in clay concentration (93)

2.7 Foaming of polymer nanocomposites in a continuous foaming system

Numerous studies on foaming of polymer nanocomposites in an extrusion system have been carried out till date(95-98, 81, 99). The foam extrusion system is different compared to the batch process in terms of the processing scheme involved as discussed earlier, hence detailed analysis becomes crucial.

PS/cloisite 20A nanocomposites have been foamed in a continuous foam extrusion system by Zeng et al (100). PS/cloisite 20A nanocomposites were produced in a twin

screw extrusion system using 0.5, 2, 5 and 7.5 wt percent clay. These samples were subsequently foamed in a foam extrusion setup. A predetermined amount of CO_2 (4 wt %) at a temperature of 40^oC and a desired pressure (generated using the syringe pump) was injected into the polymer nanocomposite melt. This two phase system was subjected to mixing inside the extruder resulting in a proper dispersion of the gas and the formation of a single phase system. This mixture was then passed through a nozzle into the extrusion die. The pressure drop at the nozzle resulted in foam cell nucleation. Finally the extrudate was expelled into the atmosphere and quenched. The

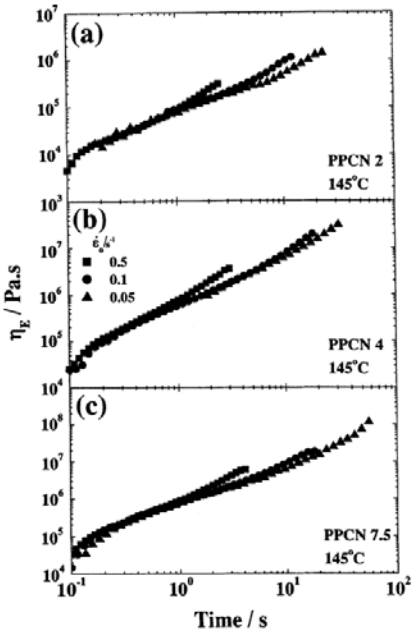

Figure 2. 22: Strain hardening behaviour observed in all PP/clay nanocomposites (93)

rate of pressure drop was controlled by the mass flow rate and the screw speed. It was found that for a given temperature and screw speed the pressure drop increases with increase in clay concentration. The highest amount of pressure drop was attained with 5 wt percent nanocomposites. The reason for increase in pressure drop is due to the increased melt viscosity caused by the addition of clay particles. Further it was found that the cell sizes decrease on addition of clay particles with the smallest cell size of 5

micron attained with 5 wt percent clay. The rate of decrease in foam cell sizes decrease with increase in clay concentration. The intercalated morphology of the clay particles at higher clay loadings results in a confined growth of bubbles between two platelets, which results in the rupture of bubbles in the stretch direction leading to an open cell morphology. This effect becomes more pronounced with 7.5 wt percent clay. The cell density was found to increase linearly with increase in clay concentration. Also the cell size initially decreases with increase in pressure drop rate but then levels off at a higher pressure drop rate. The smallest cell sizes are attained when the pressure drop rate is above 10^9MPa/sec. Overall the general observation was that of a reduced cell size and an improved surface finish on addition of clay as compared to the pure polymer.

Velasco et al (101) studied the foaming behaviour of irradiated LDPE foams and found the effect of degree of cross linking on foam cell morphology in a continuous foaming system. The results indicated that at a very high degree of cross linking the foam cell nucleation rate is very low resulting in low foam cell density. This effect is caused by the increased melt elasticity of the samples at higher degree of cross linking. On the other hand at lower irradiation dosages the degree of cross linking is too less and hence enhancement in melt strength is very low resulting in foam collapse. Thus the selection of a proper melt strength range is very essential for foam processing. Similar observations were made with the foaming of Nylon6/clay nanocomposites (99). Additionally, it was found that the dispersion of clay particles improves by the addition of supercritical CO_2. Also the smallest cell sizes are attained in the case of an exfoliated morphology.

2.8 Effect of processing parameters on the foaming of polymer nanocomposites

The effect of processing parameters on foam cell morphology is one of the most critically researched areas. Different combinations of processing parameters, and rheological and morphological properties of the polymer nanocomposites can lead to different foam cell structure. Hence a theoretical understanding of the effect of processing parameters, rheology and morphology of the polymer nanocomposites on foam cell structure becomes very important. The foam cell morphology (cell size, foam density, cell morphology) is mainly affected by parameters like saturation pressure and temperature, foaming time and temperature, depressurization rate, melt strength, clay particle distribution, and extensional viscosity (100, 101, 19, 47).

2.8.1 Gas concentration

The concentration of the dissolved gas in the polymer matrix generally governs the rate of foam cell nucleation. The foam cell nucleation rate is directly proportional to the dissolved gas concentration. Hence higher the dissolved gas concentration higher is the nucleation rate. The solubility of gases (CO_2) generally increases with increase in pressure and then levels off. The gas solubility is also strongly affected by saturation temperature. Generally the solubility is higher at lower temperatures and reduces at increased temperatures (27, 104). The increased diffusivity of the gas reduces the equilibrium solubility at higher saturation temperatures.

The presence of clay particles in polymer nanocomposites also influences the gas solubility in polymers. At low clay loadings the effect is not very significant but at higher clay loadings (above 10 wt %) the solubility is reduced. The gas escape rate is

also influenced by the presence of clay particles. Normally in an exfoliated polymer clay system, the gas diffusivity is reduced due to increased resistance to diffusivity (105). On the other hand at higher clay loading, where clay particle aggregation is dominant. an easier route for the escape of the gas from the polymer matrix exists increasing the gas escape rate (105). The change in diffusivity of the gas affects the solubility of the gas in the polymer matrix. By controlling the amount of gas and the rate at which the gas can escape out of the polymer matrix and thereby influences the foam cell morphology can be influenced.

2.8.2 Foaming pressure

Generally it has been observed that higher the saturation pressure and larger the depressurization, higher is the nucleation rate and smaller are the cell sizes for both batch and continuous foaming process. The foam cell size is very sensitive to the depressurization rate since the depressurization rate governs the time period over which a thermodynamic instability is induced. Normally with an instantaneous nucleation occurring at higher depressurization rates the cell sizes are small and the cell morphology is more uniform neglecting the rheological effects.

2.8.3 Foaming temperature

It is very difficult to exactly determine the effect of foaming temperature on foam cell morphology. A lot of foam processing factors like viscosity, surface tension, solubility, diffusivity, clay particle dispersion etc are a function of temperature. It is the combined effect of all these factors which determine the finally developed foam cell morphology. In a batch foaming process a foaming pressure and temperature is selected at which a polymer specimen is saturated until equilibrium solubility is

reached (normally the saturation times are greater than 24 hours). In presence of clay particles the saturation time is normally reduced as the presence of clay particles reduce gas escape rate and overall solubility. Once the sample is saturated the nucleation is achieved by rapid depressurization. Normally the temperature of depressurization (foaming temperature) is the saturation temperature but processes where saturation temperature and foaming temperatures are different have been used as well (93). In the latter case since the sample is saturated at a different temperature any subsequent change in temperatures will cause a change in diffusivity, interfacial tension and viscosity.

The classical homogenous nucleation theory was modified by developing an equation for interfacial tension as a function of CO_2 concentration (106, 107). It was noted that with increase in foaming temperature the interfacial tension increases due to reduction in solubility propelled by increase in gas diffusivity. This in turn results in reduced foam density and increased foam cell sizes. Experimental results at different saturation temperatures and constant saturation pressures reveal that the cell density and cell size increase with increase in foaming temperature. The simulation results using the modified classical nucleation theory also predict the same kind of result (108).

Studies on the foaming of polystyrene/nitrogen system show a similar result. The cell density is minimum and the cell size is maximum at a saturation temperature of 77^oC, which corresponds to minimum solubility of nitrogen in the polymer matrix.

Another study (72) conducted by Arora et al on polystyrene foams found that at higher temperatures the cell size is larger and cell density higher due to reduction in viscosity of the polymer matrix at higher temperatures. The polymer melt viscosity is the resisting force which restricts foam cell size. With increase in foaming

temperature the polymer viscosity reduces and the gas diffusivity increases resulting in larger foam cell sizes and lower foam density. The foaming of polyether sulfone (PES) and polysulfone (PSF) showed a reverse trend (109). It was observed that the cell sizes were smaller at a temperature of 230^{o}C as compared to a foaming temperature of 180^{o}C.

The continuous foaming system is different as compared to the batch process due to the following reasons 1) a pre determined amount of gas is dissolved in the polymer matrix 2) the pressure is determined by the flow and is not by the saturation pressure and 3) the foaming temperature is the die temperature.

The effect of die temperature and melt temperature on foam cell morphology has been investigated for the case of high impact polystyrene(HIPS) foamed with CO_2 (110). The studies reveal that microcellular foams are obtained in a continuous foam processing system at the cost of reduced volume expansion. At high melt temperatures (170^{o}C) the foam cell size is high due to increased cell coalescence and reduced melt viscosity irrespective of the die temperature. At moderate melt temperature (150^{o}C) the rate of cell coalescence is reduced resulting in a partial collapsed structure at high die temperatures (175^{o}C) to open cell structure at moderate die temperatures (135^{o}C) and to a closed cell structure at low die temperatures (120^{0}C). It was concluded that the rate of coalescence can be reduced and the foam cell structure improved by using lower melt temperatures irrespective of the die temperature. Similar results were obtained in other studies as well

The effect of die temperature and melt strength in case of polymer nanocomposites was investigated using amorphous and crystalline nylon 6 clay nanocomposites (99).

In case of polymer nanocomposites the improvement in melt strength due to the addition of clay particles helps in restricting foam cell sizes at higher foaming

temperatures as compared to pure polymer foaming. Also the gas concentration is higher in case of polymer nanocomposites due to reduction in gas loss induced by a reduced diffusion rate. Hence at any given foaming temperature the cell sizes would be smaller and uniform in case of polymer nanocomposites as compared to pure polymers except for lower die temperatures.

Interestingly, as compared to pure polymers at reduced die temperature the polymer nanocomposites show poor foaming characteristics. The stiffening of the polymer chains at reduced temperatures in presence of clay particles results in such a kind of behaviour. The presence of clay in crystalline polymers has a negative effect on the foam cell morphology. The reduced melt strength, and viscosity and higher crystallization temperature results in poor foaming characteristics. The cell coalescence rate is comparatively higher in such cases. Similar results were found in other studies as well (20, 111).

2.8.4 Foaming time

The effect of foaming time has been mostly studied in a batch process where the foam cell nucleation is induced by using a temperature superheat. The effect of foaming time in a continuous foaming process is difficult to estimate since it's a continuous flow based process although qualitative estimates are possible.

In case of a batch process the foam cell size increases rapidly in the first few seconds and then levels off as the driving force reduces. The levelling of cell sizes is due to reduction in concentration gradient driving foam growth. The same trend is observed in case of polymer nanocomposites as well though the reduced diffusivity in presence of clay particles reduces the amount of gas loss and prolongs the attainment of the constant cell size state during the growth process. Also with longer foaming times the cells are able to interact with each other resulting in transition from spherical to

pentagonal or hexagonal cell structures. In presence of clay particles this effect is restricted due to improved cell wall strength induced by flow induced alignment of clay particles.

The effect of saturation time is very straight forward to evaluate. Normally at lower saturation times the dissolved gas concentration is lower reducing the nucleation density at lower saturation times. At higher saturation times the gas concentration is higher with degree of supersaturation as well, hence the rate of nucleation is improved.

2.9 Rheology of polymer nanocomposites

The rheology of polymer nanocomposites has been found to influence foam cell size and morphology. Specifically the dynamic and the extensional rheological properties of polymer nanocomposites influence the cell sizes in polymer nanocomposites.

The use of dynamic rheological analysis for nanocomposites has been primarily in the dynamic shear analysis area. The reason being these methodologies are the simplest methods that can effectively provide structural information. The shear rheological measurements have been effectively used to study the outcome of nanofiller loading and polymer/nanofiller interactions on the shear thinning behaviour and dynamic moduli. The dynamic modulii have been used in many instances to examine the pseudo solid-like behaviour of the nanocomposites at long times and the reinforcement of properties caused by the presence of the nanofillers. Linear and non-linear viscoelastic behaviour has been investigated mainly through dynamic measurements (112). Dynamic properties have also been used to study the formation of a three-dimensional percolated network and the estimation of percolation threshold for filler loading beyond which the network formation is established and filler-filler interactions become significant (113). Dynamic properties have been further used to differentiate between an intercalated and exfoliated structure and to assess the degree

of filler dispersion within the polymer matrix (114). Moreover, dynamic measurements have been used to establish the mixing sequence for clay dispersion. Extensional rheological tests are a bit complex to initiate and involve more complicated theoretical analysis as well but this drawback is balanced by the fact that extensional rheological methods are the best method to determine the structure of a surface under the presence of a highly variable flow field (or higher shear rates) simply because extensional rheological analysis is normally carried out in absence of surfaces and hence the structural changes within the material are a sort of an inherent characteristics of the material involved in the study. Thus extensional rheology can provide first hand information on polymer nanocomposites. Extensional rheological measurements have been extensively used to study strain hardening behaviour in polymer nanocomposites (115-117).

Overall, with respect to foam processing, rheological analysis has been helpful in relating the polymer matrix structure parameters to foam cell morphology. The polymer nanocomposites that show higher melt elasticity have a better resistance to the cell growth process resulting in smaller foam cells. The improvement in melt elasticity can be achieved by using a branched polymer or using filler as well.

Also the strain hardening behaviour coupled with clay particle alignment under the influence of biaxial extensional force results in hardening of cell walls and hence helps in controlling foam cell sizes.

The functionalization of the clay particles used as fillers significantly influences the rheological response of the polymer nanocomposites. It has been found that changes in surface functionality strongly influence the rheological response of the nanocomposites (112). Studies using PS/clay nanocomposites (36) have revealed that the changes in the surface functionality of the clay particles and the polymer chains is

reflected in the dynamic rheological response of the nanocomposites. Higher interaction potential between the polymer chains and the filler results in better dispersion and higher degree of intercalation causing an improvement in the melt strength of the polymer nanocomposites. The polystyrene nanocomposites with simple intercalated structure exhibited a slight enhancement at low frequency having a distinct plateau-like behaviour, while the exfoliated PE-g-MA silicate nanocomposites generated by the functionalization of the polymer chains exhibited both a distinct plateau-like behaviour at low frequency and enhanced moduli at high frequency, due to strong attractive interaction with the silicate layers (117).

Wang et al (34) investigated the rheological behaviour of PP/organophilic montmorillonite nanocomposites. The addition of organically modified MMT leads to an increase in relaxation time and melt viscosity of the polymer. All the composites were further found to exhibit non terminal behaviour in the lower frequency regions. The polymer exhibited a pseudo solid like behaviour in presence of the nano filler particles.

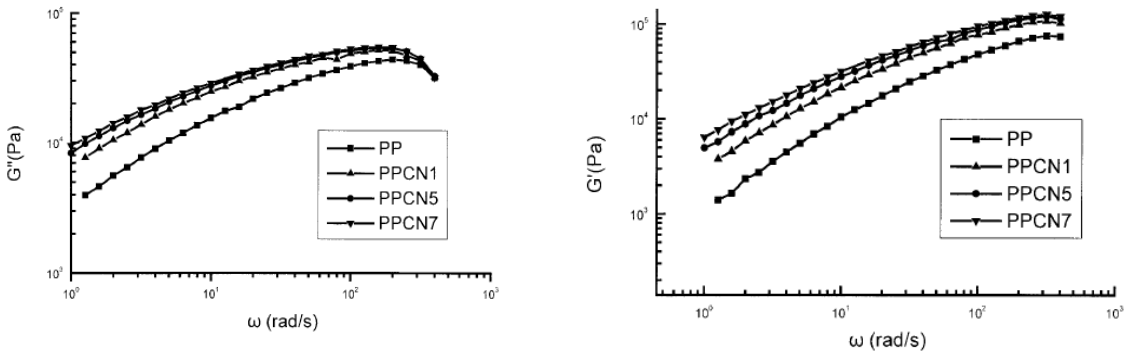

Figure 2.23: Dynamic material function for PP/clay nanocomposites (34)

Figures 2.23 show a plot of the storage and the loss modulus with respect to frequency for differing amounts of filler content. As it can be seen that the storage and the loss modulus increase with increasing amount of filler content. The increase in the storage modulus as compared to the pure polymer hints towards a possible increase in

relaxation time as well because now the matrix has a greater tendency to store energy than to disperse it away as compared to the polymer. The polymer/MMT system also shows a complete absence of nonterminal behaviour with increase in clay content. Nonterminal behaviour is characterized by the absence of a frequency independent region at lower and higher frequencies. The G' and G" exhibit power law dependencies with power law index much smaller than 2 and 1 respectively. The presence of a non terminal behaviour could be attributed to the presence of an ordered domain structure in the polymer system under flow due to presence of interacting particles. A long range order is further established in the melt state as well. This orderly structure leads to the development of a nonterminal behaviour by restriction of the segmental motion of the polymer chains.

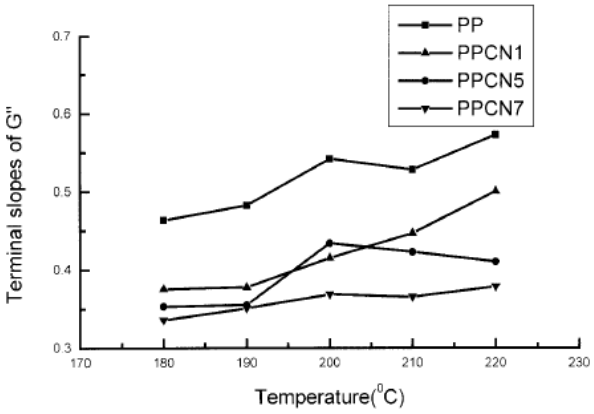

Figure 2.24: Terminal slopes for PP/clay nanocomposites (34)

Figure 2.24 shows a plot of the terminal slope of G" at different temperatures for different amounts of clay loadings. It can be seen from this Figure that the terminal slope increases with increase in temperature going more towards the ideal slope regimes. This effect could be attributed to the improved chain mobility at higher temperatures. But it can be also seen that the rate of increase of the terminal slopes is an order of magnitude lesser than that for the pure polymer and becomes lesser as clay content is increased gradually. Now this behaviour provides ample evidence towards

increase in relaxation times after addition of clay particles to the polymer system. The formation of an orderly structure even at higher temperatures is also evident by the reduced rate of change of the terminal slopes.

The linear viscoelastic behaviour, as characterized by the storage and loss moduli, has been earlier reported (118) for exfoliated nylon 6 and poly (ε-caprolactone) formed by end tethering of polymer chains by layered silicates. At high frequencies, both G' and G'' showed solid-like (non-terminal) behaviour, which was attributed to the tethering of the soft poly (ε-caprolactone) chains to the hard silicate layers. At the low frequencies, G' and G'' showed a frequency-independent plateau, with G' exceeding G'', which does not normally happen in ideal situations. This kind of behaviour can be linked to a pseudo solid-like response due to the incomplete relaxation of the polymers tethered to the silicate layers. Non-terminal flow behaviour has also been observed in intercalated poly(styrene-isoprene) di-block *co*-polymer (119). At all frequencies, both G' and G'' for the nanocomposites increased monotonically with increasing silicate loading. The viscoelastic behaviour at high frequencies was unaffected by the addition of the layered silicate, with the exception of a monotonic increase in the modulus value. Further, at low frequencies, where the unfilled system exhibited liquid-like behaviour, both G' and G'' moduli for the nanocomposites showed diminished frequency dependence.

Galgali et al (120) reported the difference in rheological behaviour of intercalated polypropylene nanocomposites with and without compatibilizer. The possibility of exfoliation was greatly enhanced by the presence of a compatibilizer. These exfoliated silicate layers easily produced percolated networks that strongly resisted shear deformation.

In general the dynamic rheological studies on polymer/clay nanocomposites have resulted in the following general observations

1) the addition of clay as compared to other fillers provides enhancement in melt strength at comparatively lower filler loadings.

2) the dynamic rheological response of the polymer nanocomposites become non linear at lower as well as higher frequencies with increase in clay loadings as indicated by the absence of a plateau region at lower frequencies and a the absence of terminal region at higher frequencies respectively

3) with anisotropic functional fillers the formation of a percolated network superstructure occurs at much lower filler loadings.

4) the relaxation spectrum of the polymer matrix is affected by the presence of clay particles and is a strong function of the dispersion state of the clay particles in the polymer matrix.

2.10 Benefits of supercritical CO_2 in polymer nanocomposites foaming

Supercritical CO_2 has been found to have a multitude of applications with polymer processing. In case of polymer nanocomposites it has been predominantly used in the preparation of polymer nanocomposites. A supercritical fluid (SCF CO_2) is used as a swelling agent for the in situ polymerization with a dispersed phase (clay particles) (26).It can be also used for dispersive mixing of clay particles with the polymer matrix caused by a reduction in viscosity due to the addition of CO_2 or it can be also used for nucleation of nanoscale bubbles in polymer nanocomposites. The effect of addition of CO_2 to the polymer nanocomposites or polymer matrix depends on the interaction of CO_2 with the polymer matrix and the dispersed phase. Generally in case of polymer nanocomposites, the use of CO_2 is to reduce the viscosity of the polymer matrix , delaminate the individual clay layers , and finally assist in dispersion of clay

layers in polymer matrix. PP/clay, HDPE/clay and PPT/clay with intercalated and exfoliated morphologies have been prepared using supercritical CO_2.

The presence of CO_2 within the polymer matrix affects a host of parameters related to foam processing. It affects crystallization kinetics of the polymer, dispersion state of clay particles, glass transition temperature, shear viscosity, diffusivity and interfacial tension. All these parameters in turn affect the foam cell morphology and structure and hence understanding the effect of CO_2 on these parameters becomes important.

The interaction of CO_2 with the polymer matrix is a Lewis acid/base kind of reaction where the ionic and Vander Waal's forces come into play. The electron deficient carbon in CO_2 acts as the electron acceptor (Lewis base group). Hence polymers with electron donor groups like carbonyl group, ether groups, fluro groups, phenyl groups or nitrogen atoms can act as an electron donor group. As a result CO_2 is found to be soluble in polymers like PDMS, PVDF, and EVA and less soluble in polymers like PVC, PS and polyolefins. The interaction mode of CO_2 with polymers needs to be explored in details since the presence of a CO_2 attractive group by itself propels solubility of CO_2 variably since the mode of interaction is different with different polymers(105). Hence CO_2 is less soluble in PMMA as compared to that in PDMS though both the polymers posses CO_2 attracting groups. The molecular level interaction of CO_2 with polymers was studied using the IR (121). PMMA was used as the base polymer in the study. It was found that the bending mode ν_2 of CO_2 changes in case it has a positive interaction with the polymer matrix. The change in bending mode was detected by the observed splitting, shift or broadening of the band corresponding to the bending mode.

In another study using polyether (122) it was found that the nature of monomeric unit, the degree of polymerization, the end group effect, the composition of copolymers,

and temperature influence the miscibility. It is shown that polymers of propylene oxide are more 'CO_2-philic' than those of ethylene oxide or tetrahydronfuran. The ether oxygen exhibits interactions with CO_2 when it is in a readily accessible position. Hydrogen bonds between polymer molecules may decrease such accessibility.

In another study the interaction between CO_2 and nine different crystalline polymers and eleven different semi-crystalline polymers was investigated on the basis of the change in appearance, weight, thermal and mechanical properties before and after the sorption of CO_2 (123). At 3000 psi and 40°C PMMA absorbed 12.96 wt.% of CO_2 while polystyrene absorbed 4.48 wt. % of CO_2. The treatment time for all reported samples was one hour. These results were compared to those from semi-crystalline polymers under the same conditions of CO2 treatment. High-density polyethylene. (HDPE) absorbed 1.22 wt.% of CO2, low-density polyethylene absorbed 1.36 wt.% of CO_2, polypropylene absorbed 1.98 wt.%, and Teflon absorbed 0.51 wt.% of CO_2. It was found that semicrystalline polymers always absorb less CO_2 than the amorphous polymers. Zhou and Huang (124) studied the rheological properties of PP/clay nanocomposites using supercritical CO_2 while processing the nanocomposites and found the effect of the use of CO_2 on the morphology of the nanocomposites.

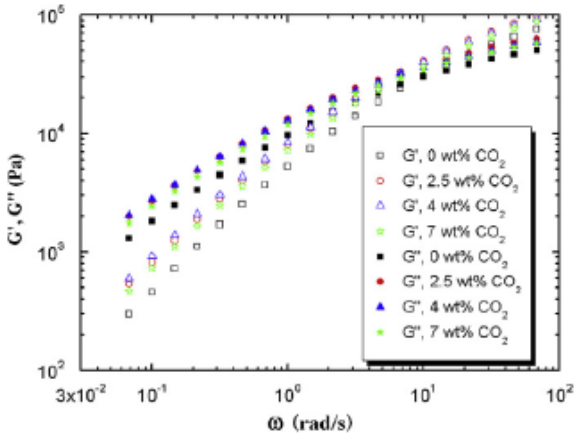

Figure 2.25: The effect of CO_2 on the dynamic properties of polymer nanocomposites (119)

Figure 2.25 shows the dynamic rheological behaviour of PP/clay (125) nanocomposites prepared at 190 ^{0}C using different wt% of CO_2.The clay concentration in all the above samples was kept constant at 3 wt%. As shown in figure 2.25 the values of G' and G" increases with increase in CO_2 concentration but interestingly the cross over frequency for the samples with different concentrations of CO_2 remains the same. The increase in the material functions with increase in CO_2 concentration can be attributed to the reduction in matrix viscosity on addition of CO_2 to the system. As a result the dynamics of the polymer chain is improved which results in a better intercalation of the polymer chains into the clay galleries causing an improvement in G' and G" respectively.

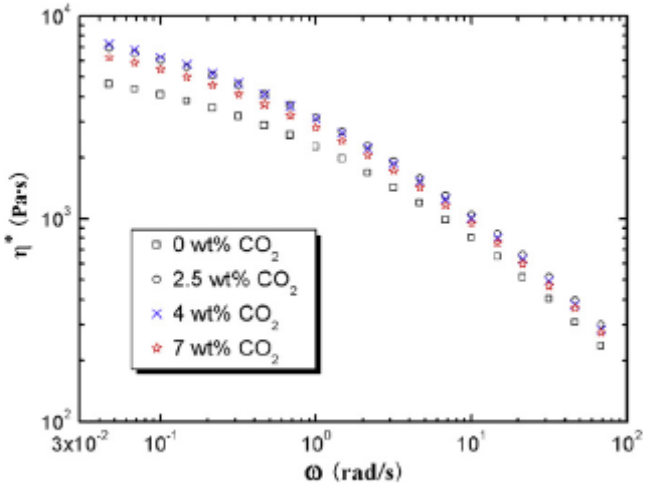

Figure 2.26: Effect of CO_2 on the complex viscosity of polymer nanocomposites (119)

The complex viscosity (Figure 2.26) also increases with increase in CO_2 loading. This could be attributed to the increase in melt strength caused by improved dispersion of the clay particles within the polymer matrix. Also it can be seen that after the use of 7wt% CO_2 in the samples the complex viscosity and G' and G" decrease. This effect could be attributed to the fact that the reduction in matrix viscosity on addition of CO_2 follows an exponential behaviour and as a result with a large amount of reduction in

matrix viscosity the clay particles have a greater tendency to aggregate thus reducing the polymer intercalation and subsequently the material functions and final matrix viscosity as well. Thus there is an optimum amount of super critical CO_2 to be used with the samples while preparing polymer nanocomposites or filled polymers

2.11 Foam process modelling and simulation

2.11.1 Modelling of gas solubility in polymer and polymer nanocomposites

The understanding of gas uptake behaviour of a polymer is important for many different applications specifically for production of ultra low density microcellular & nanocellular foams. Theoretically the problem is a case of statistical thermodynamics applied to phase equilibria. The modelling of gas solubility started in the early days for rubber like materials (126) and other polymers when the free energy of mixing was calculated using the Flory Huggins theory, In this work additional terms to consider the elastic distortion of polymer was also taken into account. More recently the Sanchez Lacombe theory (127) and Simha Smocynsky theory (128) have been applied to the case of gas solubility in polymers. In the lattice fluid theory of Sanchez Lacombe the effect of compressibility is simulated by considering the presence of vacancies in the lattice whereas in other cell theories like that by Flory et al, Prigogine et al, compressibility is modelled by considering the changes in the volume of the lattice sites or cells. The Lattice Hole theory first applied by Simha Smocynsky (SS) considers both vacancies and variable cell volumes in its form. Thus, this theory effectively combines the considerations of the lattice fluid models as well as that of cell models. The Simha Smocynsky theory has been found effective in predicting the solubility of gases in polymer nanocomposites to certain extent. However the theory does not take into account the fact that in case of nanocomposites there exists a strong

dipole – dipole interaction or other kinds of interaction between the polymer and the clay surface, hence the polymer chains will have a strong propensity to be adjacent to the clay surface. Under such circumstances the mixing of the polymer and the holes in the lattice would be non-random whereas the SS theory assumes a completely random mixing state. The non random mixing condition in turn will affect the configuration partition function and the thermodynamic variables for the system. The Holey Huggins theory (HH) (129) takes this factor into account by using the quasi – chemical approximation of Guggenheim (1952).

For commercial purposes the Sanchez Lacombe theory and the Simha Smocynsky theory have been found to be effective for solubility predictions in filled polymers at lower filler loadings. The predictions using the HH theory are very similar to that of Sanchez Lacombe theory and the Simha Smocynsky theory for lower filler loadings though deviations have been observed for higher filler loadings

The HH Theory has been discussed in depth in the literature (130). A brief review of the essential aspects of the HH theory is discussed. In this paper the non random mixing of segments and holes due to the presence of interactive forces between the polymer and other segments in the lattice results in another microscopic parameter X which accounts for the fraction of segment hole contacts in the partition function Z. The parameter X accounts for the fact that the entire polymer chain is not in contact with holes but only a certain fraction of the chain is in contact with hole resulting in a non random mixing state. As a result the partition function now is given by equation (2.1)

$$Z(N,V,T) = \sum_{q} \sum_{X} Z_{qX}(N,V,T,q,X)$$

$$Z\,(N, V, T) = \sum_{q,X} g(q,X) l_f(q,X)^{3cNc_s} \exp(-E_0(q,X)/kT \qquad (2.1)$$

where $Z_{q,X}(N,V,T,q,X)$ is the partition function for the system with fixed values of X and q where q represents the fraction of occupied sites in the lattice which varies with the thermal energy of the chain. The function g (q, X) represents the combinatorial entropy related to the mixing of holes and the polymer chain within the lattice. E_0 represents the internal energy of the lattice system where the polymer chain is under static conditions and l_f represents the segmental free length.

Guggenheim's quasi – chemical approximation equation (2.2) for Non randomness can be used to calculate the combinatorial factor g as shown below (for a single component) (129)

$$g = g_{HH} \frac{[Q(q-X^*)!][(QX^*)!]^2[Q(1-q-X^*)!]}{[Q(q-X)!][(QX)!]^2[Q(1-q-X)!]} \qquad (2.2)$$

$$E_0 = Q(q-X)\varepsilon_C \qquad (2.3)$$

$$l_f = (1-\frac{X}{q})l_s + (\frac{X}{q})l_g \equiv \bar{l}_f v^{*1/3} \qquad (2.4)$$

In the equations (2.2-2.4) q represents the net external contact fractions of the segments in the lattice, (1- X/q) is the fraction of the segment contacts and (X/q) represents the fraction of segment hole contacts.

As per the theory of partition function in statistical thermodynamics, it has been proven that for a given ensemble the property of the system in the state which is most probable, can be used to approximate the variation of that property throughout the ensemble. As a result the function on R.H.S. of equation (2.1) is replaced by its maximum value. The maximum terms in the above equations ((2.2) to (2.4)) is represented by a bar on the top of the parameter.

$$Z(N,V,T) = Z_{yx}(N,\bar{y},V,T,\overline{X}) \tag{2.5}$$

Here the parameter (equation (2.5)) y is the occupied site fraction and can be related to the external contact fraction q.

The maximum values of the above parameters are determined by equation 2.6

$$\left(\frac{\partial \ln Z_{yX}}{\partial X}\right)_{N,y,V,T} = 0$$

$$\left(\frac{\partial \ln Z_{yX}}{\partial y}\right)_{N,X,V,T} = 0 \tag{2.6}$$

Once the partition function is known the free energy of the polymer chain in the lattice can be calculated by the Hemholtz free energy function. Here the Hemholtz free energy function is considered since the system is modelled for a constant N, V, and T. The calculated Hemholtz free energy function (equation (2.7)) then can be used in determining solubility

$$A = - kT \ln Z \tag{2.7}$$

The above technique has been used to determine gas solubility for the case of interacting polymer blends and non-interacting fillers present in the polymer matrix.

The results agree very closely to the experimental results. Interestingly in both the above cases the use of Sanchez Lacombe equation and SS theory have also yielded results which closely match with experiment.

2.11.2 Cell nucleation

Foam cell nucleation and cell foam growth are the most important aspects of the foaming process, since all other processes directly or indirectly affect these two. The theoretical modelling of the foam cell nucleation process has majorly originated from the boiling literature (131, 132). The formation of vapour bubbles, condensation of liquids and mixing of liquids follow the same sort of mechanism like foam cell nucleation. The only difference being that in case of foam cell nucleation the surrounding medium is viscoelastic whereas in the former it is a Newtonian fluid. The process of nucleation is initiated when molecules overcome an activation energy barrier to accumulate together and form a new phase. Spontaneous fluctuations in density result in the formation of the embryo of the new phase. When the initial nucleus formed is less than the critical size it will collapse back into the old phase. If the embryo is greater than the critical size then it can further convert into a macroscopic bubble. The difficulties in studying nucleation can come from both experimental as well as theoretical considerations. Nucleation is induced by energy fluctuation so local changes in pressure, temperature, concentration and presence of impurities will affect the rate of nucleation and hence the repeatability of the experiment. The presence of functionalized fillers provide a theoretical challenge to nucleation theory since it is based on discrete thermodynamic changes hence the effect of functionalization of nucleants is not taken into consideration in the theory. Also empirical equations are used to take into account the effect of orientation of particles.

The most commonly used basic presumption of nucleation theory for liquid droplets-vapour is given by equation (2.8)

$$A_1 + A_{i-1} = A_i \qquad (2.8)$$

where A_1 is the monomer and Ai is the i-mer cluster.

The classical nucleation theory (133) (phenemological approach) is based on the concept of statistical thermodynamics. The cluster in this case is treated as a macroscopic spherical droplet with bulk surface tension. In the classical approach the equilibrium constant for the formation of a nucleus is related to the Gibbs free energy and the monomers collide with the cluster surface at the gas kinetic rate for an ideal gas. The classical nucleation theory can predict critical super saturations successfully for most gases, while it is in error when predicting actual nucleation rate since it works on the concept of averaging over an ensemble whereas actual nucleation rate is a local phenomenon and varies locally.

In another theory (27) of the kinetic approach the forward and the backward rate of formation of clusters is calculated without actual reference to the free energies of formation of clusters. In this case the rates are calculated as a function of the interaction potential between particles. In practice however due to locally existing uncertainties in the interaction potential it became difficult to develop an average interaction potential to be used in the model. Hence in practical cases the experimental values of surface tension, liquid density and sometimes even the nucleation rate has to be used to calculate rate constants. This limits the testing of theoretical models based on the above presumptions.

The microscopic approach is another approach that involves computer simulation with molecular dynamics and Monte Carlo techniques. This avoids many of the limitations in phenomenological approaches; however, the typical volume and time in computation work restrict simulation to the properties of isolated clusters, which requires the definition of a cluster. Also important assumptions about the influence region used, the number of frames considered, the kind of lattice assumption and profile of interaction potential assumed all significantly affect the results obtained. Dynamic simulation tools interestingly have been found to be useful in cases where dynamic properties need to be studied or monitored. Hence though the technique is a bit tedious it can be very effective in determining the nucleation rate under dynamic conditions with variable process parameters.

The nucleation of foam cells occurring from a binary homogenous solution of polymer foaming can be explained by the classical nucleation theory for a homogenous system. Hence the homogenous nucleation theory will be discussed also, since the foaming process involves the use of heterogeneous nucleants the heterogeneous nucleation theory will be discussed as well. Finally other theoretical approaches to model nucleation will be discussed.

The absence or lack of sufficient heterogeneous nucleation sites results in a predominant homogeneous nucleation. The rate of homogenous nucleation (number of clusters which grow beyond the critical cluster size per unit volume and unit time) is given by equation (2.9) (133)

$$N_0 = C_0 f_0 \exp\left(\frac{-\Delta G_{critical}}{k_B T}\right) \qquad (2.9)$$

where C_0 is the number of gas molecules dissolved per unit of the primary phase, f_0 is the frequency of collisions which is called the kinetic pre exponential factor (and is found to be a weak function of temperature), k_B is the boltzman constant and $\Delta G_{critical}$ is the free energy of formation of a critical nuclei. f_0 can be expressed by equation (2.10)

$$f_0 = \left(\frac{2\sigma}{\pi m}\right)^{1/2} \tag{2.10}$$

in which σ is the surface tension and *m* is the mass of the gas molecule. The Gibbs free energy ΔG for a spherical cluster of radius *R* (corresponding to the formation of new volume and new surface) is given by equation (2.11)

$$\Delta G = \frac{-4\pi}{3} R^3 \left(P^G - P^L\right) + 4\pi R^2 \sigma \tag{2.11}$$

The available free energy for the nucleation of a bubble is a function of the pressure differential driving force and the surface tension force. When these two forces balance each other then the critical bubble radius is reached.

The critical free energy $\frac{\partial \Delta G}{\partial R} = 0$ in this case is now given by

$\Delta G_{cri} = \frac{16\pi\sigma^3}{3\left(P_G - P_L\right)^2}$ and the critical bubble size is then given by $R_{cri} = \frac{2\sigma}{\left(P_G - P_L\right)}$

where P_G is the pressure inside the critical bubble and P_L is the pressure of the surrounding liquid. The product of the Zeldovich factor times the impingement rate was treated as a fitted parameter, for which $f_0 = Z\left(4\pi R_{cri}^{\ 2}\right) R_{impingment}$. Agreement between prediction and data was found at high saturation pressures(118, 95).

The effect of pressure drop rate on nucleation rate was studied by Xu and Wu (119). The studies revealed that at smaller pressure drop rates nucleation rate is proportional to the pressure drop rate. The nucleation rate becomes independent of the pressure

drop rates at higher pressure drop rates. Thus higher nucleation rate cannot only be achieved by increasing the pressure drop rate. Hence consideration to other methods to increase nucleation rate are very important.

Modelling studies conducted by Goel and Beckman (111) using the classical nucleation theory demonstrated the effect of saturation pressure, temperature and time on cell density using PMMA as the host polymer. The effect of CO_2 on surface tension was also taken into account.

2.11.2.1 Heterogeneous nucleation theory

The nucleation of gas bubbles in presence of a foreign material or impurities within the polymer matrix is termed as heterogeneous nucleation. Bubbles tend to nucleate at the interface between a foreign particle (impurities, initiators, nucleating agents, nanofillers) and the polymer matrix propelled by the reduction in activation energies required for nucleation on the surface of particles. The reduced activation energies improves the nucleation rate at any given temperature. The commonly used model for heterogeneous nucleation was developed by Colton and Suh and is represented by equation (2.12) (27)

$$N_1 = C_1 f_1 \exp\left(\frac{-\Delta G_{heterogenous}}{k_B T}\right) \tag{2.12}$$

where C_1 is the concentration of heterogeneous nucleation sites, f_1 is the frequency factor similar to f_0, and represents the frequency that gas molecules impinge upon the embryo nucleus. It is a complex function of the vibrational frequency of the atoms, the activation energy for diffusion in the polymer, and the surface area of the critical nucleus.

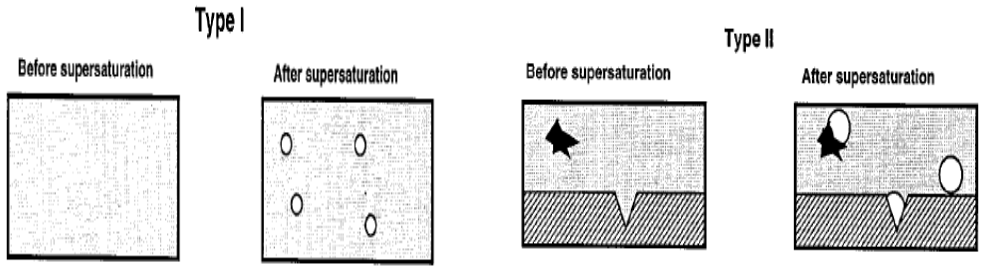

Figure 2.27: Representation of classical homogenous and Heterogeneous nucleation (27)

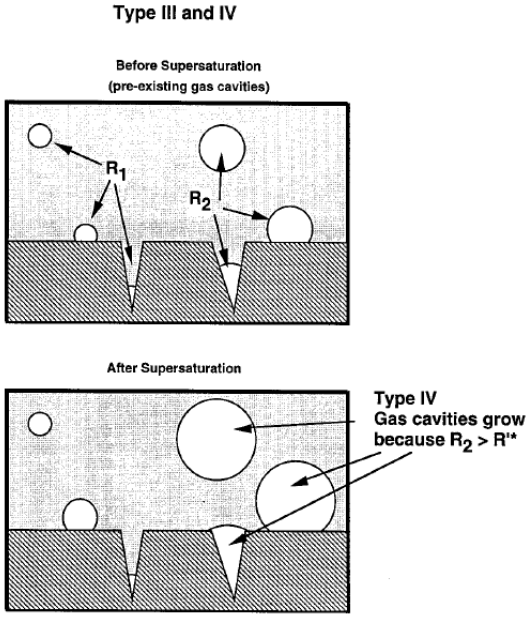

Figure 2.28: Schematic representation of pseudo classical heterogeneous nucleation (27)

The critical free energy for heterogeneous nucleation is given by equation (2.13)

$$\Delta G_{cri}^{\ het} = \frac{16\pi\sigma^3}{3(P_G - P_L)^2} S(\theta) \qquad (2.13)$$

S (θ) is a function depending only on the wetting angle θ of the particle-gas interface, and has values of less than or equal to 1. An expression of *S (θ)* is given by equation (2.14)

$$S(\theta) = (1/4)(2 + \cos(\theta))(1 - \cos(\theta))^2 \qquad (2.14)$$

The effect of addition of filler or particle on surface tension and the change in free volume caused by the introduction of CO_2 was also taken into consideration in the

model. The effect of changes in these parameters on Gibbs free energy was also evaluated and modelled. Polystyrene –Zinc state system was used to validate the model and suitably close agreement between theory and the experiment was observed. Lee et al (22) used the concept of cavitation to study the nucleation phenomenon. Pre existing cavities or voids within the host polymer composite system also causes nucleation of bubbles. In this study the critical radius of the bubble is the size at which pressure gradient balances the surface tension force. Subsequently the shear force exerted by the polymer matrix allows the bubble to escape out of the cavity. Thus the model subsequently takes into consideration the effect of shear on nucleation rate (136, 137).

The effect of shear on nucleation rate has been modelled in other studies as well (136, 138, 137). It has been found that shear rate improves nucleation rate by breaking of growing bubbles into smaller bubbles of critical radius. Interestingly at very high shear rates the shape distortion of bubbles is higher and hence cell coalescence increases where as at moderate and lower shear rates the bubble nucleation rate and density improves significantly.

2.11.3 Cell growth

Cell growth is the most complex phenomenon to model in the foaming process. It involves the use of heat, mass and momentum balances along with the use of a suitable rheological equation. A lot of research work has been done in modelling of bubble growth starting with single bubble growth models like a single bubble surrounded by infinite sea of fluid with infinite amount of gas available for growth of bubbles(133, 19, 52, 139). Further modifications have resulted in more realistic models like the cell models. The cell models take into account the effect of bubble to bubble interaction and the availability of fixed amount of dissolved gas. Models

where a swarm of non interacting bubbles are assumed to grow simultaneously have also been developed.

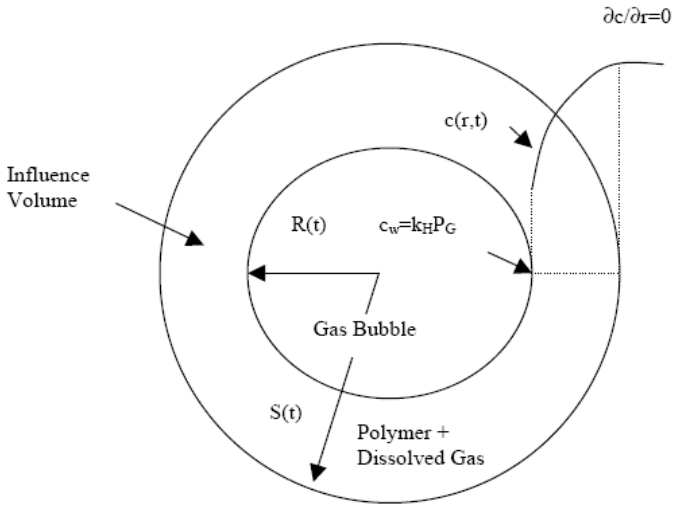

Figure 2.29: Bubble growth studies using the influence volume approach (22)

In the 'cell model', the foam is divided into spherical microscopic unit cells of equal and constant mass, each consisting of a liquid envelope surrounding a single bubble. Thus the gas available for growth is limited. A lot of complexity still exists in the modelling of foam growth process. Till date computational tools like Fluent, Star CD and Polyflow have not been found to be useful in foam growth modelling. The complexity arises with respect to the rheological description of the host polymer in which the bubble grows. Commercial computational tools are not developed to handle viscolelastic fluids. These normally work well with Newtonian fluids.

Recently polyflow and CFD have been used to model the Foam injection moulding process by using an empirical equation to represent shear viscosity within the mould. The technique has been found to be reasonably accurate in predicting foam cell size and morphology as compared to the experimental results.

As a general trend foam process modelling is normally performed by using individually developed codes in conjunction with suitable rheological models.

The basic foam growth modelling equation developed by simplifying the Naviers Stokes equation is given by equation (2.15) (19)

$$P_G - P_L - \frac{2\sigma}{R} + 2\int_{R}^{Rf}(\tau_{rr} - \tau_{\theta\theta})\frac{dr}{r} = 0 \qquad (2.15)$$

Here, P_G and P_L (equation (2.15)) are the pressures in the bubble and in the polymer melt respectively. σ is the interfacial tension. R and R_f are the radius of the bubble and the polymer shell respectively. τ_{rr} and $\tau_{\theta\theta}$ are the stresses

In case of a Newtonian fluid further simplification leads to equation (2.16)

$$\tau_{rr} = 4\eta\frac{\dot{R}}{R} = (P_G - P_L) - \frac{2\sigma}{R} \qquad (2.16)$$

where the bubble growth rate $\dot{R} = \frac{dr}{dt}$ and the Newtonian viscosity is denoted by η.

In case of a viscoelastic fluid other complex rheological models need to be used like the UCM (upper convected Maxwell model) given by (140)

$$\tau + \lambda\overset{\nabla}{\tau} = 2\eta_0^*\underline{D}$$

Where the zero shear viscosity η_0^* could be a function of temperature, pressure, and concentration of the foaming agent. $\underline{D}$ is the deformation gradient matrix.

The mass balance over the gas can be expressed by equation (2.17)

$$\frac{d}{dt}\left[\left(\frac{4\pi}{3}\rho_g R^3\right) = 4\pi R^2 D\left(\frac{\partial c}{\partial r}\right)_{r=R}\right]$$

(2.17)

The equation (2.17) simply states that the rate of change of volume of a gas bubble per unit time is equal to the amount of gas diffusing out of the bubble denoted by the change in gas concentration.

The gas diffusion in the surrounding polymer (control volume) is given by equation (2.18)

$$\frac{\partial c}{\partial t}+\frac{\dot{R}R^2}{r^2}\frac{\partial c}{\partial r}=\frac{D}{r^2}\frac{\partial}{\partial r}\left(r^2\frac{\partial c}{\partial r}\right) \tag{2.18}$$

The diffusivity D in the above case is a function of concentration of the foaming agent and the temperature. Selection of proper initial and boundary conditions are essential for simplification of the model. For example, an initial condition could be a pseudo equilibrium followed by Henry's law

$$c(r,0)=c_0^*=K_H P_{G_0}$$

The boundary conditions can be with or without gas loss at the moving boundary (r = S (t)). When the foam expansion occurs in a closed mould, such as an injection moulding process, boundary conditions without foaming agent loss are reasonable. However, in an extrusion foaming process, especially when the extruded shape is thin, the influence of gas loss on the foaming efficiency must be considered.

The initial bubble radius is assumed to be equivalent to the critical bubble radius and is given by equation (2.19)

$$R(0)=\frac{2\sigma}{(P_{G0}-P_C)} \tag{2.19}$$

where P_{G0} is the saturation pressure before nucleation and P_c is the polymer resin pressure during flowing.

Another possible way to define a boundary condition is to use the influence volume approach. In the case of influence volume approach the gas concentration at the edge of the influence volume is assumed to be $0.95c_0^*$. Here c_0^* is the initial gas concentration before nucleation. This concentration is also treated as the nucleation threshold gas concentration below which no nucleation occurs. The bubble nucleation

stops when the average gas concentration becomes less than the threshold concentration or the summation of the influence volume of all the bubbles nucleated equals the polymer initial volume.

In case of modelling a foam extrusion system the microscopic models discussed above need to be combined with other macroscopic flow models. Baldwin modified the power law model of the flow through a constant cross-section slit die with a height 2B and a width W (141). In the model, the influence of gas phase was included in the flow rate and viscosity. In other words, the apparent volumetric flow rate and viscosity are functions of volume fraction of bubbles in the flow as given by equation (2.20).

$$\frac{dP_C}{dz} = -\left[\frac{2+1/n}{2WB^2}Q\right]^n \frac{m}{B}\left(1-\frac{V_G}{Q}\right) \tag{2.20}$$

Where $Q = V_G + V_P$, and V_G is the volume flow rate of gas.

2.12 Effect of extensional viscosity on bubble growth

The viscoelasticity of the polymer matrix and the extensional viscosity of the polymer matrix significantly influence the shape and the size of bubbles in the polymer foaming process. The extensional viscosity of the polymers shows a dependence on the extensional rate and time. The extensional viscosity initially increases and then reaches a steady state. In case of filled polymers the extensional viscosity is also dependent on the dispersion state of the fillers and the filler concentration as well. It has been found that the orientation of the filler in the stretch direction induces strain hardening behaviour earlier as compared to that of pure polymers (116). Also extensional viscosity has a higher value in case of a filled polymer as compared to the pure polymers. In certain cases though where the concentration of the filler is high

and the fillers are aggregated the extensional viscosity is found to reduce as compared to the pure polymer matrix (116).

Experiments show that a bubble growth takes about 60-120 seconds in a batch process (3), while in a continuous extrusion foaming process, it takes only 1-2 seconds. In such a short time scale for (1-2 seconds), the effect of transient extensional strain hardening viscosity on bubble growth would be very noteworthy.

To understand this effect, simulation was done by Arefmanesh et al (142). based on complex constitutive equations. Simulation results indicate that increasing the melt elasticity (longer relaxation time) enhances bubble growth compared with a Newtonian medium with the same zero-shear-rate viscosity. The effect of the elasticity is more pronounced at the beginning of the bubble growth when it is mainly controlled by the hydrodynamic forces. The stresses that oppose bubble growth are much smaller in a viscoelastic fluid than those in a Newtonian fluid.

2.13 Techniques used for generation of nanocellular foams

The generation of nanocellular foams is the next frontier in polymer foam processing. The idea of generation of nanocellular foams has gained immense interest due to the possible enhancement in mechanical, physical and chemical properties as compared to microcellular foams. The generation of nanocellular cell structure with the polymer matrix would result in minimum distortion of the inherent structure of the polymer. This would result in production of rigid polymer foams with properties better than that of microcellular foams. Research into the generation of nanocellular foams has mostly been done using a batch process (85). Since this area is relatively new, researchers are still trying to figure out the controlling parameters for generation of nanocellular foams. The generation of nanocellular foams can be achieved either by

accurate control of processing conditions or by addition of a filler or some other component which propels solubility and nucleation rate. It is easier to control processing parameters in a batch process as compared to a continuous system. Also use of glass window in a batch process enables in online (photographic) measurements of the foaming process. This further helps in understanding the effect of addition of filler and other components on the foam cell size and morphology.

2.13.1 Addition of functionalized filler

The addition of functionalized filler in small proportions has resulted in generation of fine cell foams and even nanocellular foams in some cases (85). It has been found that a very high nucleation rate (heterogeneous nucleation), improvement in melt viscosity and improvement in extensional viscosity have combinedly resulted in generation of nanocellular foams. The dispersion of the clay particles within the polymer matrix also becomes critical and hence the use of a suitable organo modifier for the clay particle to ensure layer by layer separation also becomes important. Foaming studies on PLA /clay nanocomposites (85) has revealed that the clay modified with octadecyl trimethyl ammonium as compared to octadecyl ammonium would result in better dispersion of clay particles and attainment of exfoliation. This in turn would increase the rate of heterogeneous nucleation and result in the generation of fine cell foams. Similar observations were made while conducting foaming studies on HDPE/clay nanocomposites, PC/clay nanocomposites in a batch process(143, 100).

2.13.2 Blending of polymers

Blending of polymers for generation of nanocellular foams (144-146) has been found to be highly effective. The concept is to prepare a blend of the base polymer with another polymer that is immiscible and has a CO_2 attracting group in its form. Since

the blends are immiscible, a dispersed phase in the form of spherical domains can be obtained. Then further by using the batch setup the foaming agent is made to localize within the dispersed CO_2 attracting domains. Finally the samples are foamed using a temperature quench technique and foaming is performed within the dispersed phase only. If the size of the dispersed phase is in nanometre range then foaming within the dispersed phase would result in the generation of nanocellular foams.

Studies on foaming polypropylene (PP)/Thermoplastic Polystyrene elastomer (TPS) (147) revealed that the foam cell morphology was a function of blend composition, draw down ratio in the extrusion system and foaming temperature. Polymer foams with 200 -400 nm cell sizes were attained in this study. The TPS used was either hydrogenated polystyrene-block-polybutadiene-block-polystyrene (HSBR) or a hydrogenated styrene isoprene styrene (HSIS). The T_g of PP is -10^oC, hence the crystallinity of PP was used to attain a kind of stiffness for the polymer matrix. The foaming temperature was then further selected in such a way that only one of the polymers would plasticize under the influence of the blowing agent and foam. In this case the foaming temperature was 120^oC. At this temperature foaming only within the dispersed TPS phase was possible. The matrix viscosity of the PP phase was high enough to resist foaming. By localizing the foaming of bubble within the dispersed phase the size of the foam cells was controlled. Also since an extrusion system was used the stretching force experienced by the nanoscale elastomeric domains resulted in orientation of foam cells in the machine direction. This behaviour in turn created ordered foam morphology with isotropic mechanical properties(148).

The same kind of concept has been used in the generation of nanoscale foam structure in polymer thin films. The localization of CO_2 in CO_2 attractive domains of PMMA and PFMA resulted in generation of nanocellular foams in this case.

2.14 Summary

Polymer foams with nanocellular cells have a multitude of applications due to the associated improvement in properties induced by reduction in foam cell size. Foam cell size and morphology are controlled by a host of factors like polymer matrix morphology, polymer crystallinity, gas solubility, cell nucleation, cell growth and the rheological response of the polymer matrix. A careful control of these parameters along with judicious blending strategies can lead to generation of nanocellular foam cells in polymers. Fine cell foam production is easier in polymer/clay nanocomposites. The presence of nanofillers along with improvement in rheological properties results in the generation of fine cell foams in polymer nanocomposites. The use of CO_2 in supercritical state as a blowing agent results in highest amount of gas solubility in the polymer matrix, resulting in higher degree of supersaturation and hence smaller cell sizes. Also the use of immiscible blends with a CO_2 attracting component also results in the reduction of foam cell sizes by trapping CO_2 within the dispersed phase domains. The existing literature on production of fine cell foams suggested that the use of CO_2, nanoclay, CO_2 attracting groups in conjunction with accurate control of process parameters would help in the generation of fine cell foams.

Chapter 3: Materials and Measurement techniques

3.1 Materials

High melt strength polypropylene (HMS-PP) supplied by Montell (USA) is used as the host polymer for the foaming studies conducted. Cloisite 20A supplied by southern clay products is used as the nanoclay material without any modifications. Also Ethyl vinyl acetate with 28 percent vinyl acetate content (EVA-28) supplied by Dow Chemicals (USA) has also been used.

The Tables 3.1 and 3.2 provide information on the materials used (as provided by the supplier).

Melt flow index @230^{o}C/2.16kg(g/10min)	2.1
Flexural Modulus (MPa)	1900
Elongation at yield (%)	6
Tensile strength at yield (MPa)	40
Tensile Modulus (Mpa)	2000

Table 3.1: Properties of HMS–PP (PP) (trade name Daploy WB 130D)

Molecular weight M_w	72600
Polydispersity Density	8.7
Melt Flow index @190^{o}C/2.16kg(g/10min)	2.5
Peak Melting temperature	88

Table 3.2 Properties of EVA -28

3.2 Measurement techniques

The experimental techniques used in this work can be broadly categorized into two main classes. The first type is that used for the production of materials and components such as the twin screw extruder for the production of polymer nanocomposites, a batch setup for generation of polymer nanocomposite foams and a foam injection moulding system for the production of foam injection melded parts. The second type is that used for characterization studies to establish the structure property relationships between the foam cell morphology and the polymer nanocomposite structure. The characterisation studies involves the use of thermal analysis technique (DSC) to study the thermal behaviour of polymer nanocomposites, XRD and TEM for morphological analysis and mechanical testing setup to investigate the mechanical properties. In addition shear, dynamic and extensional rheological techniques have been used to study the effect of polymer nanocomposite rheology on foam cell morphology SEM and ESEM on foam cell size and morphology. A batch setup to determine solubility of gases in polymer nanocomposites has also been used.

3.3 Preparation of HMS-PP/clay nanocomposites

The materials used to make the nanocomposites are HMS – PP (Daploy WB 130 HMS) supplied by Borealis. Polypropylene grafted with maleic anhydride (PP – MA). Commercially available Cloisite 20A supplied by Southern Clay products Inc is used as received without any modification. Cloisite 20A is a Organo modified clay modified with dimethyl dihyrogenated tallow quaternary ammonium with a modified concentration of 95meq/100gm of clay. A master batch of pre mixed PP-g-MA and C20A (60/40) was prepared in a Brabender twin screw extruder (DSK 42/7).The extruder has a L/d ratio of 7 and a diameter of 42mm and a screw channel depth of 5

mm operating in a counter rotating mode. The extruder had a temperature gradient of 155, 170, and 185 ^{o}C at the feed zone, plasticization zone and extrusion zone respectively and was operated at a speed of 70 rpm. To ensure proper mixing of clay and polymer the obtained extruded samples were again recycled through the extruder at a speed of 80 rpm. The application of higher shear rates and temperatures ensured proper mixing of the components. Furthermore increased temperature and increased residence time ensured improved dispersion of clay in the (PP-g-MA) matrix. The total residence time of the material in the extruder was 15 minutes. Once the master batch was formed it was subsequently mixed with pure HMS –PP and melt extruded to form nanocomposites of the desired compositions using the same processing conditions and residence times as for the master batch. It has been found that a two step mixing technique produces a better dispersion of the clay particles in the polymer matrix(150).

The twin screw extruders was chosen since it provides better dispersive and distributive mixing. The intermeshing counter rotating twin screw extrusion system provides intensive shearing and is self cleaning as well. The dispersion of clay particles within the polymer matrix governs the properties of the polymer nanocomposites and a better dispersion of clay particles in the polymer matrix results in enhanced properties. Hence optimal mechanical shearing force and suitable residence times need to be provided. Both the above mentioned factors are a function of the screw speed. The shearing force between the static barrel and the screw is responsible for material transport and mixing. Hence if the screw speed is high then the amount of viscous heating is high resulting in degradation of the polymer being processed but at the same time the residence time of the polymer mixture is also reduced. Hence the idea is to select a mid range of screw speed. At a speed between

(60 – 80) rpm the residence time within the extruder for one pass between 80 -110 seconds. Hence the material was recycled through the extruder until a residence time of 15 minutes was achieved. To ensure that the residence time selected is not too high the polymer sample was tested for degradation by visual observation. The discoloration of the polymer is the indication for degradation of the polymer chains.

Once the samples were processed through the extruder they were subsequently pelletized and a suitable quantity of these pellets (50 gm) was compression moulded to 2mm thick plaques. The compression moulding press was operated at a temperature of 195^0C. Cooling water was used to cool the system back to room temperature or 30^0C. Also superheated steam was used for heating the compression moulding system. A two step pressurization technique was used to ensure that bubbles are not formed during compression. Hence initially the samples were kept at a lower pressure till all the resin melted (approximately 1 minute) and then the pressure was raised to the desired value.

3.4 Batch setup for foaming of polymers

The physical foaming process using a batch setup consists of four stages (2)

1) Saturation of the sample in a batch setup using supercritical CO_2 at the desired temperature.
2) Depressurization of the sample in the autoclave at the desired rate.
3) Foam cell growth and nucleation using temperature superheat.
4) Finally foam cell stabilization via cooling process of the foamed system.

The foaming process in a batch setup normally involves using a pressure vessel for saturation as well as foaming. The drawback of using a combined system is that, at higher temperatures the solubility of the physical blowing agent in the sample is low and at the same time using a pressure gradient to generate foams doesn't provide

proper control of the cell nucleation and foam cell growth since there is a competing mechanism between cell growth and nucleation. Hence a two stage process was used in this study. The saturation of the sample at lower temperatures improves the solubility of the gas within the sample; also using a subsequent superheat to generate the desired foam structure provides better control on cell nucleation and growth

The figures 3.1, 3.2 show the batch foaming setup used in this work.

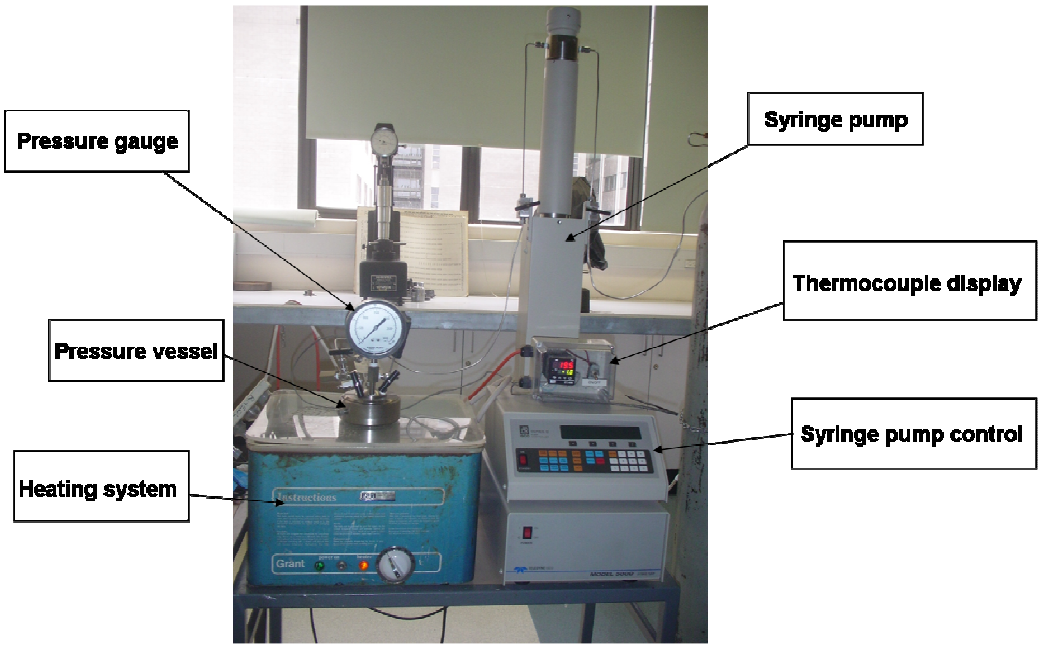

Figure 3.1 : Batch setup for dissolving CO_2 in the polymer samples

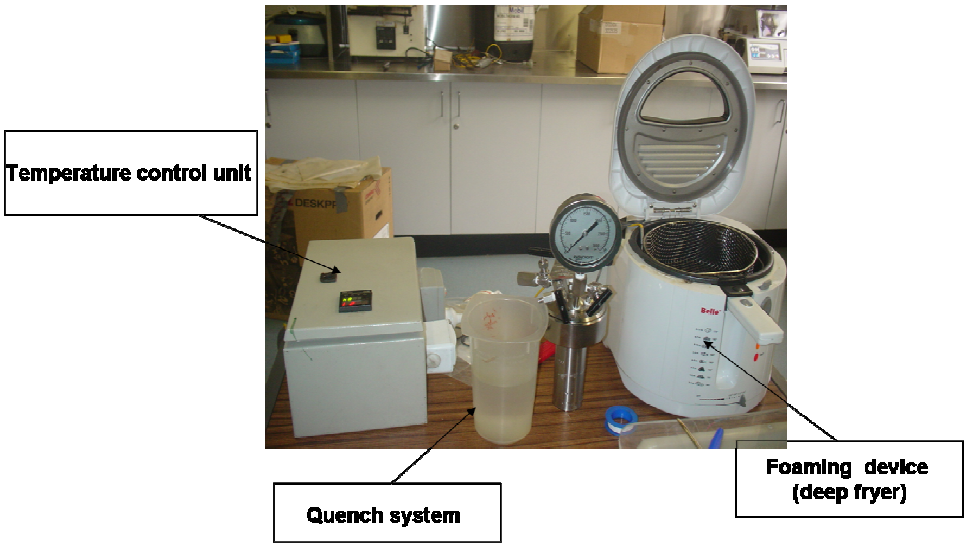

Figure 3.2 : Batch setup for foam generation.

3.4.1 Pressure vessel

The pressure vessel (figure 3.1) used was a Parr -4791 series vessel. It has a volume of 100ml and is a split ring type vessel. This vessel is provided with an externally connected detachable head. A split ring type pressure vessel can be easily dismantled since external bolts are used to hold the head and the vessel together. The pressure vessel is made up of stainless steel and can bear a maximum pressure of up to 3000 psig and a temperature of 250^{o}C. The vessel is externally provided with five connections. A gas inlet valve, a gas release valve, a safety valve, a connection for the thermocouple and a pressure gauge. A fluroelastomeric O-ring (Viton) is required to connect the vessel head to the pressure vessel. The pressure gauge connected to the vessel can measure a pressure of up to 3000 psig (20.68MPa) with a sensitivity of 10 psig. The thermocouple has a sensitivity of 0.1^{0}C and can measure a temperature up to 350^{0}C. The idea of having a smaller vessel was to minimize the time required for depressurization and hence improve the nucleation rate (152).

3.4.2 The heating and cooling systems

The pressure vessel was heated using a temperature controlled water bath (10 -100^{0}C) having a temperature sensitivity of 1^{0}C. Foaming was carried out using a temperature superheat in a deep fryer (figure 3.2) with a temperature controlled heater (70 – 250^{0}C) range and a sensitivity of 1^{0}C. The generated foams were subsequently quenched using water at room temperature.

3.5 Volumetric method for measurement of gas solubility

Figure 3.3 shows a schematic representation of the experimental technique used for the determination of equilibrium solubility within the polymer nanocomposites. The technique is equally accurate as compared to other techniques for measurement of the

equilibrium solubility(4). A mass balance approach is used for determination of equilibrium solubility. The approach physically states that the mass of the gas polymer system before absorption should be equal to the mass of the system after absorption. Hence in simple terms the mass of the gas delivered by the syringe pump should be equal to the amount of gas present in the vessel plus the mass of gas dissolved in the polymer sample. The density of the gas/polymer composite system and the gas is calculated using the Sanchez Lacombe equation of state. The benefit of this approach is that unlike the pressure decay method, volumetric decay method and the gravimetric method, the use of an expensive instrumentation like magnetic suspension balance is not required to measure equilibrium solubility. The sample chosen for gas solubility study should be of a volume which is significant enough to cause a detectable change in the volume of the gas used to determine equilibrium solubility. The accuracy of the measurement is affected if the sample is very small since then the amount of gas dissolved in the polymer matrix is very small. Also the use of Sanchez Lacombe equation of state for calculating the density of the gas provides approximate results introducing errors in measurement.

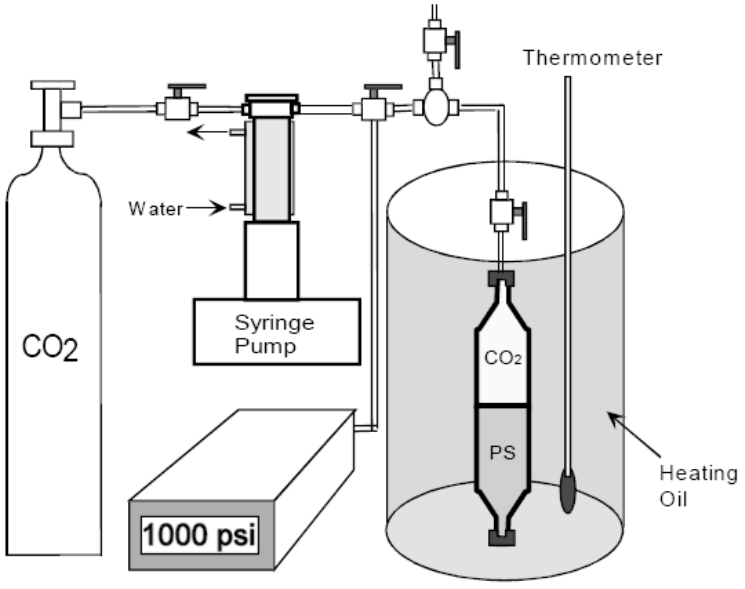

Figure 3.3 : Gas solubility measurement setup

Equation 3.1 is used for the determination of equilibrium solubility

$$m(beforesorption) = \rho(40^0 C, P)V_{pump}^{before} + \rho(25^0 C, P)V_{tubing} =$$
$$\rho(40^0 C, P)V_{pump}^{after} + \rho(25^0 C, P)V_{tubing} + \rho(T, P)(V_{vessel} - V_{polymer}) \quad (3.1)$$
$$+ m_{polymer} w = m(aftersorption)$$

where $m(beforesorption) =$ is the mass of gas in the system before absorption of gas

$\rho(40^0 C, P)$ = density of CO_2 at 40°C

V_{pump}^{before} = volume of gas in the syringe pump before pumping

V_{pump}^{after} = volume of gas in the syringe pump after pumping

V_{tubing} = volume of the tube

V_{vessel} = volume of the vessel

$m_{polymer}$ = mass of the polymer

w = weight of the gas dissolved per unit of the polymer

m (after sorption) is the mass of the gas in the system after absorption of gas

All the parameters in the equation (3.1) are known except w, which can be then effectively calculated.

3.6 Characterization of polymer nanocomposites

The characterization of the polymer nanocomposites is an important part of this study, since it helps in relating the rheological and morphological properties of the polymer nanocomposites to the foam cell size and distribution. The studies help in understanding, if the nanocomposites prepared were intercalated, exfoliated or simply a microstructure where the clay platelets retain there original periodic structure

There are several techniques like AFM (Atomic force microscopy), NMR (Nuclear magnetic resonance) and other neutron scattering methods that are being used. But none of the methods has gained popularity like the wide angle X-Ray scattering (WAXS) method and the Transmission electron microscopy (TEM). ESEM and SEM have also been used in this project for morphological characterization of foams and will be described later in this review.

3.6.1 Wide Angle X-ray Scattering (WAXS)

X –ray scattering is generally divided into two types: Small angle (SAXS) and wide angle scattering (WAXS). The classification of the technique is based on the angle of deviation (2θ) from the direct beam. SAXS as the name suggests is used to observe scattering at small angles typically less than 1^0. At angles greater than 1^0 it is classified as WAXS. The range of analysis for WAXS extends till 180^0 but for polymers, scattering effects are observed at angles well below 90^0. In this study the WAXS patterns have been used to determine the extent of intercalation of polymer chains into clay galleries and hence the degree of swelling. The analysis is done by calculating the interlayer spacing (d) as indicated by the d_{001} peak in the WAXS patterns. The d-spacing is essentially the distance between the clay layers or platelets. The calculation of the d-spacing is done using the Braggs law as represented by the equation (3.2) and figure 3.4

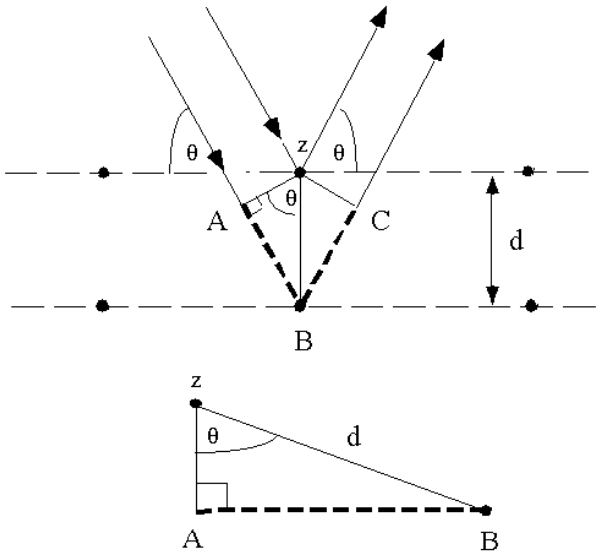

$$n\lambda=2d\sin\theta \qquad (3.2)$$

Figure 3.4 : Calculation of d-spacing in WAXD

In case of XRD analysis it is very important to understand that the wavelength of the incident beam is equivalent to the repeat distance between the scattering centres. Also the incident beam is normal to the striking surface and the reflected beam is coplanar. The angle between these two beams is always 2θ as shown in figure3.4. Equation 3.2 is used to calculate the d spacing. The transmission mode of penetration is generally preferred since in transmission mode the incident beam is allowed to penetrate the depth of the sample and then the scattered X rays are detected by the counter. Thus the result generated is actually a bulk phenomena instead of being a surface phenomena providing more concrete morphological analysis. Studies using different transmission angles revealed that at each transmission angle it is possible to obtain varying intensity peaks for the same polymer nanocomposites. This makes it difficult to analyze the polymer morphology. This problem could be eliminated by rotating the sample about its axis during the scattering test. As a result now an averaging of all possible orientations of the sample is made thereby reducing the effect.

The WAXS equipment used in this research was the Philips X-ray generator using 40kV accelerating voltage with 40 mA current. Ni filtered Cu-Kα (λ = 0.154 nm) radiation was used to record wide angle X-ray scattering intensities from 2θ = 1 to 30°. The reflection mode which is generally used for surface analysis was used to analyze clay powder. In the reflection mode the incident beam hits the surface of the clay powder and the resulting intensity of the scattered beam is measured using a detection counter. The intensities thus recorded give information about the basal spacing of the layered silicates at the surface. The transmission mode of analysis is used for analyzing PP/clay nanocomposites. The sample used was 2mm in diameter or thickness. The transmission mode is preferred to the reflection mode in this case, since with the transmission mode the incident beam penetrates to deeper levels within the sample, thereby ensuring that the measured intensities provide information about basal spacing from within the sample instead of just being a surface phenomenon. To avoid the problems of orientation as discussed above a rotating sample holder was used. A computer recorded the scattering intensities. The effect of background scattering due to particles present in the air was taken into consideration by subtracting the background intensities at small angles. Background intensities were recorder using an empty sample holder. WAXS only provides quantitative description about nanocomposite morphology only in case of ordered immiscible or ordered intercalated system. Hence in cases where periodicity is absent the use of imaging techniques to analyze morphology becomes even more essential.

3.6.2 Transmission electron microscopy (TEM)

Electron microscopy is the process of obtaining images using electrons and is frequently used when magnification required is much larger than the magnification provided by light microscopes. The electrons used are high energy matter and hence

can penetrate deep inside the material analyzed. Also the electrons have a smaller wavelength as compared to light and hence it allows for the resolution of smaller objects. Electrons also interact with samples in various ways providing a lot of information. The two main electron microscopes available for nanocomposite imaging are TEM and SEM. The main difference between the two is that the latter only provides information about the surface topology and hence the TEM method is preferred as compared to the SEM for morphological analysis of polymer nanocomposites. Also TEM provides a resolution of 0.2nm as compared to a resolution of 2 nm in case of SEM. Interestingly TEM cannot distinguish between two different phases since it works on the principle of transmission of electron beams through a sample. On the other hand the SEM works on the principle of scanning the sample using an electron beam and hence refractive index changes within the samples due to the presence of different phases can be identified and imaged. Hence SEM is more useful in analysis of polymer blends and polymer foams.

In case of a TEM a highly energized electron beam passes through the sample (thickness < 100nm) and the transmission of the electron beam helps in investigating the internal structure of the specimen.

The TEM equipment (figure 3.5) used in this study is the JEOL 1010 with an accelerating voltage of 100kV and a high vacuum. The sample preparation is very complex in the case of polymers. For polymers the samples were ultramicrotomed using a diamond knife on a Leica Ultracut S with a liquid nitrogen cooling device (LNG). The LNG operates at a temperature of -165^{0}C. The freezing of the samples was necessary due to the soft nature of the polymer samples. The thickness of these cryogenically cut samples were approximately 70nm. The samples were then placed on copper grids ready to be analyzed. Two different magnifications (25,000X and

100,000X) were chosen. The lower magnification was chosen to provide information on the dispersion and distribution of clay layers and the higher magnification was chosen to facilitate the analysis of individual layers. The clay particles appear darker due to the presence of heavier elements like silica and aluminum as compared to the polymer matrix, which appears brighter due to presence of lighter elements like carbon and hydrogen

Figure 3.5 : Picture of the TEM used.

3.6.3 Scanning Electron Microscopy (SEM):

The SEM (figure 3.6) uses a beam of electrons to scan the surface of a sample to build a three-dimensional image of the specimen**.** An electron gun generates the electron used to study the specimen. The filament in the electron gun is responsible for the production of the electrons. The filament current is well monitored to avoid the damage of the filament by not allowing the filament current to increase beyond the filament saturation point (the point after which the electron flux generated by the filament cannot increase further). Electrons are very small and are easily deflected by gas molecules in air. Therefore, to allow the electrons to reach the sample, the column is under a vacuum (normally a low vacuum mode works with polymers). Also the gas

inside the polymer keeps the material from getting charged (in case of ESEM). In case of SEM a conductive coating or gold coating becomes essential. Once the electron beam strikes the sample then a variety of beams like backscattered electrons, secondary electrons, light and heat is produced. Among these the secondary and the backscattered electrons are detected. Unlike the light microscopes where light forms an instant image, the electrons in the SEM don't form an instant image. Instead the SEM scans its electron beam line by line over the sample. It's much like using a flashlight in a dark room to scan the room from side to side. Gradually the image is built on a TV monitor (like CRT tube). Hence the scanning tendency of the SEM and ESEM enables it to detect phase differences better as compared to TEM.

Figure 3.6 : Picture of SEM used for image analysis

3.6.4 Measurement of thermal properties

Figure 3.7 shows the DSC 2920 system used for investigating the thermal properties of the polymer samples in this work. Differential scanning calorimetry (DSC) is a thermal analysis technique and has been used to measure the temperatures and heat flows associated with transitions in materials as a function of time and temperature. Such measurements provide quantitative and qualitative information about physical

and chemical changes, that involve endothermic or exothermic processes, or changes in heat capacity.

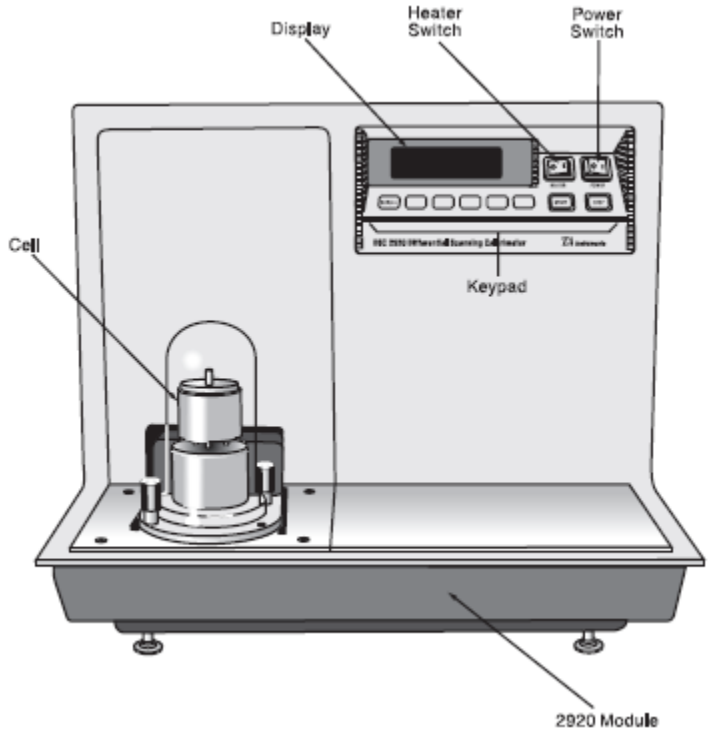

Figure 3.7 : Schematic representation of the DSC setup used.

DSC is the most widely used thermal analysis technique for use with polymers and organic materials, as well as various inorganic materials. Many thermal transitions are not accurately detectable by DSC. Examples include the enthalpic relaxation that occurs at the glass transition and the crystallization of amorphous or metastable crystalline structures prior to or during melting. Hence to detect such complex and minute changes MDSC (Modulated differential scanning Calorimetry was used in this study.

MDSC measures the difference in heat flow between the sample and an inert reference like the case of DSC. However, in MDSC a different heating profile (temperature regime) is applied to the sample and reference. Specifically, a sinusoidal modulation (oscillation) is overlaid on the conventional linear heating or cooling ramp to yield a profile in which the average sample temperature continuously changes with

time but not in a linear fashion. The net effect of imposing a more complex heating profile on the sample is the same as if two experiments were run simultaneously on the material - one experiment at the traditional linear (average) heating rate and one at a sinusoidal (instantaneous) heating rate.

Equation (3.3) is the general heat flow equation used in case of DSC or MDSC

$$\frac{dQ}{dT} = C_p\beta + f(T,t) \qquad (3.3)$$

where, $\frac{dQ}{dT}$ is the net heat flow rate ,C_p is the heat capacity of the material , β is the heating rate and f(T,t) is the heat flow from kinetic(absolute temperature and time dependent) processes. Modulated DSC determines the total, as well as these two individual heat flow components, to provide increased understanding of complex transitions in materials. MDSC is able to do this based on the two heating rates seen by the material, - the average heating rate which provides total heat flow information and the sinusoidal heating rate which provides heat capacity information from the heat flow that responds to the rate of temperature change. The heat capacity component and the kinetic component are more generally known as reversing heat flow and non reversing heat flow respectively.

3.7 Rheological measurements

Rheological measurements can be differentiated into two categories

Shear rheological measurements

Extensional rheological measurements

Both these techniques were used to gain an understanding of the microstructure and the morphology, and there response towards shear and extensional deforming. The ARES rheological setup as shown in figure 3.8 was used in this project.

Figure 3.8 : ARES setup used for rheological analysis

3.7.1 Shear Rheology

Shear rheological measurements can be classified into steady shear and dynamic oscillatory shear experiments. Both the above mentioned experiments were conducted using the Advanced Rheometric Expansion system (ARES). The rheological data were analyzed using the Rheometric Rhios V 4 software. The rheological measurements were made using a parallel plate geometry. The plates had a diameter of 25 mm. All the melded samples were cut out to the size of 25 mm disks. Before loading the sample it was essential to ensure equilibration of the system temperature. This was followed by zeroing the plate gaps when the desired temperature was attained. The samples were then loaded into the machine. Also, once the samples were loaded at the desired temperature it was necessary to ensure that the torque value (displayed) stands at zero. Non zero torque means the sample has a yield stress and

cannot be tested for dynamic rheological measurements. The sample in that case can be pre-sheared at 0.01/s or 1/s for a certain period to reduce the torque to zero and then the measurements can be started.

Generally in parallel plate or torsional flow geometries the samples are loaded in between parallel plates separated by a distance h. The lower plate oscillates (dynamic measurements) or rotates (steady shear measurements) at a constant angular velocity (Ω).The upper plate measures torque and normal stress difference functions. These parameters are related to the shear viscosity and the normal stress function using the equation (3.4) and equation (3.5). A detailed derivation can be found in (140)

$$\eta(\dot{\gamma}) = \frac{T}{2\pi R^3 \dot{\gamma}_R}\left(3 + \frac{d\ln T}{d\ln \dot{\gamma}_R}\right) \tag{3.4}$$

$$N_1(\dot{\gamma}_R) - N_2\left(\dot{\gamma}_R\right) = \frac{2F}{\pi R^2}\left(1 + \frac{1d\ln F}{2d\ln \dot{\gamma}_R}\right) \tag{3.5}$$

In equations (3.4) and (3.5) η(γ) is the steady shear viscosity measured at the rim of the plates, T is the torque measured at the rim of the plates. R is the radius of the plate from the centre to the rim. F is the normal force and $\dot{\gamma}_R$ is the shear rate measured at the rim of the plate. Although the parallel plate geometry is user friendly and relatively accurate, a setback is that strain rate (or its integral) varies radially along the plates and hence the strain rate experienced by the sample varies with the radius of the plate. The apparent shear rate (dependent on the radial position) is calculated using equation (3.6)

$$\dot{\gamma}_R = \frac{\Omega R}{h} \tag{3.6}$$

Parallel plate geometries are found to be more useful in case of small amplitude oscillatory shear measurements (SAOS). The SAOS material functions η(ω') and

$\eta(\omega^{"})$ can be related to the measured torque (T) and the phase lag (δ) using equation 3.7 and equation 3.8. The parameter $\eta(\omega^{'})$ represents the complex viscosity and $\eta(\omega^{"})$ represents the out of phase component of the complex viscosity. θ_0 in the equation (3.7) and equation (3.8) denotes the flow direction of the sample.

$$\eta^{'}(\omega) = \frac{2hT \sin \delta}{\pi R^4 \omega \theta_0} \tag{3.7}$$

$$\eta^{"}(\omega) = \frac{2hT \cos \delta}{\pi R^4 \omega \theta_0} \tag{3.8}$$

The SAOS technique can be used to study the mesostructure of the polymer nanocomposites at very small oscillation frequencies. The use of a small oscillation frequency helps in studying the inherent behaviour of the polymer matrix in presence of filler. In case of nanocomposites generally a pseudo solid like behaviour has been observed at lower frequencies with increase in filler loadings (6). Also in certain cases non linear rheological trends are observed at lower frequencies as denoted by the absence of a distinct plateau region (7). Since at lower frequencies the material is expected to behave like a solid and absorb all the energy or shear force exerted on the sample and hence show a plateau region. Alternatively at higher frequencies the material is expected to completely behave like a liquid and hence show a terminal region or a linear dependency of viscosity with increasing shear rates followed by a terminal region at high frequencies. This is because at higher frequencies the shear induced orientation of the filler material makes the shear thinning behaviour exhibited solely a function of the polymer matrix (158). Determination of the linear viscoelastic region before conducting the dynamic tests is essential since in the linear viscoelastic region the microstructure of the material is not affected by the shear induced alignment. In simple terms, once the applied shear is removed the material reverts back to its original inherent microstructure. In the nonlinear region a

permanent structural change is induced in the sample under investigation. Hence frequency sweep test to determine the linear viscoelastic region are essential before the dynamic rheological tests can be conducted. In the linear viscoelastic region the shear stress is directly proportional to the amount of strain and the torque response includes only the first harmonics (or the first normal stress difference).

In the linear viscoelastic region the material functions G' and G" are independent of the strain amplitude and hence the condition of direct proportionality between stress and strain is satisfied. Now with increase in strain amplitude the stress will increase proportionally. The constant of proportionality is the modulus. The absence of higher harmonics ensures that the stress remains sinusoidal.

The Cox –Merz rule ($\eta^*(\omega) = \eta(\gamma^0)$)has been found to be very useful to relate the shear viscosity and the complex viscosity. The rule has been found to work very well with homopolymer systems. In case of filled polymer systems the rule has not worked well. Small deviations were observed at low filler concentrations but with increase in filler concentration specifically beyond the percolation threshold large deviations were observed (159). This effect was attributed to significant changes to the polymer mesostructure beyond the percolation threshold region. The application of SAOS tests revealed that at lower frequencies the complex viscosity is higher than the shear viscosity. But with LAOS it was found that the complex viscosity is lower than the shear viscosity. This discrepancy led to the conclusion that in case of nanocomposites even at smaller oscillations rates the application of a shear force for a long duration leads to orientation of the filler material at lower frequencies.

3.7.2 Extensional rheology

Extensional rheological tests were performed using the ARES. A special extension fitting was used for making the measurements. The data generated were for the case

of uniaxial extensional viscosity. The extension fitting used is like two rectangular thin slits which can hold on a rectangular sample to the cylindrical rheometer connection ports. The cylindrical ports rotate generating an extensional force on the rectangular sample. The extensional measurements are made till the samples break out completely. The degree of stretching or the hencky strain rate applied control the frequency of rotation of the cylindrical connection ports in ARES. The new extension fitting has been found to provide repeatable results with EVA based polymers, where the generated results have been compared with the tests conducted using a RME for determining extensional viscosity (unpublished work at RMIT University, October 2008). Hence the results generated for HMS-PP are repeatable and consistent. The extensional viscosity results generated using the new extension fitting also follows the troutons ratio within the linear region or till the point where strain hardening behaviour starts. The idea of using this relation was once again to validate the results generated using the new fitting.

3.8 Foam injection moulding setup

Foam injection moulding system is a combination of a continuous extrusion system in the first part and then further an injection moulding device connected with the extrusion system. The foam injection moulding machine used was a Mucell injection moulding system. The foam moulding system has three parts, a supercritical fluid injection system, a foam extrusion system, and a foam injection moulding system. The supercritical fluid injection system is a compressor which can raise the pressure of the foaming agent (N_2) to the desired injection pressure. In this case an injection pressure of 200Mpa can be achieved using the compression system.

The extrusion system used had a screw diameter of 30mm and an L/d ratio of 12. A dispersive and distributive mixing scheme was adopted in the screw design. The

screw channel depth was accordingly varied and the screw elements were orthogonal to each other in the mixing zone. Also, another supportive mixing element was provided to ensure complete mixing. The screw speed could be varied in the range of (100-500) mm/sec. The injection pressure of the uniform gas/polymer mixture at the injection port of the mould could be controlled by varying the screw speed; hence even at a fixed injection pressure the screw speed variation could be effectively used to vary the pressure of the gas/polymer melt. The barrel of the foam extrusion system is provided with three separate band heaters which can be used to raise or lower the temperature of the melt. The shot size used for injection was 50 gm and the injection volume was 70cm^3. The next part of the system is the mould. The important parameters of the mould are listed in table 3.3.

Clamping force	min. ton	40
Closing force	kN	30-35
Opening Stroke	mm	350-400
Mould Height	min. mm	200
Daylight	max. mm	600
Distance between Tie bars	mm	300-400
Platen Size	mm	400-450

Table 3.3 : Mould parameters for the foam moulding setup

3.9 Error analysis

The experimental techniques described in this chapter would help in determining factors which control foam cell structure and morphology. But like most cases these may have errors. The errors arising from experimental measurements are discussed in this section.

3.9.1 Wide angle X-Ray scattering (WAXS):

WAXS studies were used in this work to provide information about the interaction of HMS-PP chains into the interlayer spacing of the layered silicates. From the scattering profile the morphology of the polymer nanocomposites can be analyzed qualitatively. The position and intensity of the peaks with respect to unintercalated clay particles provides information on the level of intercalation. An error that can possibly occur during WAXS measurement is the effect of X-ray scattering in presence of air. This effect can be easily eliminated by conducting WAXS studies in vacuum. In case the WAXS studies are not carried under vacuum condition, then subtraction of the background scattering intensities due to air from the sample WAXS intensities becomes essential. The background scattering intensity can be generated by placing the empty sample holder and conducting the run as normal. The effect of background subtraction is not very pronounced and is less than (+/-) 1 %, hence in most cases can be neglected except for small angles lesser than 2^0.

3.9.2 Shear Rheological measurements*:*

As described previously, shear rheological measurements can be subdivided into two categories

Oscillatory shear

Steady shear

The ARES rheometer used in this study has a torque range of $0.2g_f$-cm to $2000g_f$-cm (gram force centimetre). Its temperature accuracy is within (+/-) 0.10C. Though the time sweep tests have indicated a better accuracy (0.05^0C).

The important aspects that need to be addressed in the case of an oscillatory shear measurement are

Repeatability of the runs to ensure consistency of the results.

Thermal degradation of samples subjected to high temperatures for a long time

Stability of measurements at low frequencies especially in the range of 0.01 to 0.001rad/s that may fall into the limit of instrument sensitivity.

The results are found to be repeatable at intermediate and high frequencies using the same instrument. The tests of repeatability using other instruments have been verified by comparing the rheological tests from the literature. At lower frequencies (less than 0.01rad/s) slight deviations (1-2%) were observed and this may be due to the torque-strain relationship reaching the limit of instrument sensitivity. To eliminate the above inconsistencies an average of two runs has been taken and presented in the results and discussion part.

Thermal degradability of the sample arises due to subjecting the samples to elevated temperatures for long times. Prolonged period of high temperatures leads to micro structural changes in the sample like chain scission, cross linking and other physio-chemical processes which in turn affect the rheological results. Hence to avoid such errors, time sweep testes were conducted using the samples, where the samples were subjected to constant temperature and constant frequency for a specified time span. A frequency of 0.1 rad/s was chosen as it was in the intermediate level and the time frame chosen was (1.5hours) was given for each time sweep run. The temperature chosen was the highest temperature that the sample would be subjected to. The parameter that was monitored was G' and G"since these two parameters are highly sensitive to microstructure changes. A very little change (2%) in these two parameters over the mentioned time range denotes that the sample doesn't undergo degradation.

3.9.2.1 Errors in steady shear measurement

The possible errors that can arise in steady shear measurements are as follows

Flow instabilities (eg: sample fracture and centrifugal expulsion)

Thermal degradation of the sample (as discussed previously)

Flow instabilities usually occur at high shear rates. These can be edge fracture or centrifugal expulsion. Powell (158, 159) has discussed both of these instabilities in details. edge fracture and centrifugal expulsion of the samples occur at certain critical shear rates corresponding to critical angular speeds of the plates and can be visually observed. The identification of centrifugal expulsion and edge fracture can be made by a discontinuity in the torque time curve and a decrease of the measured torque with time respectively. The tests of thermal degradation conducted for the oscillatory measurements can be used to access thermal degradation in case of steady shear measurements as well, since the time of duration of steady shear measurements is usually lesser than that for the oscillatory shear measurements and hence the results from oscillatory shear measurements can be effectively used.

An important deficiency of the parallel plate geometry is that shear rates are not constant and vary radially across the sample. This is unlike cone and plate geometry where this inconsistency in shear rate is offset by the angle of the cone. Shear rates in case of parallel plate geometry range from zero at the centre to maximum at the edge or rim of the plate. Macosko(84) has suggested a correction for such a discrepancy, a derivative that relates shear stress to total torque. Using the basic expression of viscosity as a ratio of shear stress to shear rate a corrected version of shear viscosity can be obtained with respect to total torque. Interestingly the variation in steady shear viscosity due to plate geometries has not been found to be very significant and is

generally in the range of 0.5 to 1 % (85). Hence such an error can be quatitatively neglected

3.9.3 SEM and TEM

The samples used in morphological analysis of polymer nanocomposites using TEM are very small in volume. Hence deductions about the morphology may be unreliable. Similar deductions can be made for the case of foam cell morphology analysis using SEM. Hence it becomes very important to test these samples for repeatability and consistency. To avoid possible errors, statistical sampling techniques were used and a set of samples was randomly generated from the same bulk material for morphological analysis. Also the technique of averaging of frames at very high resolution was used to improve the accuracy of the generated images. Another possible source of error in SEM image analysis was the degradation of the sample at high electron beam energies as indicated by the generation of large black spots on the sample under investigation. Hence during SEM image analysis the samples were first tested with different spot sizes and electron beam intensities and the combination which provided the best resolution and the least degradation of the samples was chosen. In case of foam cell morphological analysis the samples used were generated from the cross section of the bulk material and hence were representative of the actual bulk foam structure.

3.9.4 The Batch foaming setup

The batch foaming setup used for the generation of fine cell foams and also for conducting solubility studies forms a major part of this project. Hence error analysis and calibration studies on this setup were essential to generate sustainable results.

The water batch (used for heating up the pressure vessel to the desired temperature) was calibrated without the pressure vessel resulting in a calibration curve between time and temperature. Also the time required for the empty pressure vessel to rise to the required temperature and equilibrate was determined. These calibration studies helped in determining the exact temperature at which the water bath needs to be operated to raise the temperature of the pressure vessel to the desired values. The thermocouple connected to the pressure vessel was also tested for accuracy by introducing a fluid of known temperature into the pressure vessel and comparing the temperature readings. The accuracy of the pressure meter was tested using the CO_2 cylinder in which the gas is filled at a pressure of around 800psig (5.6MPa). Once the cylinder was connected to the pressure vessel the pressure meter provided the same pressure reading as on the cylinder.The pressure meter connected to the pressure vessel had a sensitivity of 5 psig and an error percentage of (+/-) 1 %. The time required for dismantling the pressure vessel and subjecting the sample to temperature superheat can be neglected since calibration studies revealed that the dismantling time was on average 5 seconds. Also, since the temperature of saturation was very low (around 50^0C) as compared to the temperature required for foam cell nucleation and growth, this dismantling time did not affect the foam cell morphology. Another problem that was detected with the calibration studies is that the gasket used wore out after 5 subsequent runs causing pressure leakage. Hence the gasket was replaced after every 3 runs to maintain accuracy of the data. Another possible error source was the non uniformity of temperature when the saturated polymer sample was introduced into the oil bath for foaming. The heating setup used for foaming was very large as compared to the sample size (quantitatively at least 60 times larger than the volume of the sample) hence temperature uniformity across the sample would have been attained

very rapidly eliminating any possible chance of error. Finally all the foaming tests were repeated using the setup to ensure that the data are reproducible.

3.9.5 Foam injection moulding system

The analysis of the foam injection moulding system becomes complex due to a large number of parameters involved, such as, injection pressure , gas concentration , foaming temperature , foaming time , screw speed and quenching time. Most of the processing parameters were very effectively controlled by electronic controllers. The power requirements of the entire foaming setup were controlled by stabilizers. The fluctuation in the power supply leads to instabilities in the injection pressure. Hence the conducted tests were repeated 3 times and the average cell size was considered for a given set of processing conditions. The clamping of the foam mould was improper at times, which resulted in higher cycle times changing the overall foaming time and quenching time. Hence it was necessary to measure the cycle time for each run to ensure that the same foaming and quenching times were attained as desired. The absence of pressure measuring devices inside the mould nullified the possibilities of conducting shear rheological analysis of the two phase gas/polymer melt. The needle valve used at the injection port of the SCF system had a huge amount of pressure drop (70Mpa) reducing the inlet pressure to a value less than desired.

Chapter 4: Results and Discussions (characterization studies)

4.1 Introduction

This thesis focuses on the development of suitable strategies for the production of fine cell foams in polymers. Literature review suggested that, with careful control of processing parameters, higher rate of nucleation, controlled cell growth, increased gas solubility and fine cell foam structure can be achieved. Accordingly a batch setup was chosen for foaming since in a batch process the processing parameters can be accurately controlled. Also nanofillers (clay) were added to the host polymer matrix to enhance the rate of nucleation. A physical blowing agent along with a batch setup was used for foaming. The first step was to conduct solubility tests in the polymer nanocomposites to assess the effect of filler on degree of super saturation and gas solubility. Since it was found that addition of clay reduces gas solubility, suitable techniques to improve the gas solubility was used (addition of EVA to the polymer nanocomposite matrix). Characterization studies conducted on the HMS-PP/EVA blend revealed that the clay particles act as a compatibilizer for the incompatible HMS-PP/EVA blend. Hence characterization studies of these blends were performed. Once all the samples were foamed it was essential to study the effect of structural parameters of the polymer matrix on the foam cell morphology and hence characterization studies on HMS-PP/clay nanocomposites were conducted. Furthermore an attempt was made to scale up batch foaming results to a continuous foam injection moulding system. Finally modelling studies to determine the effect of clay particles on gas solubility and to study the effect of polymer nanocomposite rheology on foam cell structure was performed.

Accordingly this chapter starts off with gas solubility studies, then moves on to clay compatibilization studies for immiscible PP/EVA blends. The next part deals with foam processing in a batch and in a continuous foam injection moulding system. The last section deals with the characterisation and its effect on foam generation.

4.2 Gas solubility studies in polymer nanocomposites

A volumetric method (using the batch setup) was used to perform gas solubility studies on polymer nanocomposites (chapter 3, page no. 75).

Gas solubility studies were initially performed on HMS-PP/clay nanocomposites with 2, 4, 8 and 10 wt percent clay as presented in figure 4.1.

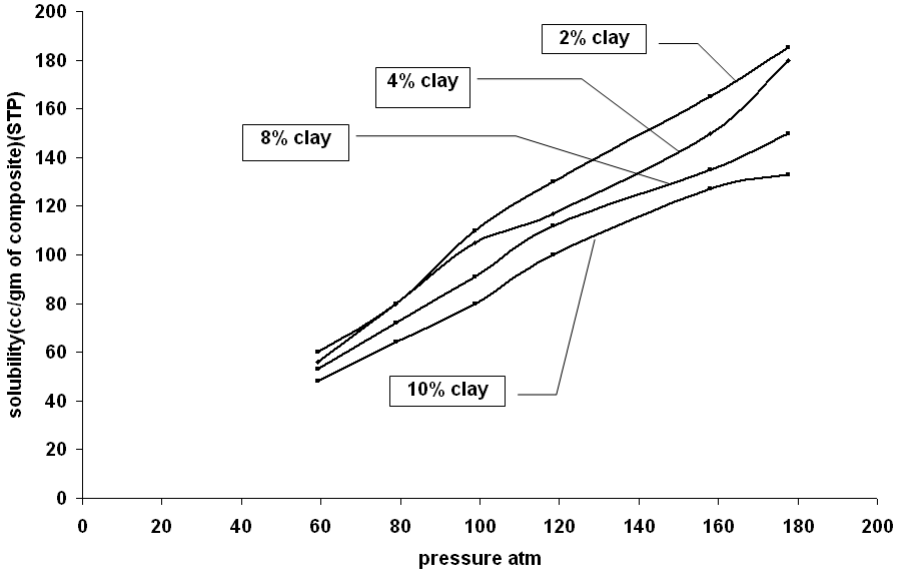

Figure 4.1 : Solubility of CO_2 in HMS-PP/clay nanocomposites

It is evident from figure 4.1 that equilibrium solubility of the blowing agent (CO_2) decreases with increase in clay concentration. Also it can be seen that the gas solubility increases nonlinearly with pressure and is higher at higher pressures. The curves also show a point of inflection around the critical point for CO_2 (8.1Mpa). The difference in gas solubility for different clay concentrations increases at higher

pressures and is more or less similar in profile for lower pressures. The possible reason could be that at higher pressures the gas molecules would have higher energy, and hence the rate of collision of gas molecules with clay particles would be higher, and hence the gas solubility would then depend on the concentration of clay particles in the polymer nanocomposite matrix. The path of diffusion of the gas would then be a function of the clay particle concentration and the dispersion state and hence overall solubility would be affected. The curves also show that the rate of rise of gas solubility decreases after 4 wt % clay even when the pressure is increased. Interestingly the overall changes in gas solubility is not very high and varies in-between (15 -20% volume percent of gas/gm of the composite) for all the clay concentrations considered in this experiment.

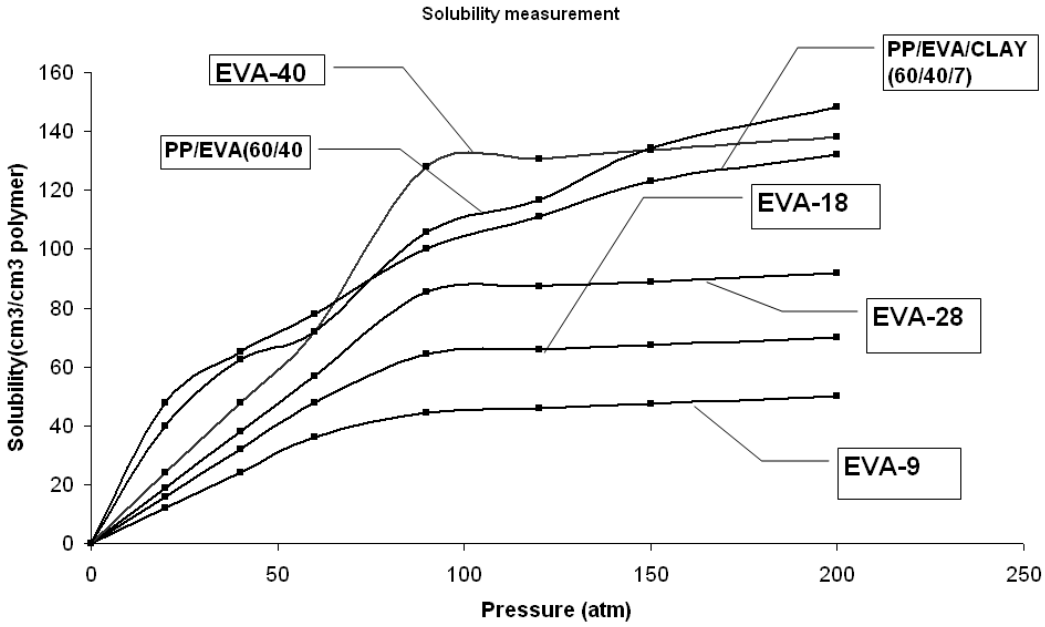

Figure 4.2 : Solubility of CO_2 in EVA and PP/EVA blends with and without clay

Gas solubility tests were also conducted on EVA containing 9, 18, 28 and 40 wt percent of vinyl acetate groups as shown in figure 4.2. The premise was to determine the effect of vinyl acetate group on gas solubility, specifically in case of CO_2, since

the literature suggests that the CO_2 interaction with C=0 group is high and vinyl acetate does have a C=0 group in its form.

The solubility curves or isotherms are shown in the figure 4.2. It can be seen from the figure 4.2 that the gas solubility does increase with increase in vinyl acetate content and also with increase in pressure. The rate of increase of gas solubility reduces at higher pressure and infact levels off at higher pressures. Subsequently EVA -40 was blended with HMS-PP and solubility behaviour of the blend was studied in presence and absence of clay particles (figure 4.2). It was found that the addition of clay particles to the blend reduces the gas solubility at higher pressures. Also after the addition of clay particles a positive deviation from the linear mixing rule (to determine solubility) is observed suggesting a compatibilization kind of action of clay particles. The aim of addition of EVA to HMS-PP was to localize CO_2 inside the nanocellular EVA domains and subsequently use it for foam nucleation.

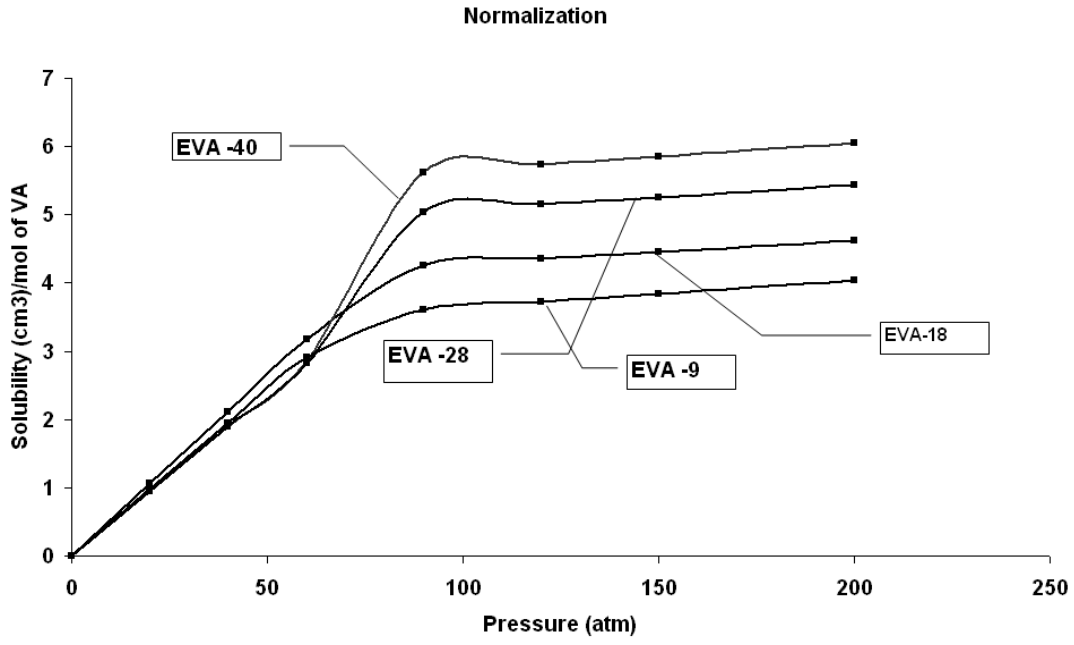

Figure 4.3 : Equilibrium solubility normalized with respect to vinyl acetate content.

Sample name	% crystallinity
EVA-9	**24.4**
EVA-18	**14.2**
EVA-28	**11.2**
EVA-40	**9.3**

Table 4.1 : Crystallinity values for EVA with different amounts of vinyl acetate content

To further evaluate the effect of vinyl acetate content on gas solubility, the solubility curves were normalized with respect to the vinyl acetate content for each sample respectively. The resulting master curves are shown in figure 4.3. The master curves reveal that below the critical point of CO_2 the gas solubility curves coincide. Hence it can be concluded that the gas solubility is a function of the vinyl acetate groups present in EVA below the critical point of CO_2. The solubility curves diverge out as the pressure is increased beyond the critical point of CO_2 (73 atmospheres). Infact the curves show a difference in solubility at the critical point of CO_2 as well. Hence it can be said that at or above the critical point of CO_2 the gas solubility is affected by other parameters like crystallinity, molecular weight distribution and other factors along with vinyl acetate content. To further support this hypothesis, crystallinity measurements were made on the EVA samples (table 4.1). The table above shows the crystallinty of the different EVA samples used in this study. The crystallinity of the EVA samples reduces with increase in vinyl acetate content indicating that the amorphous region increases with increase in vinyl acetate content. The solubility of a gas within the polymer matrix is a function of the amorphous region of the polymer

since gas is insoluble in the crystalline phase of the polymer. The high degree of order and close packing of crystals reduces the free volume available for gas to occupy and hence solubility decreases with increase in crystallinity.

4.3 Studies on PP/EVA blends

The final properties of polymer blends to a large extent depend on the size of the minor phase and the interfacial adhesion between the two phases. The processing conditions, concentration of the dispersed phase and the morphology of the blends play an important role in controlling the size of the dispersed phase. The role of a compatibilizer in a polymer alloy or blend is to improve interfacial adhesion between two immiscible polymers resulting in the formation of miscible blends. The compatibilizer can be a macro molecule or a block, star, graft co-polymer conventionally.

The addition of these compatibilizers results in a decreased domain size of the dispersed phase, stabilization of the dispersed phase during melt mixing and finally an improved interfacial adhesion in the solid state. The decreased domain size leads to increase in surface tension which should result in coalescence but the improved interfacial interaction negates out the increased surface tension resulting in a more homogenous stable blend. A newly used compatibilization technique is the use of clay particles to compatibilize immiscible blends.

The strong adsorption of polymers on the particles provides the stabilization energy for compatibilization, also the intercalation of the polymers inside the clay galleries along with a very high surface area per unit weight of the clay particles further helps in compatibilization. The addition of clay particles also results in increase in melt viscosity which further helps in reducing the size of the dispersed phase.

The objective of this work is to see the role of clay as a compatibilizer for a blend and study its effects on the properties of the immiscible glassy polymer pair. HMS-PP/ EVA is the chosen immiscible pair since HMS-PP/EVA blends lead to a phase separated structure when melt mixed. The binary blend of HMS-PP/EVA due to the addition of EVA shows improvement in properties over HMS-PP, specifically in the in impact strength of HMS-PP (163). A 60/40 HMS-PP/EVA blend is considered to study the effect of clay since in a 60/40 blend the role of interphase in controlling the final blend properties is significant and hence the role of clay as a compatibilizer can be effectively studied. A combination of XRD, SEM, TEM, DSC, rheology and mechanical properties analysis is used to study the effect of clay on immiscible blends of HMS-PP/EVA.

4.3.1 Thermodynamics

The free energy of mixing in case of a three component polymeric system is governed by the equation 4.1

$$\Delta G_m = \Delta G_{AP} + \Delta G_{BP} - \Delta G_{AB} \quad (4.1)$$

Where A and B denote polymers and P represents particle. Thus, AP, BP and AB represent polymer A - particle, Polymer B – particle and polymer-polymer interaction respectively. Now a system tries to be in a state of minimum free energy and this is only possible when $\Delta G_{AB} > 0$ and $\Delta G_{AP}, \Delta G_{BP} < 0$. Thus the addition of solid particles can stabilize the blend by adsorbing the blend components. This purpose can only be attained when the solid particles have a large surface area per unit weight, which nanoparticles have and hence they can be effectively used as compatibilizers (164). The entropic penalty of confining a polymer within the clay galleries is nullified by the increase in enthalpic contribution of the blend components due to the

presence of a high interaction potential between clay particles and the blend components. Thus the interaction potential between the clay particles and the blend components becomes a governing parameter to ensure the intercalation of both the blend components at the interphase(163). The differential interaction potential ensures that the clay particles are present at the interphase as well in the bulk system. Balanced interaction potential causes the clay particles to localize themselves only at the interphase since net attraction in that case will be maximum only at the interphase. In this case the interaction potential is different for the two blend components ensuring that clay particles are present at the interphase as well as throughout the blend matrix.

4.3.2 Miscibility and compatibility

There are differing views on the definition of miscibility and compatibility based on the kind of study or analysis undertaken. The term compatibility has been normally used to describe materials with enhanced mechanical properties after mixing of the components. In case of compatible materials there is a fairly good adhesion between the two constituent phases(164).The term miscibility on the other hand has been used to describe a mixture of components which show a behaviour like that of a single phase system. In terms of thermal properties miscibility is the easiest to determine and detect. A miscible blend is expected to show a single glass transition temperature but again there are differing opinions in this regard as well. The presence of a crystallization peak in-between the two components provides evidence in favour of co-crystallization which provides evidence of partial miscibility of the components in the melt phase in a temperature range near the crystallization temperature. In thermal analysis miscibility is determined in terms of homogeneity within the mixture at a chain length equivalent to the chain length in the crystalline region, while determining

T_g. However in case of molecular level simulations miscibility is defined in terms of homogeneity at a smaller scale normally based on the sphere of influence of the intermolecular forces. Thus the presence of a single glass transition is not a very comprehensive way to determine blend miscibility. Sometimes miscibility is used interchangeably with compatibility but normally compatibility is only used when there is improvement in mechanical properties and other properties on mixing of blend components. Also, the ease of mixing of the components is a good indicator of compatibility. The depression of melting point of a blend system or rather changes in melting point of a system has also been linked to blend compatibility in some cases.

4.3.3 XRD analysis

A Philips X-ray generator using 40 KV accelerating voltage and 40 mA current was used in the analysis. Ni filtered Cu-Kα (λ = 0.154 nm) radiation was used to record wide angle X-ray scattering intensities from 2θ = 1 to 30°. XRD analysis was carried out to study the dispersion state of clay in the polymer matrix. As shown in Figures 4.4 and 4.5, the polymer chains have expanded the clay galleries. The complete absence of a peak in the samples denotes an exfoliated morphology but needs further validation from the TEM images (Figures 4.6 and 4.7). The rheologically determined percolation threshold for HMS-PP and EVA clay nanocomposite is around 4%.The HMS-PP/EVA/Clay (60/40/7) system shows a WAXD pattern with complete absence of peak which hints towards an exfoliated morphology. If both the polymers would not intercalate the clay galleries then once a phase is saturated there would be aggregation of the remaining clay particles which would be indicated by the absence of an exfoliated or mixed morphology. For individual polymers the percolation threshold is around 4 wt % clay (165) and above the percolation threshold no further exfoliation is possible.

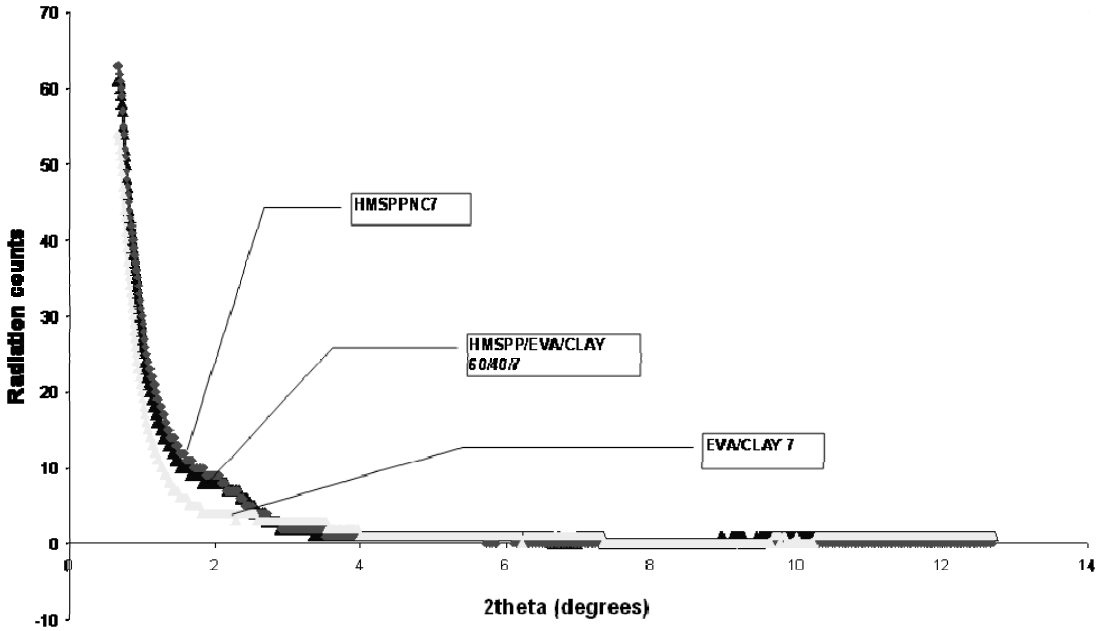

Figure 4.4 :WAXD plots for HMS-PP/EVA blend nanocomposites

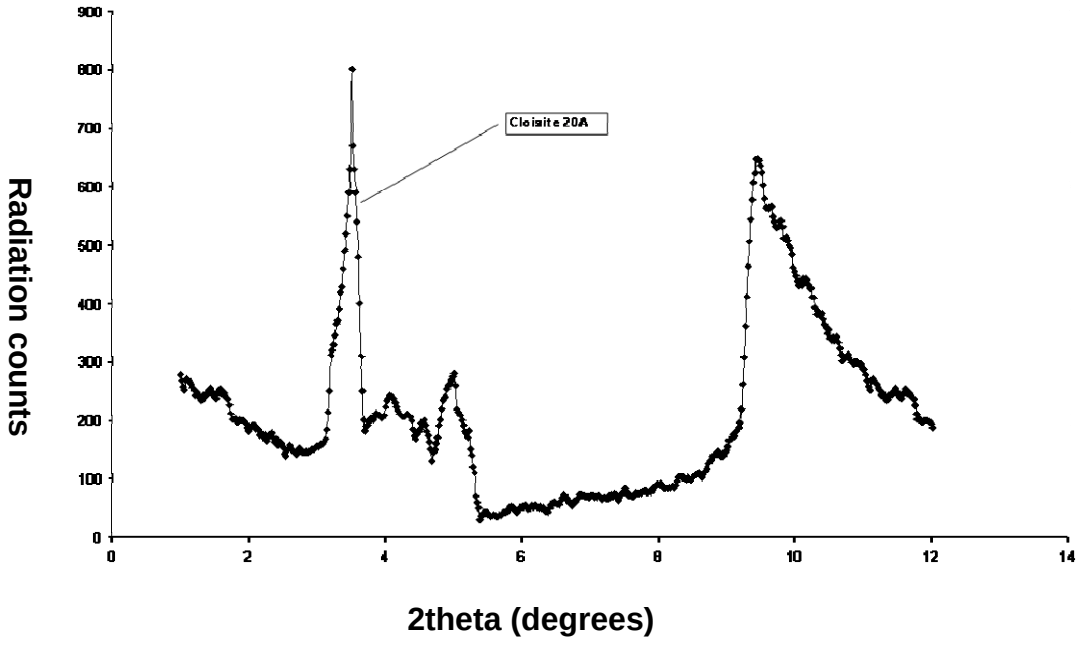

Figure 4.5 : WAXD pattern for cloisite 20A

Thus it can be concluded that both the blend components have entered the clay galleries. Due to simultaneous intercalation by both the blend components there would be a common region of intercalation which can be probably the interphase

between the two blend components. The presence of clay coupled with simultaneous intercalation of both the blend components results in a compatibilization effect between the two blend components. The same hypothesis can be verified using the TEM images.

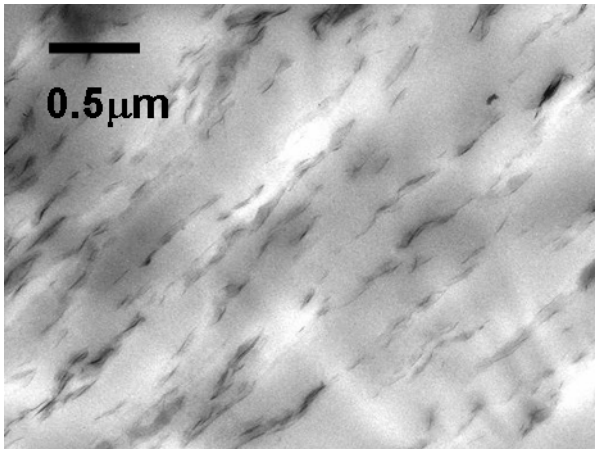

Figure 4.6 : TEM image of PP/EVA/clay blend (60/40/7)

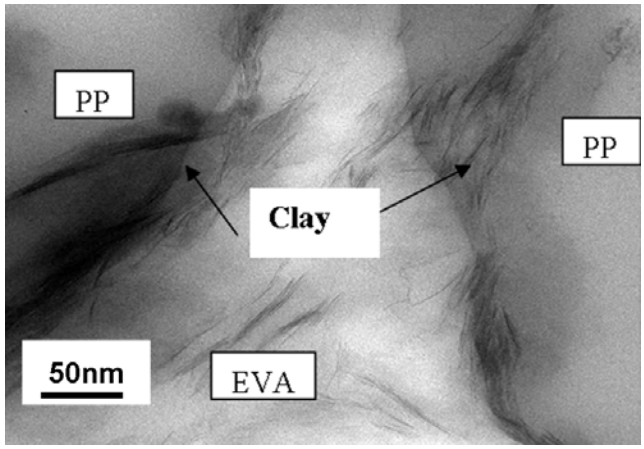

Figure 4.7 : TEM image of a PP/ EVA/clay blend (60/40/7)

As shown by the TEM images (Figures 4.6 and 4.7) the clay particles are dispersed homogenously throughout the polymer blend matrix. The micrographs also reveal that the clay particles are present at the interphase between the two blend components. The possible explanation for this could be the limited presence of groups in blend components which can intercalate the clay galleries. The excess clay particles move out to the interphase between the two blend components. Also as shown in the XRD images, both the components intercalate the clay galleries and hence there has to be a region of common intercalation which can only take place at the interphase. This further leads to a reduction in interfacial tension and also subsequent reduction in dispersed phase size. The white part in the above images represents the EVA phase and the black part the HMS-PP phase. The images were obtained by extracting the PP phase out by using a solvent. Once a phase is extracted out then under a SEM it appears to be black. If it is assumed further that the clay particles are fully exfoliated

and are located at the surface of the dispersed phase then the volume fraction of clay needed to saturate the dispersed EVA phase is given by equation 2 (166).

$$\phi_c = \frac{3e}{R}\phi_{EVA} \tag{4.2}$$

In equation (4.2), e is the thickness of the clay platelets, R is the EVA average drop diameter and ϕ_{EVA} is the volume fraction of the EVA phase in the blend .The above equation assumes that the clay particles are located at the surface of the EVA drops and are supposedly spherical with an average radius of R.Thus for a EVA volume fraction of 40% (R = 0.51 μm and e = 1 nm) the amount of clay particles needed to saturate the surface of the dispersed phase is approximately 1%. This shows that the saturation concentration is relatively small as compared to the amount of clay loading and hence supports the fact that the clay particles emulsify the blends. Also with a concentration of 7 wt % clay, one expects the excess amount of clay to migrate towards the bulk phases of the blend components. The relative position of the clay particles depends on the relative attraction potential of the blend components towards the clay particles. The presence of clay particles at the interphase thermodynamically provides the case of least amount of free energy under equilibrium conditions and hence is the most preferred state for the system.

4.3. 4 Mechanical properties

The mechanical properties of the blends show an improvement after the addition of clay to the system as compared to pure HMS-PP/EVA blends (table 4.2 and table 4.3). A 60/40 blend is chosen since the role of the interphase in such a blend will govern the mechanical properties of the system.

Sample	Modulus (MPa)	Tensile strength (MPa)	% Elongation at break
HMS PP	20	231	237.81
HMS-PP/EVA(60/40)	15	102	312.64
HMS-PP/EVA/CLAY(60/40/7)	21	147	569.98
EVA	17	10	899.82

Table 4.2 : Mechanical properties of PP/EVA blend with and without clay.

Property	HMS-PP/EVA(60/40)	HMS-PP/EVA/CLAY(60/40/7)	% INCREASE
Modulus (MPa)	15.23	20.78	36.41%
Tensile strength(MPa)	102.22	147.32	44.1%
% Elongation	312.64	569.98	82.3%

Table 4.3 : Comparison of mechanical properties of PP/EVA blend with and without clay

The absence of compatibility between the blend components would result in reduced interfacial adhesion which is turn will lead to reduction in mechanical properties. The addition of clay to the blend does improve the mechanical properties of the system since clay migrates to the interphase and also to the bulk phase (167). The presence clay at the interphase with intercalation of the clay galleries by both the blend components does provide a possible evidence of improved compatibility at the interphase.The presence of organoclay in amounts greater than the quantity required for saturation of the interphase results in dispersion of clay in the component phases, which changes the morphology and the mechanical behaviour of the blend (168).The reduction in the size of the dispersed phase (169) as compared to the pure blends causes improvement in the mechanical properties of the blends. This improvement could be attributed to a sort of homogenization introduced in the blend system by the addition of clay particles.

The improved modulus and elongational properties can be attributed to the reinforcement provided by the clay particles by shear transfer to the clay particles during stretching of the samples(170). As shown, the blends with clay follow the linear mixing rule for (171) all the properties and show positive deviations in case of the percent elongation. The presence of positive deviation indicates a partial compatibility between the blend components(172). Also the relatively high increase in percentage elongation for the blends with clay particles does indicate a molecular level interaction between the blend components because if there is no interaction between the blend components then the failure under applied stress or load will occur relatively quickly due to incompatibility and generation of stress concentration areas within the system causing failure which will further lead to negative deviation as compared to the pure component(173).

4.3.5 SEM Images

As shown by the SEM images (Figure 4.9) the pure blends are incompatible and immiscible but with the addition of clay the size of the dispersed phase has reduced. The average size of the dispersed phase in the pure blend is around 3.38 μm and in the case of a blend with clay particles it is around 0.511μm(figure 4.8). Thus there is a significant size reduction in the size of the dispersed phase domains of around 84%. An image analysis technique was used to measure the size of the dispersed phase as shown in Figure 4.10 and Figure 4.11, statistical analysis results are shown in table 4.4. The image was sampled from five different zones with 10 sample points from each zone to determine the distribution of the dispersed phase within the blend. The distribution is skewed to the right for pure as well as the blends with clay particles.

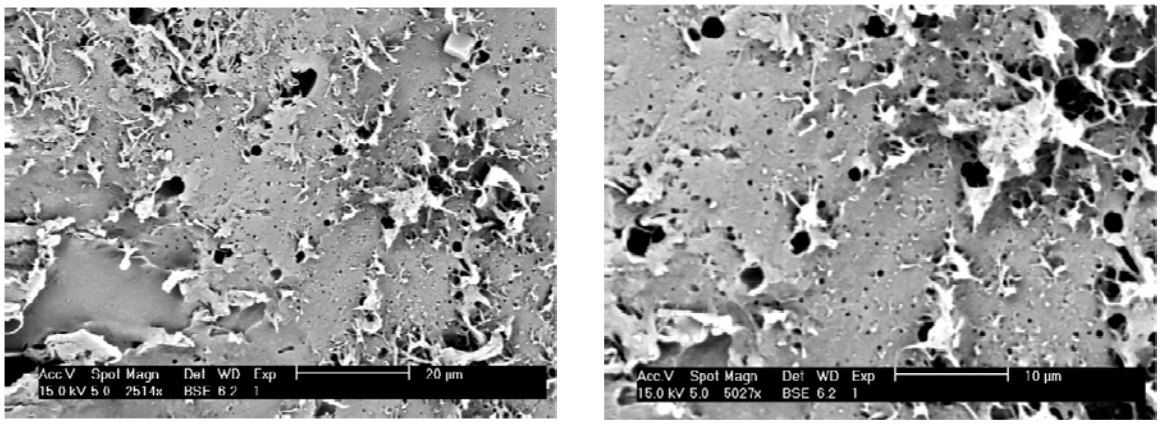

Figure 4.8 : SEM images of PP/EVA /clay (60/40) with 7 % clay at different magnifications.

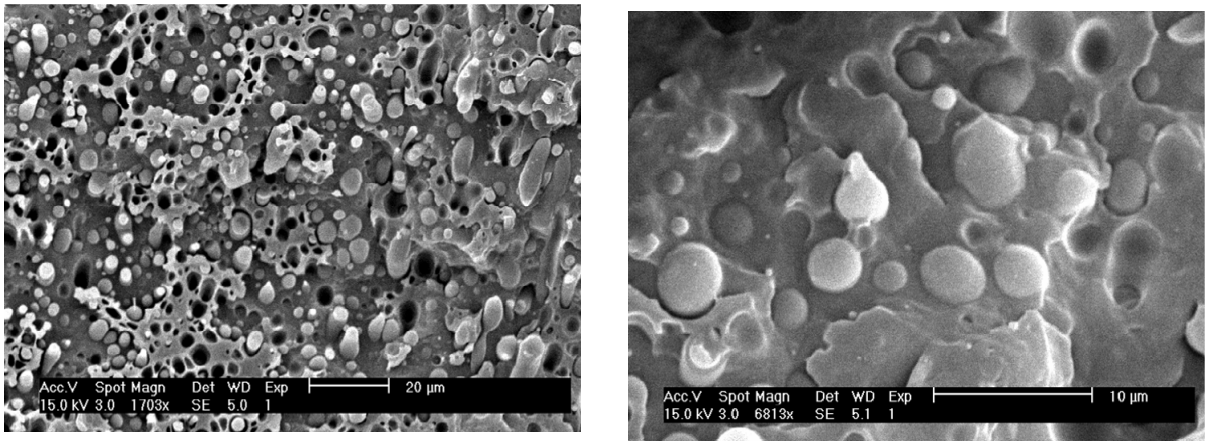

Figure 4.9 : SEM image of PP/EVA blend (60/40) at different magnifications

	HMS-PP/EVA /60/40 (μm)	HMS-PP/EVA/CLAY/60/40/7 (μm)
Mean	3.38	0.51
Median	3.299	0.42
Mode	3.50	0.141
Standard Deviation	1.185	0.36
Skewness	0.57	2.54
Kurtosis	0.19	9.05

Table 4.4 : Size distribution in μm of dispersed phase in pure and blends with clay particles

The distribution is more scattered in case of the pure blend but is significantly skewed in the right in case of the blend with clay particles indicating that the non homogeneity in the size of the dispersed phase has reduced in case of blends with clay particles. Also a very high value of kurtosis for the blend with clay particles denotes that the distribution of the size is more concentrated and more peaked as compared to a normal distribution with almost 95% of the distribution curve lying within two standard deviation. Overall there is a 50% reduction in standard deviation for the blends with clay particles as compared to the blends without them.

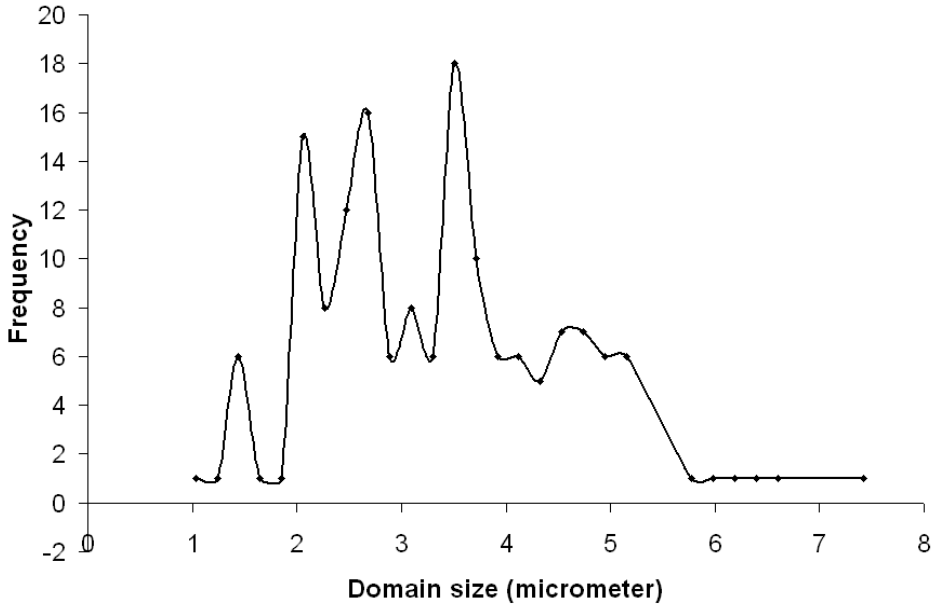

Figure 4.10 : Domain size distribution for PP/EVA (60/40) pure blend

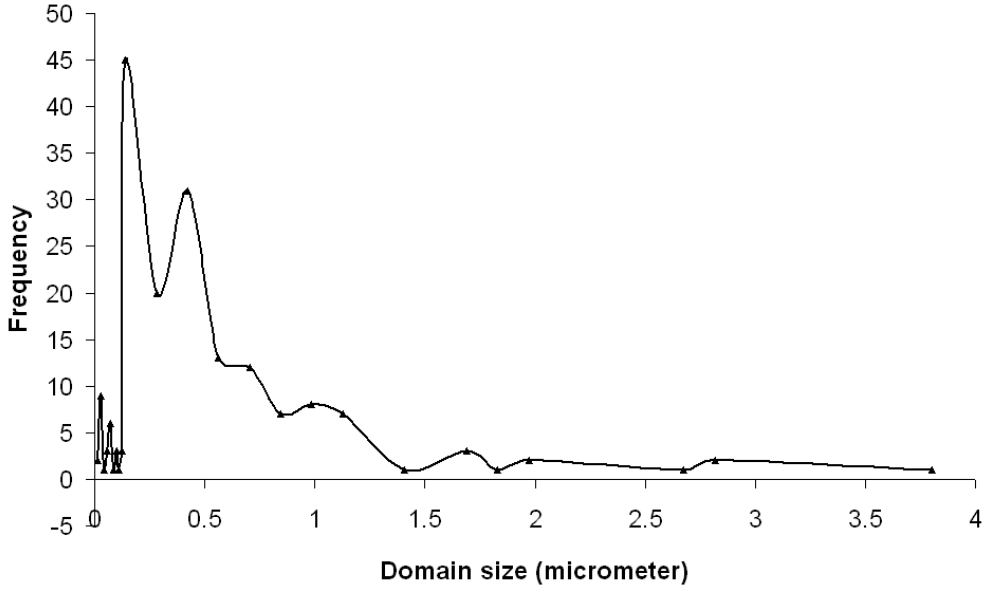

Figure 4.11 : Domain size distribution for PP/EVA/clay (60/40/7) nanocomposite blend.

4.3.6 Thermal analysis

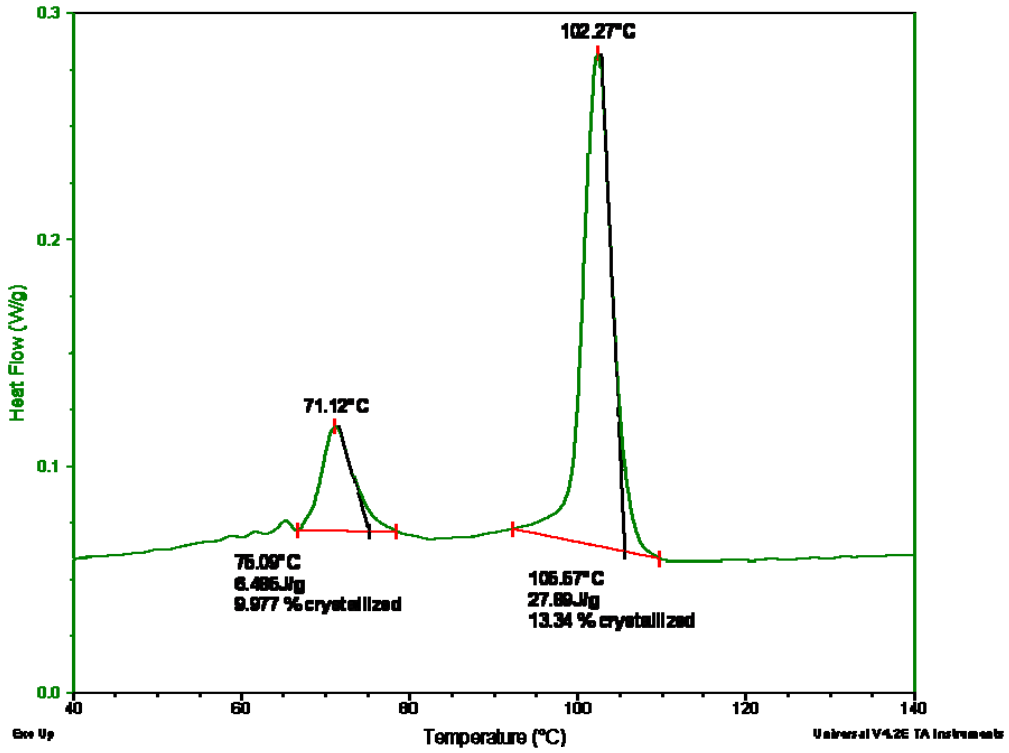

Figure 4.12 : Crystallization peak for pure PP/EVA blend (60/40)

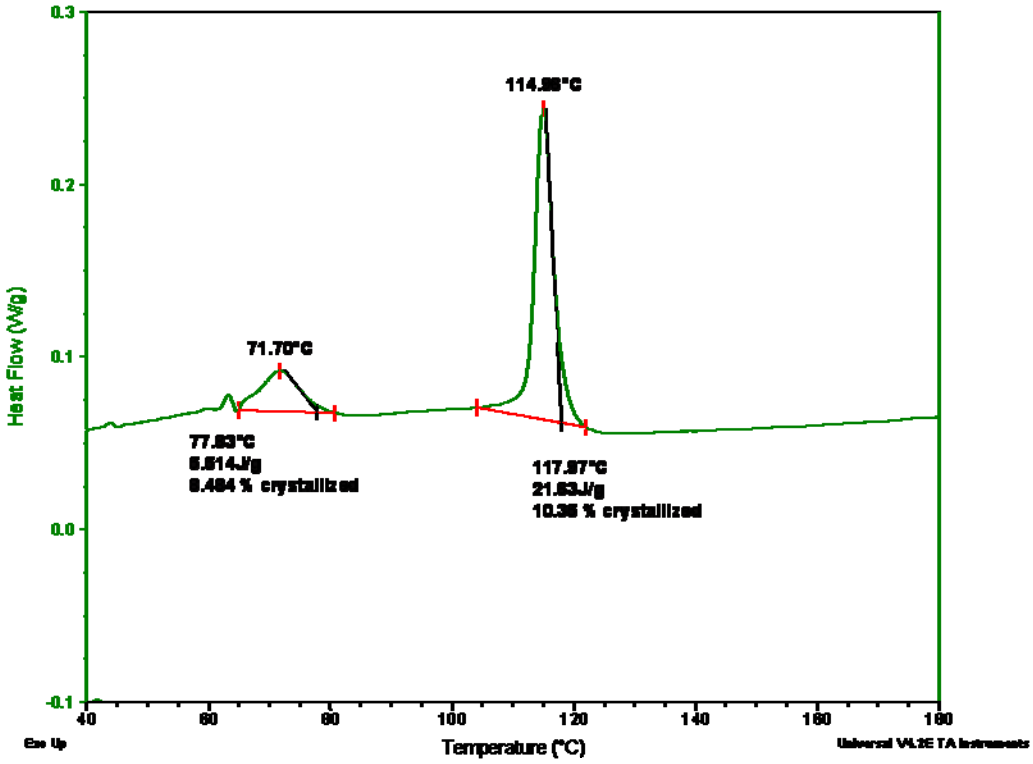

Figure 4.13 : Crystallization peak for PP/EVA blend with 7 % clay

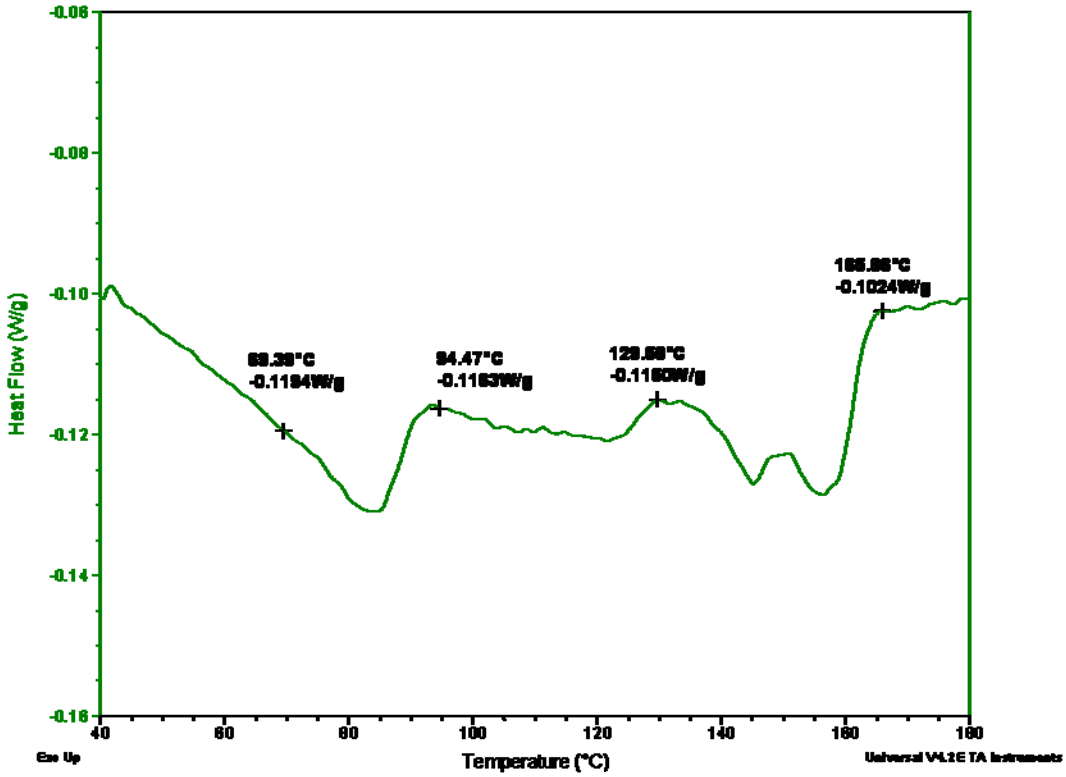

Figure 4.14 : Melting peaks for pure PP/EVA blend (60/40) with clay

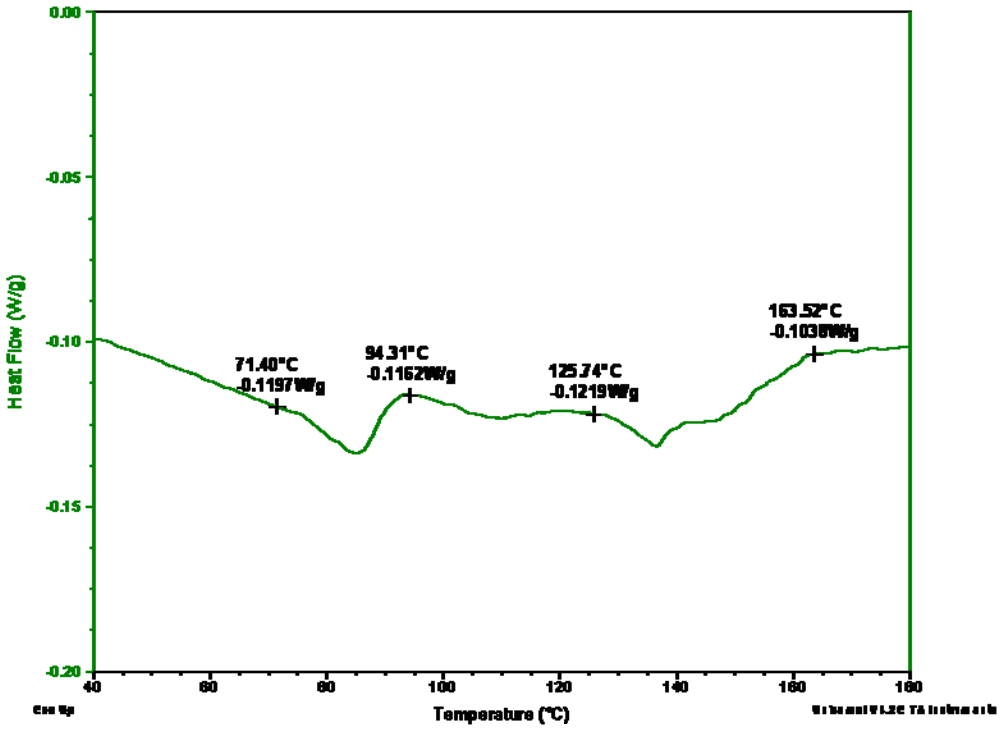

Figure 4.15 : Melting peak for PP/EVA blend (60/40)

Sample Name	Crystallization temperature (^{0}C)	Melting temperature Range (^{0}C)	Percentage crystallinity
HMS PP	102.87	125.26- 164.05	19.20%
EVA	70.66	71.42 – 95.21	44.22%
HMS-PP/EVA (60/40) (EVA phase)	71.12	71.40-94.31	9.977%
HMS-PP/EVA(60/40) (HMS-PP Phase)	102.27	125.74 – 163.52	13.34%
HMS-PP/EVA/clay(60/40/7) (EVA phase)	71.70	69.39 – 94.47	8.484%
HMS-PP/EVA/clay (60/40/7) (HMS-PP phase)	114.96	129.58 – 165.86	13.34%

Table 4.5 : Differential Scanning Calorimetry (DSC) results for HMS-PP, EVA and HMS-PP/EVA blends

The melting and crystallization behaviour of the blends and the blends with clay particles were studied in a Perkin Elmer DSC -6 under a nitrogen atmosphere with samples sealed in Aluminium pans and weighing between 5 – 10mg. The crystallization and the melting behaviour of the blend components were studied to determine compatibility of the blends. The crystallization temperature of HMS-PP and that of EVA decreased by around 1 degree each after combination of the blend components (figure 4.12) suggesting that the crystallization of both the blend components is suppressed by blending them(174). Table 4.5 reports the thermal analysis results for the HMS-PP/EVA blend system. Similarly in the case of blends with clay particles (Figure 4.13) the crystallization temperature increased by about 1 degree for the EVA phase and increase by about 12 degrees for the HMS-PP phase. The melting and crystallization temperature depression or change is normally associated with miscibility(168). The relatively high increase of crystallization temperature of the HMS-PP phase after addition of clay particles suggests that the

clay particles affect the crystallization of HMS-PP more than that of EVA in a blend of HMS-PP/EVA. This could be partly attributed to the nucleation effect of clay particles causing crystallization early in the DSC cooling cycle (169), The relatively higher increase in the crystallization temperature of HMS-PP phase after addition of clay particles suggests that the clay particles have a greater effect on the nucleation of crystals in the HMS-PP phase but as such affects the crystallization of both the phases. The relative decrease in the size of the crystallization peak as indicated by the presence of negative deviations (177) in heat of fusion after the addition of clay beyond the scaling law (for a 60:40 blend) and the heat of crystallization for both the blend components with clay as compared to the pure system, suggest a partial amount of co crystallization of the blend components which is a sign of partial compatibility(178).

The decrease in the melting temperature (168) ranges of the blend components after addition of clay particles as compared to the pure blends (Figures 4.14 and 4.15) suggests that the molecular weight distribution of the blend components changes after addition of clay particles causing a change in the melting range of the blends. Thus there is a possible interaction of the blend components at the molecular level after addition of clay particles. The increase in the melting temperature range of the EVA phase and that of the HMS-PP to the higher side indicates a probable case where the lower molecular weight fractions of the HMS-PP phase interact with that of the EVA phase. This causes an increase in the EVA melting range and a decrease in the HMS-PP melting range. Thus clay particles result in an interaction of the lower molecular weight fractions between the two blend components.

The presence of double melting peaks caused by addition of a nanofiller (figure 4.15) or clay particles has been generally attributed to recrystallization during the heating cycle. The crystallization process during the cooling phase is incomplete and as a result during the heating cycle a recrystallization occurs producing a secondary melting peak at a lower temperature. This behaviour is attributable for slower crystallization rate for some crystals during the cooling cycle. This lower rate doesn't allow the crystals to reorganize quickly and hence a metastable phase is generated once the polymer solidifies. Now during the heating cycle with increase in temperature the polymer chains acquire greater mobility providing freedom to metastable crystals to reorganize and recrystallize producing a smaller secondary melting peak.

4.3.7 Steady shear and dynamic rheology:

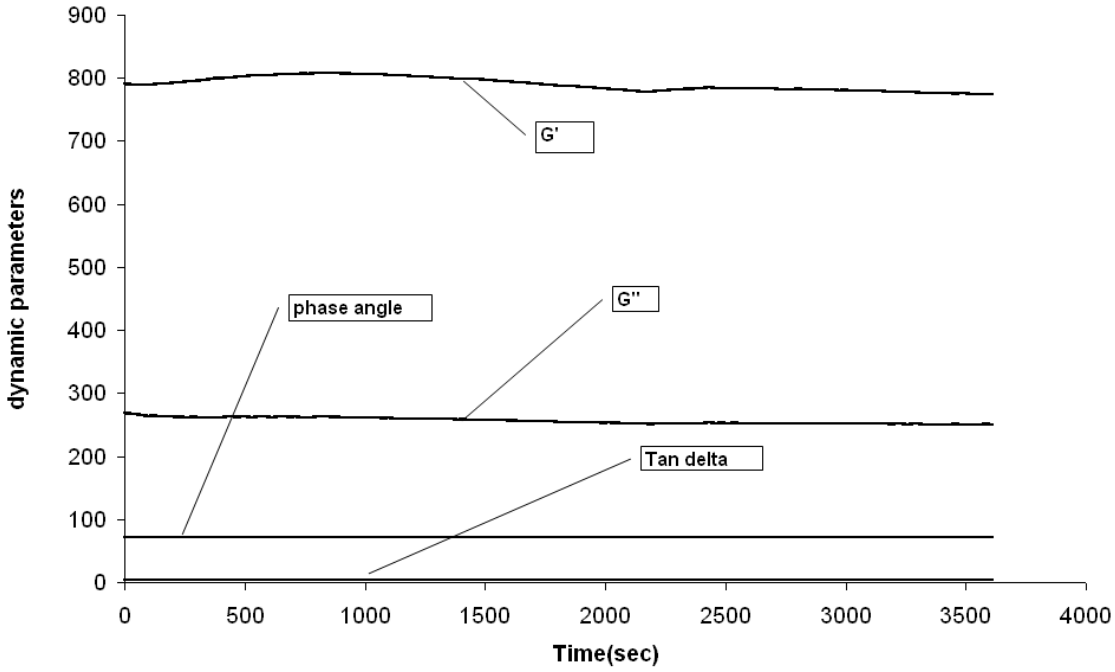

Figure 4.16 : Time sweep test for pure PP/EVA blend (60/40)

The time sweep behavior for the blends was studied at a frequency of 0.1 rad/sec (figure 4.16). It was observed that there is not a very significant change in G' and G" even after an elapsed time period of one hour and hence as such the blend components do not undergo degradation at the desired temperature of 190^{O}C even after one hour.

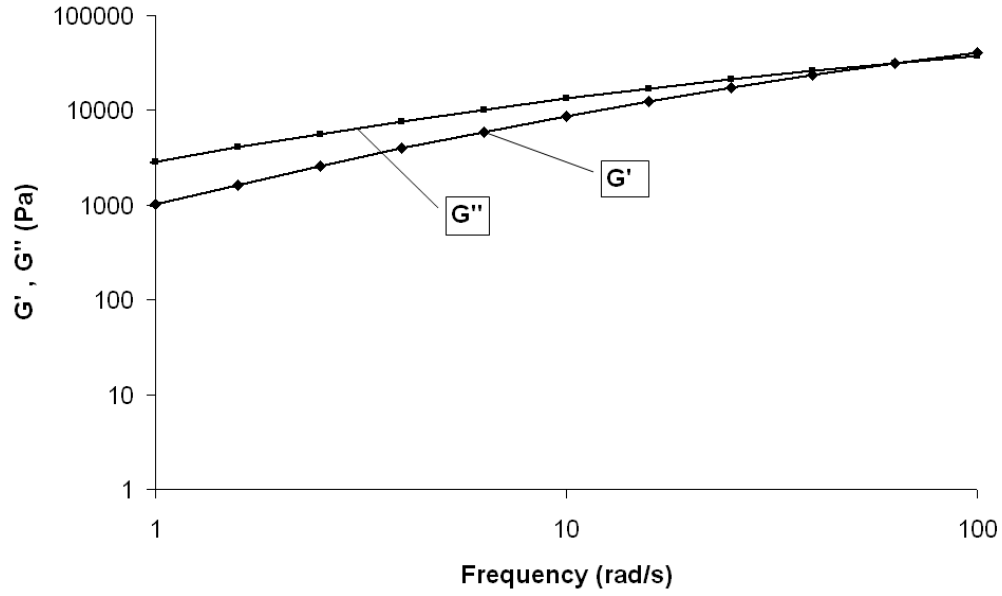

Figure 4.17 : Dynamic material functions for the pure PP/EVA blend (60/40)

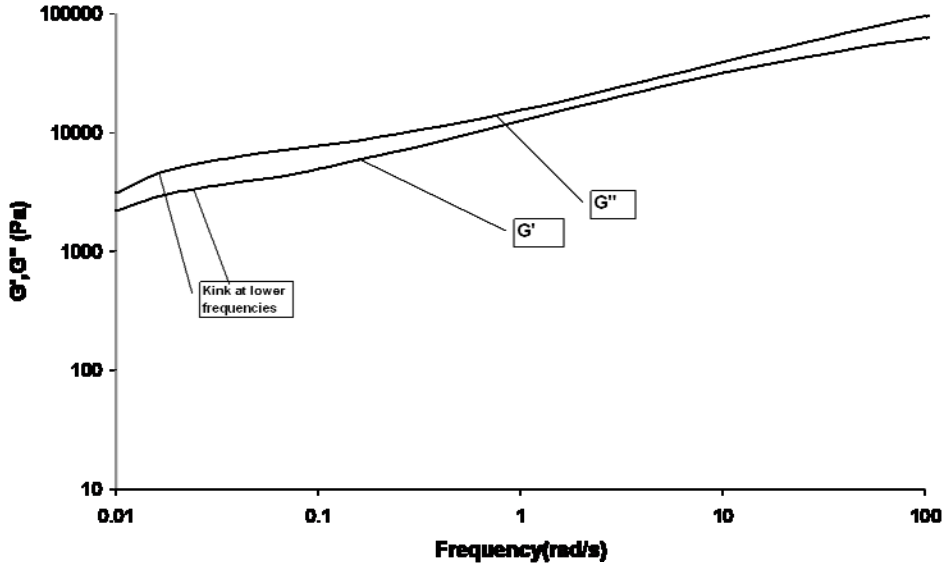

Figure 4.18 : Dynamic material function for PP/EVA blend (60/40) with 7% clay

Figures 4.17 and 4.18 show the dynamic behaviour of the pure blend as well as the blend with clay particles, both the blend show a deviation from the standard behaviour

as proved by the absence of the typical 2 and 1 slope (for G' and G" respectively) behaviour for miscible blends. Also the polymer blend system with clay particles shows a secondary plateau region at lower frequencies which can be attributed to a solid like behavior in the polymer blend system generated by the addition of clay particles. At lower frequencies a typical kink develops in the curves of G' and G" respectively. The increase in elasticity of incompatible polymer blends at lower frequencies can be interpreted in context of the emulsion models (2). The curvature in G' and G" at lower frequencies can be attributed to the relaxation of the dispersed phase as per the emulsion models(179). It can be seen that the curvature is higher for the case of blend with clay particles (figure 4.18). This could be attributed to the decrease in size of the dispersed phase since at lower frequencies at decreased dispersed phase size the number of dispersed phase domains per unit volume of the blend matrix increases causing a increase in the relaxation time and hence a subsequent increase in the amount of curvature at lower frequencies(180)

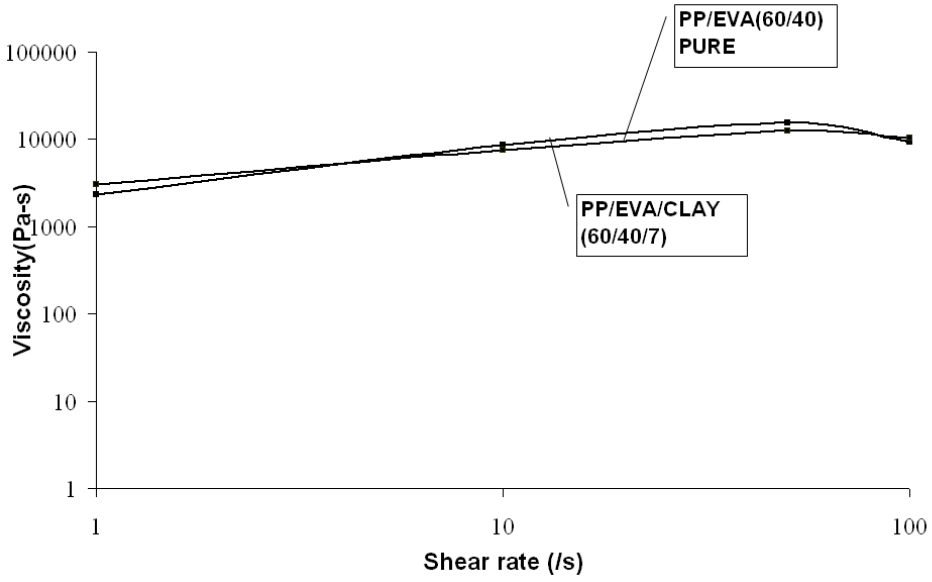

Figure 4.19 : Steady shear viscosity plots pure PP/EVA (60/40) blend and blend with 7 % clay

As shown in Figure 4.19 the shear viscosity only increases by a small amount around 5 % due to the addition of clay particles at higher frequencies, that means reduction in the size of dispersed phase is just not due to increase in viscosity but also due to the partial compatibilization caused by the clay particles (173). Higher frequencies are considered to take into account the shear rate existing within the extruder while processing the polymers since the viscosity of the system plays an important role in controlling the size of the dispersed phase while mixing. The pure blend as well the blend with clay particles show a strong characteristic shear thinning behavior with increase in frequency. The viscosity profile doesn't show terminal zone behavior at lower frequencies like for the case of pure polymers which could be attributed to the addition of clay particles to the system.

The blends of HMS-PP/EVA as such are immiscible. Addition of clay to the blends improves the compatibility between the two components partially due to migration of clay particles to the interphase as shown by the TEM analysis. Also the thermal analysis of the blends sample indicates a change in the melting range on addition of clay particles hinting towards an interaction between the lower molecular weight chains of the two blend components. The crystallization peaks reveal the presence of clay in both the phases but a higher interaction with the HMS-PP phase thus providing evidence for the fact that the enthalpic interactions between the blend components and the clay particles do affect the location of clay particles within the blend. The decrease in the percentage crystallization on addition of clay and change in heat of fusion more than the linear mixing rule suggest that there is a possible interaction between the two phases in the crystallization temperature ranges. The steady shear rheology tests reveal that the zero shear viscosity or the matrix viscosity changes only

by a small amount on addition of clay particles and hence the reduction in the size of the dispersed phase cannot be only due to increase in matrix viscosity. Also the increase in elasticity at lower frequencies can be attributed to the relaxation of the dispersed phase using the emulsion models and subsequent size reduction of the dispersed phase on addition of clay.

4.4 Foaming behaviour of PP/clay nanocomposites

Polymer foams have found application in multitude of industries over the years due to their improved properties such as light weight, high impact strength, and improved insulation properties. The cell size and the morphology of the foam (open, closed cell, shape of cells) in turn control the enhancement in properties. The processing window for foaming of linear polyolefin's (e.g. linear polypropylene) is small due to limited strain hardening behaviour exhibited by these polymers to withstand stretching during bubble growth. Also the presence of a sharp melting point and the semi crystalline nature of polypropylene makes it further difficult to foam such polymers. Linear polyolefin's like Linear Polypropylene have low melt strength and elasticity resulting in poor foam structure(181). But linear polymers tend to have better nucleation rates as compared to branched polymers as indicated by higher cell density in case of linear polymers. The possible reason could be that branched polymer have shorter chains and hence lesser free volume available for nucleation as compared to linear polymers (182) which reduces the survival rate of micro voids and therefore impedes nucleation. On the other hand a more stable, closed and homogenous cell structure is developed in case of branched polymer due to improved melt elasticity and extensional viscosity(183). Further the branched polymers have a broader melting range as compared to linear polymers improving the processing window for such

polymers. The homogenous nucleation process inside unfilled polymers results in foams with large cell sizes and non uniform distribution thereby limiting the possible enhancement in properties. The branching of polymers, addition of a co-polymer, blending of linear and branched polymer (184) and addition of nano filler are some of the techniques used to improve the extensional viscosity, melt strength and the nucleation efficiency within the polymer in an attempt to generate better foams. Hence the above discussion leads to the conclusion that a branched polymer with filler would be the best option for the production of fine cell foams and hence high melt strength Polypropylene (HMS-PP) nanocomposites would be a suitable material to be used to generate fine cell foams.

Considerable amount of work has been devoted to the generation of foams characterized by smaller cell sizes and narrower distribution specifically in production of sub microcellular and nanocellular foams(185-187). The foams with reduced cell sizes have been found to provide improved mechanical and insulating properties as compared to the larger microcellular foams. The addition of a filler to improve nucleation rate propelled by the low energy of activation required in heterogeneous nucleation does provide a way to generate sub micron and nanocellular foams(185). The internal structure of the material and its rheological characteristics play an important role in determining the potential of a polymer to be used in making fine cell foams (188). Hence the production of fine cell foams is dependent on the polymer structure, its rheological behaviour, the effect of filler and careful control of processing conditions.

In this study high melt strength polypropylene nanocomposites, PPNC/Cloisite 20A (clay) with exfoliated and intercalated morphologies were prepared and subsequently foamed in a batch setup under different foaming conditions. The foaming parameters

were varied to relate the foam cell structure to these parameters and determine the efficiency of clay in producing fine cell foams. The effect of clay dispersion on the foam cell structure was investigated by using TEM and SEM images. Also the correlation between the dynamic and extensional rheological properties on foam cell morphology was also studied. The use of DSC analysis helped in understanding the effect of addition of clay on the melting and crystallization behaviour of the polymer and their subsequent effect on foam structure

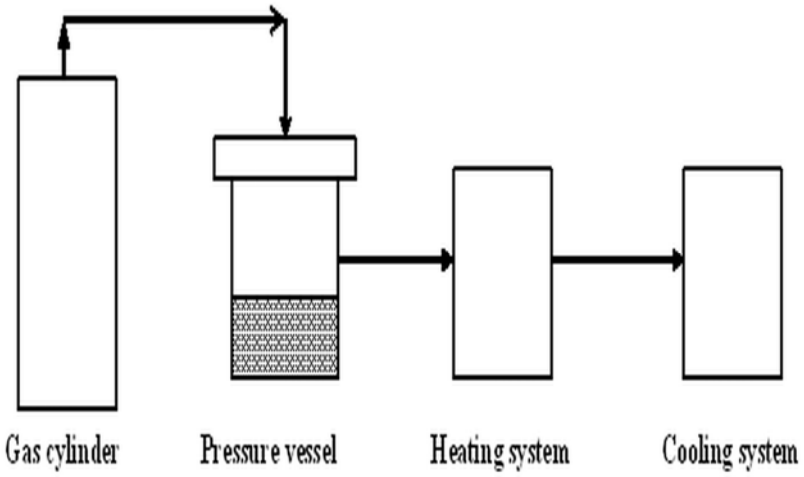

Figure 4.20 : Schematic diagram of the batch process used for foaming

As described above a batch foaming process (figure 4.20) was used to prepare the nanocomposites foams used in this study. All the polymer nanocomposites samples were saturated with the gas within the auto clave for a period of 12 -15 hours to attain equilibrium solubility at different saturation temperature and pressure. The subsequent depressurization of the sample led to supersaturation within the sample. The autoclave was then quickly dismantled and the samples were then foamed using a temperature superheat for the desired foaming time. Finally the foam samples were quenched using water with a variable quenching gradient as per requirement.

4.4.1 WAXD patterns

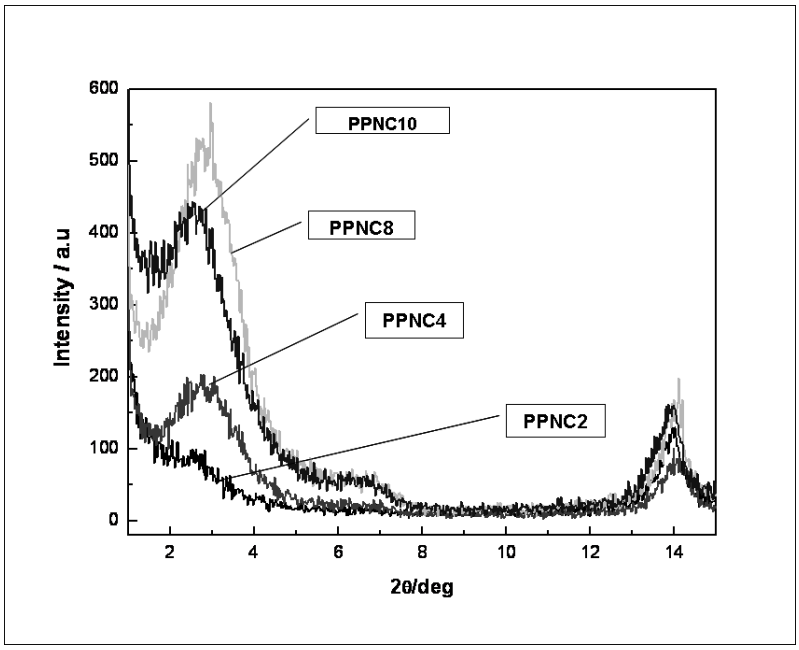

Figure 4.21 : WAXD patterns for PP/clay nanocomposites

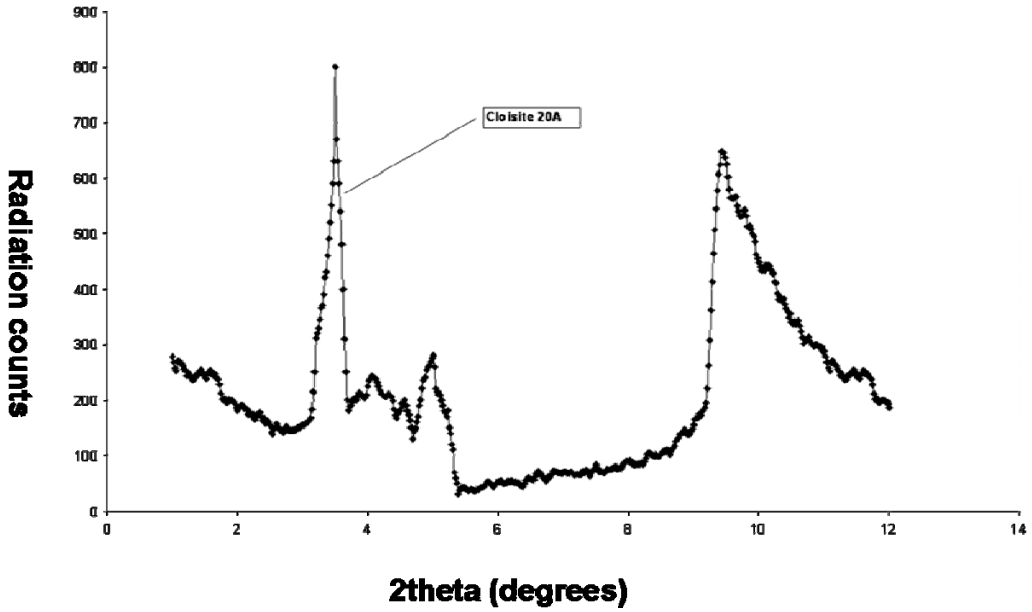

Figure 4.22 : WAXD patterns for cloisite 20A

	Type	dspacing (nm)
	Cloisite 20A	**2.521**
2wt% nanocomposites	**PPCN2**	**2.921**
4wt% nanocomposites	**PPNC4**	**2.883**
8wt% nanocomposites	**PPCN8**	**2.865**
10wt%nanocomposite	**PPCN10**	**2.845**

Table 4.6 : d- spacing for PP/clay nanocomposites

Figure 4.21 and 4.22 shows WAXD scattering curves of Cloisite 20A and PPNCs. The increase in *d (001)*-spacing (table 4.6) for the polymer nanocomposites relative to Cloisite 20A organo clay shows that the silicate layers have expanded because of intercalation of polymer chains into the gallery spaces. Also the shifting of the peak to lower angle indicates an increase in gallery spacing. A very small peak was detected for PPNC2 indicating an intercalated morphology but further verification through the TEM images is needed to verify these findings. The presence of a peak at lower angle as compared to clay indicates an intercalated structure for 4, 8 and 10 weight% nanocomposites respectively. This result needs to be verified further using TEM images since WAXD patterns just by itself donot provide sufficent evidence on the dispersion state of clay particles within the polymer samples(189).

The Braggs law equation given by ($n\lambda = 2d \sin \theta$) was used to calculate d spacing. The values of d-spacing are listed in Table 4.6. From the Table 4.6 it can be seen that the d (001) spacing reduced for 10 wt % clay loading as compared to other samples. This behaviour could be attributed to the fact that at higher clay loadings the interaction potential between clay particles increases and as a result the level of intercalation reduces although the changes in the d spacing is very small hence it can

be argued that the morphology for 4 , 8 , 10 wt % clay cocncentrations is nearly the same and all of these nanocomposites intercalate the clay galleries to the same extend.

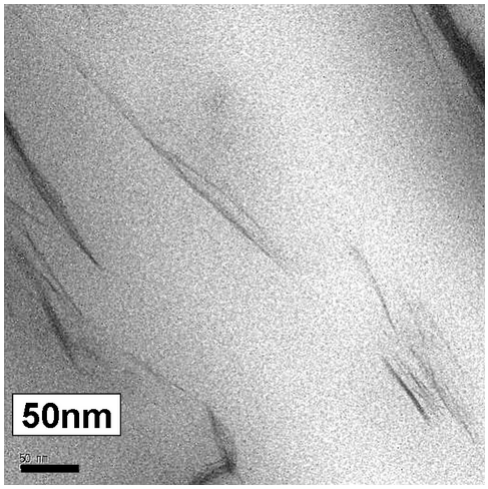

Figure 4.23 : TEM for PPNC2

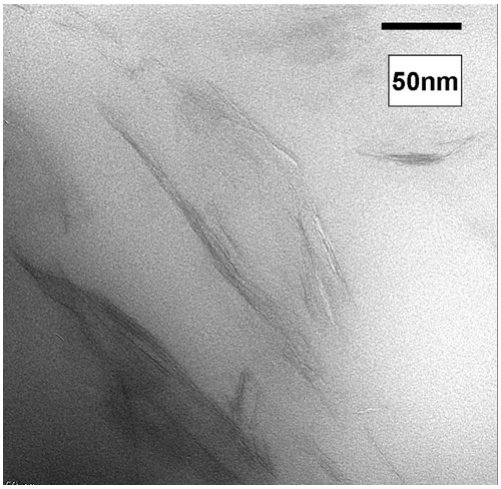

Figure 4.24 : TEM for PPNC4

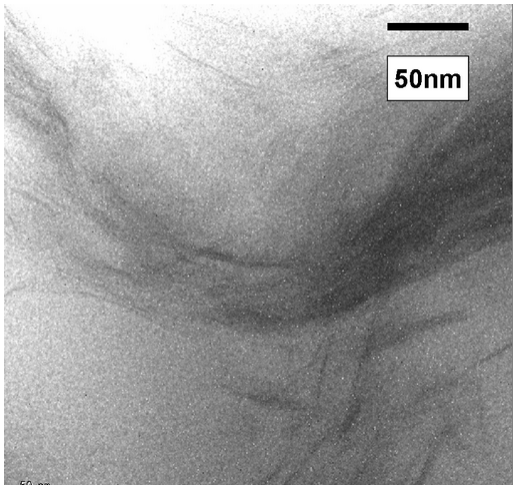

Figure 4.25 : TEM for PPNC8

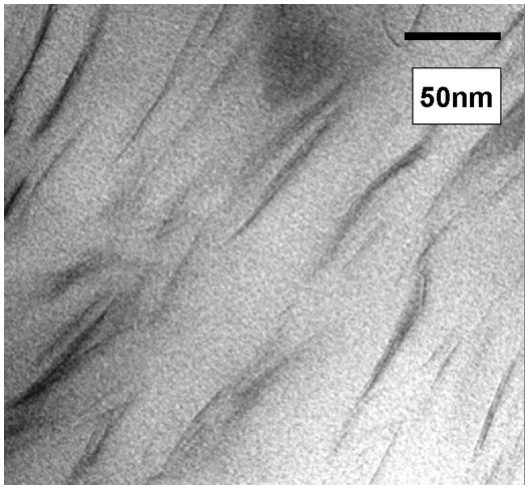

Figure 4.26 : TEM for PPNC10

TEM images reveal that the clay platelets are well dispersed within the polymer matrix. Figure 4.23 shows a random distribution of clay particles within the polymer matrix. Also individual clay layers are also visible showing that the clay platelets have completely separated into individual layers. In addition clay aggregates are also visible. Therefore it could be argued that a mixed morphology is established in case of PPNC2 as well. Similar observations can be made from Figure 4.24 and Figure 4.25 when coupled with the WAXD patterns providing evidence of intercalation of

polymer chains in clay galleries for PPNC4 and PPNC8 as well. Figure 4.24 also reveals that a mixed morphology is established in case of PPNC4 since the image shows a random distribution of the clay platelets. Further it can be concluded that an exfoliated morphology is not established even at lower clay (Cloisite 20A) loadings for PPNC. Figure 4.26 shows an ordered distribution of clay platelets within the polymer matrix; also clay aggregates are visible in certain places hinting an intercalated morphology for PPNC10. It would be interesting to try different types of clay (with respect to the organic modifier used) and variable amounts of compatibilizer in order to achieve exfoliation for these nanocomposites.

4.4.2 Thermal analysis

	Crystallization temp.(Tc) ^{o}C	Melting Peak (Tm) ^{o}C	Onset Point ^{o}C	Melting Range ^{o}C
HMS -PP	103.5	156.7	133.2	133.2 - 162.17
PPNC2	114.9	158.6	138.1	138.1 - 164.7
PPNC4	116.5	158.5	139.1	139.1 - 165.2
PPNC8	116.9	158.4	136.7	136.5 - 165.6
PPNC10	116.9	158.3	135.3	135.3 - 165.2

Table 4.7 : Thermal analysis of PPNC's

Thermal analysis was carried out on PPNCs to determine the effect of clay on the crystallization and melting temperature range. A Perkin Elmer DSC instrument was used to conduct the thermal analysis tests. The testes were conducted within a temperature range of -60 – 210 ^{o}C, with a temperature modulation of 0.5 ^{o}C per/5 min. The temperature in the DSC test was raised at 2 ^{0}C/min.

It was found that the addition of clay resulted in crystallization at a higher temperature in the cooling cycle. This effect could be attributed to the early nucleation of crystals

in presence of clay. The melting temperature range as compared to the pure sample was not affected much, although the peak melting temperature was altered in presence of clay (190). This effect could be associated with the restricted chain mobility in presence of clay causing an increase in peak melting temperature. Table 4.7 summarizes the DSC results for HMS –PP and PPNC for different amounts of clay.

4.4.3 Foam processing

HMS-PP and PPNCs were foamed at different temperature within the melting range specified in the DSC results and just above it as well. The foaming temperature choice is based on the premise of reduced but sufficient melt viscosity to sustain nucleated cells and produce closed cell foams (184). As the foaming temperature increased beyond the melting point the rate of cell coalescence increased and foam with bigger cell size was produced. The smallest foam cell sizes were achieved within the melting range just near the end of melting peaks.

The expansion ratio (v_a) of each sample was calculated as the ratio of bulk density (ρ_p) of the pure sample to bulk density of the foamed sample (ρ_f) as shown in equation (4.3) (192).

$$v_a = \frac{\rho_p}{\rho_f} \qquad (4.3)$$

The void fraction of the foam samples was calculated on the basis of the bulk density of the foamed sample (ρ_f) to that of the unfoamed sample or pure sample (ρ_p).

The cell population density was calculated using the number of cells per unit volume with respect to the un-foamed polymer. The number of cells (n_b) is determined for a selected area (l^2) in the SEM images and the value is extrapolated to total number of cells per cubic centimetre using equation (4.4) (192)

$$n = \left(\frac{n_b}{l^2}\right)^{3/2} * 10^{12} * v_a \qquad (4.4)$$

The average cell wall thickness is calculated using the foam cell diameter determined from the SEM images using equation (4.5)

$$\delta = d\left(1/\sqrt{1-(\rho_f/\rho_p)}-1\right) \qquad (4.5)$$

Alternatively the cell population density can also be determined from the foam cell diameter determined from the SEM images and using the bulk density of the foamed sample and the pure polymer respectively. The calculation using both the methods is presented in this paper. Equation (4.6) used to calculate cell population density is given below (192)

$$n = 10^4\left(1-(\rho_f/\rho_p)\right)/d^3 \qquad (4.6)$$

A two stage batch setup technique is used to produce foamed samples since in a two step process the process of saturation and cell growth can be effectively separated and thus PPNC samples can be saturated with the blowing agent at different saturation pressures and temperatures and subsequently foamed. The production of fine cell foams is mainly governed by the foam cell nucleation and growth process. The other two processes (i.e. sample saturation and quenching of foams) are subsidiary methods to improve foam nucleation and control foam growth respectively. Consequently it is essential to know first the effect of the above mentioned processes on foam cell nucleation and growth so that the experimental design can be simplified.

4.4.4 Effect of processing parameters on foam structure

The HMS –PP and PPNCs were saturated in the autoclave under different saturation temperature and pressure respectively. Gas solubility studies using supercritical CO_2 have revealed that the highest amount of solubility is attained at lower temperatures and higher pressures respectively (193). The increase in the saturation temperature imparts increasing amount of kinetic energy to the gas molecules inside the polymer samples, which results in an increased tendency of the gas to escape from the polymer samples resulting in lower solubility and vice versa. Similarly the pressure of the gas used to saturate the polymer sample solubility increases due to increased potential energy of the gas molecules accompanied by the higher penetration power of the gas molecules. Interestingly the pressure differential generated during the subsequent depressurization of the sample is also higher at higher saturation pressure causing an improvement in the degree of supersaturation (188). Higher solubility of blowing agent within the polymer samples causes supersaturation at lower foaming temperature and improves the nucleation rate within the polymer sample since the nucleation rate is directly proportional to the amount of gas dissolved in the polymer due to the presence of a competing mechanism between cell nucleation and growth. The quicker super saturation of the sample at lower temperature also additionally increases the tendency of the gas to escape from the sample with an increase in the degree of superheat. All these factors when combined cause a reduction in foam cell size by reducing the amount of gas available for foam cell growth and nucleation.

The foaming temperature governs the rate of nucleation of foam cells in a foaming process (193). This can be explained by the fact that the free energy for nucleation is directly proportional to temperature and hence raising the temperature raises the free

energy of the gas towards the amount needed for conversion of sub critical micro bubbles into the supercritical state at a faster rate. The molecular diffusion rate is also increased with increase in foaming temperature favouring foam growth as well but interestingly the rate of nucleation is propelled by a higher degree since the net free energy needed to nucleate on a particle surface is lesser than the free energy needed to diffuse through a polymer film into the cells (185). As a result the overall rate of foam growth is partially retarded resulting in the formation of fine cell foams. At the same time the selected foaming temperature should not be too high as well since with increase in temperature the polymer chain mobility also increases and the melt viscosity reduces. The increased chain mobility reduces the rate of survival of individual micro voids within the polymer producing larger cells (198).

The rate of quenching of the polymer foam sample also affects the final cell size. The aim of the quenching process is to go below the glass transition temperature of the polymer. Since below the glass transition temperature the polymer would behave like a solid and so the foam cell walls would be strong enough to resist further cell growth. The rate of quenching controls the time available to the foam cells to keep growing and then stabilize subsequently. Thus a very low quenching temperature would increase the temperature differential between the foam sample and the quench fluid restricting the foam cell size (197). Application of a force balance helps in understanding the quenching process. The cell walls experience two different opposing forces during the quenching process. The growing bubbles tend to stretch the cell walls at the same time the cooling of the foam cells tend to contract them. In case of a high quenching rate the cell walls are not able to quickly respond to the abrupt change in temperature and relax which may cause foam collapse. Therefore the best quenching temperature is one where the contracting force on the cell walls is

exactly balanced by the stretching force acting on them. Alternatively another way would be to reduce the foaming time resulting in thicker cell walls right from the outset and then quench the sample very quickly to stop any further cell growth.

4.4.5 Selection of parameters for foam processing and experimental design

Saturation pressure, temperature, foaming temperature, foaming time and quenching temperature all affect the foam cell morphology. Consequently the design of experiments becomes intricate in studying the role of all the above mentioned parameters on foam processing. Now the addition of clay particles to the polymer samples further complicates the situation. For this reason a clearly defined experimental approach is needed to reduce the number of experiments required but at the same time it is important to study the effect of all the above mentioned parameters. Interestingly all the above mentioned parameters either affect cell nucleation or cell growth. Hence the two process variables are cell nucleation and cell growth. Cell nucleation and growth is mostly affected by foaming temperature. Saturation pressure and temperature affect the solubility level and degree of super saturation and are like supporting systems to improve cell nucleation. On the other hand foaming time and quench temperature are supporting parameters for foam growth. So, the major process variables that define the foam cell structure are foaming temperature and foaming time. Ideally the solubility of supercritical CO_2 is the highest when the saturation temperature is low and the saturation pressure is high (183, 186), both above the supercritical limits for CO_2. But the effect of temperature on solubility is not very profound till the point where the samples tend to change phase. This simplifies the experimental design. The idea is to first determine the foaming temperature range or

processing window for generation of closed cell foam for a polymer sample with a certain amount of filler loading. Once this is determined the next step is to vary the saturation pressure and foaming time for each sample and then determine the optimum values for these two parameters till the point where the cell size stops reducing further down. The quench temperature chosen for this system is room temperature for all samples since in actual foaming condition in a continuous process the quench temperature is the atmospheric temperature.

A box Benkhen design approach was used initially to determine the effect of processing parameters on foam cell morphology and also to perform optimization studies. The optimization process helped in identifying the range of operating conditions needed to minimize foam cell sizes. Saturation pressure and temperature and foaming time and temperature are the four processing variables used in these studies. The Box Benkhen approach resulted in overall 30 experimental runs

Sat pressure(MPa)	**Sat temp(^{o}C)**	**Foam temp(^{o}C)**	**Foam time(sec)**
17	46	170	20
14	57	152.5	30
17	46	152.5	30
17	35	170	30
14	35	152.5	30
17	46	135	40
17	46	152.5	30
17	57	135	30
17	46	152.5	30
17	46	152.5	30

20	46	135	30
17	57	152.5	20
20	46	152.5	40
17	57	170	30
17	46	170	40
14	46	152.5	40
20	46	152.5	20
14	46	152.5	20
20	35	152.5	30
17	35	135	30
14	46	135	30
14	46	170	30
17	35	152.5	40
17	46	152.5	30
20	46	170	30
17	46	152.5	30
17	57	152.5	40
17	46	135	20
20	57	152.5	30
17	35	152.5	20

Table 4.8 : Experimental runs using the Box Benkhen method

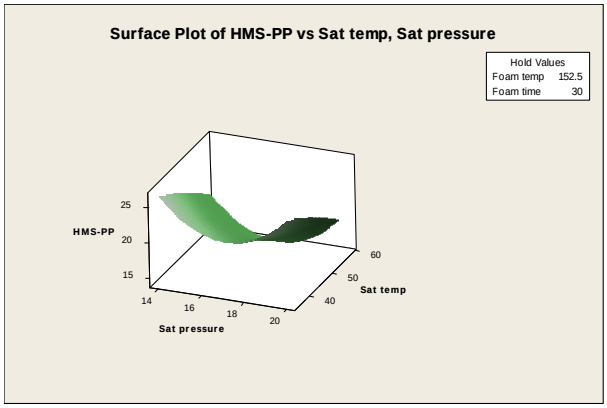

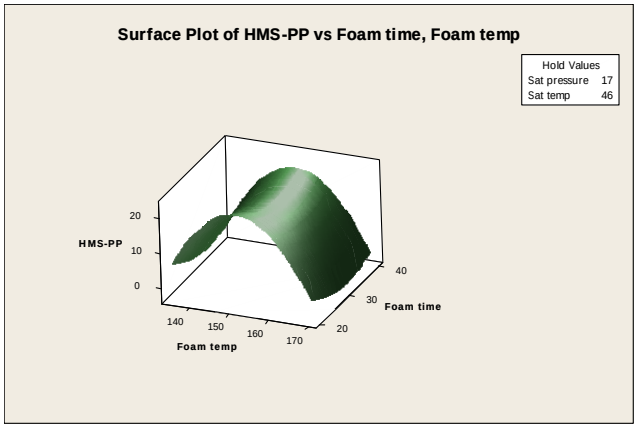

Figure 4.27 : Effect of processing parameters on HMS-PP pure foams (closed cells)

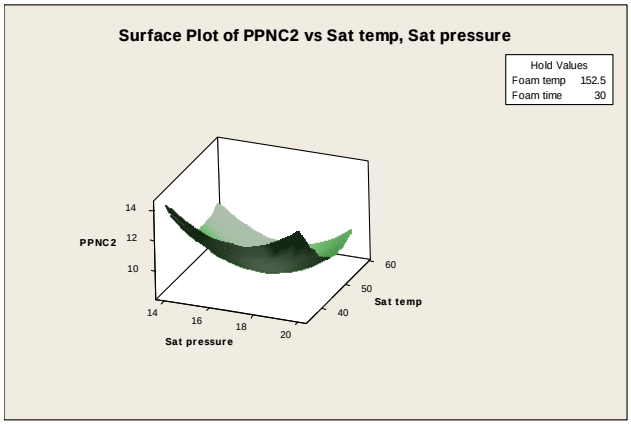

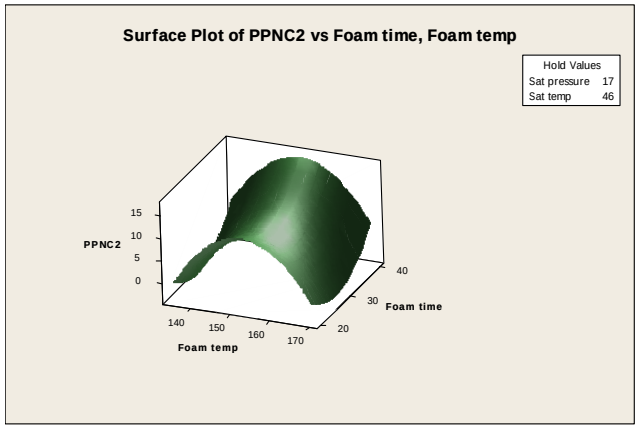

Figure 4.28 : Effect of processing parameters on PPNC 2 foams (closed cells)

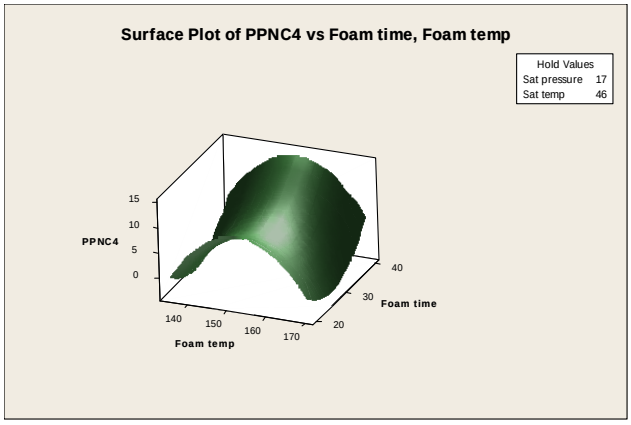

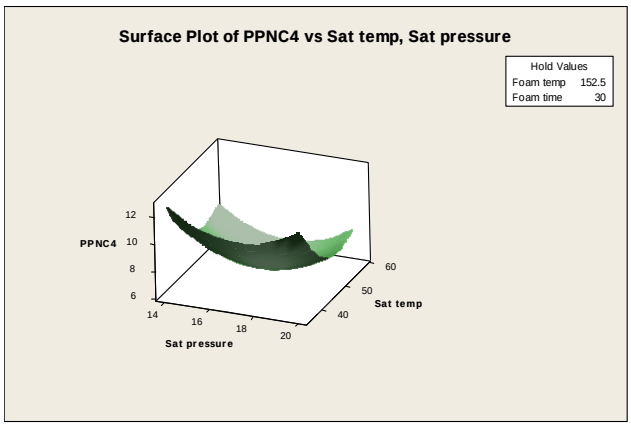

Figure 4.29 : Effect of processing parameters on PPNC 4 foams (closed cells)

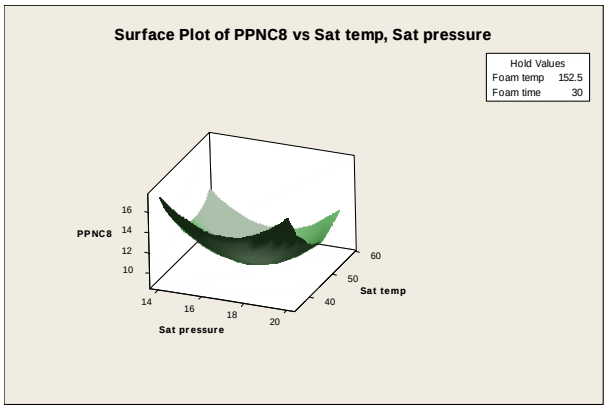

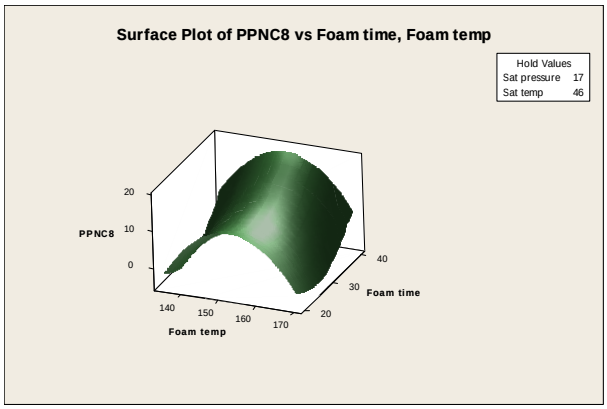

Figure 4.30 : effect of processing parameters on PPNC 8 foams (closed cells)

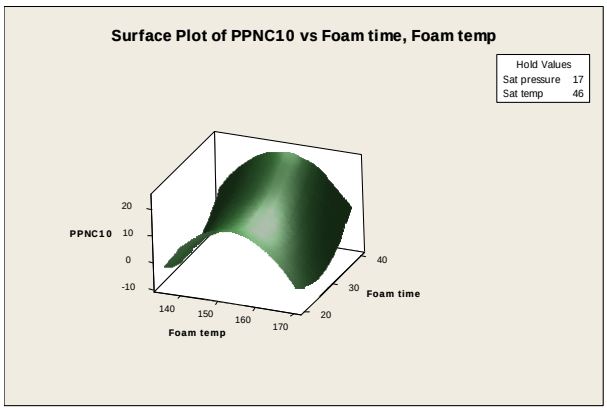

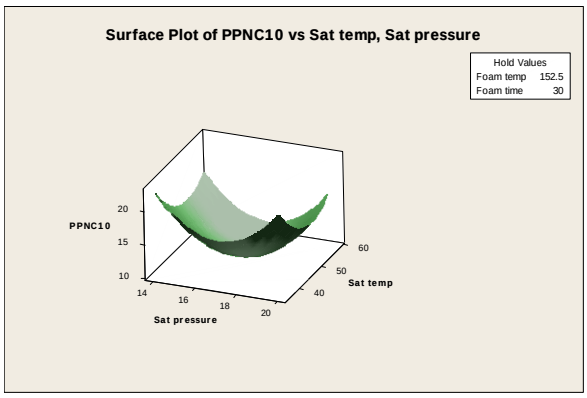

Figure 4.31 : Effect of processing parameters on PPNC 10 foams (closed cells)

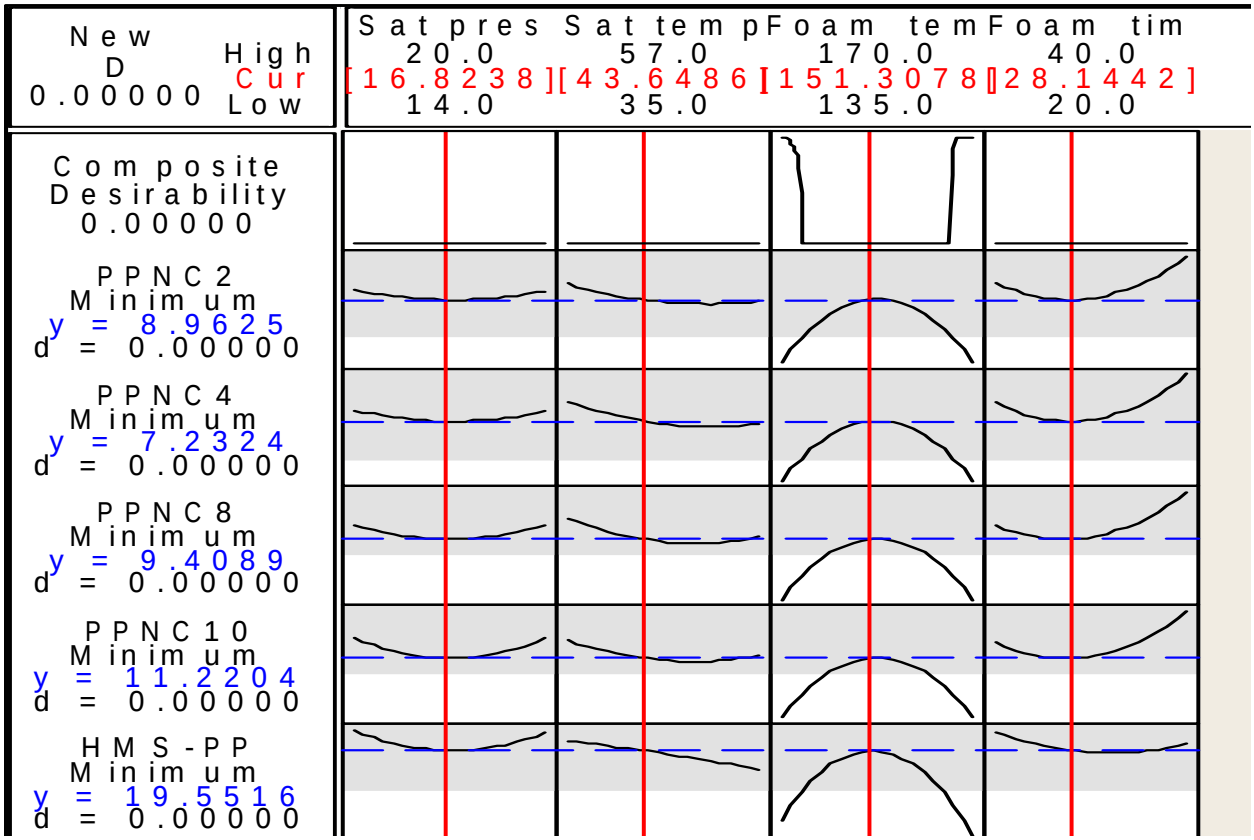

Figure 4.32 : Optimization of processing parameters using the Box Benkhen design approach for production of fine cell foams (closed cells).

It is evident from the surface plots (figures 4.27 -4.31) that the foam cell sizes (for closed cells) reduces with increase in saturation pressure and reduction in saturation temperature. Similarly the foam cell sizes also reduce as the foaming temperature is raised and the foaming time is reduced. The U shaped nature of all the surface plots reveals that there is an optimum condition at which smallest cell sizes would be generated. Since the foam cell size is a function of the foaming time, foaming temperature, saturation pressure and temperature, direct linear methods of optimization cannot be used to determine the optimum processing conditions for generation of fine cell foams. Hence a Langranges optimization algorithm is used to

determine the optimum processing conditions. The optimization is performed with respect to foam cell sizes. In other words the optimum points (singularities) in the surface plots are determined on the basis of the first derivative of all the mentioned process parameters with respect to foam cell sizes for determination of Eigen values. Eigen values are like scale factors which can shift a curve with a specific boundary curve proportionally without changing the optimization conditions. The foam cell sizes are inversely proportional to the foaming temperature and directly proportional to the saturation pressure, saturation temperature and foaming time as seen in the optimization plots (figure 4.32). The dependency of the foam cell sizes on saturation temperature changes trend on addition of clay particles as evident from the plots. Thus the saturation temperature is highly sensitive to the degree of clay concentration, when the aim is to reduce foam cell sizes. All other processing parameters have the same trends in presence or absence of clay except for changes in the overall gradient or slope. From the optimization plot (figure 4.32) (values in red) in the top of the table provide the optimum parameters for reduction in foam cell sizes. The first point of intersection between the blue lines (lines depicting boundaries for reducing foam cell sizes) and the parameter curves provide the optimum processing conditions for generation of fine cell foams with respect to each processing condition. The values of all the processing parameters were correct except for foaming temperature which was later found to be 147^{o}C instead of 151^{o}C.

Based on the above mentioned methodology (Box Benkhen approach), a wide range of foaming temperature for processing foams from 139 -170^{o}C were investigated with a one degree temperature gap. The saturation pressure used was also varied from 1800 -2700 psi. The processing window for generation of closed cell foam was found to be

around 143 -148^{o}C. Now different saturation pressure and foaming time combination was tried for the samples within the processing window with a minimum foaming time and saturation pressure used as per literature. Further the polymer samples were foamed beyond the processing window as well to understand the sensitivity of the foam cell structure to foaming time. It was found that beyond the processing window the variation in foam time always results in generation of open cell foams and high degree of cell coalescence. Table 4.9 shows the various processing conditions employed for production of polymer nanocomposites foams. HMS –PP and PPNCs were foamed at six different foaming conditions as shown in Table 4.9. When the foaming temperature is very close to the onset melting point, there is no foaming taking place although some amount of gas does dissolve into the sample which subsequently escapes from the sample with increase in temperature without the formation of foams. The sample viscosity is very high near to the onset of melting which results in no foam generation. Alternatively, in cases where the foaming temperature is very high (i.e. higher than the melting point) leads to high degree of cell coalescence and a partial collapse of the foam cells formed. The best foam structure is obtained when the foaming temperature is within the melting range but close to the higher end of the melting range used. The foaming temperature employed in case of a batch process needs to be such that the melt viscosity is high enough to restrict foam cell sizes and resist foam collapse but at the same time low enough for the initially nucleated cells to survive and grow. The rate of gas escape from the sample is also a function of temperature and increases with increase in foaming temperature. At higher gas escape rates foam cells get lesser time to grow and nucleation rate improves resulting in smaller cell sizes. Therefore the foaming

temperature employed is a balancing act with respect to cell nucleation rate and cell growth rate.

Case	Foam Temp (^{O}C)	Foam Time(sec)	Saturation Pressure (MPa)	Saturation Temp (^{O}C)	Visual observations
(1)	139	34	14.3	35	No foaming
(2)	159	30	16.3	42	Predominantly closed but larger cells foams
(3)	170	28	17.7	50	Foam collapse
(4)	149	25	18.6	57	Closed cell sizes crossover to micrometer region
(5)	146	30	16.3	42	Closed cell foam non uniform distribution
(6)	147	30	16.3	42	Closed nanocellular foams

Table 4.9 : Effect of processing parameters on foam cell morphology

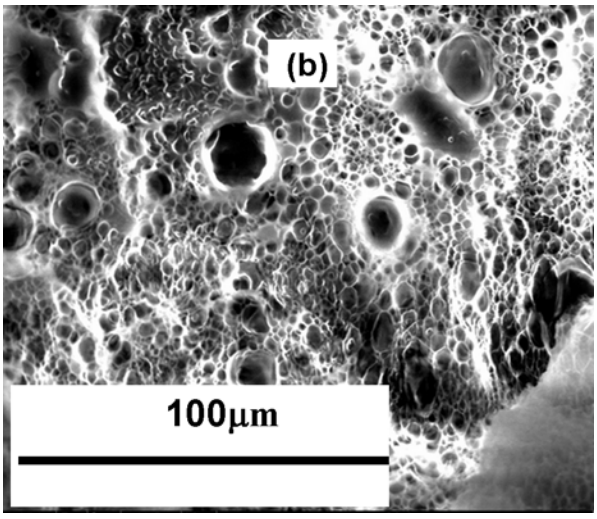

Figure 4.33 : SEM of HMS-PP foams case (6)

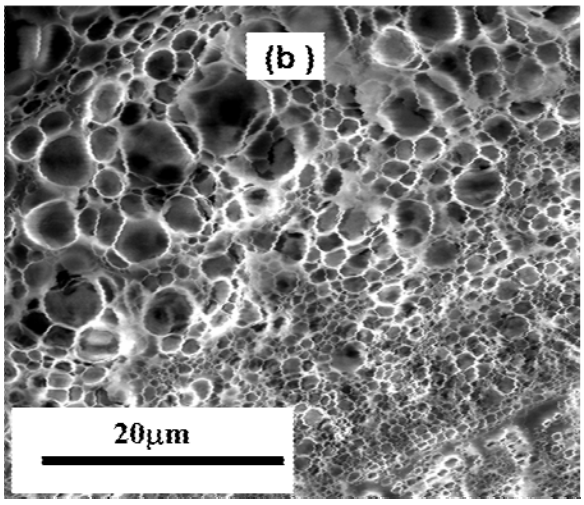

Figure 4.34 : SEM of PPNC2 foams case (6)

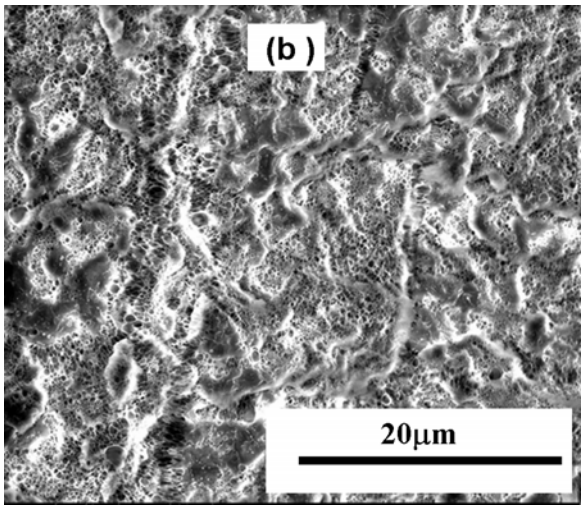

Figure 4.35 : SEM of PPNC4 foams case (6)

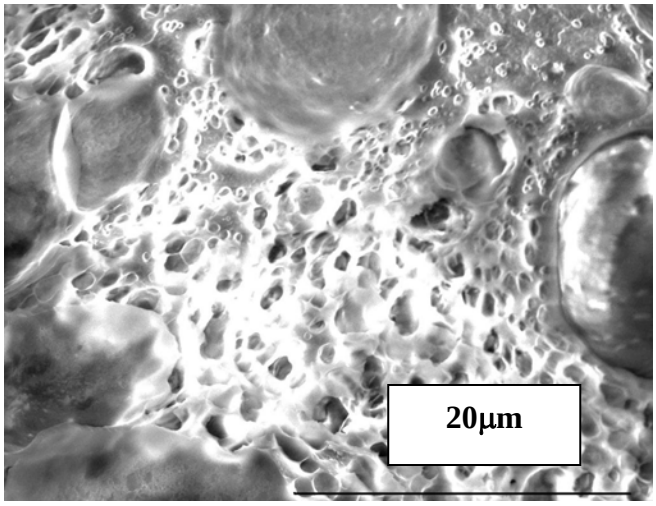

Figure 4.36 : SEM of PPNC8 foams case (6)

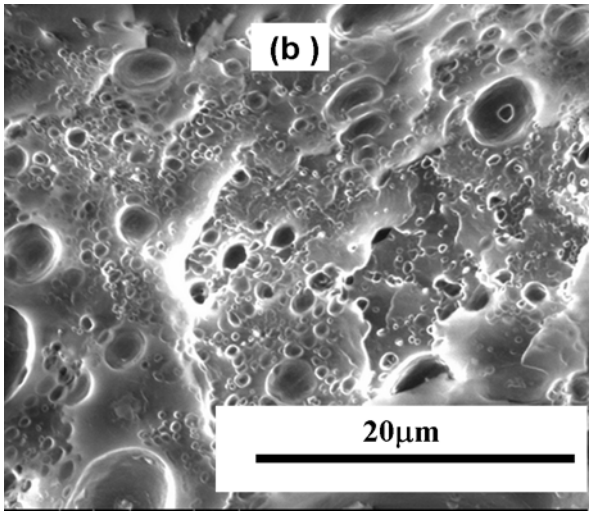

Figure 4.37 : SEM of PPNC10 foams case (6)

Figures 4.33 -37 and figures A-5 to A-24 (appendix A) shows the SEM images for the pure HMS–PP foams. The foam samples were freeze fractured using liquid nitrogen and subsequently the cross section of the samples were investigated using SEM. At very low foaming temperature there is no foaming (Figure A-5) although the image shows that the foam cells were nucleated but could not grow out due to very high melt viscosity of the samples. The subsequent increase of foaming temperature results in

production of foams but at the same time it can be seen that the cell size increases with increase in foaming temperature. The rate of cell coalescence also increase with foaming temperature (Figure 4.35 and Figure 4.36) as proved by the presence of larger cells at higher temperatures along with a non-homogenous distribution of cells. At temperatures beyond the melting point of the sample (Appendix A , figures A-5 to A-24)), SEM image indicates the formation of open cell foams with a high degree of coalescence. Thus at very high temperatures there is a partial collapse of the generated foams. The same can be true for the case of PPNC2, PPNC4, PPNC8 and PPNC10 foams also (Figures A-5 to A-24). The images also reveal that the cell sizes and foam structure vary with the percentage of clay loadings as well. The cell size initially decreases with increase in clay loading until the threshold of 4 wt % clay loading and then again starts increasing. At 10 wt % clay loading only open cell foam morphology is developed irrespective of the processing conditions used, in case of other samples though closed cell morphology is established when case 6 (Table 3) processing conditions are used. The images also reveal that the cell wall thickness increases with increase in processing temperature and clay loadings.

The cell number or cell density increases rapidly as shown in the (table 4.10 -4.14) in presence of clay particles. This effect could be attributed to heterogeneous nucleation in conjunction with homogenous nucleation occurring within the polymer matrix in presence of clay particles. The combined presence of both the nucleation mechanisms in presence of clay particles causes an increase in the cell density. The increased cell density counteracts the growth of foam cells and as a result a large number of small cells are formed resulting in the production of ultra microcellular or fine cell foams. The cell wall thickness increases with increase in foaming temperature. At higher foaming temperature the gas has a greater tendency to escape and since foaming was

done at atmospheric conditions using temperature superheat there is a significant amount of gas loss which restricts the foam cell growth to smaller sizes. The strain hardening effect of the polymer also adds on to restricting foam cell sizes and increasing the cell wall thickness. Interestingly the cell wall thickness first decreases with clay loading until 4 wt % and then again starts increasing with further increase in clay loading. The presence of an intercalated structure at higher clay loadings increases the amount of cell coalescence (198) since in absence of exfoliation the clay particles are not separated out into individual platelets, The ordered distribution of clay particles in the case of an intercalated morphology reduces the nucleation efficiency of clay particles since available surface area of clay particles in an intercalated morphology reduces, also the nucleation of cells on clay aggregates present in an intercalated structure causes cell coalescence and increases the foam cell size and results in a non homogenous foam cell distribution. Accordingly even if the cell density linearly increases with increase in clay loading propelled by the lesser free energy required for nucleation in presence of solid particles the cell size does tend to increase with increase in clay loadings. Due to this opposite trend between cell sizes and cell density in presence of clay particles only an optimum amount of clay can be used as a nucleating agent with the polymer matrix. The cell wall thickness is inversely proportional to the cell number or cell density (table 4.10 -4.14). A reduction in cell density causes an increase in cell wall thickness and vice versa (192). For a given volume of a polymer sample the increase in cell density causes a decrease in the volume of the polymer present between two nucleating foam bubbles. The subsequent strain hardening effect exhibited by the polymer at high stretching rates due to large number of cells nucleating simultaneously causes orientation of the filler material present within that volume (184). This further provides the strength to the

cell walls to resist any further cell growth and so the cell wall thickness is maintained at that value.

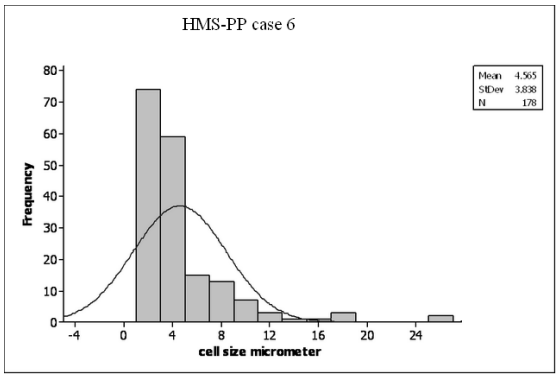

Figure 4.38 : Cell size distribution for pure HMS-PP foams case (6)

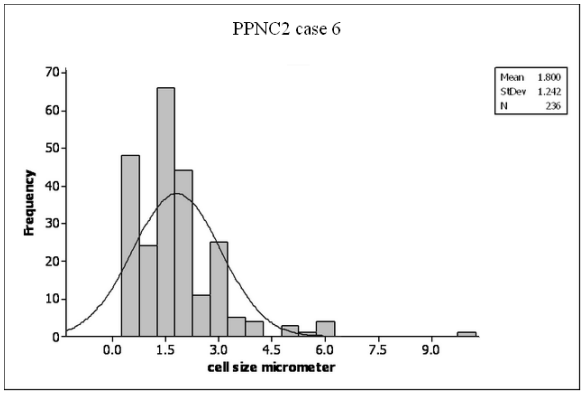

Figure 4.39 : Cell size distribution for PPNC2 foams case (6)

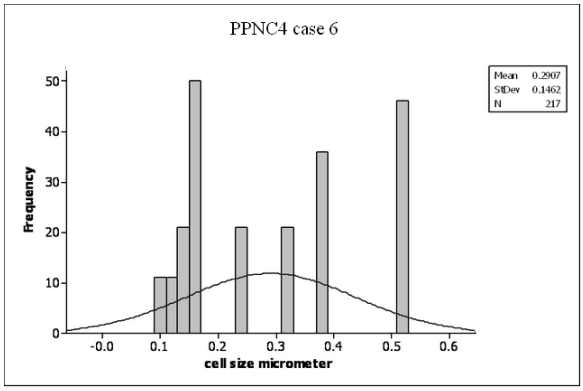

Figure 4.40: Cell size distribution for PPNC4 foams case (6)

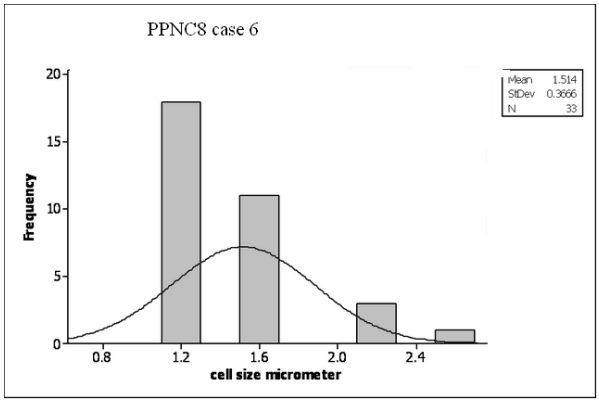

Figure 4.41: Cell size distribution for PPNC8 foams case (6)

Sample name	Mean cell size (μm)	Standard deviation	Foam type
HMS-PP case 2	14.73	7.97	Closed cell
HMS –PP case 3	25.58	9.16	Open cell/collapsed
HMS –PP case 4	4.3	6.23	Closed cell
HMS –PP case 5	4.5	5.12	Closed cell
HMS –PP case 6	4.57	3.84	Closed cell
PPNC2 case 2	2.26	3.25	Mixed
PPNC2 case 3	3.46	2.74	Open cell
PPNC2 case 4	1.9	2.34	Mixed
PPNC2case 5	1.8	1.98	Closed cell
PPNC2case 6	1.8	1.23	Closed cell
PPNC4 case 2	1.15	0.48	Closed cell
PPNC4 case 3	5.55	2.64	Closed cell
PPNC 4 case 4	1.1	3.21	Closed cell
PPNC4case 5	0.3	3.79	Closed cell
PPNC4case 6	0.29	0.14	Closed cell
PPNC8 case 2	2.96	0.85	Closed cell
PPNC 8 case 3	1.51	0.37	Closed cell
PPNC8case 4	1.5	0.92	Mixed
PPNC8case 5	2.3	2.1	Mixed
PPNC8 case 6	5.14	2.29	Open/collapsed
PPNC 10 case 2	1.02	1.13	Open cell
PPNC10 case 3	4.4	2.13	Open cell
PPNC10case4	2.3	1.12	Open cell
PPNC10case 5	2.1	3.1	Mixed
PPNC10 case 6	1.31	0.61	Open cell

Table 4.10 : Calculation of foam cell sizes using image analysis technique

Figures (4.38- 4.41) show the cell size distribution for the foam samples with variable amount of clay loadings prepared under varying conditions specifically for the cases where closed cell foams were produced. An image analysis technique was used to determine the foam cell size. The foam images were broken down into 5 zones and then sampled from each zone to determine the cell size and distribution. The distribution plots reveal that the cell size increases with increase in clay loading and foaming temperature. The cell size distribution for the pure polymer (HMS –PP) foam samples appears to be symmetric and homogenous. The distribution graphs do show a positive kurtosis value. All the samples show a pretty much symmetric distribution of

cell sizes closely following normal distribution. The images also reveal that the distribution becomes broader and flatter as the clay loading increases indicating that the cell size distribution range increases with the increase in clay loading. This effect could be attributed to a non homogenous nucleation mechanism in presence of clay. The standard deviation and mean cell size for all the samples increases as the foaming temperature is increased indicating that larger cells are generated at higher foaming temperatures and the cell size distribution is more non homogenous too. The increase in cell size and formation of open cell foams with increase in clay loading and foaming temperature does indicate that the degree of coalescence is not only a function of the foaming temperature but also of the of clay loading in the polymer samples respectively. Table 4.10 lists the mean cell size and type of foam formed for PPNCs under different processing conditions. It is clear from this table that the formation of closed cell foams starts at around 144 ^{0}C and continues until 149 ^{0}C. The smallest cell size is attained for a processing temperature of 147 ^{0}C.

Sample	Cell Number 10^8	Cell wall thickness δ(μm)	Volume Exp.	Cell Dia (μm)
HMSPP(1)	0	0	0.02	0
HMSPP(2)	2.1	1.4	0.89	14.7
HMSPP(3)	0.2	0	0.22	25.6
HMSPP(4)	2.3	1.2	0.7	6.1
HMSPP(5)	3.1	1.2	1.37	4.3
HMSPP(6)	3.2	1	1.37	4.5

Table 4.11 : Foam cell parameters for HMS-PP foams

Sample	Cell Number 10^{11}	Cell wall thickness d(μm)	Volume Exp.	Cell Dia (μm)
PPNC2(1)	0	0	0.02	0
PPNC2(2)	2.2	1.5	3.46	2.26
PPNC2(3)	0.8	3	0.92	3.46
PPNC2(4)	3.6	2	2.7	2.3
PPNC2(5)	4	1	1.72	1.9
PPNC2(6)	5	0.5	2.32	1.8

Table 4.12 : Foam cell parameters for PPNC2 foams

Sample	Cell Number 10^{13}	Cell wall thickness d(μm)	Volume Exp.	Cell Dia (μm)
PPNC4(1)	0	0	0.02	0
PPNC4(2)	876	1.1	3.23	1.15
PPNC4(3)	5	2	3.21	5.52
PPNC4(4)	570	1.3	2.54	1.1
PPNC4(5)	2.9	1	1.12	0.3
PPNC4(6)	1253	0.65	2.58	0.29

Table 4. 13: Foam cell parameters for PPNC4 foams

Sample	Cell Number 10^{9}	Cell wall thickness d(μm)	Volume Exp.	Cell Dia (μm)
PPNC8(1)	0	0	0.03	0
PPNC8(2)	2.1	3.3	2.23	2.97
PPNC8(3)	0.2	collapsed	1.76	5.15
PPNC8(4)	1.7	2.7	1.32	1.5
PPNC8(5)	2.1	2.4	1.71	2.3
PPNC8(6)	3.2	1.8	2.21	1.51

Table 4.14: Foam cell parameters for PPNC8 foams

Sample	Cell Number 10^{8}	Cell wall thickness d(μm)	Volume Exp.	Cell Dia (μm)
PPNC10(1)	0	0	0.03	0
PPNC10(2)	1.41	1.7	1.92	1.024
PPNC10(3)	0	collapsed	0.55	4.4
PPNC10(4)	1.7	3	1.67	2.3
PPNC10(5)	3.1	1.5	1.44	2.1
PPNC10(6)	3.1	1.5	2.09	1.31

Table 4.15: Foam cell parameters for PPNC10 foams

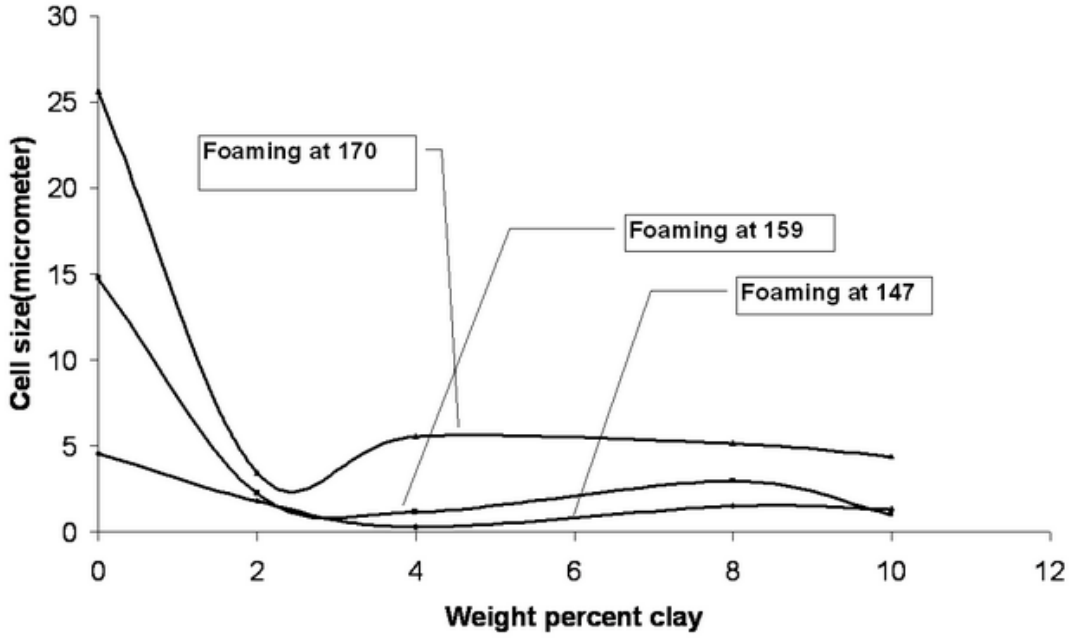

Figure 4.42 : Effect of clay loading on foam cell morphology

Figure 4.42 shows the variation in cell sizes with changes in clay loading for different foaming temperatures. It can be seen that initially the cell size decreases with increase in clay loading but after a threshold limit the cell size again starts increasing. The lowest cell size of 0.29μm. is attained for 4 wt % clay loading. Thus the efficiency of clay in nucleating foam cells goes down with increase in loading levels. One of the possible reasons can be the absence of a randomized clay distribution at higher clay loadings. Smallest cell size therefore would be attained only with an exfoliated structure and hence the clay loading should not increase beyond the percolation threshold limit since after that point the rate of reduction in cell sizes starts decreasing with an increased tendency towards intercalation and then finally when the clay particle - particle attraction potential is high enough then large clay aggregates are formed resulting in increased cell sizes. At very high foaming temperature (170^{o}C) SEM images have revealed the highest amount of coalescence and foam cell collapse. As a result the trend line for foaming at 170^{o}C denotes that the possible lowest amount of cell coalescence would be for samples with 2 wt % clay loading and then the coalescence rate starts increasing. Although significant increase in coalescence takes place beyond 4 wt % or very high clay loadings.

4.4.6 The effect of clay on foam cell morphology

The efficiency of functionalized filler as compared to other conventional fillers is much higher in increasing nucleation rate of polymer cells as indicated by the fact that only small amount of clay is needed to propel nucleation rate. The dispersion state of clay particles within the polymer has a considerable effect on cell size and density. Randomly dispersed completely separated clay platelets have the highest efficiency in nucleating foam cells and that's why producing the smallest foam cells as well [4]. The dispersion state of clay particles in turn is a function of concentration of clay

particles in the polymer. Clay agglomerates provide areas of coalescence with a polymer as shown by the experimental results.

4.4.7 Effect of vinyl acetate content on foam cell morphology

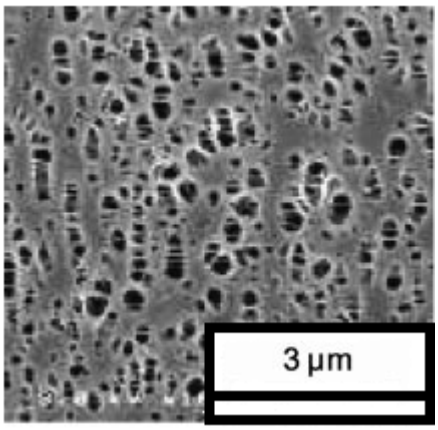

Figure 4.44 : SEM of PPNC4 foam case (6)

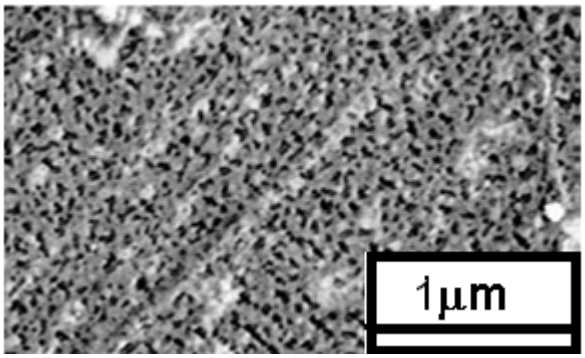

Figure 4.43 : SEM of PP/EVA/clay foam case (6)

The addition of EVA to the HMS-PP nanocomposite matrix causes a reduction in foam cell sizes as shown in figure 4.43. Figure 4.43 shows that the average cell size in case of PPNC4 foam is around 0.29µm. The subsequent addition of EVA (40%) to the nanocomposite matrix causes a reduction in foam cell sizes to about 100nm (figure 4.44). The distribution of the cell sizes after addition of EVA becomes non uniform.

4.4.8 Dynamic and Extensional rheology

The rheological behaviour of the polymer matrix also affects the final foam morphology attained. The dynamic rheological properties of the polymer matrix at the subsequent foaming temperature provide an insight in to the properties of the melt and its relaxation behaviour which in turn govern the foam cell structure. The extensional viscosity comes into play during the growth process when the polymer sample is stretched biaxially due to the growth of foam bubbles (184). The presence of strain

hardening behaviour at those high extension rates limits the growth of foam bubbles to smaller sizes [197, 198]. These measurements are hence essential to gain an insight into the physical reasoning behind the developed foam morphology.

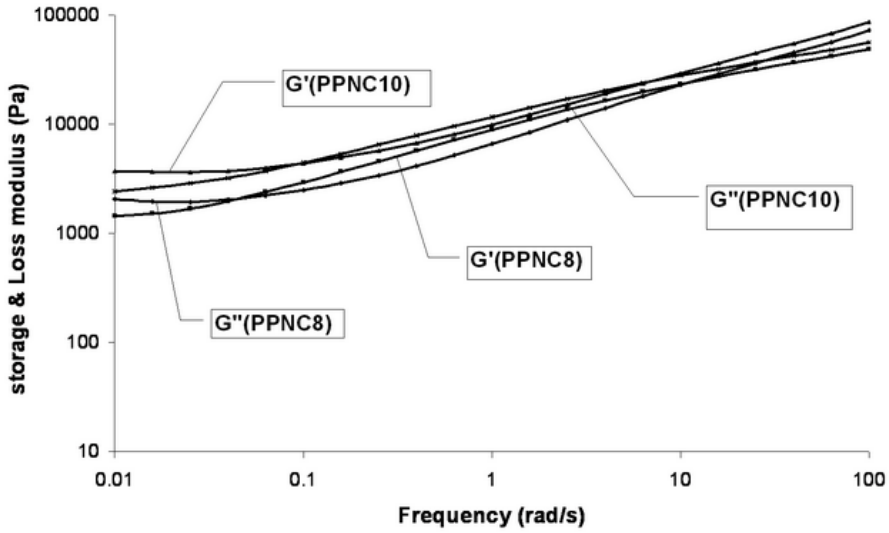

Figure 4.45 : Dynamic properties for PPNC8 and PPNC10

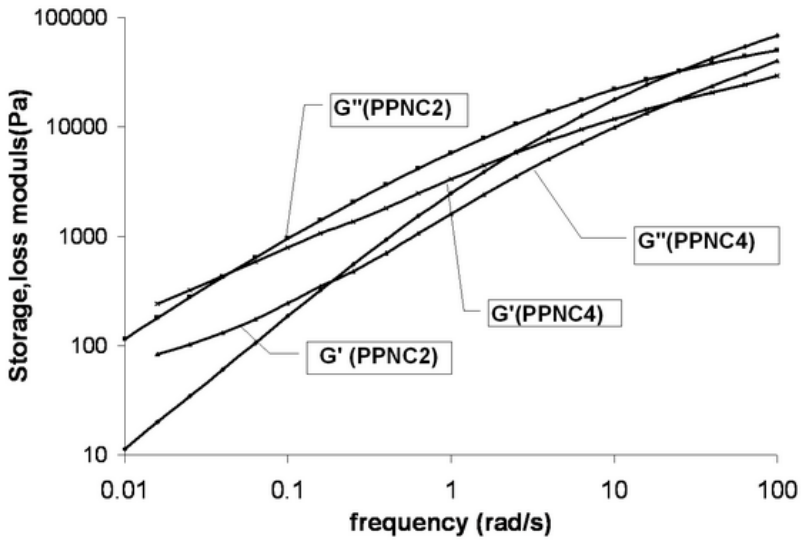

Figure 4.46 : Dynamic properties for PPNC2 and PPNC4

Figures (4.45and 4.46) show the dynamic rheological testes performed of various PPNCs. A time sweep test was first performed on all the samples and it was found

that the samples do not degrade even after a period of 1 hour. Strain sweep tests carried out at a strain rate of 1/s helped in determining the linear viscoelastic region for the sample at the applied strain rate and so the strain rate of 1/s was used for the dynamic frequency tests. These tests were conducted at a temperature of 160 ^{0}C. Figure 17 shows the storage modulus (G') and loss modulus (G") plots for PPNC2 and PPNC4 at 160 ^{0}C. It can be concluded that a typical terminal behaviour is exhibited by PPNC2. PPNC4 doesn't exhibit a terminal behaviour at low frequencies. The storage and loss modulus both gradually increase with clay loading but the rate of increase of storage modulus is higher as compared to loss modulus. The increase in material function of the nanocomposites with increase in clay loadings is due to the increased frictional resistance provided by the clay particles to the motion of the polymer chains. Also the unequal rate of increase of storage and loss modulus indicates that PPNCs tend to become more solid like with increase in clay loading. The cross over frequency for both the nanocomposites is around the frequency of 10 rad/s. The material functions for both the nanocomposites become independent of frequency at higher frequencies by developing a typical plateau region. At higher frequencies the relaxation time of the polymer is higher than the applied frequency and hence the polymer sample is not able to respond to the frequency change quickly resulting in such behaviour. Figure 4.61 shows the storage and loss modulus plots for PPNC8 and PPNC10 at 160^{o}C. It can be seen from Figure 4.61 that both the nanocomposites exhibit non terminal type behaviour at lower frequencies and tend to develop a small secondary plateau region at lower frequencies with increase in clay loading. The development of a secondary plateau region at lower frequencies is due to a solid like behaviour. Figure 4.61 also shows the absence of a typical plateau region at higher frequencies, interestingly the cross over frequency is still around the 10 rad/s

region for all the nanocomposites. The cross over frequency is the frequency of transition from a liquid like to solid like behaviour. The samples exhibit a solid like behaviour after the cross over frequency. This effect can be attributed to the fact that after the cross over frequency the relaxation time of the polymer chains is higher than the applied dynamic frequency and hence the polymer is not able to react to the abrupt change of frequency resulting in a solid like behaviour.

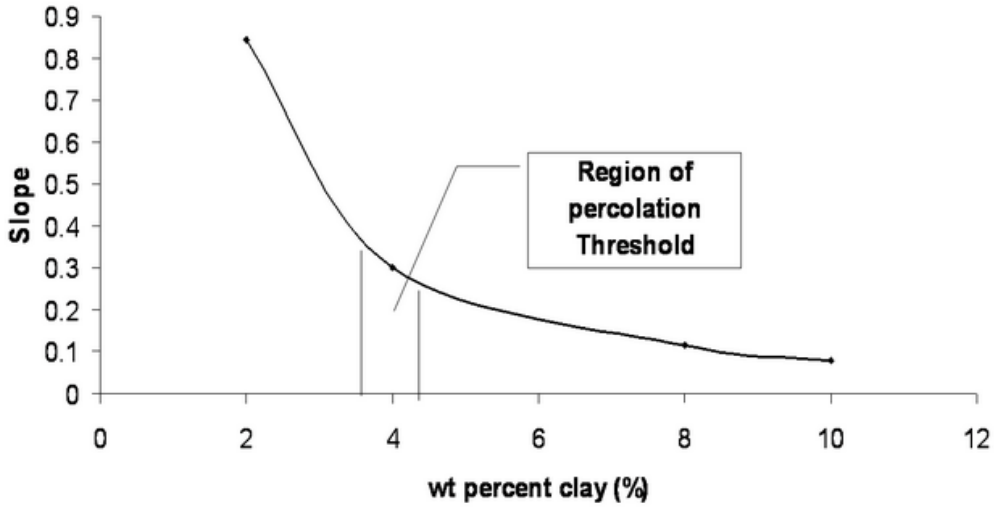

Figure 4.47 : Percolation threshold calculation of PPNC nanocomposites

Figure 4.47 shows the percolation threshold for the polymer samples determined from the slopes of the terminal region from the dynamic frequency plots (i.e. Figure 4.45 and Figure 4.46. Figure 4.63 shows that an abrupt change in the slope takes place at around the 4 wt % clay loading region indicating that the percolation threshold for the PPNC is around the 3 – 4 wt %. The percolation threshold is the clay loading value after which no further exfoliation is possible even if the shear rate applied to the sample is increased. It is to be noted here that as discussed earlier that the optimum clay content for the samples is ~ 4 wt % for the generation of fine cell foams because after 4 wt % clay loading the cell size tends to increase and even open cell foams are

formed. This result leads to an important conclusion that the optimum clay loading for generation of fine cell foams is around the percolation threshold .This result also makes physical sense since after the percolation threshold no further exfoliation is possible and hence the rate of foam cell nucleation is bound to reduce since the nucleation rate is highest for an exfoliated disordered structure. The increase order in an intercalated structure probably leads to increased cell coalescence and so increased cell sizes. The nucleation efficient of clay in an intercalated morphology is lesser than in an exfoliated morphology since unlike the exfoliated morphology clay platelets are not completely separated in an intercalated structure and there might be presence of clay aggregates as well. All of these reasons result in the reduction of nucleation rate and hence increase in foam cell sizes provided that the foam processing conditions remain same.

4.4.9 Extensional Rheology

The extensional viscosity measurements were made using the special extension fitting designed for the ARES rheometer. The strain hardening behaviour is caused by the orientation of the clay particles in the stretch direction which reduces the dynamic mobility of the polymer chain within the clay galleries causing a substantial increase in extensional viscosity. Figure 4.48 shows the dynamic extensional viscosity of PPNC at a strain rate of 3 1/s at 150^{o}C. The stretching rate during foam formation would be much higher than this due to a very high rate of cell nucleation. The selection of this stretching rate is to see the extensional behaviour of the polymer matrix at high stretching rates. This temperature is chosen since it is close to the actual foaming temperature used in this study. The stretching rates of the polymer for the case of PPNC4 (the smallest cell size and highest cell density) is much higher than that used in this experiment

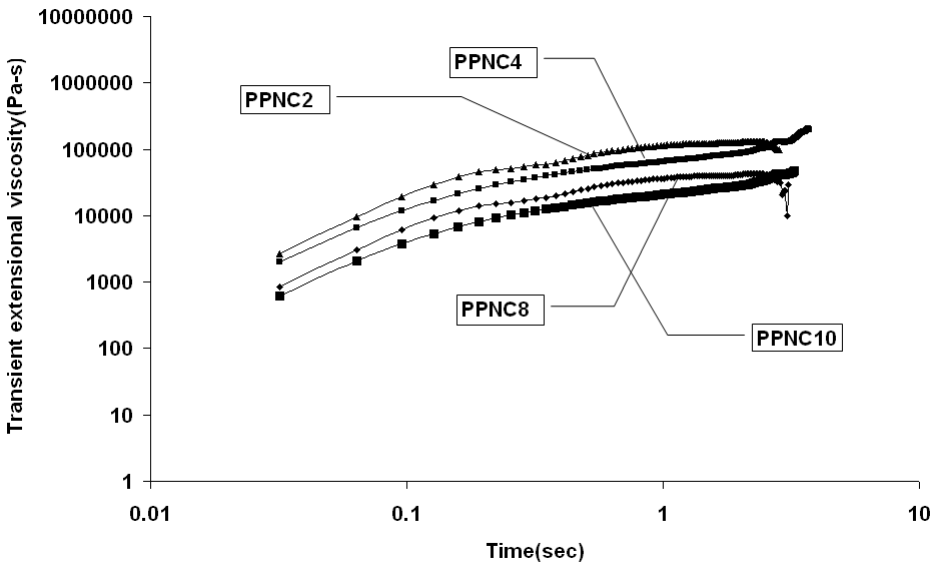

Figure 4.48 : Extensional viscosity of PPNC nanocomposites

All the polymers show a typical strain hardening behaviour after an elapsed time of 10 seconds. Thus an improved nucleation rate in presence of clay particles along with higher stretching rates during bubble growth strain hardening effect would appear much faster than 10 seconds enabling the restriction of cell growth to smaller sizes. The subsequent increase in clay loading does not effect the strain hardening behaviour but increases the melt elasticity and decreases the nucleation efficiency due to formation of intercalated morphology .These two supporting effects result in increased cell coalescence , non uniform cell shapes , generation of open cell foams and increased cell sizes as well further providing evidence for the fact that the optimum clay content for the foamed samples is around the percolation threshold region respectively. Also as compared to linear PP nanocomposites, PPNCs exhibit a much abrupt and extended strain hardening effect and thereby a higher extensional viscosity(184). This behaviour in turn results in production of smaller foam cell sizes in case of PPNCs as compared to linear PP nanocomposites.

The foaming behaviour of pure HMS –PP and PPNCs was studied for different foam processing conditions. The generation of closed cell foams and the degree of cell coalescence was found to be minimum when the foaming temperature of the sample was at the higher end of the melting temperature range. Cell coalescence and collapse was higher when the foaming temperature was raised beyond the melting range by 4 to 5^{o}C. The efficiency of clay in nucleation of foam cells was found to decrease with increase in clay loading with the maximum foam cell density and smallest cell size attained for a clay loading of 4 wt %. The decrease in nucleation efficiency of clay with increase in clay loading can be attributed to a non random ordered dispersion of clay at higher loadings coupled with increased interaction potential between the clay particles respectively. The foam cell density and cell size followed an inverse relationship, also with increasing in clay loading the cell wall thickness tends to increase. The smallest cell sizes in polymer nanocomposites foams are generated when a two step batch setup is used because the saturation of the sample can be carried out at much lower temperature and higher pressure improving solubility and degree of super saturation then a subsequent use of temperature superheat result in generation of fine cell foams. Foam cell sizes ranging from 0.294μm to 9 μm were obtained. The dynamic rheological tests reveal that the percolation threshold for the nanocomposites is in between 3-4 wt %. This helps in developing an important understanding that for interacting filler the nucleation efficiency will be the highest till percolation threshold after the percolation threshold the rate of increase of nucleation due to the presence of fillers reduces finally becoming very low at very high clay loadings. The extensional tests reveal that all the polymers exhibit a strain hardening effect in the foaming temperature ranges investigated. The strain hardening

effect in case of PPNCs is more pronounced and appears in a short time after the stretching of the sample thereby helping in restricting foam cell sizes.

4.5 Foaming of HMS –PP Clay nanocomposites in a foam injection moulding system

The L9 orthogonal DOE was used to study the effect of processing parameters on foam cell sizes. This experimental design approach was chosen since it minimizes the number of trials required. The table below shows the experimental runs performed using the above mentioned approach

Gas conc. (vol %)	Foaming Temperature °C	Injection Pressure MPa	Foaming Time (Sec)	Foam cell size 2 % (microns)	Foam cell size 4 % (microns)
20	195	70	30	150	120
20	205	90	40	120	100
20	215	110	50	90	60
30	195	90	50	110	80
30	205	110	30	80	50
30	215	70	40	100	40
40	195	110	40	70	70
40	205	90	50	50	20
40	215	70	30	60	80

Table 4.16 : Experimental runs using the L9 orthogonal experimental design approach

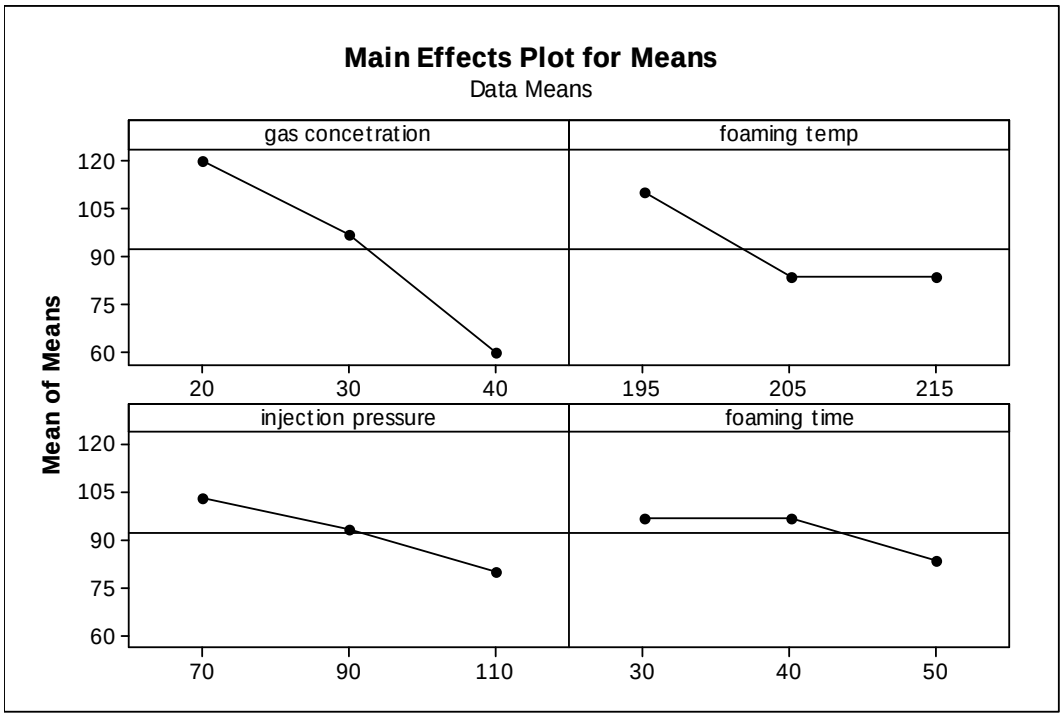

Figure 4.49 : effect of processing parameters on PPNC2 foams

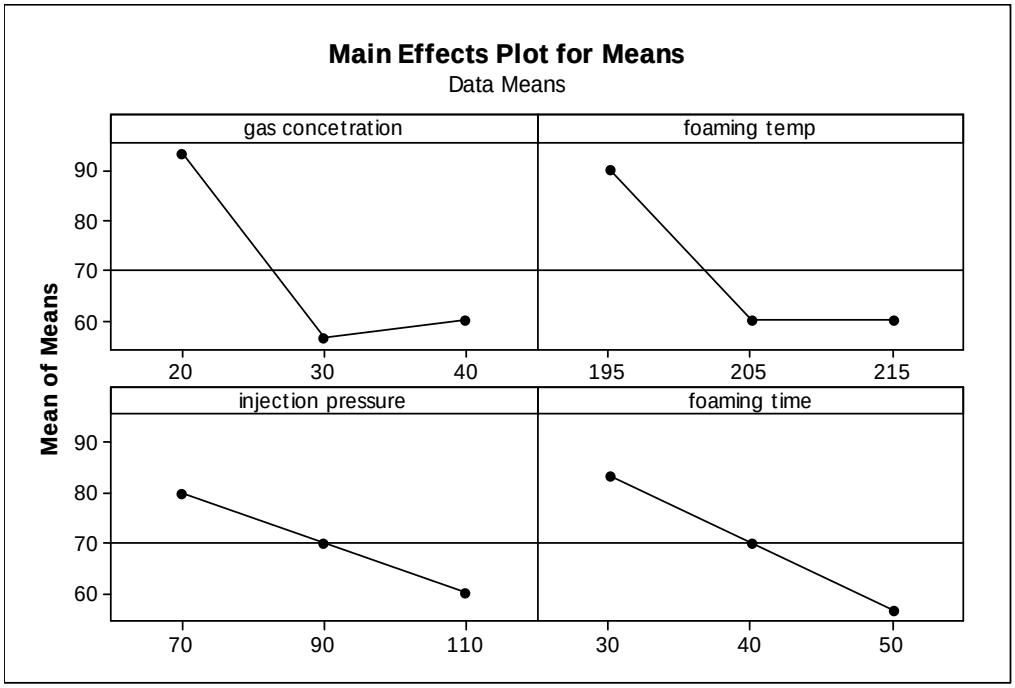

Figure 4.50 : Effect of processing parameters on PPNC4 foams

Figures 4.49 and 4.50 show the effect of processing parameters on foam cell sizes. It can be seen from both the figures that with increase in gas concentration foam cell

sizes are reduced. This effect can be attributed to the fact that increase in gas concentration increase the gas flux available for foam cell nucleation resulting in higher nucleation rates and reduced foam cell sizes(200). The reduction in melt temperature also results in reduction in foam cell sizes .This effect can be attributed to the fact that at reduced temperatures the melt viscosity is high which resists cell growth resulting in smaller foam cell sizes (185). Interestingly at reduced melt temperature the dissolved gas concentration increase and the nucleation rate increase as well resulting in smaller foam cell sizes. Also it can be seen from figure 4.65 and 4.66 that the foam cell size becomes independent of melt temperature after 205^0C. The shear viscosity response of a polymer with respect to temperature levels of at higher temperature which probably makes foam cell sizes independent of melt temperature at higher temperatures. It is also observed that the foam cell sizes decreases with increase in injection pressure. The increased injection pressure results in a higher pressure drop at the mould gate. At higher pressure drop rates the rate of nucleation is increased resulting in smaller foam cell sizes (Baldwin 1995)(199). The foam cell sizes also have an inverse relationship with respect to foaming time or holding time. In case of foam injection moulding system it is necessary to provide sufficient time for foam cells to grow and stabilize. At very small foaming times the foam growth process in incomplete hence during the quenching process the rate of cell collapse is high resulting in increase in cell sizes. Interestingly if the foaming time is very high then the foam growth time increase to a value where the foam cells become too big and hence the rate of coalescence is increase resulting in higher foam cell sizes. The key is to provide sufficient foaming time so that neither foam cell collapse nor foam cell coalescence occurs.

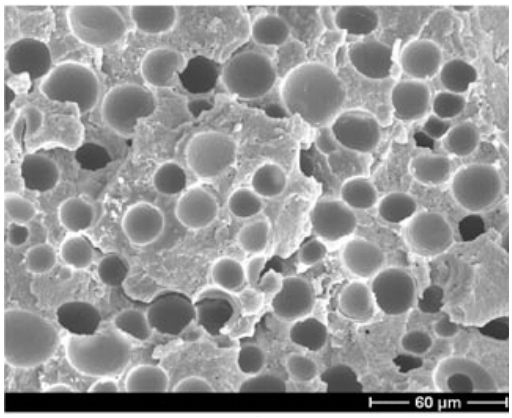

Figure 4.51 : SEM of PPNC4 foam

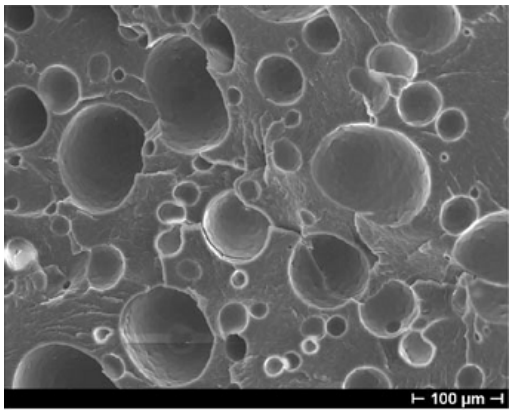

Figure 4.52 : SEM of PPNC2 foam

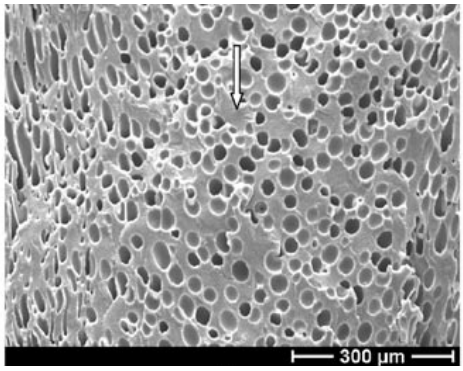

Figure 4.53: Orientation of cells in PPNC2 foams

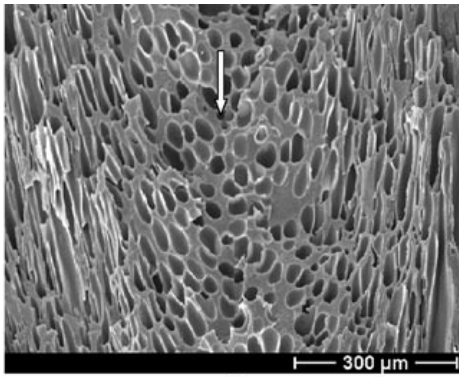

Figure 4.54 : Orientation of cells in PPNC4 foams

The SEM images (figure 4.51 -4.52) show that the cell sizes in case of a foam injection moulding is much larger as compared to the batch foaming process. The cell size is smaller for the case of PPNC4 nanocomposite as compared to PPNC2. Interestingly the cell size distribution is more uniform in case of PPNC2 nanocomposites as compared to PPNC4. (Figure 4.53 -4.54) reveal that there is orientation of the foam cells along the flow direction. The orientation or alignment of

the foam cells in the flow direction results in improvement in mechanical properties although the properties become non isotropic.

4.6 Summary

The foam cell morphology in case of polymer nanocomposites is affected by the foam processing parameters and the morphological and rheological properties of the host polymer nanocomposite matrix. The improvement in polymer melt viscosity accompanied with an improved strain hardening behaviour results in smaller foam cell sizes by restricting the foam growth process. The distribution of the clay particles within the polymer matrix affects the foam cell distribution. In case of randomized clay particles distribution the foam cells are randomly distributed whereas in case of ordered clay particles distribution the foam cell distribution is more uniform. This behaviour can be explained by the dependency of the initial nucleation rate on the clay particle distribution. The rate of coalescence of foam cells increases with increase in clay concentration as indicated by generation of mixed foam morphologies with increase in clay concentration. Also, the cell wall thickness increases with increase in clay particle concentration. The addition of clay particles causes an overall reduction in foam cell sizes due to improvement in foam cell nucleation rate. The reduction in foam cell sizes with increase in clay concentration only takes place untill the rheologically determined percolation threshold is reached. Once the percolation threshold is reached the foam cell sizes begin to increase. The gas solubility is very sensitive to clay concentration as indicated by the optimization plots specifically where the aim is to reduce foam cell sizes. Experimental design schemes like L9 orthogonal and Box Benkhen design was used with foaming studies. The use of such experimental design schemes reduced the number of experimental runs and at the same time helped in conducting optimization studies.

Chapter 5: Results and Discussions (Modelling and simulation)

5.1 Introduction

The generation of fine cell foams is affected by the presence of filler (nanoclay) in the polymer matrix. The rate of foam cell nucleation is improved significantly by the addition of nanoclay in the polymer matrix resulting in finer foam cells. Also the melt strength and extensional properties of the polymer matrix is improved which further helps in reduction of foam cell sizes. Interestingly the literature suggests that the solubility of the blowing agent is reduced by the addition of filler. The reduction in gas solubility would result in lower degree of supersaturation which would in turn lead to lower initial nucleation rates and hence lower cell densities. Thus, the addition of nanofiller would on the one hand propel the nucleation rate but on the other hand would cause a reduction in the degree of supersaturation. These two mechanisms counteract each other and hence result in opposite trends with respect to foam cell sizes and densities. Hence it is very important to understand the effect of addition of filler on gas solubility in the polymer matrix. A statistical thermodynamic model has been developed to study the effect of addition of filler on gas solubility. The model involves the use of molecular parameters like polymer chain flexibility, chain length and contact fractions. The use of these factors in the model provides a qualitative and quantitative insight on the effect of filler on gas solubility and hence foam cell morphology. The next part of this chapter simulates the effect of polymer matrix rheology on foam cell structure. Modelling the effect of polymer nanocomposite rheology on foam cell structure would lead to an understanding of the sensitivity of the foam cell sizes to the rheological properties of the polymer nanocomposites. It would also provide an understanding of the controlling resistance to foam cell growth.

This knowledge in turn would help in synthesizing polymer matrix structures with the desired molecular weight distribution for producing fine cell polymeric foams.

5.2 Modelling of gas solubility

The HH Theory has been discussed in depth in the literature (207).

A brief review of the essential aspects of the HH theory is discussed here. The non random mixing of segments and holes due to presence of interactive forces between the polymer and other segments in the lattice results in another microscopic parameter X which accounts for the fraction of segment hole contacts in the partition function Z. As a result the partition function now is given by equation (5.1)

$$Z(N,V,T) = \sum_{q}\sum_{X} Z_{qX}(N,V,T,q,X)$$

$$= \sum_{q,X} g(q,X) l_f(q,X)^{3cNc_s} \exp(-E_0(q,X)/kT \qquad (5.1)$$

Where $Z_{q,X}(N,V,T,q,X)$ is the partition function for the system with fixed values of X and y where y represents the fraction of occupied sites in the lattice which varies with the thermal energy of the chain. g(q,X) represents the combinatorial entropy related to the mixing of holes and the polymer chain with in the lattice E_0 represents the internal energy of the lattice system where the polymer chain is under static conditions and l_f represents the segmental free length.

Guggenheim's quasi – chemical approximation for Non randomness can be used to calculate the combinatorial factor g given by equation (5.2)

$$g = g_{HH} \frac{[Q(q-X^*)!][(QX^*)!]^2[Q(1-q-X^*)!]}{[Q(q-X)!][(QX)!]^2[Q(1-q-X)!]} \qquad (5.2)$$

$$E_0 = Q(q - X)\varepsilon_C$$

$$l_f = (1 - \frac{X}{q})l_s + (\frac{X}{q})l_g \equiv \bar{l}_f v^{*1/3} \qquad (5.3)$$

In the equations (5.2) and (5.3) q represents the net external contact fractions of the segments in the lattice, (1- X/q) is the fraction of the segment segment contacts and (X/q) represents the fraction of segment hole contacts.

As per the theory of partition function in statistical thermodynamics it has been proven that for a given ensemble the property of the system in the state which is most probable can be used to approximate the variation of that property throughout the ensemble. As a result the equation to the right of Z (N, V, T) is replaced by its maximum value. The maximum terms in the above equations is represented by a tilde on the top of the parameter as shown in equation (5.4).

$$Z(N,V,T) = Z_{yx}(N,\bar{y},V,T,\overline{X}) \qquad (5.4)$$

Here the parameter y is the occupied site fraction and can be related to the external contact fraction q.

The maximum values of the above parameters are determined by equation (5.5)

$$\left(\frac{\partial \ln Z_{yX}}{\partial X}\right)_{N,y,V,T} = 0$$

$$- \qquad (5.5)$$

$$\left(\frac{\partial \ln Z_{yX}}{\partial y}\right)_{N,X,V,T} = 0$$

Once the partition function is known the free energy of the polymer chain in the lattice can be calculated by the Hemholtz free energy function. Here the Helmholtz

free energy function is considered since the system is modelled for a constant N, V, and T. The calculated Helmholtz free energy (equation (5.6)) function then can be used in determining solubility

$$A = - kT \ln Z - \qquad (5.6)$$

5.3MODIFICATIONS IN THE MODEL

5.3.1 Internal energy

The polymer in the lattice has three types of possible interactions 1) segment to segment interaction

2) Segment to particle interaction 3) particle to particle interaction. All the three interaction are characterized by the 6 – 12 Lennard's Jones pair potential. It has been proven in the literature that the nanoparticles cannot easily come close enough to each other to consider the repulsive interaction between them. This could be related to the strong repulsion between the particles due to presence of charged exchangeable cations on their surface. As a result in this analysis only the attractive interaction between the nanoparticles (Wander Waals interaction) is taken in to consideration. It is interesting to note that this interaction force can be expressed as a function of the end to end distance between the particles. Thus the dispersion state (exfoliated, intercalated) of the particles can be accounted for. The segment - segment interaction is given by (modified form of the LJ potential).The simplified form of the LJ potential (equation (5.7)) results because a square well approximation is made (203)

$$\varepsilon_C = \varepsilon^* \left(A\varpi^{-4} - 2B\varpi^{-2} \right) \qquad (5.7)$$

The internal energy contribution of gas contacts can be given by equation 5.7. The same equation will be used to represent the interaction potential between the gas and the polymer denoted by $\varepsilon_{GG.}$

where $\varpi = \frac{yV}{Nsv^*}$ represents the reduced cell volume ε^* & v^* represent maximum attraction energy and the corresponding segmental volume. The reduced cell volume takes in to consideration the fact that the volume of the cells are variable and also at maximum attraction the cell volume is reduced since the polymer chains are closely spaced, also further it is assumed that the number of holes in the lattice is a function of temperature as a result the lattice is now represented by the reduced cell volume to make the above assumption true.

5.3.2 The segment to particle interaction:

It is assumed that the particles are spherical and the concept of equivalent radius is used to take in to account the non spherical nature of the particle. This is done because the complexity of the volume integral involved for calculating the interaction potential for the entire volume of the nanoparticle from a differential element is significantly reduced in case of spherical particles. Also a square well approximation cannot be made in case of interaction between solid particles and polymer chains as a result the final form of the equation cannot be expressed in reduced cell volume form The interaction between the clay particles and the polymer chains do not affect the cell volume significantly since clay particles are present in minor amounts.

The interaction between a differential element dV of the particle and the polymer is given by equation (5.8)

$$d\varepsilon_{mp} = \varepsilon_{ads}\left(\frac{r_1^{12}}{R^{12}} - \frac{2r_1^{6}}{R^{6}}\right)dV \qquad (5.8)$$

$\varepsilon_{mp} = \int_V d\varepsilon_{mp}$ Performing the integration we have equation (5.9)

$$\varepsilon_{mp} = \varepsilon_{ads}\left[\frac{r_1^{9}}{30(D_{eq}+2r_{mp}}\left(\frac{4D_{eq}-r_{mp}}{r_{mp}^{9}} + \frac{5D_{eq}+r_{mp}}{r_{mp}+D^{9}} - 2\frac{D_{eq}^{3}r_1^{3}}{r_{mp}^{3}\left(D_{eq}+r_{mp}\right)^{3}}\right)\right] \qquad (5.9)$$

Here r_{mp} denotes the shortest distance between the particle and the polymer in a given interaction state

The attractive potential (Vander Waals potential) between two spherical particles is easily found in the literature (214, 215). The modification made in here is that equivalent diameter is used to take in to account non spherical nature of the nano-particles as shown in equation (5.10). The overall attraction potential is given by equation (5.11)

$$D_{eq} = \sqrt[3]{Ldh/C} \qquad (5.10)$$

$$\varepsilon_{pp} = -\varepsilon_p'\left(\frac{D_{eq}^{2}}{r_{pp}\left(r_{pp}+2D_{eq}\right)} + \frac{D_{eq}^{2}}{\left(r_{pp}+D_{eq}\right)^{2}} + 4\ln\frac{r_{pp}\left(r_{pp}+2D_{eq}\right)^{1/2}}{r_{pp}+D_{eq}}\right) \qquad (5.11)$$

Where $\varepsilon_p' = \frac{C^2\pi^2\varepsilon_p}{6}$

Where L is the length of the particle, d is the width of the particle and h is the thickness of the particles

5.4 Model system

The system is a binary mixture of polymer (represented by component A) and that of clay particles (represented by B). Let N_A and N_B represent the number of molecules of polymer and number of clay particles with modifiers. It is assumed further that each clay particle along with the modifier occupies a lattice site. s_A and s_B denote the number of segments of component A and that of clay + modifier (component B) M_{0A} & M_{0B} the molar mass of components A and B respectively. P, V, T the pressure total volume and temperature of the system. The following parameters are introduced as given below

N the total number of molecules

N_h the total number of holes in the lattice

z co – ordination number of the lattice

y occupied site fraction $y = (N_A s_A + N_B s_B + N_g s_g)/ (N_A s_A + N_B s_B + N_h + N_g s_g)$

ϕ_A segment fraction of component A = $(N_A s_A) / (N_A s_A + N_B s_B + N_h + N_g s_g)$

ϕ_B fraction of component B = $(N_B s_B) / (N_A s_A + N_B s_B + N_h + N_g s_g)$

ϕ_g segment fraction of the gas = $N_g s_g/ (N_A s_A + N_B s_B + N_h + N_g s_g)$

c_{sA} flexibility parameter of segment A c_{sA}/s_A

The flexibility parameter for component B clay particles is zero but the modifiers will have flexibility given by c_{SB}/s_B

C_{sg} flexibility parameter of gas = c_{sB} /s_B

zq_A number of external contact sites of the polymer = $s_A (z-2) + 2$

zq_B number of external contact sites for component B = $Ns_B(z-1)$ where s_B is the no. of modifiers on the clay surface

where N is the number of clay particles.

zq_g number of external contact sites for gas = $s_g (z-2) + 2$

$\langle s \rangle$ average number of segments $=1/ (\phi_A/ s_A + \phi_B/ s_B + \phi_g /s_g)$

$\langle c_s \rangle$ average flexibility parameter $\phi_A c_{sA} + \phi_g c_g$

u the contact fraction of the polymer $u = N_A zq_A /(N_A zq_A + N_B zq_B + zN_h + zNg)$

v the contact fraction of component B $v = N_B zq_B/(N_A zq_A + N_B zq_B + z N_h + zNg)$

w the contact fraction of holes $w = z N_h/(N_A zq_A + N_B zq_B + z N_h + zNg)$

r the contact fraction of gas molecules $r = zNg/ (N_A zq_A + N_B zq_B + z N_h + zNg)$

q total contact site fraction of polymer, clay & Gas $q = u + v + r$

Q total external contact pairs $Q = (N_A zq_A + N_B zq_B + z N_h + zNg)/2$

To consider the non randomness in mixing for the system which affects the net entropy of mixing of the system the following microscopic parameters have to be considered as follows

Polymer – clay	QX_1
Clay – clay	$Q (v – X_1 – X_2)$
Holes – holes	$Q (w – X_2 - X_3)$
Clay – holes	QX_2
Polymer – holes	QX_3
Polymer – polymer	$Q (u – X_1 – X_3 – X_4)$
Gas – polymer	QX_4
Gas - hole	$Q(r – X_4 – X_{5)}$
Gas – Gas	QX_5

$$Z(N, y, V, \phi_A, T) = \sum_{X_1, X_2, X_3, X_4, X_5} Z_x(N, y, V, T, \phi_A, X_1, X_2, X_3, X_4, X_5) \quad (5.12)$$

The partition function for the subsystem Z_x is given by equation (5.12-5.13)

$$Z_X = g l_f^{3N<s><c_s>} \exp(-E_0 / kT) \qquad (5.13)$$

According to Guggenheim the combinatorial factor or the factor contributing to the configurational state of the system in the lattice is given by equation (5.14)

$$g = N_{HH} \frac{\left(Q\left(u - X_1^* - X_3^* - X_4^*\right)\right)!\left(Q\left(v - X_1^* - X_2^*\right)\right)!\left(Q\left(w - X_2^* - X_3^*\right)\right)!\left(Q\left(r - X_4^* - X_5^*\right)\right)!}{(Q(u - X_1 - X_3 - X_4))!(Q(v - X_1 - X_2))!(Q(w - X_2 - X_3))!(Q(r - X_4 - X_5))!}$$

$$X \frac{\left(\left(QX_1^*\right)!\right)^2\left(\left(QX_2^*\right)!\right)^2\left(\left(QX_3^*\right)!\right)^2\left(\left(QX_4^*\right)!\right)^2\left(\left(QX_5\right)!\right)^2}{\left(\left(QX_1\right)!\right)^2\left(\left(QX_2\right)!\right)^2\left(\left(QX_3\right)!\right)^2\left(\left(QX_4\right)!\right)^2\left(\left(QX_5\right)!\right)^2} \qquad (5.14)$$

here X* denotes the corresponding value for that fraction in case of random mixing

The segmental free length remains the same as per the previous theory for a single component given by equation (5.15)

$$l_f = \left(\frac{1 - X_2 + X_3 + X_4}{u + v + r}\right)\langle l_s \rangle + \left(\frac{X_2 + X_3 + X_4}{u + v + r}\right)\langle l_g \rangle = \left(1 - \frac{X}{q}\right)\langle l_s \rangle + \left(\frac{X}{q}\right)\langle l_g \rangle \qquad (5.15)$$

The solid like and gas like free lengths given by l_s and l_g respectively also remains the same and are similar in nature to that for a pure component. They are a function of the hardcore volume and overall site contact fractions.

The net internal energy for the system is now given by equation (5.16)

$$E_0 = Q(u - X_1 - X_3 - X_4)\varepsilon_c + Q(v - X_1 - X_2)\varepsilon_{pp} + QX_1\varepsilon_{mp} + QX_4\varepsilon_{gp} + QX_5\varepsilon_{gg} \qquad (5.16)$$

$$= Qu\varepsilon_c + Qv\varepsilon_{pp} + QX_1(\varepsilon_{mp} - \varepsilon_c - \varepsilon_{pp}) - QX_2\varepsilon_{pp} - QX_3\varepsilon_c + QX_4\varepsilon_{gp} + QX_5\varepsilon_{gg}$$

Let

$$\varepsilon_1 = \varepsilon_{mp} - \varepsilon_c - \varepsilon_{pp}$$
$$\varepsilon_2 = -\varepsilon_{pp}$$
$$\varepsilon_3 = -\varepsilon_c$$
$$\varepsilon_4 = \varepsilon_{gp} - \varepsilon_c$$
$$\varepsilon_5 = \varepsilon_{gg}$$

Then equation 5.16 reduces to equation (5.17)

$$E_0 = Qu\varepsilon_c + Qv\varepsilon_{pp} + Q(\varepsilon_1 X_1 + \varepsilon_2 X_2 + \varepsilon_3 X_3 + X_4\varepsilon_4 + X_5\varepsilon_5) \qquad (5.17)$$

Now the next step is to determine the value of $\overline{X_i}$ which can be determined by maximization of the partition function Z_X. The method of Gamma functions (due to presence of a factorial function) is used in solving the equation 5.18 to determine maximum values of the parameter X_i.

$$\left(\frac{\partial \ln Z_X}{\partial X_i}\right)_{N,\phi,y,V.T,X_{j\neq i}} = 0 \qquad (5.18)$$

The determination of maximum values is essential since the entire system could be described in terms of the maximum value of the parameter X_i as per statistical thermodynamic theory.

$\ln Z_x$ is given by

$$\ln Z_x = \ln[Q(u - X_1 - X_3 - X_4)]! + [Q(v - X_1 - X_2)]! + \ln[Q(w - X_2 - X_3)]! +$$

$$\ln[Q(r - X_4 - X_5)]! + 2\ln(QX_1)! + 2\ln(QX_2)! + 2\ln(QX_3)! + 2\ln(QX_4)! + 2\ln(QX_5)!$$

$$- 3 < c_s > N < s > \ln\left[\left(1 - \frac{X}{q}\right) < l_s > + \left(\frac{X}{q}\right) < l_g >\right]$$

$$+\frac{Q}{kT}\left(\varepsilon_1 X_1+\varepsilon_2 X_2+\varepsilon_3 X_3+\varepsilon_4 X_4+\varepsilon_5 X_5\right) \tag{5.19}$$

The solid like and gas like free length <ls > and <lg> respectively of the polymer/clay system is like the case of a HH theory applied to a multicomponent polymer system since the presence of the solid particles do not alter the cell volume significantly, the modifiers on the clay surface alter the free length which is taken in to consideration by applying the concept of multi component mixtures of polymers as a result we have equation (5.20) (209)

$$\ln\left[\left(1-\frac{X}{q}\right)<l_s>+\left(\frac{X}{q}\right)<l_g>\right]=\ln\left[1-\beta\left(1-\frac{X}{q}\right)\right] \tag{5.20}$$

Using the Stirlings approximation ($\ln N!=N\ln N-N$) and combining equation (5.19) and (5.20) we have the following relations.

$$\begin{aligned}
\left(\overline{X_1}\right)\eta_{e1} &= \left(u-\overline{X_1}-\overline{X_3}-\overline{X_4}\right)\left(v-\overline{X_1}-\overline{X_2}\right)\eta_{s1}\\
\overline{X_2}\eta_{e2} &= \left(v-\overline{X_1}-\overline{X_2}\right)\left(w-\overline{X_2}-\overline{X_3}\right)\eta_{s2}\\
\overline{X_3}\eta_{e3} &= \left(u-\overline{X_1}-\overline{X_3}-\overline{X_4}\right)\left(w-\overline{X_2}-\overline{X_3}\right)\eta_{s3}\\
\overline{X_4}\eta_{e4} &= \left(u-\overline{X_1}-\overline{X_3}-\overline{X_4}\right)\left(r-\overline{X_4}-\overline{X_5}\right)\eta_{s4}\\
\overline{X_5}\eta_{e5} &= \left(r-\overline{X_4}-\overline{X_5}\right)\eta_{s5}
\end{aligned} \tag{5.21}$$

Where $\eta_{ei}=\exp\left(\varepsilon_i/kT\right)$ (5.22)

$$\eta_{s1} = \exp\left[\frac{2<c_s>q}{z(1-2/z(1-1/s))}\frac{\beta\left(1-\frac{\overline{X}}{q}\right)}{1-\beta\left(1-\frac{\overline{X}}{q}\right)}\frac{\partial \ln <v^*>}{\partial \overline{X_1}}\right] \quad (5.23)$$

$$\eta_{s2} = \exp\left[\frac{<c_s>q}{z(1-2/z(1-1/s)}\frac{2^{-1/6}}{\overline{l_f}}\right]X \exp\left[\frac{2<c_s>q}{z(1-2/z(1-1/s))}\frac{\beta\left(1-\frac{\overline{X}}{q}\right)}{1-\beta\left(1-\frac{\overline{X}}{q}\right)}\frac{\partial \ln <v^*>}{\partial \overline{X_2}}\right] \quad (5.24)$$

$$\eta_{s3} = \exp\left[\frac{<c_s>q}{z(1-2/z(1-1/s)}\frac{2^{-1/6}}{\overline{l_f}}\right]X \exp\left[\frac{2<c_s>q}{z(1-2/z(1-1/s))}\frac{\beta\left(1-\frac{\overline{X}}{q}\right)}{1-\beta\left(1-\frac{\overline{X}}{q}\right)}\frac{\partial \ln <v^*>}{\partial \overline{X_3}}\right] \quad (5.25)$$

$$\eta_{s4} = \exp\left[\frac{<c_s>q}{z(1-2/z(1-1/s)}\frac{2^{-1/6}}{\overline{l_f}}\right]X \exp\left[\frac{2<c_s>q}{z(1-2/z(1-1/s))}\frac{\beta\left(1-\frac{\overline{X}}{q}\right)}{1-\beta\left(1-\frac{\overline{X}}{q}\right)}\frac{\partial \ln <v^*>}{\partial \overline{X_4}}\right] \quad (5.26)$$

$$\eta_{s5} = \exp\left[\frac{2<c_s>q}{z(1-2/z(1-1/s))}\frac{\beta\left(1-\frac{\overline{X}}{q}\right)}{1-\beta\left(1-\frac{\overline{X}}{q}\right)}\frac{\partial \ln <v^*>}{\partial \overline{X_5}}\right] \quad (5.27)$$

The above relations (equation 5.21-5.27) can be used to determine the maximum values of the contact fraction X.

The next step is to determine X^*_i. Now the case of random mixing arises when other contact fractions are zero. This condition can be mathematically stated as the case of minimization of the partition function for X = 0 as given by equation (5.28).

$$\left(\frac{\partial Z_x^{\,0}}{\partial X_i}\right) = 0 \quad (5.28)$$

$$\ln Z_X^0 = \ln\left[Q(u - X_1 - X_3 - X_4)\right]! + \left[Q(v - X_1 - X_2)\right]! + \ln\left[Q(w - X_2 - X_3)\right]! +$$

$$\ln\left[Q(r - X_4 - X_5)\right]! + 2\ln(QX_1)! + 2\ln(QX_2)! + 2\ln(QX_3)! + 2\ln(QX_4)! + 2\ln(QX_5)! \quad (5.29)$$

Combining the equations (5.28) and (5.29) we have and again using the Stirlings approximation we have equation (5.30)

$$\left(X_1^*\right)^2 = \left(u - X_1^* - X_3^* - X_4^*\right)\left(v - X_1^* - X_2^*\right)$$

$$\left(X_2^*\right)^2 = \left(v - X_1^* - X_2^*\right)\left(w - X_2^* - X_3^*\right)$$

$$\left(X_3^*\right)^2 = \left(w - X_2^* - X_3^*\right)\left(u - X_1^* - X_3^* - X_4^*\right) \qquad (5.30)$$

$$\left(X_4^*\right)^2 = \left(u - X_1^* - X_3^* - X_4^*\right)\left(r - X_4^* - X_5^*\right)$$

$$\left(X_5^*\right)^2 = \left(r - X_4^* - X_5^*\right)$$

Solving the above equations and using the condition that X* =q (1-q) which applies to a pure polymer should also be valid for the case of a multicomponent system we have $X_1^* = uv$, $X_2^* = vw$ and $X_3^* = uw$ $X_4^* = ur$ $X_5^* = wr$

The expression for internal energy with modifications for the interaction energies is given below and is used as the final form equation (5.31).

$$-E_0(N,\phi_A,y,V,\overline{X_1},\overline{X_2},\overline{X_3})/kT = -\frac{N<s>z(1-2/z(1-1/s)}{2qRT}\left[u-\overline{X_1}-\overline{X_3}-\overline{X_4}\right]\varepsilon_c + \left[v-\overline{X_1}-\overline{X_2}\right]\varepsilon_{pp}$$
$$+2\overline{X_1}\varepsilon_{mp} + \overline{X_4}\varepsilon_{gp} + 2(r-\overline{X_4}-\overline{X_5})\varepsilon_{gg} \qquad (5.31)$$

According to HH Theory

$\ln N_{HH}$ =

$$N<s>\left[-\phi_A\ln(\phi_A/s_A) - \phi_B\ln(\phi_B/s_B) - \frac{1}{<s>}\ln y - \frac{1-y}{y}\ln(1-y) + \frac{1}{\gamma}\left(\frac{1-\alpha<y>}{y}\right)\ln(1-<\alpha>y)\right]$$

The free energy function is then given by equation (5.32)

$$A/n < s > RT = \phi_A \ln(\phi_A / s_A) + \phi_B \ln(\phi_B / s_B) + \phi_g \ln(\phi_g / s_g) + \frac{1}{< s >} \ln y$$

-

$$\left[-\frac{1-y}{y} \ln(1-y) + \frac{1}{\gamma} \left(\frac{1-(1-2/z(1-1/s)) < y >}{y} \right) \ln(1-y) \right]$$

-

$$\frac{z(1-2/z(1-1/s)}{2q} \left[2u \ln u + 2v \ln v + 2w \ln w + 2r \ln r \right] - (u - \overline{X_1} - \overline{X_3}) \ln(u - \overline{X_1} - \overline{X_3}) -$$

$$(v - \overline{X_1} - \overline{X_2}) \ln(v - \overline{X_1} - \overline{X_2}) - (w - \overline{X_2} - \overline{X_3}) \ln(w - \overline{X_2} - \overline{X_3}) - (r - \overline{X_4} - \overline{X_5}) \ln(r - \overline{X_4} - \overline{X_5})$$

-

$$\left[2\overline{X_1} \ln \overline{X_1} - 2\overline{X_2} \ln \overline{X_2} - 2\overline{X_3} \ln \overline{X_3} \right] - < c_s > \ln \left[\overline{\omega} < v^* > \left(1 - \beta \left(1 - \frac{\overline{X}}{q} \right)^3 \right) \right]$$

$$+ \frac{N < s > z(1-2/z(1-1/s)}{2qRT} \left[u - \overline{X_1} - \overline{X_3} - \overline{X_4} \right] \varepsilon_c + \left[v - \overline{X_1} - \overline{X_2} \right] \varepsilon_{pp}$$

$$+ 2\overline{X_1} \varepsilon_{mp} + \overline{X_4} \varepsilon_{gp} + 2(r - \overline{X_4} - \overline{X_5}) \varepsilon_{gg} \qquad + k_1 < c_s > \ln \left(k_2 \left(M_0 \right) / T \right)$$

(5.32)

The equation for free energy equation (5.32) in conjunction with the equation of internal energy, equation (5.31) can be used to determine a host of thermodynamic properties. All thermodynamic potentials can be expressed as a function of the Helmholtz free energy and the Internal energy of the system as shown below.

5.5 Determination of Equilibrium solubility:

The equilibrium solubility is determined by equating the chemical potential of the gas in the polymer/clay matrix and in the pure gas phase. The state of mixing between the

gas and the polymer/clay matrix will be completely random. As a result the combinatorial factor in this case can be used as per Prigorine et al's cell model for random mixing where the hardcore volume is simply replaced by the weighted average hardcore volume. It has been assumed that the gas and the clay particles do not interact since the clay particles are impermeable

The chemical potential in the pure phase as per SS theory is given by equation (5.33) (207)

$$\mu_{11} = RT \ln\left[\left(p / KT\right)\left(\left(N_a h\right)^2 / 2\pi mRT\right)^{3/2}\right] \qquad (5.33)$$

The chemical potential in phase 2 is given by

$$\mu_{12} = G_m + (1 - x_1)\frac{\partial G_m}{\partial x_1}$$

Where x_1 is the mole fraction of the dissolved gas in the system.

The contact site fraction of the gas with the polymer is given by equation (5.34) and equation (5.35)

$$X_4 = x_1 q_4 / \sum_i x_i q_i \qquad (5.34)$$

Also we have $x_i = r / q$ (5.35)

Now the mole fraction of a component in the system will be equivalent to its volume fraction

Hence we also have equation (5.36)

$$x = \frac{r(S_g N_g v_g)}{u(S_p N_p v_p) + v(s_{pp} N_{pp} v_{pp}) + r(s_g N_g v_g)} \qquad (5.36)$$

Equation 5.36 can be used to express x_i in terms of parameter X and then the calculation can be easily done

5.6 Simulation Algorithm

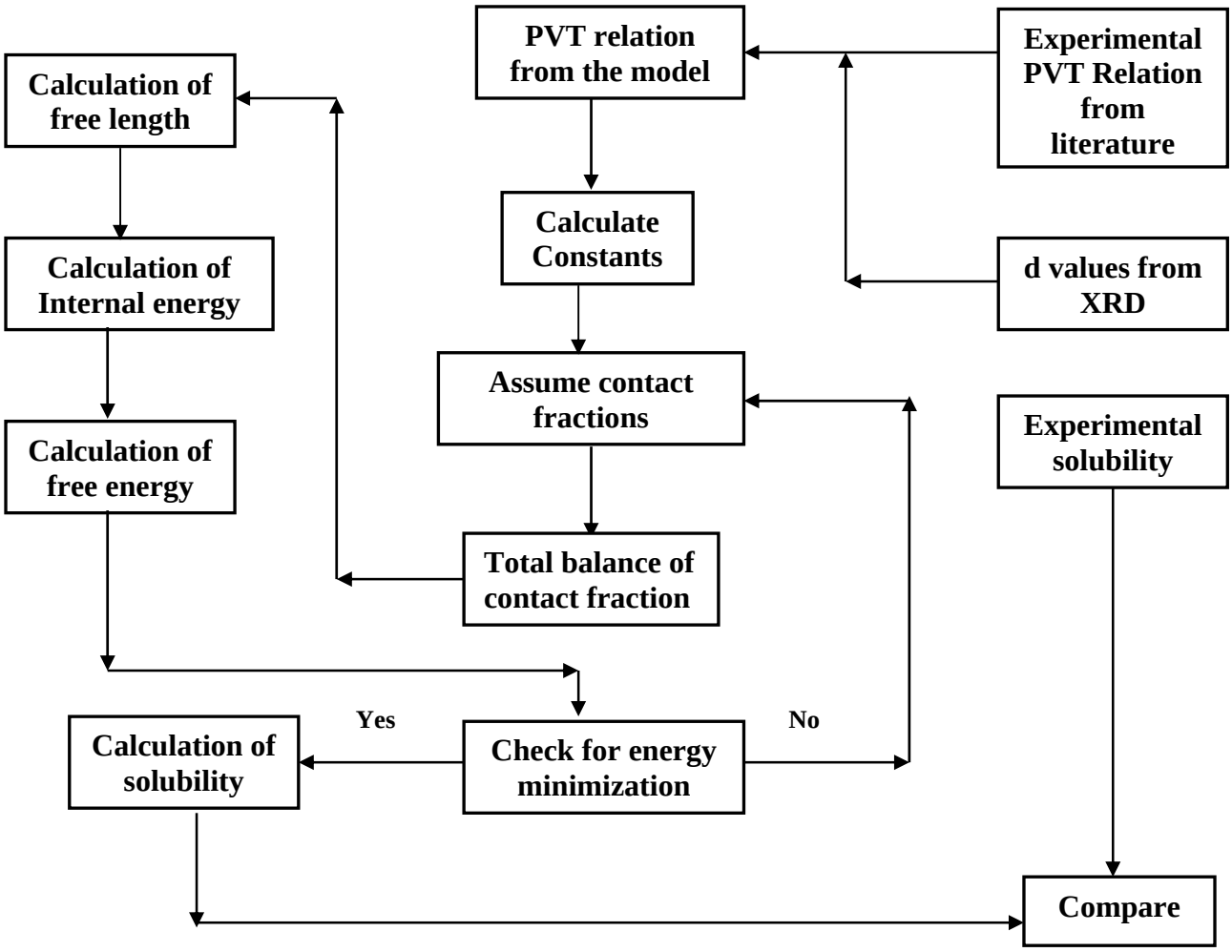

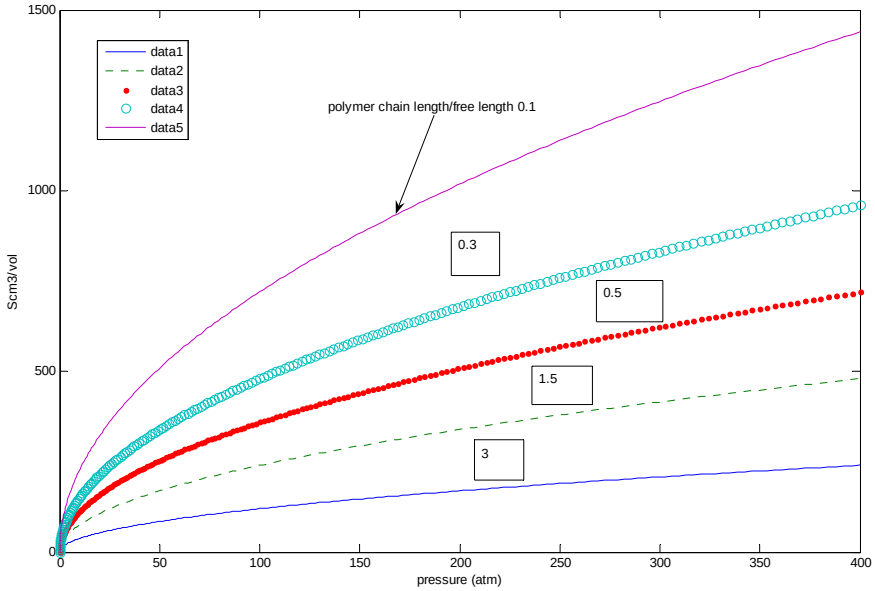

Figure 5.1: Variation in gas solubility with changes in pressure

Figure 5.1 shows the variation in gas solubility with changes in pressure for different polymer chain length. As it can be seen from the figure 5.1 that with increase in pressure the solubility increases. The increase in pressure increases the net energy of the gas molecules to overcome the resistance of polymer chains and hence the gas solubility increases. The rate of increase in solubility becomes sluggish at higher pressures. With increase in pressure the gas solubility increase and approaches towards equilibrium and hence the overall rate of increase reduces. Also the gas solubility decreases with increase in polymer chain length. This effect can be attributed to the fact that increase in polymer chain length reduces the overall free volume; also the contact fraction between the gas molecules and the free volume reduces. Also with increase in polymer chain length the contact fraction between the gas molecules and the polymer chain increase resulting in increased mobility of gas molecules , which further allows the gas molecule to escape from the matrix resulting in decrease in solubility.

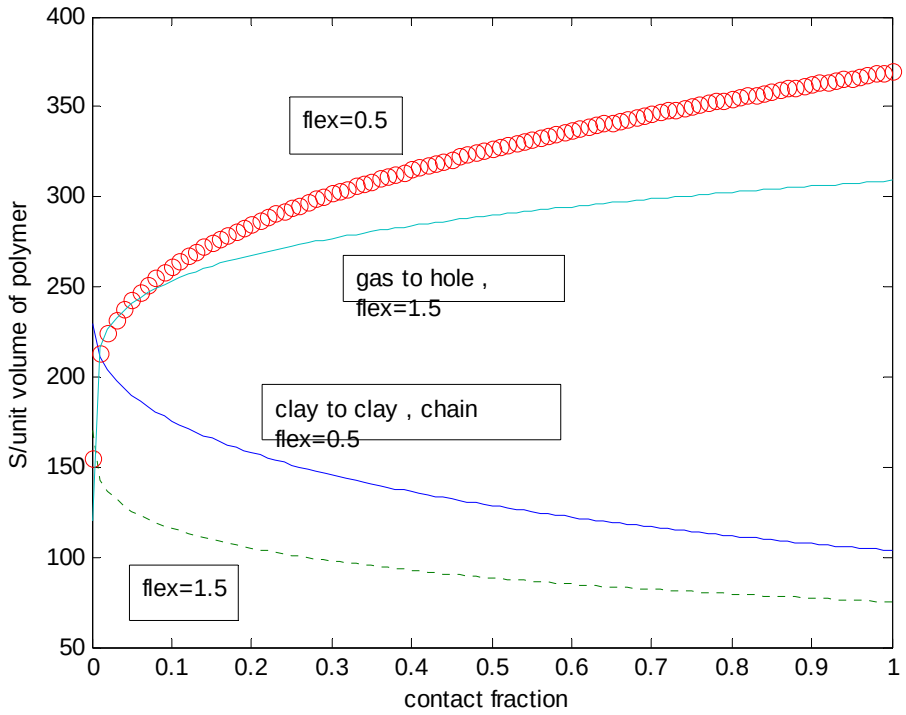

Figure 5.2: Effect of chain flexibility on gas solubility

Figure 5.2 shows an interesting result. As the chain flexibility increase the gas solubility decreases with increase in gas to hole contact fraction. At increased chain flexibility the mobility of the polymer chains is higher which allows higher interaction between the polymer chains and the gas molecules increasing the mobility of the gas molecules and hence decreasing overall solubility. Interestingly a reverse trend is seen for the case of clay to clay contact fraction. As the clay to clay contact fraction increase the chain flexibility increases since the clay particles are in a aggregated state and hence the polymer chains have a higher degree of independence to move around in the lattice (due to reduced interaction between the polymer chains and the clay particles) and hence the gas solubility decreases. Also with reduction in chain flexibility characterized by a reduced clay to clay contact fraction the gas solubility increases. This is due to the fact that with decrease in chain flexibility the overall

interaction between the clay particles and the polymer chains increases which results in creation of a solid like network structure. This network structure has very low mobility and hence allows the gas molecules to occupy free voids with out much interaction or exchange of kinetic energy between the gas molecules and the polymer chains.

5.7 Change in solubility with variation in clay loading

For a given polymer volume or lattice volume V the increase in clay loading will decrease the end to end distance between the particles at the same time the contact fraction between the polymer and the clay surface will increase (equation 5.21). The interaction potential between the particles (equation 5.11) will now be a strong function of the equivalent diameter of the particles (Deq). The increase in the contact fraction of the polymer chains will clay particles will significantly reduce its contact fraction with holes and other components in the system. The result will be that most of the polymer in the lattice will be bound in a small volume close to the clay particles in a highly entangled state. The close packing of the polymer chains with the clay will cause a reduction in solubility and permeability as well. The solid like free length of the polymer will increase and the gas like free length decrease (equation 5.15) due to decrease in X_2 , X_3 , X_4. This can be physically explained by the fact that due to close packing of the polymer chains close to the solid clay particles the polymer/clay matrix will behave more like a solid. The increase in equivalent diameter of the particle will cause aggregation of particles which will in turn reduce the contact fraction of the polymer with particles since the available sites for the contact of the polymer and the clay particles is reduced. Subsequently the contact fraction between the clay particles and the other components will also reduce. It could be assumed that even at higher clay loading the clay loading is significantly lesser than the volume fraction of the

polymer in the lattice, since the contact between the clay particles and the holes in the lattice has reduced due to aggregation the contact fraction between the holes and the polymer and the other components will increase which in turn will reduce fraction of holes available in the lattice, this reduction will cause subsequent reduction in solubility. At the same time the increase in the internal energy part of the free energy (211,216) and generation of large scale voids in the lattice due to aggregation of the clay particles will partially help increasing the solubility but overall the solubility will reduce. The generation of large scale voids in the system will increase permeability and the diffusion of gas with in the system.

The decrease in clay loading will have a reverse effect and the polymer/clay system will tend towards the case of random mixing and the solubility in that case will be like that for a pure polymer in the Random mixing state.

5.8 Effect of dispersion state of clay particles:

The effect of intercalation/exfoliation of the clay particles can be studied by varying the end to end distance between the polymer and the clay particles

In case of intercalated state the end to end distance will be lower as a result the attractive potential between the clay particles will be higher(from equation 5.10) which in turn will increase the clay to clay contact fraction (equation 5.21) and decrease the polymer to clay contact fraction(equation 5.24). The interaction potential between the clay-clay and polymer- clay particles will increase which will cause a subsequent reduction in the partition function (equation 5.14) and free energy (equation 5.32) and the equilibrium solubility will go down. In case of exfoliation the interaction potential between the clay particles will be weaker decreasing the internal energy of the system which in turn will increase (equation 5.13) the partition function

and the free energy (equation 5.32) quantitatively increasing solubility. At very low clay loadings (with an exfoliated state) this increase will be negligible (subsequent reduction in polymer/clay contact fraction) and the net solubility will be almost equivalent to the case of a pure polymer

5.9 Change in solubility with variation of the L/d ratio of clay particles.

The change in the L/d ratio of the particles produces a proportional change in the equivalent diameter of the particles causing a change in the interaction potential between the particles and the polymer-particle pair subsequently causing a change in equilibrium solubility with a change in the free energy of the system

5.10 Change in solubility due to changes in interaction potential

The effect of variation in the interaction potential between the particles and the polymer chains affects solubility. With increase in interaction potential between the polymer-clay systems (for a constant polymer-particle contact fraction) the polymer chains in contact with the particles will form entangled aggregates close to the particles. This structure will be repeated throughout as per the dispersion state of the clay particles. This will further cause a decrease in the free cell volume of the lattice , also the presence of holes with in the polymer will be reduced causing a decrease in solubility also the polymer self diffusion coefficient will reduce due to a very high proportion of the non random mixing in the matrix which in turn will further suppress diffusivity.

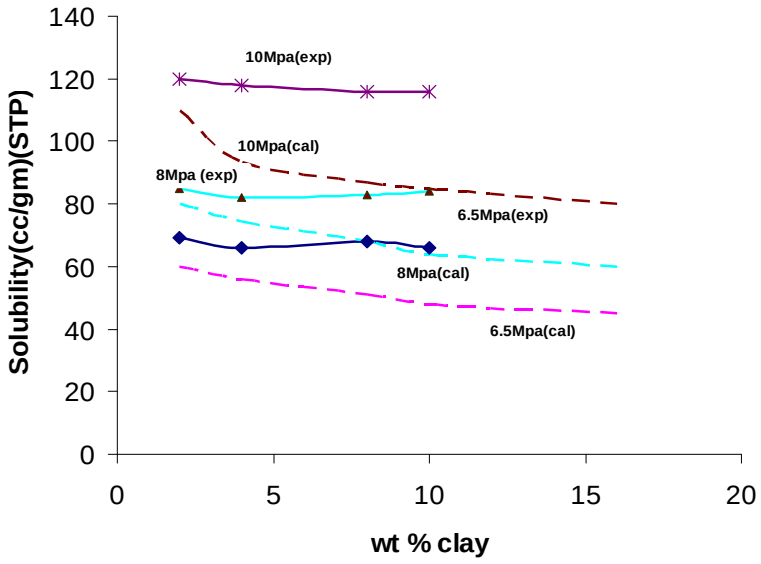

Figure 5.3: Comparison of simulation and experiment

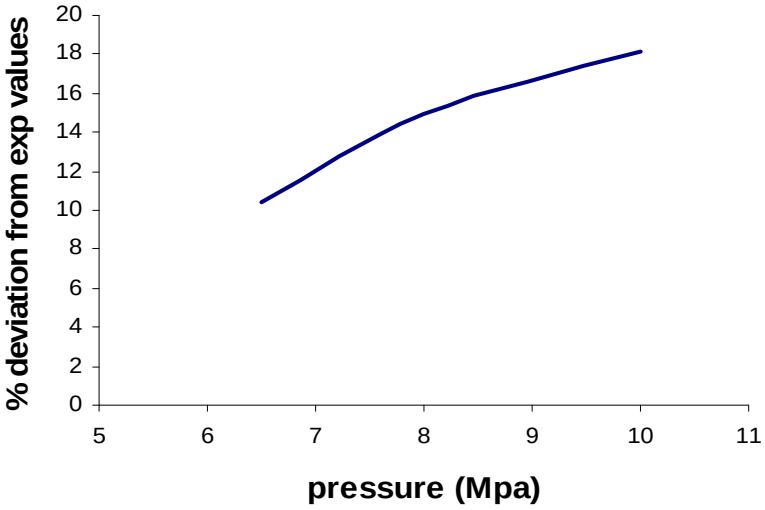

Figure 5.4: Deviations of model predictions from experimental values

Figure 5.3 and 5.4 show that the model predictions closely match the experimental observations with a maximum deviation of 18%.

5.11 Foam process simulation

Foam process simulation was performed with a view to analyze the effect of shear as well as extensional viscosity on the bubble growth process.

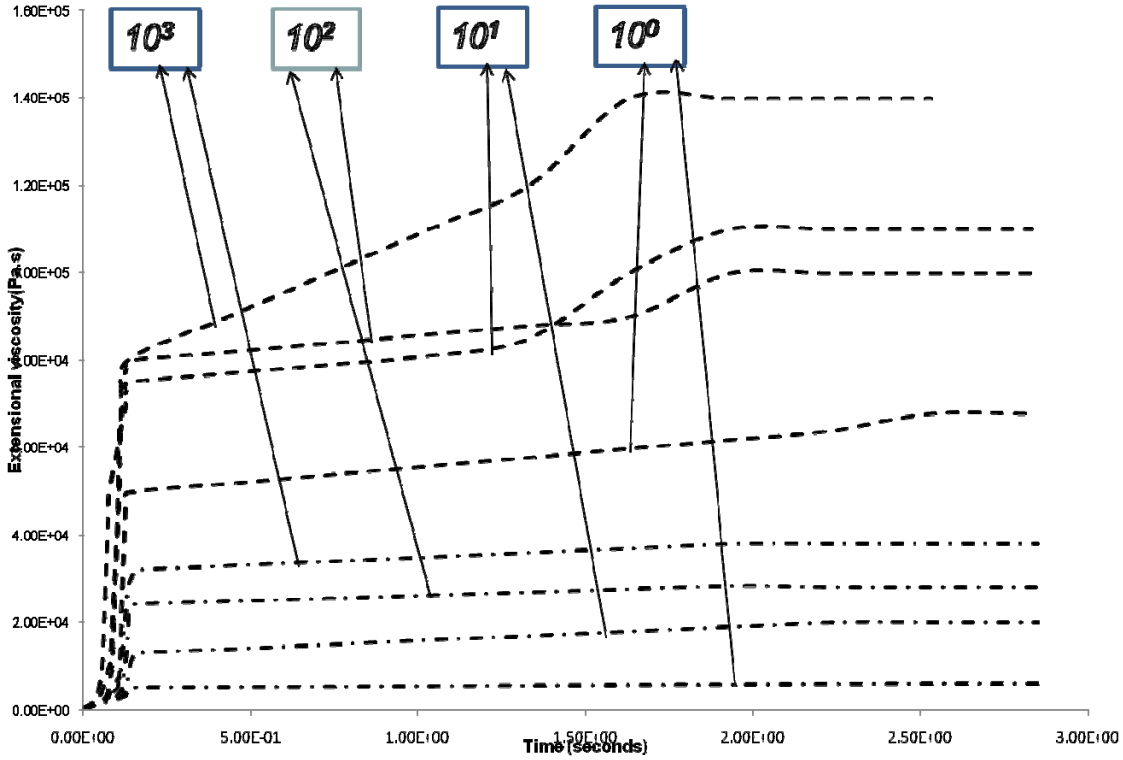

Figure 5.5: Variation of extensional viscosity with time

Figure 5.5 shows the simulation results for variation in extensional viscosity with time. It can be seen from the above figure that extensional viscosity increase rapidly in the first few seconds of foam growth and then becomes more or less constant. Also the extensional viscosity is higher for polymer chains with higher relaxation times since for higher relaxation times the polymer matrix has to branched or the polymer chain has to be long

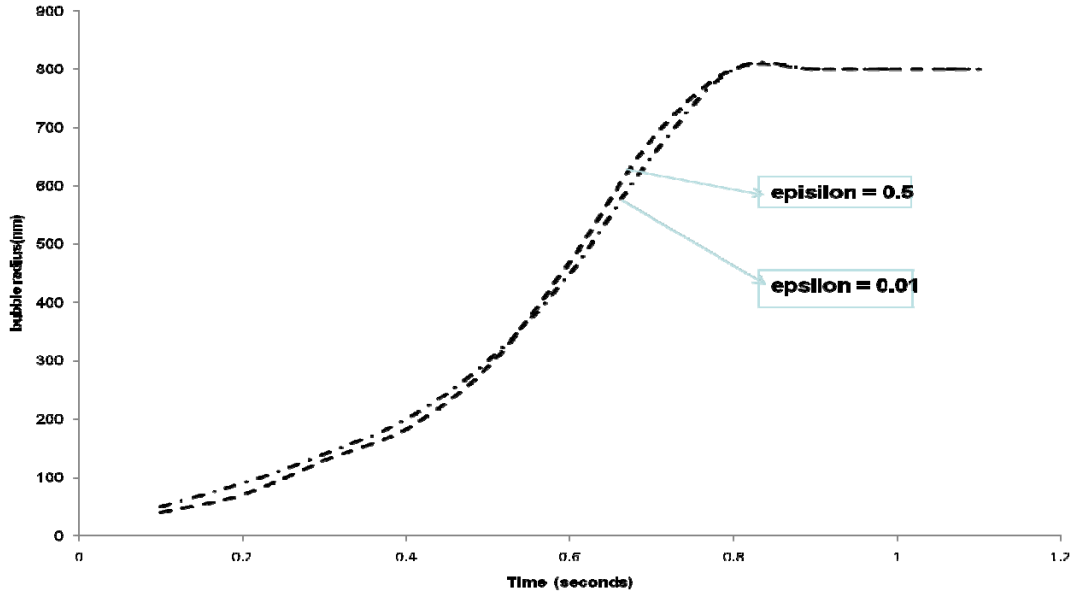

Figure 5. 6: Effect of hencky strain rate on bubble radius

To further understand the sensitivity of bubble radius to extensional viscosity the variation in bubble radius was tested for different hencky stretch rate (figure 5.6) and it was found that the bubble radius is insensitive to different stretch rates validating the fact that extensional viscosity is not the controlling parameter for cell growth. The reason being the extensional viscosity initially increase and then is almost constant throughout the bubble growth process

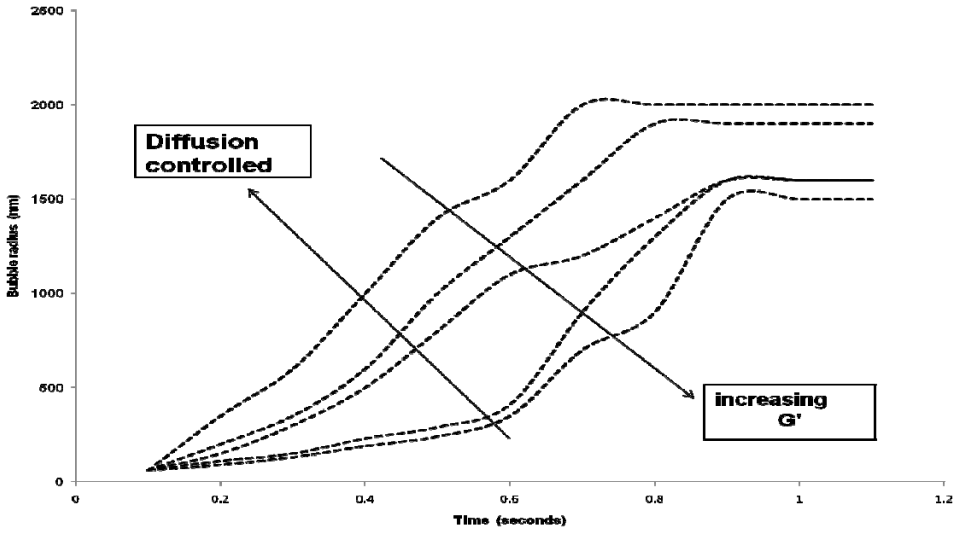

Figure 5.7: Effect of polymer matrix viscoelasticity on foam cell size

Now since it was concluded that extensional viscosity is not a controlling parameter the next step was to determine the effect of viscoelasticity on foam cell structure. Figure 5.7 shows the effect of viscoelasticity of the polymer matrix on bubble radius for different relaxation time and schemes and a sample molecular weight distribution (184). As it can be seen from the figure that the bubble growth becomes sluggish as the relaxation time increase or as the storage modulus increases. The elasticity of the polymer matrix increase with increase in relaxation time. Interestingly the bubble growth in this region is diffusion controlled where the gas actually has to diffuse through a viscoelastic film surrounding the growing bubble. Lastly it was necessary to understand the role of relaxation time on bubble growth The improvement in melt viscosity and elasticity of a polymer matrix by the addition of nanofiller causes a reduction in foam cell sizes. This reduction is due to the increased resistance to foam cell growth with improvement in melt viscosity and elasticity. Also the addition of a filler results in improved strain hardening behaviour which again causes reduction in rate of coalescence and foam growth, hence a reduction in foam cell sizes. Hence it is necessary to access the importance of these rheological parameters (melt elasticity and extensional viscosity) on the foam cell size.

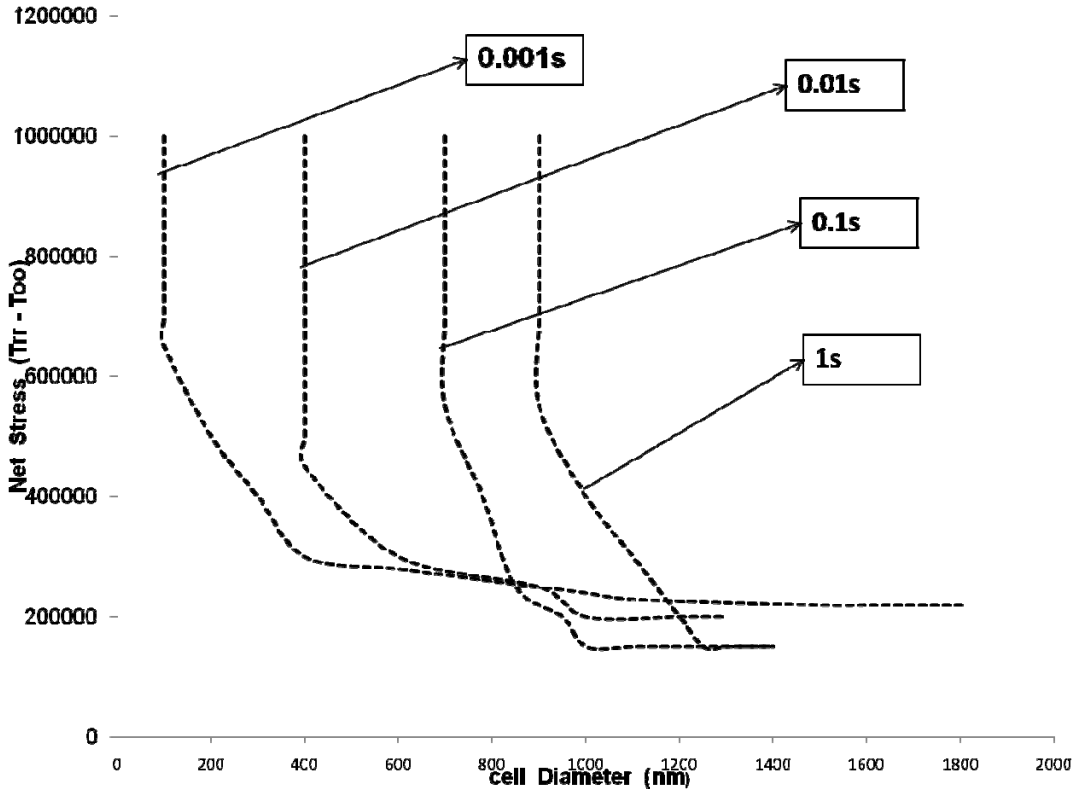

Figure 5.8: Effect of stress relaxation on foam cell radius

The figure 5.80 shows the net stress relaxation mechanism for different assumed relaxation time. It can be seen from the figure that the stress relaxation for 0.001 seconds is the quickest and hence the effect of net stress on bubble growth is more sluggish for a relaxation time of 0.001 seconds. Hence this relaxation time is very important in controlling the cell sizes. Also a small relaxation time hints towards the use of a branched polymer or a polymer with smaller chain length to control or restrict cell sizes

5.12 Summary

The simulation studies revealed that the contact fraction of the polymer with the clay particles affects solubility. The chain flexibility and the overall net chain length also effect solubility. In cases where the polymer chain length is small the polymer chains are closely packed and hence the free volume of the entire system increases and hence the gas has more free space to occupy. As the polymer chain length increases the free volume reduces also a reduction in the surface charge density for the same amount of surface charge with increase in length results in increase in the polymer chain mobility. An increased polymer chain mobility would cause a decrease in solubility since the gas molecules would collide with polymer chains and would hence gain enough kinetic energy to move around in the polymer matrix and finally escape. The chain flexibility also effects solubility. In case where the clay to clay contact fraction and the clay to polymer contact fraction is allowed to change keeping other contact fractions constant. An increase in chain flexibility denotes reduced clay to polymer contact and improved clay to clay contact. This reduction improves the polymer chain mobility and hence causes a reduction in overall solubility. In case where the chain flexibility reduces. The polymer chain has an increased contact with clay particles and hence the chain mobility is lower and hence the overall solubility improves. Interestingly the structure of the polymer chain (linear or branched would also affect solubility but that case has not been explored in these simulation studies. The rheological modelling studies around a growing bubble indicate that the viscoelasticity (net stress) around the growing bubble plays a significant role in controlling cell sizes since the overall net stress around the growing bubble decomposes throughout the growth life of the bubble. The extensional viscosity rises rapidly during the initial stages of bubble growth and then levels off. Thus the

extensional viscosity levels off after a few seconds once bubble growth starts. The change in the hencky strain rate also doesnot change the behaviour of extensional viscosity. In case of a growing bubble chains with the lower relaxation time are important as compared with chains with larger relaxation times. This can be attributed to the fact that chains with lower relaxation times are smaller and hence branched which increase the overall capacity of the chains to absorb stress energy and hence exponential decay of stress energy happens sluggishly and takes longer duration. This result quantitatively points towards the fact that use of a branched polymer would help in restricting bubble radius to smaller values.

Chapter 6: Conclusions

6. 1 Gas solubility studies

Experimental gas solubility studies revealed that the addition of clay to the polymer matrix causes reduction in gas solubility especially at higher pressures. The gas solubility can be increased by blending with polymers which have a strong interaction with the blowing agent used. Since in this work CO_2 was used as the physical blowing agent EVA was chosen as the additive. It was found that the addition of EVA enhances the gas solubility in the host polymer nanocomposite matrix. Normalization studies revealed that the effect of the interaction of the vinyl acetate content is only significant below the critical point of CO_2. After the critical point, other parameters like crystallinity, molecular weight distribution and interfacial adhesion affect the overall gas solubility.

6. 2 Clay compatibilization of immiscible PP/EVA blends

The addition of nanofillers (clay) to the HMS-PP/EVA blend resulted in improved adhesion at the blend intephase. To further investigate the compatibilization action, characterization studies were conducted on the immiscible HMS-PP/EVA/clay (60/40/7) blends. WAXD analysis showed a complete absence of a peak even with 7 wt percent of clay particles in the blend. This means that the clay particles are present in both the phases because in case they were only present in any one phase, there would be establishment of an intercalated morphology in atleast one of the phases which would be indicated by a peak in the WAXD patterns. SEM images revealed that the size of the dispersed phase (EVA) reduces significantly due to the addition of clay particles to the blend. TEM images revealed the presence of clay particles at the

blend interphase as well as within the bulk matrix. Measurement of mechanical properties revealed that the addition of clay particles causes an improvement in mechanical properties indicative of a compatibilization action of clay particles. The broadening of the melting peaks for both the blend components and the depression of heat of crystallization indicate molecular level interaction between the two phases after the addition of clay particles. In particular the lower molecular weight fractions of HMS-PP interact with the EVA phase. Dynamic rheological studies further validate the compatibilization action of clay particles as indicated by the presence of a small bulge or kink at lower frequencies. This kink represents a reduction in the size of the dispersed phase and increase in the relaxation time. Shear rheological studies show that at higher frequencies the shear viscosity of the blend with and without clay particles is almost same. Hence it was concluded that the reduction in size of the dispersed phase is just not because of increase in melt viscosity but also because of interaction between the two phases.

6. 3 Foam processing of HMS-PP/clay nanocomposites

The foam processing studies on polymer clay nanocomposites was carried out in a batch as well as in a continuous foam injection moulding system. The batch studies revealed that there is a reduction in foam cell size on addition of nanofillers to the host polymer matrix. The reduction in foam cell sizes occurs only till the point of rheologically determined percolation threshold. Once the percolation threshold is exceeded the cell sizes start to increase due to increased degree of cell coalescence. The degree of cell coalescence increases due to aggregation of nanoparticles added to the polymer matrix. The melt strength and extensional viscosity of the host matrix has a controlling influence on foam cell sizes. The strain hardening effect causes

hardening of the cell walls and hence helps in restricting foam cell sizes. The increase in melt viscosity on addition of clay particles also results in smaller foam cell sizes. The addition of nanoparticles results in reduction of foam cell sizes but doesn't lead to generation of nanocellular foams. The addition of CO_2 philic groups causes further reduction in foam cell sizes resulting in nanocellular foams.

Studies using foam injection moulding system reveal that the moulding parameters have a governing influence on foam cell sizes and it is difficult to attain nanocellular foams in a continuous system.

Modelling studies on gas solubility reveal that there is a case of nonrandom mixing, once nanoparticles are introduced into the polymer matrix. This mixing pattern affects the configurational entropy and the overall solubility of the system. The developed model is able to predict the experimentally observed gas solubility. The model can further provide insight into the effect of surface functionality, shape, size and overall interaction potential of the nanoparticles on gas solubility.

Rheological modelling studies revealed that the viscoelasticity of the polymer matrix has a controlling influence in determining foam cell sizes.

6.4 Future Work

Research on the generation of nanocellular polymer foams is still at a very nascent stage. Infact nanocellular foam cellular structure has never been achieved in a continuous foam processing systems. Hence it would be interesting to scale up the results from the batch processing of nanocellular foams to a continuous foaming system. The mechanism of foaming inside immiscible polymer blends with CO_2 absorbing groups is not known. The foam cell sizes attained is generally lesser than the size of the dispersed domains. Hence probably there is a different foam growth and nucleation mechanism which needs to be explored. Also the effect of polymer

blend rheology on foam cell growth also needs to be assessed. Further the effect of addition of different surfactants (for surface tension reduction) and also other different CO_2 absorbing groups needs to assessed. Once nanocellular foams can be commercially produced using a continuous foam processing system, it would be interesting to study the mechanism of mechanical fracture and heat transfer in such foams. Innovative applications of nanocellular foams viz: as data storage devices, in cases of rigid packaging and also as smart foams needs to be explored. The effect of clay particle dispersion state on final foam cell morphology also needs to be evaluated with a modelling perspective. Also other strategies (chemical and physical) to develop such nanocellular foam cell structures needs to be explored.

References

1. S. Lee, C. Park and N. Ramesh, *Polymeric Foams: Science and Technology*. 2006: CRC Press.

2. M. Shimoda, M. Tanigaki, M. Ohshima and I. Tsujimura, *Journal of Cellular Plastics*, **37**. 517.(2001).

3. C.B.P. Hani E. Naguib, U. Panzer, Norbert Reichelt, *Polymer Engineering & Science*, **42**. 1481. (2002).

4. S. Lee, *Foam Extrusion: Principles and Practice*. 2000: CRC Press.

5. D. Tomasko, X. Han, D. Liu and W. Gao, *Current Opinion in Solid State & Materials Science*, **7**. 407. (2003).

6. X. Sun, H. Liu, G. Li, X. Liao and J. He, *Journal of Applied Polymer Science*, **93**. 163. (2004).

7. P. Nam, P. Maiti, M. Okamoto, T. Kotaka, T. Nakayama, M. Takada, M. Ohshima, A. Usuki, N. Hasegawa and H. Okamoto, *Polymer Engineering and Science(USA)*, **42**. 1907. (2002).

8. P. Lee, J. Wang and C. Park, *Industrial and Engineering Chemistry Research*, **45**. 175. (2006).

9. C. Liu, D. Wei, A. Zheng, Y. Li and H. Xiao, *Journal of Applied Polymer Science*, **101**. 4114. (2006).

10. Y. Fujimoto, S. Ray, M. Okamoto, A. Ogami, K. Yamada and K. Ueda, *Macromolecular Rapid Communications*, **24**. 457. (2003).

11. Y. Lee, C. Park, K. Wang and M. Lee, *Journal of Cellular Plastics*, **41**. 487. (2005).

12. M. Okamoto, P. Nam, P. Maiti, T. Kotaka, T. Nakayama, M. Takada, M. Ohshima, A. Usuki, N. Hasegawa and H. Okamoto, *Nano Lett*, **1**. 503. (2001).

13. Y. Sato, T. Takikawa, S. Takishima and H. Masuoka, *The journal of Supercritical fluids*, **19**. 187. (2001).

14. I. Sanchez and P. Rodgers, *Pure Appl. Chem*, **62**. 2097. (1990).

15. C. Zhong and H. Masuoka, *Fluid Phase Equilibria*, **144**. 49. (1998).

16. H. Xie and R. Simha, *Polymer International*, **44**. 348. (1997).

17. D. Klempner and K. Frisch, *Handbook of polymeric foams and foam technology*. 1991: Hanser.

18. A. Landrock, *Handbook of Plastic Foams: Types, Properties, Manufacture, and Applications*. 1995: Noyes Publications.

19. S. Lee, *Foam Extrusion: Principles and Practice*. 2000: CRC Press.

20. H. Fischer, *Materials Science & Engineering C*, **23**. 763.(2003).

21. L. Lee, C. Zeng, X. Han, D. Tomasko and K. Koelling. *Polymer Nanocomposite Foams Prepared by Supercritical Fluid Foaming Technology*. in M*aterials research society symposium proceedings*. 2002: Warrendale, Pa.; Materials Research Society; 1999.

22. S. Lee, C. Park and N. Ramesh, *Polymeric Foams: Science and Technology*. 2006: CRC Press.

23. S. Doroudiani, C. Park and M. Kortschot, *Polymer Engineering & Science*, **36**. 2645.(1996).

24. G. Nam, J. Yoo and J. Lee, *Journal of Applied Polymer Science*, **96**. 1793.(2005).

25. A. Sinsawat, K. Anderson, R. Vaia and B. Farmer, *Journal of Polymer Science, Part B, Polymer Physics*, **41**. 3272.(2003).

26. D. Tomasko, X. Han, D. Liu and W. Gao, *Current Opinion in Solid State & Materials Science*, **7**. 407.(2003).

27. J. Colton and N. Suh, *Polymer Engineering and Science*, **27**. 500.(1987).

28. L. Lee, K. Koelling, D. Tomasko, X. HanandC. Zeng, *Polymer nanocomposite foams*. 2004, Google Patents.

29. E. Giannelis. , *Polymer nanocomposite foams* , 2005 , google patents

30. J. Gilman, C. Jackson, A. Morgan, R. Harris, E. Manias, E. Giannelis, M. Wuthenow, D. Hilton and S. Phillips, *Chemistry of Materials(USA)*, **12**. 1866.(2000).

31. A. Morgan and J. Harris, *Polymer*, **44**. 2313.(2003).

32. M. Alexandre and P. Dubois, *Materials Science & Engineering R*, **28**. 1.(2000).

33. E. Giannelis, R. Krishnamoorti and E. Manias, A*dvances in polymer science*, **138**. 107.(1998).

34. P. LeBaron, Z. Wang and T. Pinnavaia, *Applied Clay Science*, **15**. 11.(1999).

35. S. Sinha Ray and M. Okamoto, *Progress in Polymer Science*, **28**. 1539.(2003).

36. X. Fu and S. Qutubuddin, *Polymer*, **42**. 807.(2001).

37. T. Fornes, P. Yoon, H. Keskkula and D. Paul, *Polymer*, **42**. 9929.(2001).

38. P. Nam, P. Maiti, M. Okamoto, T. Kotaka, N. Hasegawa and A. Usuki, *Polymer*, **42**. 9633.(2001).

39. M. Biswas and S. Ray, A*dvances in polymer science*, **155**. 167.(2001).

40. L. Liu, Z. Qi and X. Zhu *Journal of Applied Polymer Science*, **71**. 1133.(1999).

41. J. Yoon, W. Jo, M. Lee and M. Ko, *Polymer*, **42**. 329.(2001).

42. M. Okamoto, P. Nam, P. Maiti, T. Kotaka, T. Nakayama, M. Takada, M. Ohshima, A. Usuki, N. HasegawaandH. Okamoto, *Nano Lett*, **1**. 503.(2001).

43. Y. Ema, M. Ikeya and M. Okamoto, *Polymer*, **47**. 5350.(2006).

44. X. Sun, H. Liu, G. Li, X. Liao and J. He, *Journal of Applied Polymer Science*, **93**. 163.(2004).

45. D. Baldwin, P*olymer engineering and science*, **35**. 433.(1995).

46. S. Lee, *Foam extrusion: Principles and Practice*. 81–124.(2000)
.

47. M. Shafi and R. Flumerfelt, *Chemical Engineering Science*, **52**. 627.(1997)
.

48. V. Kumar and H. Schirmer, *ANTEC'95.*, **2**. 2189.(1995).

49. V. Kumar and H. Schirmer, *A Semi-Continuous Process to Produce Microcellular Foams*. 1997, US Patent 5,684,055.

50. C. Han, *Multiphase Flow in Polymer Processing*. 1981: Academic Press.

51. D. Johnson, C. Krutchen and G. Sharps Jr, *Polymer foam extrusion system*. 1982, US Patent 4,344,710.

52. C. Rauwendaal, *Mixing in Polymer Processing*. 1991: Marcel Dekker.

53. G. Atlanta and M. Cambridge, *Polymer engineering and science*, **36**.(1996).

54. X. Han, K. Koelling, D. Tomasko and L. Lee, *Polymer engineering and science*, **43**. 1206.(2003).

55. H. Naguib, C. Park, U. Panzer and N. Reichelt, P*lymer engineering and science*, **42**. 1481.(2002).

56. R. Gendron and L. Daigneault , *Foam Extrusion: Principles and Practice*.(2000).

57. C. Lee, K. Lee, H. Jeong and S. Kim, *Advances in Polymer Technology*, **19**. 97.(2000).

58. L. Hyde, L. Kishbaugh and J. Katterman, *SAE Transactions: Journal of Materials & Manufacturing*, **111**. 463.(2003).

59. D. Pierick and K. Jacobsen, *Plastics engineering*, **57**. 46.(2001).

60. G. Atlanta and M. Cambridge, *Polymer engineering and science*, **27**. 493.(1987).

61. J. Xu and D. Pierick, *Journal of Injection Molding Technology(USA)*, **5**. 152.(2001).

62. J. Martini-Vvedensky, N. Suh and F. Waldman, *Microcellular closed cell foams and their method of manufacture*. 1984.

63. C. Park, S. Doroudiani and M. Kortschot, *Polymer Engineering and Science(USA)*, **38**. 1205.(1998).

64. N. SUH, P*olymer engineering and science*.(1990).

65. M. Yuan, L. Turng, S. Gong, D. Caulfield, C. Hunt and R. Spindler, *Polymer Engineering and Science*, **44**. 673.(2004).

66. J. Stevenson, *Specialized Molding Techniques*.(2001).

67. R. Gosselin, D. RodrigueandB. Riedl, *Journal of Thermoplastic Composite Materials*, **19**. 639.(2006).

68. M. Hosur, A. Mohammed, S. Zainuddin and S. Jeelani, *Materials Science & Engineering A*, **498**. 100.(2008).

69. J. Shen, C. Zeng and L. Lee, *Polymer*, **46**. 5218.(2005).

70. L. Turng, M. Yuan, H. Kharbas, H. Winata and D. Caulfield. *Applications of nanocomposites and woodfiber plastics for microcellular injection molding., May 19-20, 2003... Madison, Wisconsin, USA. Madison, WI: Forest Products Society, 2003*.

71. C. Park, *Foam Extrusion: Principles and Practice*. 263–305.(2000).

72. S. Doroudiani and M. Kortschot, *Journal of Applied Polymer Science*, **90**. 1412.(2003).

73. X. Han, C. Zeng G, L. Lee, K. Koelling and D. Tomasko , *Polymer engineering and science*, **43**. 1261.(2003).

74. T. Lickly, K. Lehr and G. Welsh, *Food and Chemical Toxicology*, **33**. 475.(1995).

75. Y. Oyanagi and J. White, *Journal of Applied Polymer Science*, **23**. 1013.(1979).

76. B. Rodeheaver and J. Colton, *Polymer engineering and science*, **41**. 380.(2001).

77. J. Schubert and E. LeDuc, *Method of extruding a polystyrene foam using both a physical blowing agent and water*. 1984, Google Patents.

78. S. Sumarno, S. Takishima and H. Masuoka, *Journal of Applied Polymer Science*, **77**. 2383.(2000).

79. M. Yazawa, *Process for continuously producing shaped articles of polystyrene foam*. 1976, Google Patents.

80. C. Zeng, X. Han, L. Lee, K. Koelling and D. Tomasko, *Advanced Materials*, **15**.(2003).

81. W. Strauss and N. D'Souza, *Journal of Cellular Plastics*, **40**. 229.(2004).

82. Y. Ke, C. Long and Z. Qi, *Journal of Applied Polymer Science*, **71**. 1139.(1999).

83. P. Maiti, P. Nam, M. Okamoto, N. Hasegawa and A. Usuki, *Macromolecules*, **35**. 2042.(2002).

84. X. Cao, L. James Lee, T. Widya and C. Macosko, *Polymer*, **46**. 775.(2005).

85. Y. Fujimoto, S. Ray, M. Okamoto, A. Ogami, K. YamadaandK. Ueda, *Macromolecular Rapid Communications*, **24**. 457.(2003).

86. E. Di Maio, C. Marrazzo, Y. Di, S. Iannace and L. Nicolais, P*resent situation and forecasts of nanotechnology in: materials, health and medicalsystems*.

87. Y. Di, S. Iannace, E. Di Maio and L. Nicolais, *Journal of Polymer Science, Part B, Polymer Physics*, **43**. 689.(2005).

88. S. Lee, H. Chen and M. Hanna, *Industrial Crops & Products*.(2008).

89. M. Okamoto, *Polymeric Foams: Technology and Developments in Regulation, Process, and Products*. 175.(2008).

90. S. Ray and M. Okamoto, M*acromolecular materials and engineering*. 936.(2003).

91. M. Mitsunaga, Y. Ito, S. Ray, M. Okamoto and K. Hironaka, *Macromolecular Materials and Engineering*, **288**. 543.(2003).

92. J. Fu and H. Naguib, *Journal of Cellular Plastics*, **42**. 325.(2006).

93. Y. Lee, C. Park, K. Wang and M. Lee, *Journal of Cellular Plastics*, **41**. 487.(2005).

94. P. Nam, P. Maiti, M. Okamoto, T. Kotaka, T. Nakayama, M. Takada, M. Ohshima, A. Usuki, N. HasegawaandH. Okamoto, P*olymer engineering and science*, **42**. 1907.(2002).

95. W. Daming, M. Qingyun, L. Ying, D. Yumei, C. Weihong, X. Hong and R. Dongyun, *Journal of polymer science part b polymer physics*, **41**. 1051.(2003).

96. H. Huang and J. Wang, *Journal of Applied Polymer Science*, **106**. 505.(2007).

97. K. KOELLING, *Polymer engineering and science*, **43**. 1261.(2003).

98. C. Park, *Journal of Cellular Plastics*, **38**. 129.(2002).

99. W. Zheng, Y. Lee and C. Park, *Journal of Cellular Plastics*, **42**. 271.(2006).

100. C. Zeng, X. Han, L. Lee, K. Koelling and D. Tomasko, *Advanced Materials*, **15**. 1743.(2003).

101. J. Velasco, M. Antunes, O. Ayyad, J. López-Cuesta, P. Gaudon, C. Saiz-Arroyo, M. Rodríguez-Pérez and J. de Saja, *Polymer*, **48**. 2098.(2007).

102. L. Chen, K. Blizard, R. Straff and X. Wang, *Journal of Cellular Plastics*, **38**. 139.(2002).

103. L. Chen, H. Sheth and X. Wang, *Journal of Cellular Plastics*, **37**. 353.(2001).

104. M. Shafi, K. Joshi and R. Flumerfelt, *Chemical Engineering Science*, **52**. 635.(1997).

105. C. Lu and Y. Mai, *Composites Science and Technology*, **67**. 2895.(2007).

106. S. Goel and E. Beckman, P*olymer engineering and science*, **34**. 1137.(1994).

107. S. Leung, H. Li and C. Park.

108. N. Ramesh, D. Rasmussen and G. Campbell, *Polymer engineering and science*, **34**. 1698.(1994).

109. J. Yokohama, *Cellular and Microcellular Materials*, **496**. 0.25.(1994).

110. C. Park, A. Behravesh and R. Venter. *A Strategy for the Suppression of Cell Coalescence in the Extrusion of Microcellular High-Impact Polystyrene Foams*. in ACS*s symposium series*. 1997: american chemical society.

111. S. Goel and E. Beckman, *Polymer Engineering & Science*, **34**.(1994).

112. R. Krishnamoorti and K. Yurekli, *Current Opinion in Colloid & Interface Science*, **6**. 464.(2001).

113. U. CNRS, R. du Maine and F. Le Mans Cedex, *Europhys. Lett*, **3**. 297.(1987).

114. M. Seo and S. Park, *Chemical Physics Letters*, **395**. 44.(2004).

115. S. Muke, I. Ivanov, N. Kao and S. Bhattacharya, *Journal of Non-Newtonian Fluid Mechanics*, **101**. 77.(2001).

116. V. Pasanovic-Zujo, R. Gupta and S. Bhattacharya, *Rheologica Acta*, **43**. 99.(2004).

117. R. Prasad, V. Pasanovic-Zujo, R. Gupta, F. Cser and S. Bhattacharya, *Polymer Engineering and Science*, **44**.(2004).

118. R. KrishnamoortiandE. Giannelis, M*acromolecules*, **30**. 4097.(1997).

119. C. MitchellandR. Krishnamoorti, *Journal of polymer science part b polymer physics*, **40**. 1434.(2002).

120. G. Galgali, S. Agarwal and A. Lele, *Polymer*, **45**. 6059.(2004).

121. S. Kazarian, M. Vincent, B. West and C. Eckert, *The Journal of Supercritical Fluids*, **13**. 107.(1998).

122. C. Drohmann and E. Beckman, *The Journal of Supercritical Fluids*, **22**. 103.(2002).

123. Y. Shieh, J. Su, G. Manivannan, P. Lee, S. SawanandW. Spall, *Journal of Applied Polymer Science*, **59**. 695.(1996).

124. Y. Zhao and H. Huang. *Effect of Supercritical Co2 on Morphology and Rheology of Polymer Nanocomposites Prepared by Melt Compounding*. in *The 2006 Annual Meeting*. 2006.

125. S. Gu, J. Ren and Q. Wang, *Journal of Applied Polymer Science*, **91**. 2427.(2004).

126. J. Rowen and R. Simha, *The Journal of Physical Chemistry*, **53**. 921.(1949).

127. I. Sanchez and R. Lacombe, *The Journal of Physical Chemistry*, **80**. 2352.(1976).

128. R. Simha and T. Somcynsky, *Macromolecules*, **2**. 342.(1969).

129. E. Nies and H. Xie, *Macromolecules*, **26**. 1683.(1993).

130. H. Xie and R. Simha, *Polymer International*, **44**. 348.(1997).

131. H. Hu, G. Peterson, X. Peng and B. Wang, *International Journal of Heat and Mass Transfer*, **41**. 3483.(1998).

132. S. Yang and R. Kim, *International journal of heat and mass transfer*, **31**. 1127.(1988).

133. S. goel and E. Beckman, *Polymer engineering and science*, **34**. 1148.(1994).

134. M. BlanderandJ. Katz, *AIChE Journal*, **21**.(1975).

135. M. Shimoda, M. Tanigaki, M. Ohshima and I. Tsujimura, *Journal of Cellular Plastics*, **37**. 517.(2001).

136. L. Chen, X. Wang, R. Straff and K. Blizard, *Polymer Engineering & Science*, **42**.(2002).

137. S. Lee, *Journal of Cellular Plastics*, **37**. 221.(2001).

138. J. Han and C. Han, *Polymer Engineering & Science*, **28**.(1988).

139. R. Upadhyay, *Advances in Polymer Technology*, **5**. 55.(1985).

140. R. Larson, *Journal of Rheology*, **28**. 545.(1984).

141. D. Baldwin, *Cellular and Microcellular Materials*, **53**. 85.(1994).

142. A. Arefmanesh and S. Advani, *Rheologica Acta*, **30**. 274.(1991).

143. Y.H. Lee, C.B. Park, K.H. Wang and M.H. Lee, *Journal of Cellular Plastics*, **41**. 487.(2005).

144. T. Otsuka, K. Taki and M. Ohshima, *Die Angewandte Makromolekulare Chemie*, **293**. 78.(2007).

145. S. Siripurapu, Y. Gay, J. Royer, J. DeSimone, R. Spontak and S. Khan, *Polymer*, **43**. 5511.(2002).

146. K. Taki, T. Otsuka, Y. Waratani and M. Ohshima.

147. T. Nemoto, J. Takagi and M. Ohshima, *Die Angewandte Makromolekulare Chemie*, **293**. 991.(2008).

148. T. Otsuka, K. Taki and M. Ohshima, *Macromolecular Materials and Engineering*, **293**.(2008).

149. (www.plastemart.com).

150 R. Shah and D. Paul, *Polymer*, **45**. 2991. (2004).

151. Y.H. Lee, C.B. Park, K.H. Wang and M.H. Lee, *Journal of Cellular Plastics*, **41**. 487. (2005).

152. D.F.B. Chul B. Park, Nam P. Suh, *Polymer Engineering & Science*, **35**. 432. (1995).

153. Y. Sato, T. Takikawa, S. Takishima and H. Masuoka, *The journal of Supercritical fluids*, **19**. 187. (2001).

154. F. Morrison, *Understanding rheology*. 2001: Oxford University Press, USA.

155. R. Krishnamoorti and E. Giannelis, *Macromolecules*, **30**. 4097. (1997).

156. R. Krishnamoorti and K. Yurekli, *Current Opinion in Colloid & Interface Science*, **6**. 464. (2001).

157. S. Lim, C. Lee, H. Choi and M. Jhon, *Journal of Polymer Science, Part B, Polymer Physics*, **41**. 2052. (2003).

158. V. Pasanovic-Zujo, R. Gupta and S. Bhattacharya, *Rheologica Acta*, **43**. 99. (2004).

159. P. Powell, *Polymer Engineering & Science*, **14**. (1974).

160. J. Stickel and R. Powell. (2005).

161. C. Macosko and W. Davis, *Rheologica Acta*, **13**. 814. (1974).

162. C. Ferraris and N. Martys, *Technology*, **108**. 229. (2003).

163. S. Sinha Ray, S. Pouliot, M. BousminaandL. Utracki, *Polymer*, **45**. 8403. (2004).

164. M. Bousmina, *Rheologica Acta*, **38**. 73.(1999).

165. R.A. Vaia and E.P. Giannelis, *Macromolecules*, **30**. 7990.(1997).

166. A. Gupta, B. Ratnam and K. Srinivasan, *Journal of Applied Polymer Science*, **46**. 281.(1992).

167. W.N. Kim and C.M. Burns, *Journal of Applied Polymer Science*, **32**. 2989.(1986).

168. P.B. Rim and J.P. Runt, *Macromolecules*, **17**. 1520.(1984).

169. S. Ray, *Progress in Polymer Science*, **28**. 1539.(2003).

170. D. Chaudhary, R. Prasad, R. Gupta and S. Bhattacharya, *Thermochimica Acta*, **433**. 187.(2005).

171. Y. Wang, Q. Zhang and Q. Fu, *Macromolecular Rapid Communications*, **24**. 231.(2003).

172. D. Hoppner and J. Wendorff, *Colloid & Polymer Science*, **268**. 500.(1990).

173. S. RAY and M. BOUSMINA, *Macromolecular rapid communications*, **26**. 450.(2005).

174. S. Tjong, S. Liu and R. Li, *Journal of Materials Science*, **31**. 479.(1996).

175. A. Yee and M. Maxwell, *Journal of Macromolecular Science, Part B*, **17**. 543.(1980).

176. A. Yee, *Polymer Engineering and Science*, **17**. 213.(1977).

177. J. Barlow and D. Paul, *Polymer Engineering and Science*, **21**. 985.(1981).

178. T. Malik, *Journal of Applied Polymer Science*, **46**. 303.(1992).

179. Y. Chun, Y. Kyung, H. Jung and W. Kim, *Polymer*, **41**. 8729.(2000).

180. M. Shahlari, P. Roberts, L. Leavitt, M. Factor and S. Lee, *The 2007 Annual Meeting*.(2007).

181. C.W.M. Pieter Spitael, *Polymer Engineering and Science*, **44**. 2090.(2004).

182. C.B.P. Hani E. Naguib, U. Panzer, Norbert Reichelt,, *Polymer Engineering & Science*, **42**. 1481.(2002).

183. C. Liu, D. Wei, A. Zheng, Y. Li and H. Xiao, *Journal of Applied Polymer Science*, **101**. 4114.(2006).

184. P. Nam, P. Maiti, M. Okamoto, T. Kotaka, T. Nakayama, M. Takada, M. Ohshima, A. Usuki, N. HasegawaandH. Okamoto, *Polymer Engineering and Science(USA)*, **42**. 1907.(2002).

185. Y. Fujimoto, S. Ray, M. Okamoto, A. Ogami, K. Yamada and K. Ueda, *Macromolecular Rapid Communications*, **24**. 457.(2003).

186. Y.H. Lee, C.B. Park, K.H. Wang and M.H. Lee, *Journal of Cellular Plastics*, **41**. 487.(2005).

187. M. Wagner, H. Bastian, P. Hachmann, J. Meissner, S. Kurzbeck, H. Münstedt and F. Langouche, *Rheologica Acta*, **39**. 97.(2000).

188. Y. JahaniandM. Barikani, *Iranian Polymer Journal*, **14**. 361.(2005).

189. S. Sinha Ray and M. Okamoto, *Progress in Polymer Science*, **28**. 1539.(2003).

190. M. Varma-Nair, P. Handa, A. Mehta and P. Agarwal, *Thermochimica Acta*, **396**. 57.(2003).

191. W. Kaewmesri, P. Lee, C. Park and J. Pumchusak, *Journal of Cellular Plastics*, **42**. 405.(2006).

192. D.F.B. Chul B. Park, Nam P. Suh,, *Polymer Engineering & Science*, **35**. 432.(1995).

193. D.H.R. N. S. Ramesh, Gregory A. Campbell,, *Polymer Engineering & Science*, **31**. 1657.(1991).

194. D.H.R. N. S. Ramesh, G. A. Campbell,, *Polymer Engineering & Science*, **34**. 1698.(1994).

195. X. Sun, H. Liu, G. Li, X. Liao and J. He, *Journal of Applied Polymer Science*, **93**. 163.(2004).

196. J.M.P. D. D. Liu, *Journal of Applied Polymer Science*, **24**. 725.(1979).

197. Y. Ito, M. Yamashit and M. Okamoto, *Macromolecular materials and engineering(Print)*, **291**. 773.(2006).

198. M. Okamoto, P. Nam, P. Maiti, T. Kotaka, T. Nakayama, M. Takada, M. Ohshima, A. Usuki, N. Hasegawa and H. Okamoto, *Nano Lett*, **1**. 503.(2001).

199. D. BALDWIN, P*olymer engineering and science*, **35**. 433.(1995).

200. Y. Lee, C. Park, K. Wang and M. Lee, *Journal of Cellular Plastics*, **41**. 487.(2005).

201. Simha R, Somcynsky T, , " *Macromolecules*, 1969 (2) ,4.

202. Jain R.K. Simha R, 1980, "*Macromolecules* 13, 1501-1508.

203. Simha R, 1996, , *Polymer Engineering & Science*,3 ,12.

204. Simha R, Jain R.K, *Polymer Physics Edition*, 1996,16, 1471-1489.

205. Olabisi O, Simha R, 1977, "*Macromolecules*, 21, 149-163.

206. Quak T.Y. , Masoori G.A., *Chemical engineering Science* , ,1986 41,5,1303-1309.

207. Xie H , Simha R , *Polymer International* , 1977,44.

208. Sanchez I ,Lacombe RH , *The Journal of Physical Chemistry* ,1976, 80, 21

209. Xie H ,Nies E , Stroeks A, *Polymer Engineering & Science* ,1992,32,

210. Xie H , Nies E , *Macromolecules* ,26, 1993,1689-1695.

211. Xie H , Nies E , *Macromolecules* , 1993,26, 1683-1688

212. W. B. Russel, D. A. Saville, and W. R. Schowalter, *Colloidal Dispersions*, Cambridge University Press, Cambridge, 1989

213. Vaia R.A., *Macromolecules* ,30,1997, 7990-7999.

214. Rowen, J. W. & Simha, R., *J. Phys. Chem*., 53 (1949) 921.

215. Gee., G., Quant. *Revs. Chem. Soc*., I (1947).

216. Jain, R. K.; Simha, R. *Macromolecules* 1980, 13, 1501.

References

1. S. Lee, C. Park and N. Ramesh, *Polymeric Foams: Science and Technology*. 2006: CRC Press.

2. M. Shimoda, M. Tanigaki, M. Ohshima and I. Tsujimura, *Journal of Cellular Plastics*, **37**. 517.(2001).

3. C.B.P. Hani E. Naguib, U. Panzer, Norbert Reichelt, *Polymer Engineering & Science*, **42**. 1481. (2002).

4. S. Lee, *Foam Extrusion: Principles and Practice*. 2000: CRC Press.

5. D. Tomasko, X. Han, D. Liu and W. Gao, *Current Opinion in Solid State & Materials Science*, **7**. 407. (2003).

6. X. Sun, H. Liu, G. Li, X. Liao and J. He, *Journal of Applied Polymer Science*, **93**. 163. (2004).

7. P. Nam, P. Maiti, M. Okamoto, T. Kotaka, T. Nakayama, M. Takada, M. Ohshima, A. Usuki, N. Hasegawa and H. Okamoto, *Polymer Engineering and Science(USA)*, **42**. 1907. (2002).

8. P. Lee, J. Wang and C. Park, *Industrial and Engineering Chemistry Research*, **45**. 175. (2006).

9. C. Liu, D. Wei, A. Zheng, Y. Li and H. Xiao, *Journal of Applied Polymer Science*, **101**. 4114. (2006).

10. Y. Fujimoto, S. Ray, M. Okamoto, A. Ogami, K. Yamada and K. Ueda, *Macromolecular Rapid Communications*, **24**. 457. (2003).

11. Y. Lee, C. Park, K. Wang and M. Lee, *Journal of Cellular Plastics*, **41**. 487. (2005).

12. M. Okamoto, P. Nam, P. Maiti, T. Kotaka, T. Nakayama, M. Takada, M. Ohshima, A. Usuki, N. Hasegawa and H. Okamoto, *Nano Lett*, **1**. 503. (2001).

13. Y. Sato, T. Takikawa, S. Takishima and H. Masuoka, *The journal of Supercritical fluids*, **19**. 187. (2001).

14. I. Sanchez and P. Rodgers, *Pure Appl. Chem*, **62**. 2097. (1990).

15. C. Zhong and H. Masuoka, *Fluid Phase Equilibria*, **144**. 49. (1998).

16. H. Xie and R. Simha, *Polymer International*, **44**. 348. (1997).

17. D. Klempner and K. Frisch, *Handbook of polymeric foams and foam technology*. 1991: Hanser.

18. A. Landrock, *Handbook of Plastic Foams: Types, Properties, Manufacture, and Applications*. 1995: Noyes Publications.

19. S. Lee, *Foam Extrusion: Principles and Practice*. 2000: CRC Press.

20. H. Fischer, *Materials Science & Engineering C*, **23**. 763.(2003).

21. L. Lee, C. Zeng, X. Han, D. Tomasko and K. Koelling. *Polymer Nanocomposite Foams Prepared by Supercritical Fluid Foaming Technology*. in M*aterials research society symposium proceedings*. 2002: Warrendale, Pa.; Materials Research Society; 1999.

22. S. Lee, C. Park and N. Ramesh, *Polymeric Foams: Science and Technology*. 2006: CRC Press.

23. S. Doroudiani, C. Park and M. Kortschot, *Polymer Engineering & Science*, **36**. 2645.(1996).

24. G. Nam, J. Yoo and J. Lee, *Journal of Applied Polymer Science*, **96**. 1793.(2005).

25. A. Sinsawat, K. Anderson, R. Vaia and B. Farmer, *Journal of Polymer Science, Part B, Polymer Physics*, **41**. 3272.(2003).

26. D. Tomasko, X. Han, D. Liu and W. Gao, *Current Opinion in Solid State & Materials Science*, **7**. 407.(2003).

27. J. Colton and N. Suh, *Polymer Engineering and Science*, **27**. 500.(1987).

28. L. Lee, K. Koelling, D. Tomasko, X. HanandC. Zeng, *Polymer nanocomposite foams*. 2004, Google Patents.

29. E. Giannelis. , *Polymer nanocomposite foams* , 2005 , google patents

30. J. Gilman, C. Jackson, A. Morgan, R. Harris, E. Manias, E. Giannelis, M. Wuthenow, D. Hilton and S. Phillips, *Chemistry of Materials(USA)*, **12**. 1866.(2000).

31. A. Morgan and J. Harris, *Polymer*, **44**. 2313.(2003).

32. M. Alexandre and P. Dubois, *Materials Science & Engineering R*, **28**. 1.(2000).

33. E. Giannelis, R. Krishnamoorti and E. Manias, A*dvances in polymer science*, **138**. 107.(1998).

34. P. LeBaron, Z. Wang and T. Pinnavaia, *Applied Clay Science*, **15**. 11.(1999).

35. S. Sinha Ray and M. Okamoto, *Progress in Polymer Science*, **28**. 1539.(2003).

36. X. Fu and S. Qutubuddin, *Polymer*, **42**. 807.(2001).

37. T. Fornes, P. Yoon, H. Keskkula and D. Paul, *Polymer*, **42**. 9929.(2001).

38. P. Nam, P. Maiti, M. Okamoto, T. Kotaka, N. Hasegawa and A. Usuki, *Polymer*, **42**. 9633.(2001).

39. M. Biswas and S. Ray, A*dvances in polymer science*, **155**. 167.(2001).

40. L. Liu, Z. Qi and X. Zhu *Journal of Applied Polymer Science*, **71**. 1133.(1999).

41. J. Yoon, W. Jo, M. Lee and M. Ko, *Polymer*, **42**. 329.(2001).

42. M. Okamoto, P. Nam, P. Maiti, T. Kotaka, T. Nakayama, M. Takada, M. Ohshima, A. Usuki, N. HasegawaandH. Okamoto, *Nano Lett*, **1**. 503.(2001).

43. Y. Ema, M. Ikeya and M. Okamoto, *Polymer*, **47**. 5350.(2006).

44. X. Sun, H. Liu, G. Li, X. Liao and J. He, *Journal of Applied Polymer Science*, **93**. 163.(2004).

45. D. Baldwin, P*olymer engineering and science*, **35**. 433.(1995).

46. S. Lee, *Foam extrusion: Principles and Practice*. 81–124.(2000)
.

47. M. Shafi and R. Flumerfelt, *Chemical Engineering Science*, **52**. 627.(1997)
.

48. V. Kumar and H. Schirmer, *ANTEC'95.*, **2**. 2189.(1995).

49. V. Kumar and H. Schirmer, *A Semi-Continuous Process to Produce Microcellular Foams*. 1997, US Patent 5,684,055.

50. C. Han, *Multiphase Flow in Polymer Processing*. 1981: Academic Press.

51. D. Johnson, C. Krutchen and G. Sharps Jr, *Polymer foam extrusion system*. 1982, US Patent 4,344,710.

52. C. Rauwendaal, *Mixing in Polymer Processing*. 1991: Marcel Dekker.

53. G. Atlanta and M. Cambridge, *Polymer engineering and science*, **36**.(1996).

54. X. Han, K. Koelling, D. Tomasko and L. Lee, *Polymer engineering and science*, **43**. 1206.(2003).

55. H. Naguib, C. Park, U. Panzer and N. Reichelt, P*lymer engineering and science*, **42**. 1481.(2002).

56. R. Gendron and L. Daigneault , *Foam Extrusion: Principles and Practice*.(2000).

57. C. Lee, K. Lee, H. Jeong and S. Kim, *Advances in Polymer Technology*, **19**. 97.(2000).

58. L. Hyde, L. Kishbaugh and J. Katterman, *SAE Transactions: Journal of Materials & Manufacturing*, **111**. 463.(2003).

59. D. Pierick and K. Jacobsen, *Plastics engineering*, **57**. 46.(2001).

60. G. Atlanta and M. Cambridge, *Polymer engineering and science*, **27**. 493.(1987).

61. J. Xu and D. Pierick, *Journal of Injection Molding Technology(USA)*, **5**. 152.(2001).

62. J. Martini-Vvedensky, N. Suh and F. Waldman, *Microcellular closed cell foams and their method of manufacture*. 1984.

63. C. Park, S. Doroudiani and M. Kortschot, *Polymer Engineering and Science(USA)*, **38**. 1205.(1998).

64. N. SUH, P*olymer engineering and science*.(1990).

65. M. Yuan, L. Turng, S. Gong, D. Caulfield, C. Hunt and R. Spindler, *Polymer Engineering and Science*, **44**. 673.(2004).

66. J. Stevenson, *Specialized Molding Techniques*.(2001).

67. R. Gosselin, D. RodrigueandB. Riedl, *Journal of Thermoplastic Composite Materials*, **19**. 639.(2006).

68. M. Hosur, A. Mohammed, S. Zainuddin and S. Jeelani, *Materials Science & Engineering A*, **498**. 100.(2008).

69. J. Shen, C. Zeng and L. Lee, *Polymer*, **46**. 5218.(2005).

70. L. Turng, M. Yuan, H. Kharbas, H. Winata and D. Caulfield. *Applications of nanocomposites and woodfiber plastics for microcellular injection molding., May 19-20, 2003... Madison, Wisconsin, USA. Madison, WI: Forest Products Society, 2003*.

71. C. Park, *Foam Extrusion: Principles and Practice*. 263–305.(2000).

72. S. Doroudiani and M. Kortschot, *Journal of Applied Polymer Science*, **90**. 1412.(2003).

73. X. Han, C. Zeng G, L. Lee, K. Koelling and D. Tomasko , *Polymer engineering and science*, **43**. 1261.(2003).

74. T. Lickly, K. Lehr and G. Welsh, *Food and Chemical Toxicology*, **33**. 475.(1995).

75. Y. Oyanagi and J. White, *Journal of Applied Polymer Science*, **23**. 1013.(1979).

76. B. Rodeheaver and J. Colton, *Polymer engineering and science*, **41**. 380.(2001).

77. J. Schubert and E. LeDuc, *Method of extruding a polystyrene foam using both a physical blowing agent and water*. 1984, Google Patents.

78. S. Sumarno, S. Takishima and H. Masuoka, *Journal of Applied Polymer Science*, **77**. 2383.(2000).

79. M. Yazawa, *Process for continuously producing shaped articles of polystyrene foam*. 1976, Google Patents.

80. C. Zeng, X. Han, L. Lee, K. Koelling and D. Tomasko, *Advanced Materials*, **15**.(2003).

81. W. Strauss and N. D'Souza, *Journal of Cellular Plastics*, **40**. 229.(2004).

82. Y. Ke, C. Long and Z. Qi, *Journal of Applied Polymer Science*, **71**. 1139.(1999).

83. P. Maiti, P. Nam, M. Okamoto, N. Hasegawa and A. Usuki, *Macromolecules*, **35**. 2042.(2002).

84. X. Cao, L. James Lee, T. Widya and C. Macosko, *Polymer*, **46**. 775.(2005).

85. Y. Fujimoto, S. Ray, M. Okamoto, A. Ogami, K. YamadaandK. Ueda, *Macromolecular Rapid Communications*, **24**. 457.(2003).

86. E. Di Maio, C. Marrazzo, Y. Di, S. Iannace and L. Nicolais, P*resent situation and forecasts of nanotechnology in: materials, health and medicalsystems*.

87. Y. Di, S. Iannace, E. Di Maio and L. Nicolais, *Journal of Polymer Science, Part B, Polymer Physics*, **43**. 689.(2005).

88. S. Lee, H. Chen and M. Hanna, *Industrial Crops & Products*.(2008).

89. M. Okamoto, *Polymeric Foams: Technology and Developments in Regulation, Process, and Products*. 175.(2008).

90. S. Ray and M. Okamoto, M*acromolecular materials and engineering*. 936.(2003).

91. M. Mitsunaga, Y. Ito, S. Ray, M. Okamoto and K. Hironaka, *Macromolecular Materials and Engineering*, **288**. 543.(2003).

92. J. Fu and H. Naguib, *Journal of Cellular Plastics*, **42**. 325.(2006).

93. Y. Lee, C. Park, K. Wang and M. Lee, *Journal of Cellular Plastics*, **41**. 487.(2005).

94. P. Nam, P. Maiti, M. Okamoto, T. Kotaka, T. Nakayama, M. Takada, M. Ohshima, A. Usuki, N. HasegawaandH. Okamoto, P*olymer engineering and science*, **42**. 1907.(2002).

95. W. Daming, M. Qingyun, L. Ying, D. Yumei, C. Weihong, X. Hong and R. Dongyun, *Journal of polymer science part b polymer physics*, **41**. 1051.(2003).

96. H. Huang and J. Wang, *Journal of Applied Polymer Science*, **106**. 505.(2007).

97. K. KOELLING, *Polymer engineering and science*, **43**. 1261.(2003).

98. C. Park, *Journal of Cellular Plastics*, **38**. 129.(2002).

99. W. Zheng, Y. Lee and C. Park, *Journal of Cellular Plastics*, **42**. 271.(2006).

100. C. Zeng, X. Han, L. Lee, K. Koelling and D. Tomasko, *Advanced Materials*, **15**. 1743.(2003).

101. J. Velasco, M. Antunes, O. Ayyad, J. López-Cuesta, P. Gaudon, C. Saiz-Arroyo, M. Rodríguez-Pérez and J. de Saja, *Polymer*, **48**. 2098.(2007).

102. L. Chen, K. Blizard, R. Straff and X. Wang, *Journal of Cellular Plastics*, **38**. 139.(2002).

103. L. Chen, H. Sheth and X. Wang, *Journal of Cellular Plastics*, **37**. 353.(2001).

104. M. Shafi, K. Joshi and R. Flumerfelt, *Chemical Engineering Science*, **52**. 635.(1997).

105. C. Lu and Y. Mai, *Composites Science and Technology*, **67**. 2895.(2007).

106. S. Goel and E. Beckman, P*olymer engineering and science*, **34**. 1137.(1994).

107. S. Leung, H. Li and C. Park.

108. N. Ramesh, D. Rasmussen and G. Campbell, *Polymer engineering and science*, **34**. 1698.(1994).

109. J. Yokohama, *Cellular and Microcellular Materials*, **496**. 0.25.(1994).

110. C. Park, A. Behravesh and R. Venter. *A Strategy for the Suppression of Cell Coalescence in the Extrusion of Microcellular High-Impact Polystyrene Foams*. in ACS*s symposium series*. 1997: american chemical society.

111. S. Goel and E. Beckman, *Polymer Engineering & Science*, **34**.(1994).

112. R. Krishnamoorti and K. Yurekli, *Current Opinion in Colloid & Interface Science*, **6**. 464.(2001).

113. U. CNRS, R. du Maine and F. Le Mans Cedex, *Europhys. Lett*, **3**. 297.(1987).

114. M. Seo and S. Park, *Chemical Physics Letters*, **395**. 44.(2004).

115. S. Muke, I. Ivanov, N. Kao and S. Bhattacharya, *Journal of Non-Newtonian Fluid Mechanics*, **101**. 77.(2001).

116. V. Pasanovic-Zujo, R. Gupta and S. Bhattacharya, *Rheologica Acta*, **43**. 99.(2004).

117. R. Prasad, V. Pasanovic-Zujo, R. Gupta, F. Cser and S. Bhattacharya, *Polymer Engineering and Science*, **44**.(2004).

118. R. KrishnamoortiandE. Giannelis, M*acromolecules*, **30**. 4097.(1997).

119. C. MitchellandR. Krishnamoorti, *Journal of polymer science part b polymer physics*, **40**. 1434.(2002).

120. G. Galgali, S. Agarwal and A. Lele, *Polymer*, **45**. 6059.(2004).

121. S. Kazarian, M. Vincent, B. West and C. Eckert, *The Journal of Supercritical Fluids*, **13**. 107.(1998).

122. C. Drohmann and E. Beckman, *The Journal of Supercritical Fluids*, **22**. 103.(2002).

123. Y. Shieh, J. Su, G. Manivannan, P. Lee, S. SawanandW. Spall, *Journal of Applied Polymer Science*, **59**. 695.(1996).

124. Y. Zhao and H. Huang. *Effect of Supercritical Co2 on Morphology and Rheology of Polymer Nanocomposites Prepared by Melt Compounding*. in *The 2006 Annual Meeting*. 2006.

125. S. Gu, J. Ren and Q. Wang, *Journal of Applied Polymer Science*, **91**. 2427.(2004).

126. J. Rowen and R. Simha, *The Journal of Physical Chemistry*, **53**. 921.(1949).

127. I. Sanchez and R. Lacombe, *The Journal of Physical Chemistry*, **80**. 2352.(1976).

128. R. Simha and T. Somcynsky, *Macromolecules*, **2**. 342.(1969).

129. E. Nies and H. Xie, *Macromolecules*, **26**. 1683.(1993).

130. H. Xie and R. Simha, *Polymer International*, **44**. 348.(1997).

131. H. Hu, G. Peterson, X. Peng and B. Wang, *International Journal of Heat and Mass Transfer*, **41**. 3483.(1998).

132. S. Yang and R. Kim, *International journal of heat and mass transfer*, **31**. 1127.(1988).

133. S. goel and E. Beckman, *Polymer engineering and science*, **34**. 1148.(1994).

134. M. BlanderandJ. Katz, *AIChE Journal*, **21**.(1975).

135. M. Shimoda, M. Tanigaki, M. Ohshima and I. Tsujimura, *Journal of Cellular Plastics*, **37**. 517.(2001).

136. L. Chen, X. Wang, R. Straff and K. Blizard, *Polymer Engineering & Science*, **42**.(2002).

137. S. Lee, *Journal of Cellular Plastics*, **37**. 221.(2001).

138. J. Han and C. Han, *Polymer Engineering & Science*, **28**.(1988).

139. R. Upadhyay, *Advances in Polymer Technology*, **5**. 55.(1985).

140. R. Larson, *Journal of Rheology*, **28**. 545.(1984).

141. D. Baldwin, *Cellular and Microcellular Materials*, **53**. 85.(1994).

142. A. Arefmanesh and S. Advani, *Rheologica Acta*, **30**. 274.(1991).

143. Y.H. Lee, C.B. Park, K.H. Wang and M.H. Lee, *Journal of Cellular Plastics*, **41**. 487.(2005).

144. T. Otsuka, K. Taki and M. Ohshima, *Die Angewandte Makromolekulare Chemie*, **293**. 78.(2007).

145. S. Siripurapu, Y. Gay, J. Royer, J. DeSimone, R. Spontak and S. Khan, *Polymer*, **43**. 5511.(2002).

146. K. Taki, T. Otsuka, Y. Waratani and M. Ohshima.

147. T. Nemoto, J. Takagi and M. Ohshima, *Die Angewandte Makromolekulare Chemie*, **293**. 991.(2008).

148. T. Otsuka, K. Taki and M. Ohshima, *Macromolecular Materials and Engineering*, **293**.(2008).

149. (www.plastemart.com).

150 R. Shah and D. Paul, *Polymer*, **45**. 2991. (2004).

151. Y.H. Lee, C.B. Park, K.H. Wang and M.H. Lee, *Journal of Cellular Plastics*, **41**. 487. (2005).

152. D.F.B. Chul B. Park, Nam P. Suh, *Polymer Engineering & Science*, **35**. 432. (1995).

153. Y. Sato, T. Takikawa, S. Takishima and H. Masuoka, *The journal of Supercritical fluids*, **19**. 187. (2001).

154. F. Morrison, *Understanding rheology*. 2001: Oxford University Press, USA.

155. R. Krishnamoorti and E. Giannelis, *Macromolecules*, **30**. 4097. (1997).

156. R. Krishnamoorti and K. Yurekli, *Current Opinion in Colloid & Interface Science*, **6**. 464. (2001).

157. S. Lim, C. Lee, H. Choi and M. Jhon, *Journal of Polymer Science, Part B, Polymer Physics*, **41**. 2052. (2003).

158. V. Pasanovic-Zujo, R. Gupta and S. Bhattacharya, *Rheologica Acta*, **43**. 99. (2004).

159. P. Powell, *Polymer Engineering & Science*, **14**. (1974).

160. J. Stickel and R. Powell. (2005).

161. C. Macosko and W. Davis, *Rheologica Acta*, **13**. 814. (1974).

162. C. Ferraris and N. Martys, *Technology*, **108**. 229. (2003).

163. S. Sinha Ray, S. Pouliot, M. BousminaandL. Utracki, *Polymer*, **45**. 8403. (2004).

164. M. Bousmina, *Rheologica Acta*, **38**. 73.(1999).

165. R.A. Vaia and E.P. Giannelis, *Macromolecules*, **30**. 7990.(1997).

166. A. Gupta, B. Ratnam and K. Srinivasan, *Journal of Applied Polymer Science*, **46**. 281.(1992).

167. W.N. Kim and C.M. Burns, *Journal of Applied Polymer Science*, **32**. 2989.(1986).

168. P.B. Rim and J.P. Runt, *Macromolecules*, **17**. 1520.(1984).

169. S. Ray, *Progress in Polymer Science*, **28**. 1539.(2003).

170. D. Chaudhary, R. Prasad, R. Gupta and S. Bhattacharya, *Thermochimica Acta*, **433**. 187.(2005).

171. Y. Wang, Q. Zhang and Q. Fu, *Macromolecular Rapid Communications*, **24**. 231.(2003).

172. D. Hoppner and J. Wendorff, *Colloid & Polymer Science*, **268**. 500.(1990).

173. S. RAY and M. BOUSMINA, *Macromolecular rapid communications*, **26**. 450.(2005).

174. S. Tjong, S. Liu and R. Li, *Journal of Materials Science*, **31**. 479.(1996).

175. A. Yee and M. Maxwell, *Journal of Macromolecular Science, Part B*, **17**. 543.(1980).

176. A. Yee, *Polymer Engineering and Science*, **17**. 213.(1977).

177. J. Barlow and D. Paul, *Polymer Engineering and Science*, **21**. 985.(1981).

178. T. Malik, *Journal of Applied Polymer Science*, **46**. 303.(1992).

179. Y. Chun, Y. Kyung, H. Jung and W. Kim, *Polymer*, **41**. 8729.(2000).

180. M. Shahlari, P. Roberts, L. Leavitt, M. Factor and S. Lee, *The 2007 Annual Meeting*.(2007).

181. C.W.M. Pieter Spitael, *Polymer Engineering and Science*, **44**. 2090.(2004).

182. C.B.P. Hani E. Naguib, U. Panzer, Norbert Reichelt,, *Polymer Engineering & Science*, **42**. 1481.(2002).

183. C. Liu, D. Wei, A. Zheng, Y. Li and H. Xiao, *Journal of Applied Polymer Science*, **101**. 4114.(2006).

184. P. Nam, P. Maiti, M. Okamoto, T. Kotaka, T. Nakayama, M. Takada, M. Ohshima, A. Usuki, N. HasegawaandH. Okamoto, *Polymer Engineering and Science(USA)*, **42**. 1907.(2002).

185. Y. Fujimoto, S. Ray, M. Okamoto, A. Ogami, K. Yamada and K. Ueda, *Macromolecular Rapid Communications*, **24**. 457.(2003).

186. Y.H. Lee, C.B. Park, K.H. Wang and M.H. Lee, *Journal of Cellular Plastics*, **41**. 487.(2005).

187. M. Wagner, H. Bastian, P. Hachmann, J. Meissner, S. Kurzbeck, H. Münstedt and F. Langouche, *Rheologica Acta*, **39**. 97.(2000).

188. Y. JahaniandM. Barikani, *Iranian Polymer Journal*, **14**. 361.(2005).

189. S. Sinha Ray and M. Okamoto, *Progress in Polymer Science*, **28**. 1539.(2003).

190. M. Varma-Nair, P. Handa, A. Mehta and P. Agarwal, *Thermochimica Acta*, **396**. 57.(2003).

191. W. Kaewmesri, P. Lee, C. Park and J. Pumchusak, *Journal of Cellular Plastics*, **42**. 405.(2006).

192. D.F.B. Chul B. Park, Nam P. Suh,, *Polymer Engineering & Science*, **35**. 432.(1995).

193. D.H.R. N. S. Ramesh, Gregory A. Campbell,, *Polymer Engineering & Science*, **31**. 1657.(1991).

194. D.H.R. N. S. Ramesh, G. A. Campbell,, *Polymer Engineering & Science*, **34**. 1698.(1994).

195. X. Sun, H. Liu, G. Li, X. Liao and J. He, *Journal of Applied Polymer Science*, **93**. 163.(2004).

196. J.M.P. D. D. Liu, *Journal of Applied Polymer Science*, **24**. 725.(1979).

197. Y. Ito, M. Yamashit and M. Okamoto, *Macromolecular materials and engineering(Print)*, **291**. 773.(2006).

198. M. Okamoto, P. Nam, P. Maiti, T. Kotaka, T. Nakayama, M. Takada, M. Ohshima, A. Usuki, N. Hasegawa and H. Okamoto, *Nano Lett*, **1**. 503.(2001).

199. D. BALDWIN, P*olymer engineering and science*, **35**. 433.(1995).

200. Y. Lee, C. Park, K. Wang and M. Lee, *Journal of Cellular Plastics*, **41**. 487.(2005).

201. Simha R, Somcynsky T, , " *Macromolecules*, 1969 (2) ,4.

202. Jain R.K. Simha R, 1980, "*Macromolecules* 13, 1501-1508.

203. Simha R, 1996, , *Polymer Engineering & Science*,3 ,12.

204. Simha R, Jain R.K, *Polymer Physics Edition*, 1996,16, 1471-1489.

205. Olabisi O, Simha R, 1977, "*Macromolecules*, 21, 149-163.

206. Quak T.Y. , Masoori G.A., *Chemical engineering Science* , ,1986 41,5,1303-1309.

207. Xie H , Simha R , *Polymer International* , 1977,44.

208. Sanchez I ,Lacombe RH , *The Journal of Physical Chemistry* ,1976, 80, 21

209. Xie H ,Nies E , Stroeks A, *Polymer Engineering & Science* ,1992,32,

210. Xie H , Nies E , *Macromolecules* ,26, 1993,1689-1695.

211. Xie H , Nies E , *Macromolecules* , 1993,26, 1683-1688

212. W. B. Russel, D. A. Saville, and W. R. Schowalter, *Colloidal Dispersions*, Cambridge University Press, Cambridge, 1989

213. Vaia R.A., *Macromolecules* ,30,1997, 7990-7999.

214. Rowen, J. W. & Simha, R., *J. Phys. Chem*., 53 (1949) 921.

215. Gee., G., Quant. *Revs. Chem. Soc*., I (1947).

216. Jain, R. K.; Simha, R. *Macromolecules* 1980, 13, 1501.

Appendix A

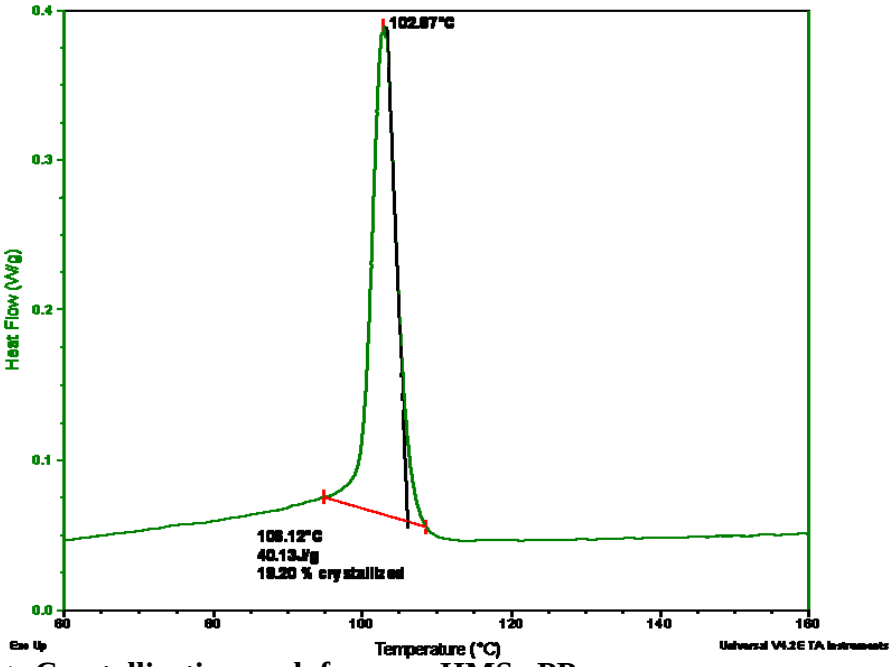

Figure A. 1: Crystallization peak for pure HMS –PP

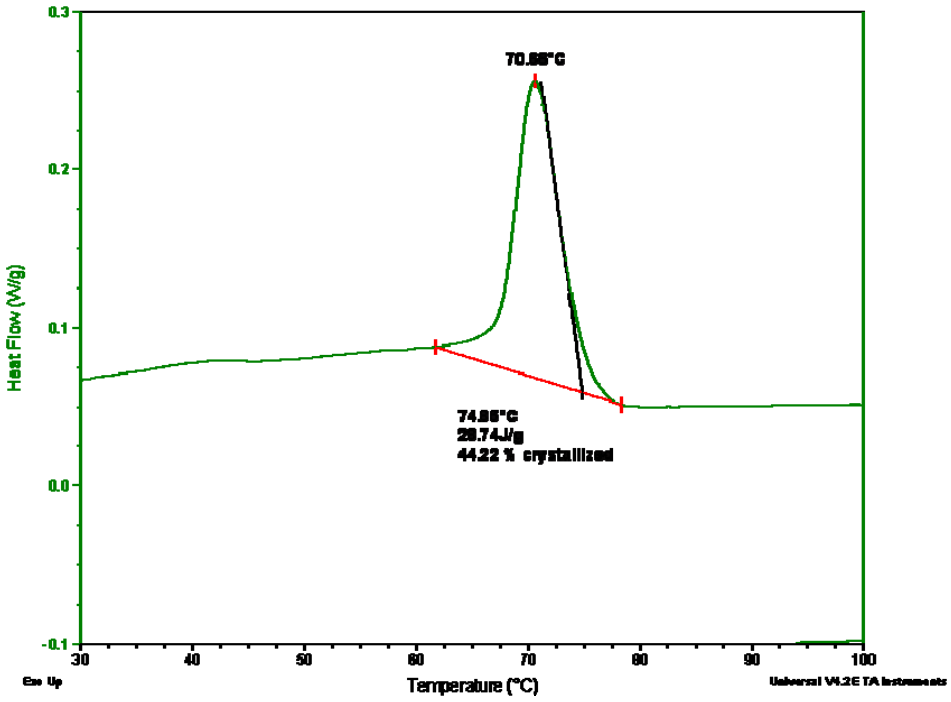

Figure A. 2: Crystallization peak for pure EVA -28

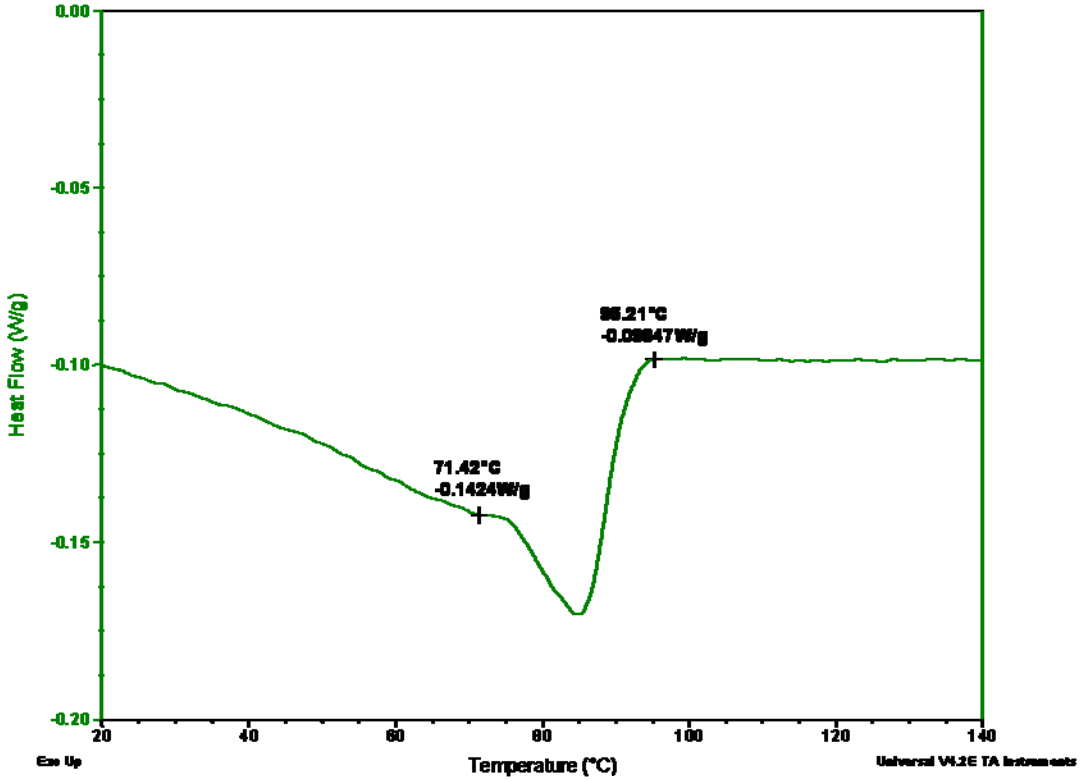

Figure A. 3: Melting peak for pure EVA -28

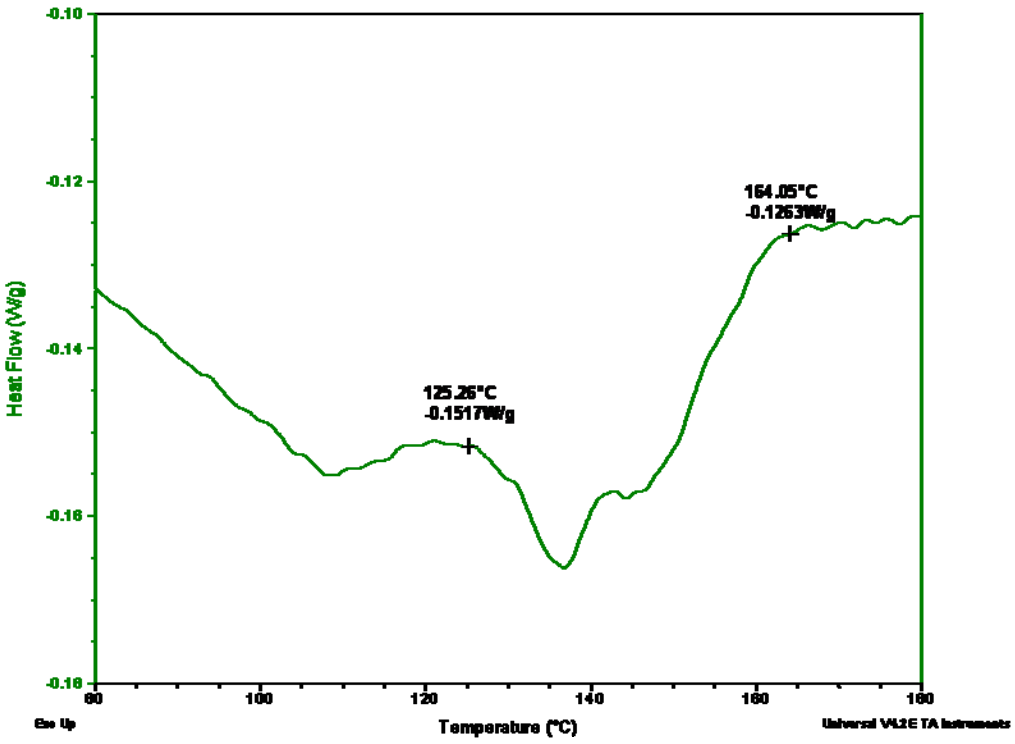

Figure A. 4: Melting peak for pure HMS-PP

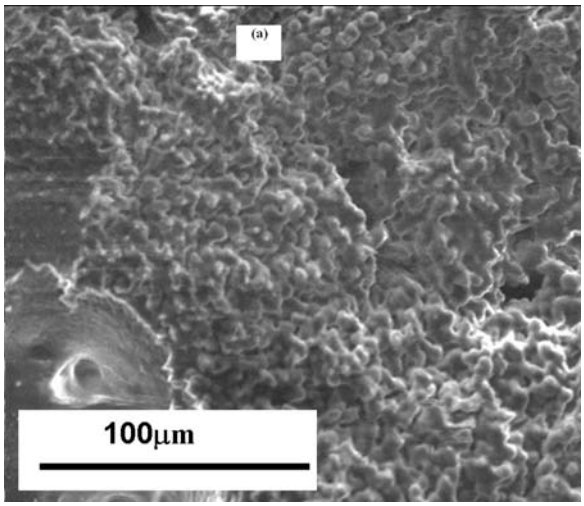

Figure A. 5: SEM of pure HMS-PP foams case (1)

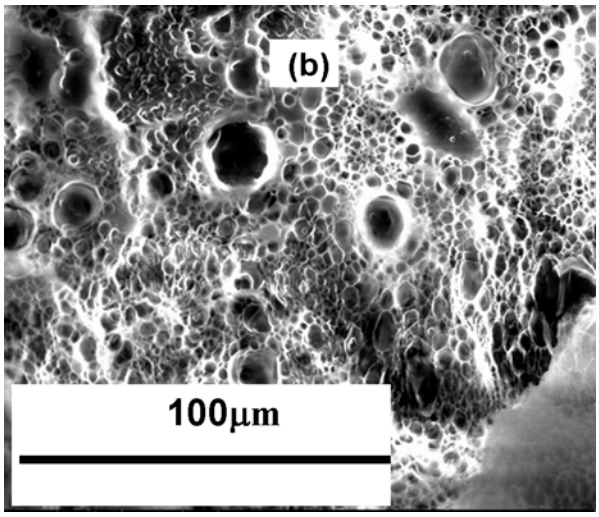

Figure A. 6: SEM of pure HMS-PP foams case (6)

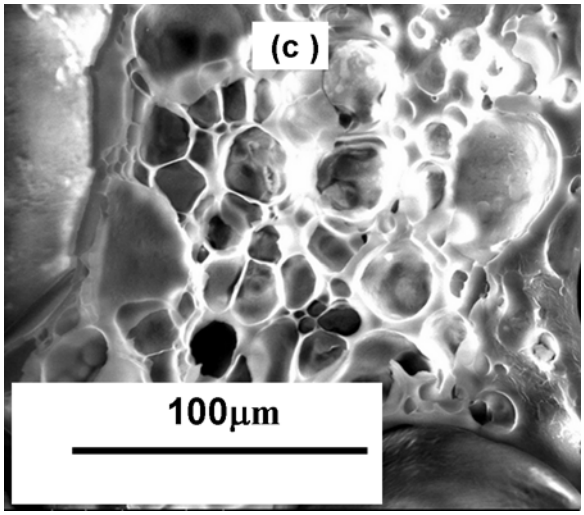

Figure A. 7; SEM of pure HMS-PP foams case (2)

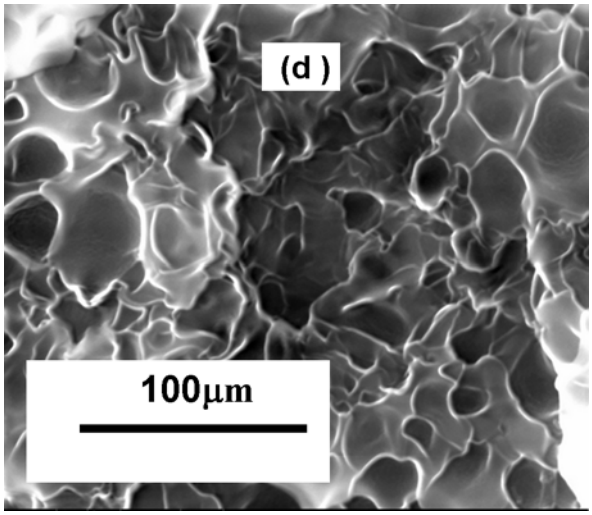

Figure A. 8: SEM of pure HMS-PP foams case (3)

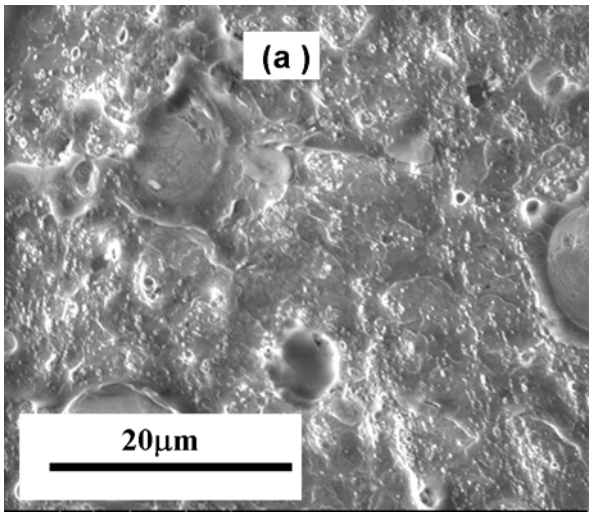

Figure A. 10: SEM of PPNC2 foams case (1)

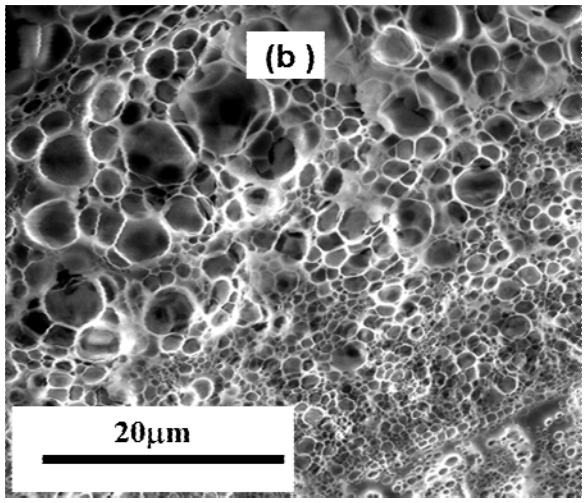

Figure A. 9: SEM of PPNC2 foams case (6)

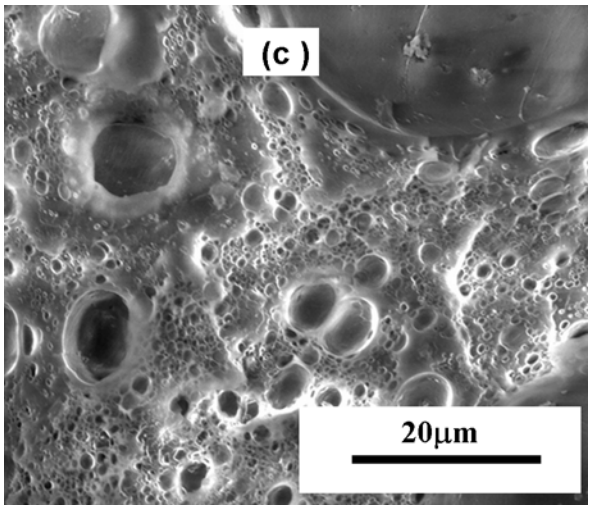

Figure A. 11: SEM of PPNC2 foams case (2)

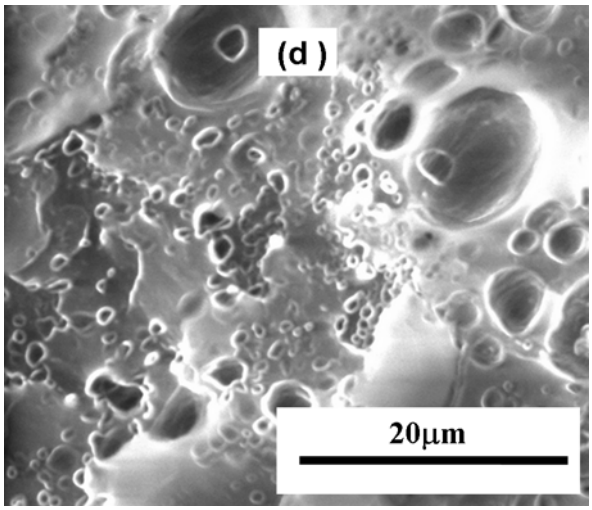

Figure A. 12: SEM of PPNC2 foams case (3)

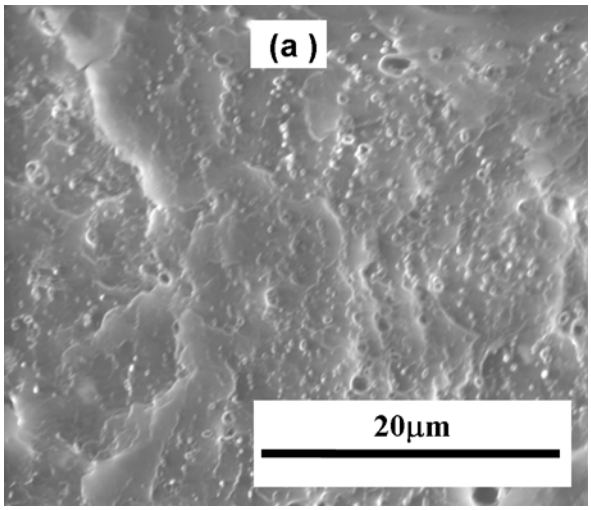

Figure A. 13: SEM of PPNC4 foams case (1)

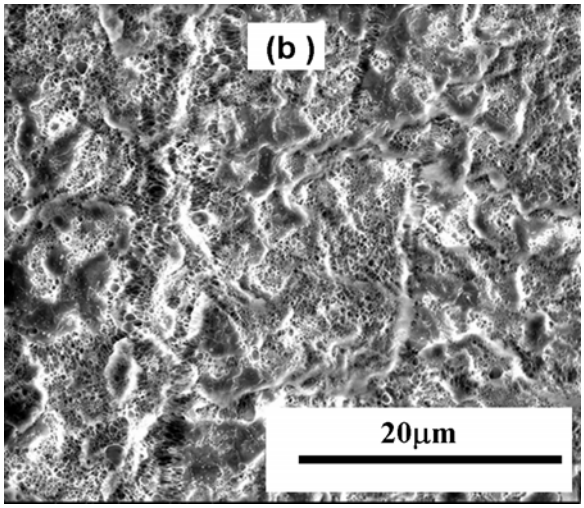

Figure A. 14: SEM of PPNC4 foams case (6)

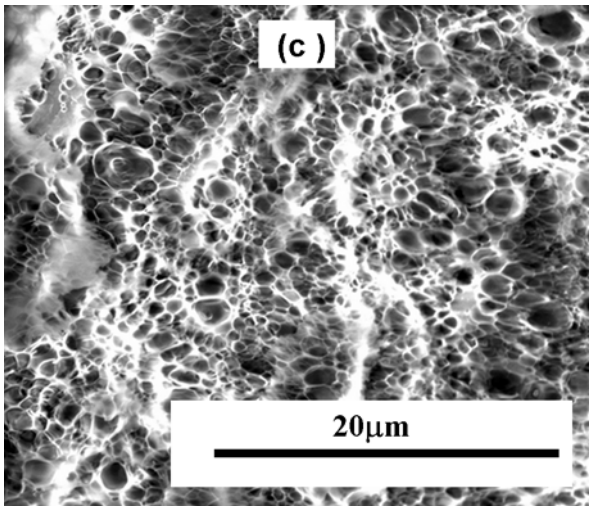

Figure A. 15: SEM of PPNC4 foams case (2)

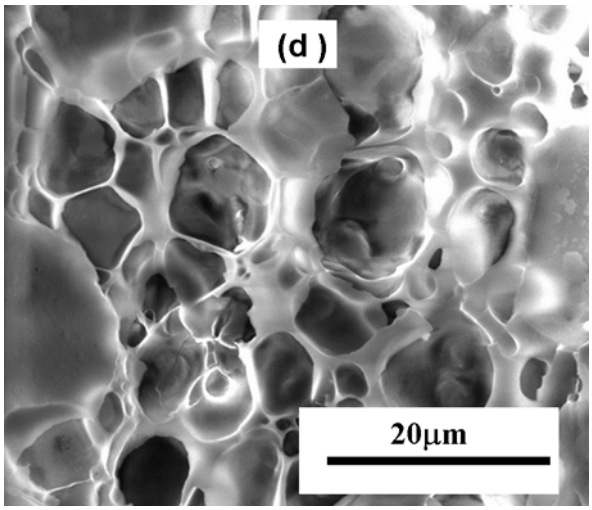

Figure A. 16: SEM of PPNC4 foams case (3)

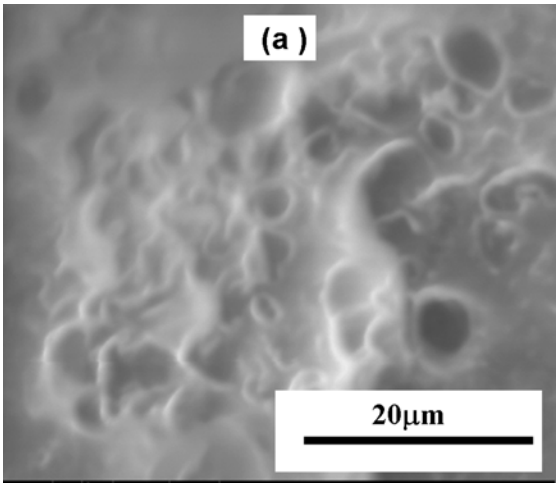

Figure A. 17: SEM of PPNC8 foams case (1)

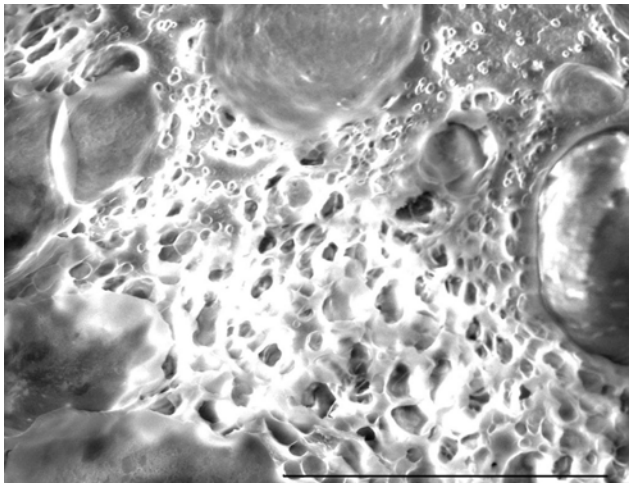

Figure A. 18: SEM of PPNC8 foams case (6)

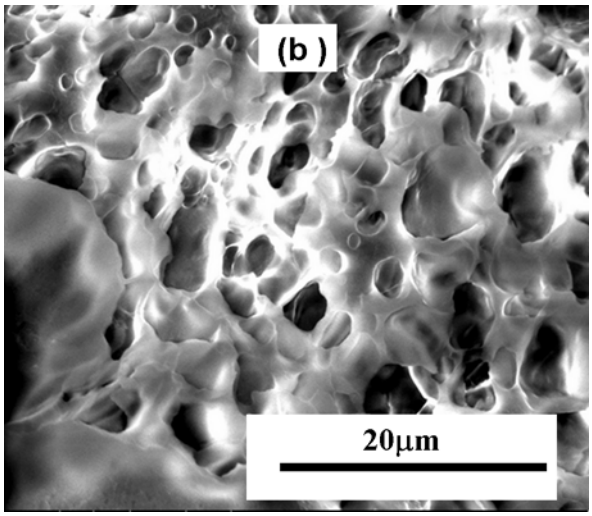

Figure A. 19: SEM of PPN8 foams case (2)

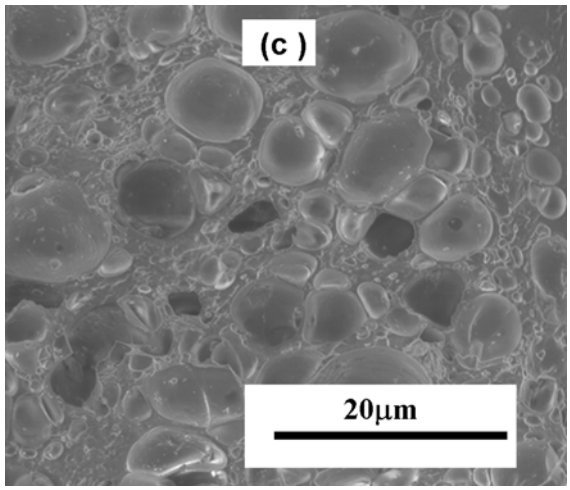

Figure A. 20: SEM of PPNC8 foams case (3)

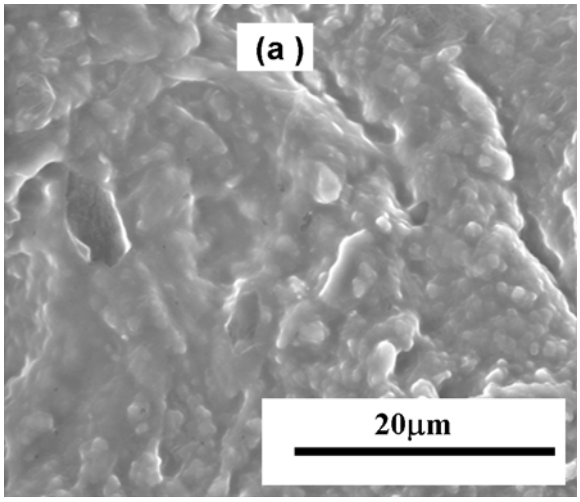

Figure A. 21: SEM of PPNC10 foams case (1)

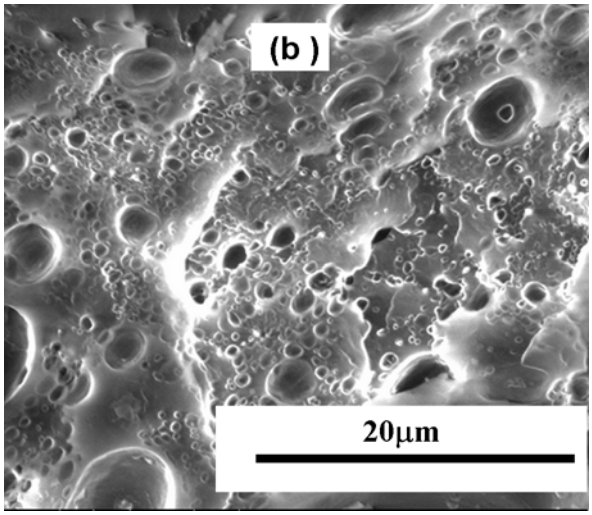

Figure A. 22: SEM of PPNC10 foams case (6)

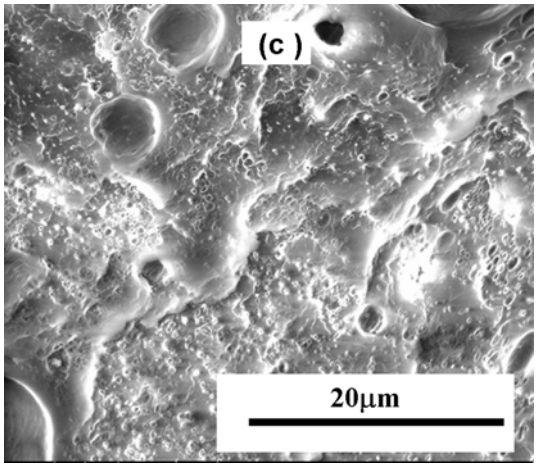

Figure A. 23: SEM of PPNC10 foams case (2)

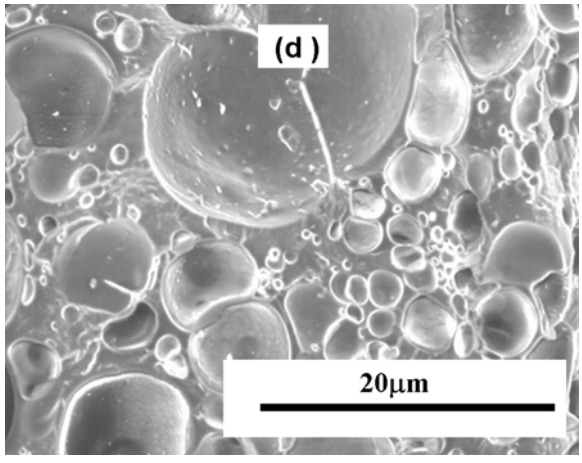

Figure A. 24: SEM of PPNC10 foams case (3)

Appendix B

Assumptions

Before the MATLAB code is presented it is essential to provide details about the assumptions made. Since the equations developed use molecular parameters they are big. Hence simplifying assumptions are essential but then again the assumptions should not result in loss of actual physical behaviour. The chain flexibility parameter has been scaled to make them non dimensional and are values represented with respect to the overall flexibility. Physically a gas molecule should have the highest amount of chain flexibility followed by the polymer chain and then by the modifiers on the clay surface. But in this case the polymer chains have the highest amount of flexibility. This is because the gas molecule flexibility depends on the polymer chain flexibility. In case the chain flexibility is high then the gas molecules can be easily entrapped and hence would have lower flexibility and vice versa. The scaled values of chain flexibility have been calculated using the equilibrium PVT relations for a polymer nanocomposite in the exfoliated state. Similar values have been calculated for the intercalated state as well and the difference in the trend can be observed from the code. Unlike the exfoliated state, in the intercalated state the gas molecules have higher flexibility. The random number generator has been used to simulate complete randomized probabilities of occurrence of the components in the system except for energy potential. The energy potential is scaled by assuming a standard normal distribution. This assumption can be quantitatively explained. Under equilibrium conditions the system would be in the state of minimum energy (characterized by the zero mean of the normal distribution). Random fluctuations would cause the particles , polymer and the gas molecules to come close to each other but once the equilibrium distance is reached the repulsion potential would cause all these elements to repel

away bound by the condition that the repulsion can be only to the point where the approach to equilibrium is still possible. Hence if a standard normal distribution is assumed then it can be said that the molecular potential varies between -1 to 0 or between 0 to 1 with zero representing the equilibrium state on no interaction. Also the overall segmental density of the different components would be directly proportional to the number of molecules and hence the number of segments has been scaled by the number of molecules of the respective components present within the system

MATLAB CODE

```
format long
>> Va = 0;
>> Vb = 0;
>> Vc =0;
>> V = Va + Vb + Vc; %total segement fraction %
>> Va = rand ; %generates vlaues between 0 & 1 %
>> Vb = rand ; %generated vlaues between 0 & 1 %
>> if (Va + Vb) <= 0.5
V = 1;
Vc = V - Va -Vb; %by total balance of segmental volume fraction%
format long
Va = 0;
Vb = 0;
Vc =0;
V=1;
if (Va + Vb) <= 1
Vc = V - Va -Vb; %by total balance of segmental volume fraction%
else
Va = rand
Va = rand;
Vb=rand;
disp (Va , Vb , Vc );
%this complets the random assumption of segmental fractions%
z = 12 ; % assuming a FCC lattice structure %
CsA = [0.6 , 0.3];
CsB = [0.1 , 0.1];
Csg = [0.3 , 0.6];
V=1 %this represnts the overall segmental volume fraction which cannot exceed 1%
V=1 ;%this represnts the overall segmental volume fraction which cannot exceed 1%
Vafinal = [0 : 1 : 1000];
224
Vbfinal = [0 : 1 : 1000];
Vcfinal = [0 :1 :1000];
Vafinal = [0 : 1 : 1000];
z = 12 ; %the co ordination number in case of FCC lattice structure%
for i =1 : 1000;
Va = rand;
Vb = rand ;
if (Va + Vb)<=1
Vc = V - Va - Vb ;
Vafinal(i)= Va;
Vbfinal(i)= Vb;
Vcfinal(i)=Vc;
else
Va= rand;
Vb=rand;
for j = 1 :1000;
```

```
N = i * 6.023 *(10^23);
Nh= rand * N ;
Ng = rand *N;
Na = rand * N ;
Nb = rand * N ;
Zqa = Na (z-2) + 2;
Zqb = Nb (z-2) + 2;
Zqg = Ng * (z-2) + 2;
Zqb = Nb (Z-1);
Nh = [0 :1 : 1000];
Ng = [0 :1 :1000];
Na = [0 : 1 :1000];
Nh(i)= rand * N ;
Nb(i) = rand * N ;
Na(i) = rand * N ;
Zqa = [0:1:1000];
Zqb = [0:1:1000];
Zqg = [0 :1 :1000];
Zqa(i) = (Na(i)* (z-2)) + 2;
Zqb (i) = (Nb(i)* (Z-1));
Zqg (i) = (Ng(i) * (z-2) + 2);
Ufinal = [0:1:1000]
Vfinal = [0:1:1000]
Wfinal = [0:1:1000];
Rfinal = [0:1:1000];
Ufinal (i)= Na(i)*.Zqa(i)/ (Na(i)*.Zqa + Nb(i)*.Zqb + Z*.Nh(i)+ Z*.Ng(i));
Ufinal (i)= Na(i)*.Zqa(i)/ (Na(i)*.Zqa + Nb(i)*.Zqb + Z*.Nh(i)+ Z*.Ng(i));
|
>> Ufinal (i)= Na(i)*Zqa(i)/ (Na(i)*Zqa + Nb(i)*Zqb + Z*Nh(i)+ Z*Ng(i));
>> Ufinal (i)= Na(i)*Zqa(i)/ (Na(i)*Zqa + Nb(i)*Zqb + Z*Nh(i)+ Z*Ng(i));
>> Vfinal (i) = Nb(i)*Zqb(i)/(Na(i)*Zqa(i)+ Nb(i)*Zqb(i)+z*Nh(i)+Z*Ng(i))
>> Wfinal(i) = Z*Nh(i)/(Na(i)*Zqa(i)+Nb(i)*Zqb(i)+z*Nh(i)+z*Ng(i));
225
>> Rfinal (i) = z*Ng/ (Na(i)*Zqa(i)+Nb(i)*Zqb(i)+z*Nh(i)+z*Ng(i));
>> savg = [0:1:1000];
>> savg(i) = 1/(Vafinal(i)+Vbfinal(i)+Vcfinal(i));
>> X1min = [0:1:1000];
>> X2min = [0:1:1000];
>> X3min = [0:1:1000];
>> X4min = [0:1:1000];
>> X5min = [0:1:1000];
>> X1min(i) = Ufinal(i) * Vfinal(i);
>> X2min(i)= Vfinal(i)*Wfinal(i);
>> X3min (i)= Vfinal(i)*Wfinal(i);
>> X3min (i)= Ufinal(i)*Wfinal(i);
>> X4min(i)= Ufinal(i)*Rfinal(i);
>> X5min(i)=Wfinal(i)*Rfinal(i);
>> c = 3/(4*3.142);
>> Ep = 1.3 ; %from literature%
>> Deq = 0.001 %assuming a length of 100nm , thickness of 1 nm and width of
```

```
50nm%
Deq =
1.000000000000000e-003
>> Emp= [0 :1 :1000];
>> r1=[0.000001 :0.0000001 :0.00001];
>> rpp = [0.0001:0.0001 :0.001];
>> Epp = [0:1:1000];
>> Epp(i) = -Ep * (((Deq^2)/(rpp(i)*(rpp(i)+2 *Deq))+(Deq^2/(rpp(i)+Deq)^2)+4*ln
(rpp +2*Deq)^0.5);
??? Epp(i) = -Ep * (((Deq^2)/(rpp(i)*(rpp(i)+2 *Deq))+(Deq^2/(rpp(i)+Deq)^2)+4*ln
(rpp +2*Deq)^0.5);
T0 = 150;
z = 12;
T0 = 150;
T0 = 150;
T0 = 150;
z = 12;
temp = 0:0.1:180 ;
temp = 0:0.1:40 ;
for j =1 :40
for j =0.1 :40
for i =0.1 :12
T0=150;
226
for j =0.1 :40
for i =0.1 :12
T = 0.0189*T0 -0.9622T0-0.0189T0;
T = 0.0189*T0 -0.9622*T0-0.0189*T0;
T0 =T0+T;
end
end
temp = 0.1:0.1:12 ;
for j =0.1 :40
if temp<12
T = 0.0189*T0 -0.9622*T0-0.0189*T0;
T0 =T0+T;
end
disp(T,j)
end
temp = 0.1:0.1:12 ;
for j =0.1 :40
if temp<=12
T = 0.0189*T0 -0.9622*T0-0.0189*T0;
T0 =T0+T;
plot3(T,j,temp)
end
end
temp = 0.1:0.1:12 ;
for j =0.10:40
if temp<=12
```

```
T = 0.0189*T0 -0.9622*T0-0.0189*T0;
temp = 0.1:0.1:12 ;
T0 =150;
if temp<=12
T = 0.0189*T0 -0.9622*T0-0.0189*T0;
end
T0 =T0+T;
plot3(T,j,temp)
end
temp = 0.1:0.1:12 ;
T0 =150;
for j =0.10:40
if temp<=12
T = 0.0189*T0 -0.9622*T0-0.0189*T0;
end
T0 =T0+T;
plot3(T,j,temp)
end
plot3(T,j,temp)
temp = 0.1:0.1:12 ;
T0 =150;
for j =0.10:40
if temp<=12
T = 0.0189*T0 -0.9622*T0-0.0189*T0;
227
T0 =T0+T;
disp(T)
end
plot3(T,j,temp)
end
Ne1= [0:1:1000];
Ne2= [0:1:1000];
Ne3= [0:1:1000];
Ne4= [0:1:1000];
Ne5= [0:1:1000];
For i= 1:1000;
Ne(i) + Emp(i)*(exp Ep./K*T);
Ns1= [0:1:1000];
Ns2= [0:1:1000];
Ns3= [0:1:1000];
Ns4= [0:1:1000];
Ns5= [0:1:1000];
Ns1(i) = exp( (2*Csavg*q/(z(1-2./z(1-1/Savg))) * exp (1- X(i)/q*diff(vfinal(i) ,x1(i));
Ns1(i) = exp( (2*Csavg*q/(z(1-2./z(1-1/Savg))) * exp (1- X(i)/q*diff(vfinal(i) ,x2(i));
Ns1(i) = exp( (2*Csavg*q/(z(1-2./z(1-1/Savg))) * exp (1- X(i)/q*diff(vfinal(i) ,x3(i));
Ns1(i) = exp( (2*Csavg*q/(z(1-2./z(1-1/Savg))) * exp (1- X(i)/q*diff(vfinal(i) ,x4(i));
Ns1(i) = exp( (2*Csavg*q/(z(1-2./z(1-1/Savg))) * exp (1- X(i)/q*diff(vfinal(i) ,x5(i));
A = [0:1:1000];
A(i)/R*(T) = Va(i)ln(Va(i)/Saavg(i))+Vb(i)ln(Vbavg(i)/Svavg(i)) +
Vg(i)*ln(Vg(i)/Sgavg(i));+ 1/Svg (i) + ln normdist(y) – Normdist(1-y) + Rand(g)(1-
```

```
(2./z(1-1/s(i)*Yavg(i)))Ln nordist(y)-z*(1-2/z *1-1/s)/2*q{Ufinal(i)*ln U +
Vfinal(i)lnv + Wfinal(i)lnW + Rfinal (i) ln R; + p*(w*v ) + N(i) + 2*X1(i)Epp(i) +
X4(i)*(Egp(i) + 2(R)(i) –X4(i) –X5(i))Egg + Ln(K2(M/T(i))
P = (Vfinal(i) – X1avg(i) –X2avg(i))ln(vfian(i)-X1avg(i-X2(i) )ln (wiX2(i) –
X3avg(i))*ln(r-X4avg(i)In(r-(X4(i)- X5avg(i);
E11(i) = [0:1:1000]
E(i) = trapzod(2 : Ns1 , Ns2 , Ns3 , Ns4, Ns5);
U11 = 2314.32 ;
For j=1:1000;
U12(i) = A(i) + (1-x) diff(A(i)/X(i))
E11(i) = E(i) *(U(i) – X1(i)-X3(i)-X4(i)) Epp(i) +(V(i) – X1(i)- X2(i))Ecp(i)
+2*X1(i) Emp(i) +X4(i) +2 *(R9i)-X4(i)-X5(i));
x = U11 – A(i) /Diff(A(i)/X(i)) -1 ;
if x >= 1
A(i) = rand;
Goto A(i);
Elseif x <=1;
Disp(x , T(i));
End.
```